Global and Pacific Temperature, Productivity, and Western North America Hydroclimate Change during the Holocene

by

Anson H. Cheung

B.S. The University of Arizona, 2017

Sc.M. Brown University, 2019

A Dissertation submitted to the Department of Earth, Environmental and Planetary Sciences at Brown University in partial fulfillment of the requirements for the Degree of Doctor of Philosophy

Providence, Rhode Island

May 2023

This dissertation by Anson H. Cheung is accepted in its present form by the Department of Earth, Environmental and Planetary Sciences as satisfying the dissertation requirement for the degree of Doctor of Philosophy.

Date: _____ _____

Timothy D. Herbert, Ph.D, Advisor

Date: _____ _____

Baylor Fox-Kemper, Ph.D, Advisor

Recommended to the Graduate Council

Date: _____ _____

Tripti Bhattacharya, Ph.D, Reader

Date: _____ _____

Karianne Bergen, Ph.D, Reader

Date: _____ _____

James M. Russell, Ph.D, Reader

Approved by the Graduate Council

Date: _____ _____

Thomas A. Lewis, Dean of the Graduate School

ANSON H. CHEUNG

anson_cheung@brown.edu
Department of Earth, Environmental, and Planetary Sciences,
324 Brook Street, Box 1846, Providence, RI 02912
website: https://sites.google.com/view/ansonhcheung/

EDUCATION

Brown University 2017 - May 2023 (expected)
Ph.D Candidate, Earth, Environmental, and Planetary Sciences
Advisors: Dr. Timothy Herbert and Dr. Baylor Fox-Kemper

Sc.M. Earth, Environmental, and Planetary Sciences 2017-2019
Advisors: Dr. Timothy Herbert and Dr. Baylor Fox-Kemper

University of Arizona 2013-2017
B.S. Geosciences – Earth System Science

RESEARCH EXPERIENCE

Graduate Research Assistant September 2017 - Present
Department of Earth, Environmental, and Planetary Sciences, Brown University
Advisors: Dr. Timothy Herbert and Dr. Baylor Fox-Kemper

Undergraduate Research Assistant January 2014 - May 2017
Department of Geosciences, University of Arizona
Advisor: Dr. Julia Cole

Undergraduate Research Assistant (Independent Study) January 2016 - May 2016
Research School of Earth Sciences, Australian National University
Advisor: Dr. Nerilie Abram

Undergraduate Research Assistant (REU) May 2015 - August 2015
Department of Meteorology and Atmospheric Science, Pennsylvania State University
Advisors: Dr. Michael Mann, Dr. Byron Steinman, Sonya Miller

NASA Space Grant Intern September 2014 - May 2015
Department of Geosciences, University of Arizona
Advisors: Dr. Luke Parsons and Dr. Jonathan Overpeck

Undergraduate Research Assistant June 2014 - August 2014
Department of Earth Sciences, The University of Hong Kong
Advisor: Dr. Zhonghui Liu

FELLOWSHIPS/SCHOLARSHIPS

Brown University Presidential Fellowship	2017-2020
Galileo Circle Scholarship	2017
Astronaut Scholarship Foundation Scholarship	2016-2017
Arizona Excellence Tuition Award Scholarship	2013-2017
Benjamin A Gilman International Scholarship	Spring 2016
Kissling Spirit of Inquiry Scholarship	2015-2016

Van de Verde Undergraduate Research Scholarship	2015-2016
UA/NASA Space Grant Internship	2014-2015

GRANTS (TOTAL = $16,600)

AMQUA Student Travel Grant ($300)	2022
Institute at Brown for Environment and Society Research Grant (total = $9550)	2020,2022
Brown University Graduate School Doctoral Research Travel Grant ($700)	2019
Brown University Graduate School International Travel Grant (total = $1400)	2018,2019
Brown University Graduate School Conference Travel Grant (total = $2600)	2017,2019, 2021,2022
Brown University Graduate Student Council Travel Grant (total = $1050)	2017,2019, 2020,2022
Honors College Alumni Legacy Grant (Honors Thesis) ($1000)	2016-2017

ACADEMIC HONORS

Outstanding Senior in the Department of Geosciences	2017
First Level Honors	2015
Academic Year Academic Distinction	2015
Academic Year Highest Academic Distinction	2014
Deans List with Distinction	Fall 2013, Spring 2014, Spring 2015
Deans List	Fall 2014, Fall 2015

PUBLICATIONS

†: Undergraduate Student *: Equal Contribution

PEER REVIEWED:

[1] R. S. Vachula and **A. H. Cheung**. A meta-analysis of studies attributing significance to solar irradiance. *Earth and Space Science*, 10(1):e2022EA002466, 2023. doi: https://doi.org/10.1029/2022EA002466.

[2] **A. H. Cheung**, S. Sandwick†, X. Du, J. Abella-Gutiérrez, R. S. Vachula, T. D. Herbert, B. Fox-Kemper, and J. C. Herguera. Middle to Late Holocene sea surface temperature and productivity changes in the northeast Pacific. *Paleoceanography and Paleoclimatology*, 37(11): e2021PA004399, 2022. doi: https://doi.org/10.1029/2021PA004399.

[3] V. J. Clementi, Y. Rosenthal, S. C. Bova, E. K. Thomas, J. D. Wright, R. A. Mortlock, O. C. Cowling, L. V. Godfrey, L. B. Childress, and **Expedition 379T Scientists**. Deep submarine infiltration of altered geothermal groundwater on the south Chilean Margin. *Communications Earth & Environment*, 3(218), 2022. doi: https://doi.org/10.1038/s43247-022-00541-3.

[4] R. S. Vachula, R. Y. Sheppard, and **A. H. Cheung**. Preservation biases are pervasive in Holocene paleofire records. *Palaeogeography, Palaeoclimatology, Palaeoecology*, page 111165, 2022. doi: https://doi.org/10.1016/j.palaeo.2022.111165.

[5] C. Li, V. J. Clementi, S. C. Bova, Y. Rosenthal, L. B. Childress, J. D. Wright, Z. Jian, and **Expedition 379T Scientists**. The sediment green-blue color ratio as a proxy for biogenic silica productivity along the Chilean Margin. *Geochemistry, Geophysics, Geosystems*, page e2022GC010350, 2022. doi: https://doi.org/10.1029/2022GC010350.

[6] D. Thompson, M. McCulloch, J. E. Cole, E. V. Reed, J. P. D'Olivo, K. Dyez, M. Lofverstrom, J. Lough, N. Cantin, A. W. Tudhope, **A. H. Cheung**, L. Vetter, and R. L. Edwards. Marginal Reefs Under Stress: Physiological Limits Render Galápagos Corals Susceptible to Ocean Acidification and Thermal Stress. *AGU Advances*, 3(1):e2021AV000509, 2022. doi: https://doi.org/10.1029/2021AV000509.

[7] **A. H. Cheung**, J. E. Cole, D. M. Thompson, L. Vetter, G. Jimenez, and A. W. Tudhope. Fidelity of the coral Sr/Ca paleothermometer following heat stress in the northern Galápagos. *Paleoceanography and Paleoclimatology*, 36(12):e2021PA004323, 2021. doi: https://doi.org/10.1029/2021PA004323.

[8] E. V. Reed, D. M. Thompson, J. E. Cole, J. M. Lough, N. E. Cantin, **A. H. Cheung**, A. Tudhope, L. Vetter, G. Jimenez, and R. L. Edwards. Impacts of Coral Growth on Geochemistry: Lessons From the Galápagos Islands. *Paleoceanography and Paleoclimatology*, 36 (4):e2020PA004051, 2021. doi: https://doi.org/10.1029/2020PA004051.

[9] R. S. Vachula and **A. H. Cheung**. Late Neogene surge in sedimentary charcoal fluxes partly due to preservation biases, not fire activity. *Palaeogeography, Palaeoclimatology, Palaeoecology*, 567:110273, 2021. doi: https://doi.org/10.1016/j.palaeo.2021.110273.

[10] **A. H. Cheung***, R. S. Vachula*, E. Clifton†, S. Sandwick†, and J. M. Russell. Humans dominated biomass burning variations in Equatorial Asia over the past 200 years: Evidence from a lake sediment charcoal record. *Quaternary Science Reviews*, 253:106778, 2021. doi: https://doi.org/10.1016/j.quascirev.2020.106778.

[11] N. A. O'Mara, **A. H. Cheung**, C. S. Kelly, S. Sandwick†, T. D. Herbert, J. M. Russell, J. Abella-Gutiérrez, S. G. Dee, P. W. Swarzenski, and J. C. Herguera. Subtropical Pacific Ocean Temperature Fluctuations in the Common Era: Multidecadal Variability and Its Relationship With Southwestern North American Megadroughts. *Geophysical Research Letters*, 46(24): 14662–14673, 2019. doi: https://doi.org/10.1029/2019GL084828.

[12] **A. Cheung**, B. Fox-Kemper, and T. Herbert. Can we use sea surface temperature and productivity proxy records to reconstruct Ekman upwelling? *Climate of the Past*, 15(6):1985–1998, 2019. doi: https://doi.org/10.5194/cp-15-1985-2019.

[13] **A. H. Cheung**, M. E. Mann, B. A. Steinman, L. M. Frankcombe, M. H. England, and S. K. Miller. Reply to "Comment on 'Comparison of Low-Frequency Internal Climate Variability in CMIP5 Models and Observations'". *Journal of Climate*, 30(23):9773–9782, 2017a. doi: https://doi.org/10.1175/JCLI-D-17-0531.1.

[14] **A. H. Cheung**, M. E. Mann, B. A. Steinman, L. M. Frankcombe, M. H. England, and S. K. Miller. Comparison of Low-Frequency Internal Climate Variability in CMIP5 Models and Observations. *Journal of Climate*, 30(12):4763–4776, 2017b. doi: https://doi.org/10.1175/JCLI-D-16-0712.1.

[15] M. E. Mann, B. A. Steinman, S. K. Miller, L. M. Frankcombe, M. H. England, and **A. H. Cheung**. Predictability of the recent slowdown and subsequent recovery of large-scale surface warming using statistical methods. *Geophysical Research Letters*, 43(7):3459–3467, 2016. doi: https://doi.org/10.1002/2016GL068159.

IN PROGRESS:

[1] **A. H. Cheung**, X. Du, M. C. Parish, R. S. Vachula, B. Fox-Kemper, and T. D. Herbert. Changes and relationships between Pacific sea surface temperature and western North America hydroclimate during the Holocene. in prep.

[2] **A. H. Cheung***, T. Lee*, T. D. Herbert, C. E. Lawrence, and B. Thompson. A Gaussian Process Calibration Model for Alkenone Paleothermometry. in prep.

CONFERENCE/WORKSHOP PRESENTATIONS

*: Equal Contribution

ORAL:

[1] **Cheung*, A. H.**, R. Cleveland-Stout*, R. Hébert*, and X. Zhang*. From simple models and physics. In *PAGES 2k-CVAS Meeting: Centennial climate variability at regional scale in models and reconstructions*, Potsdam, Germany, March 2023. PAGES CVAS– PAGES2k.

[2] **Cheung, A. H.**, L. A. Parsons, and B. Fox-Kemper. Time of emergence in the Last Millennium Reanalysis and CCSM4. In *AGU Fall Meeting 2022*, Chicago, IL, USA, December 2022. American Geophysical Union.

[3] **Cheung, A. H.**, B. Fox-Kemper, and T. D. Herbert. Can we use sst and productivity records from eastern boundary current systems to reconstruct upwelling? In *Climate Variability Across Scales (CVAS) Workshop*, Seattle, WA, USA, January 2019. PAGES CVAS.

[4] **Cheung, A.H.**, J. E. Cole, L. Vetter, G. Jimenez, D. M. Thompson, and A. W. Tudhope. Multiproxy Reconstructions of the Eastern Equatorial Pacific: Measuring Sr/Ca, Ba/Ca, and Li/Mg in Modern Corals using ICP-OES. In *Goldschmidt Conference 2018*, Boston, MA, USA, August 2018. European Association of Geochemistry and the Geochemical Society.

[5] **Cheung, A.H.**, J. E. Cole, L. Vetter, C. Shaver, and G. Jimenez. New approaches to reconstruct oceanic conditions in the Eastern Equatorial Pacific. In *GeoDaze 2017*, Tucson, AZ, USA, March 2017. University of Arizona Geosciences.

[6] **Cheung, A.H.**, L. A. Parsons, J. E. Cole, and J. T. Overpeck. Analysis of Amazon rainfall datasets and the importance of paleoclimate records. In *Arizona Space Grant Consortium Statewide Symposium*, Phoenix, AZ, USA, March 2015. Arizona Space Grant Consortium.

POSTER:

[1] **Cheung, A. H.**, B. Fox-Kemper, and T. D. Herbert. Changes in Pacific sea surface temperature and western North America hydroclimate during the Holocene. In *American Quaternary Association Biennial Meeting*, Madison, WI, USA, June 2022. American Quaternary Association.

[2] **Cheung, A. H.**, T. D. Herbert, and B. Fox-Kemper. Middle to Late Holocene sea surface temperature and productivity changes in the Northeast Pacific. In *AGU Fall Meeting 2020*, Virtual, December 2020. American Geophysical Union.

[3] **Cheung, A. H.**, T. D. Herbert, and S. Sandwick. North Pacific sea surface temperature changes from Mid to Late Holocene. In *AGU Fall Meeting 2019*, San Francisco, CA, USA, December 2019a. American Geophysical Union.

[4] **Cheung, A. H.**, T. D. Herbert, and S. Sandwick. North Pacific sea surface temperature changes from Mid to Late Holocene. In *Graduate Climate Conference 2019*, Woods Hole, MA, USA, November 2019b.

[5] **Cheung, A.H.**, J. E. Cole, L. Vetter, G. Jimenez, D. M. Thompson, and A. W. Tudhope. Multiproxy Reconstructions of the Eastern Equatorial Pacific: Measuring Sr/Ca, Ba/Ca, and Li/Mg in modern Corals using ICP-OES. In *AGU Fall Meeting 2017*, New Orleans, LA, USA, December 2017. American Geophysical Union.

[6] **Cheung, A. H.**, M. E. Mann, L. M. Frankcombe, M. H. England, B. A. Steinman, and S. K. Miller. Internal interdecadal variability in CMIP5 control simulations. In *AGU Fall Meeting 2015*, San Francisco, CA, USA, December 2015. American Geophysical Union.

[7] **Cheung, A.H.**, L. A. Parsons, J. E. Cole, and J. T. Overpeck. Analysis of Amazon rainfall datasets and the importance of paleoclimate records. In *GeoDaze 2015*, Tucson, AZ, USA, March 2015. University of Arizona Geosciences.

[8] **Cheung, A.H.** and J. E. Cole. Defining El Nino variability using coral isotopes and elemental records from Central Line Islands (Jarvis Island). In *UA Honors College First Years Honors Showcase*, Tucson, AZ, USA, May 2014. University of Arizona Honors College.

FIELD EXPERIENCE

JOIDES Resolution July 20, 2019 - August 18, 2019
JR100: Chilean Margin Paleoclimate
Inorganic Geochemist

CCGS Vector November 8, 2018
Saanich Inlet High Resolution Paleoclimate Piston and Gravity Coring
Scientist

TEACHING

Guest Lectures

Brown University – Environmental Science in a Changing World Fall 2018
Instructor: Dr. Allison Jacobel
Lecture: Energy, Natural Gas, Fracking

Brown University – Principles of Planetary Climate Fall 2022
Instructor: Dr. Jung-Eun Lee
Lectures: Carbon Dioxide and Climate; Climate Variability

Teaching Assistant

Brown University – Principles of Planetary Climate Fall 2022
Instructor: Dr. Jung-Eun Lee

Brown University – Face of the Earth Spring 2023
Instructor: Drs. Steve Parman and Yan Liang

MENTORING

Undergraduate Students:

Cameron Tripp (Brown '21) – Honors Thesis	Spring 2020 - Spring 2021
Elizabeth Clifton (Brown '21)	Fall 2018 - Spring 2019
Samantha Sandwick (Brown '20) – Senior Thesis	Fall 2017 - Spring 2020

High School Students:

Ellie Hamilton (Wheeler School '19)	Summer 2018
Omeed Siadati (Carroll Senior High School '23)	Summer 2022

SERVICE

Service to the Department

Coordinator First Years Mentoring Program	Spring 2020 - Spring 2021
Mentor First Years Mentoring Program	Fall 2020 - Spring 2021, Fall 2022 - Spring 2023
Co-organizer Department Graduate Student Conference	Spring 2020
Coordinator Department Elementary School Outreach Program	Fall 2019 - Spring 2020
Coordinator Climate and Environment Group Lunch Bunch	2018
Treasurer Department Graduate Student Geology Club	Fall 2018 - Spring 2019

Service to the Profession and Community

Peer Reviewer *International Journal of Climatology, Ocean Science, Geophysical Research Letters, Journal of Geophysical Research–Oceans, Paleoceanography & Paleoclimatology, Mathematical Geosciences*	2018 - Present
Expert Reviewer *IPCC SROCC, IPCC AR6*	2018, 2019
Session Convener *AGU Fall Meeting*	2021, 2022
Volunteer Teacher *Department Elementary School Outreach Program*	2017 - 2020

ADDITIONAL TRAINING

Brown University Sheridan Center Course Design Seminar	Spring 2023
Community Earth System Model Tutorial	Summer 2020
Brown University Sheridan Center Teaching Certificate I (Reflective Teaching)	Spring 2018

SKILLS

Languages	Cantonese, English, Mandarin
Computer	MATLAB, Python
Certificate	PADI Open Water Diving

PROFESSIONAL MEMBERSHIPS

American Geophysical Union	2015 - Present
American Quaternary Association	2022 - Present

Acknowledgements

Doing a PhD is not a simple and an easy task. When I signed up do to a PhD six years ago, I never thought the challenge I face would be way more than I was expecting and that I would undergo tremendous growth intellectually and personally. I am extremely grateful to be able to grow in a supportive and welcoming environment and be supported by faculty members, staff, colleagues, friends, and family. I would like to take this opportunity to thank and acknowledge them.

Although my dissertation work is done at Brown, my science journey started earlier and it would not do justice if I did not credit the people that I have crossed path with through my research experience as an undergraduate at the University of Arizona. I would especially like to thank Julie Cole, who allowed me to work in her lab when I was freshman and showed me the world of paleoclimatology. I would also like to thank Stephan Hlohowskyj, Elizabeth Patterson, Luke Parsons, Emma Reed, and Diane Thompson, who all guided and helped me to be a better person and a better scientist.

I would like to thank my advisors Tim Herbert and Baylor Fox-Kemper for all their support and advice throughout my PhD. Discussions with Tim are always interesting and fruitful, he showed me how to be a scientist with humility, pushed me to think deeper and broader about different science topics, and made sure I grow holistically. His feedback and comments, although sometimes brutal, are always extremely constructive and have helped me become a better writer and a scientist. Baylor, on the other hand, infuses energy and provides enthusiasm to everything that I work on. The short (bi-)weekly meetings are always refreshing and give me the right amount

of time to talk and get feedback. His thoughts as a physicists and ocean modeller also brings my research into a new dimension. Both of them have given me a lot of encouragement, freedom, trust, and guidance over the past few years and I am very thankful for that. I would also like to thank my past and current committee members, Jim Russell, Chris Huber, Jung-Eun Lee, Karianne Bergen, and Tripti Bhattacharya for taking their time to learn about my work, collaborate with me, and provide their expertise and advice in navigating my career and life.

People from the DEEPS community have played a significant role in my years at Brown. The graduate students, staff, C&E people, the Herbert lab and Fox-Kemper lab groups together have created an environment that I enjoyed working in. I would like to thank Brendan Anzures, Richard Vachula, Nora Richter, Leif Tokle, Sydney Clark for being welcoming when I first started at Brown and providing timely encouragement and advice for me whenever I needed them. Emily Joyce, Sarah McGrath, Bryce Mitsunaga, Rosa Xu, Sloane Garelick, Karen Wang, Xiangming Zhao made going through graduate school a lot easier and more fun before COVID and other life events put a twist to the experience. Chats with Aakash Sane, Dani Blum, Kristin Kimble, and Meredith Parish are always highlights of my day at work. I am thankful for the opportunities to collaborate with Xiaojing Du (first a collaborator, now a friend!), who helped me a lot in my research projects. I am also grateful that I got to work with Sam Sandwick, Cam Tripp, Elizabeth Clifton, and thank them for their patience as I learn how to work with undergraduates. Of course, all my lab work would not have be done without Becky Rose, who taught me all the nuts and bolts of the lab. JB Novak, Weimin Si, Allison Jacobel, Jared Nirenburg, Jenna Pearson, Abbie Bodner, and Brodie Pearson also provided a warm and welcoming intellectual environment for me to learn about topics that I am less familiar and comfortable with. Lastly, I thank Olga Huber for the constant encouragement in outreach work at DEEPS STEP.

Aside from the DEEPS community, I would also like to thank my friends outside of DEEPS and family. I thank you all for keeping me in your prayers and thoughts as I go through ups and downs in life and graduate school. I would also like to thank my siblings, Brian, Reanna and Roland, and my mom for being there every step of the way and for showing up when I needed the most. It makes a world of difference to know that there is always someone supporting me. Last but not least, I thank God for guiding me through the journey and giving me the peace, wisdom, and joy.

Contents

List of Figures

List of Tables

Chapter 1

Introduction

Anson Cheung

Department of Earth, Environmental, and Planetary Science, Brown University,

Providence, RI 02912, USA

1 Background

The Earth's climate system varies across a wide range of spatial and temporal scales (Kunz & Laepple, 2021; von der Heydt et al., 2021). These spatiotemporal variations play an important role in determining global and regional climate patterns, marine and terrestrial ecosystem habitats, and natural resources. Understanding the characteristics and drivers of climate variations can therefore advance our knowledge on the evolution and changes of the Earth system and improve our capability to predict climate changes. Paleoclimatology offers a good avenue to decipher climate changes across a wide range of spatiotemporal scales that cannot be achieved by solely looking into the instrumental record.

The Holocene is an ideal period to understand how the climate system varies on interannual to millennial timescales. Covering the last $\sim 11,700$ years and representing the most recent interglacial (warm) period within the climate history, the Holocene climate is relatively stable compared to earlier periods of Earth's history, with minimal planetary radiative imbalance (< 0.1 W/m^2) (Baggenstos et al., 2019) and small changes in global mean surface temperature (< 1°C) (Kaufman & Broadman, 2023). Its boundary conditions are fairly well constrained, with orbital parameters (precession and obliquity) exhibiting the most prominent change in magnitude compared to other drivers of the climate system such as greenhouse gases and volcanic activity (Figure 1.1) (Kaufman & Broadman, 2023; Wanner et al., 2008). Because of the relatively large number of proxy records with radiocarbon constraints available compared to earlier periods, the capability for climate models to simulate transient changes during the Holocene, and the relatively similar climate mean state compared to the present, Holocene climate has been used to understand whether temperature changes in the past were globally synchronous (Cartapanis et al., 2022) and to contextualize modern climate change (Gulev et al., 2021).

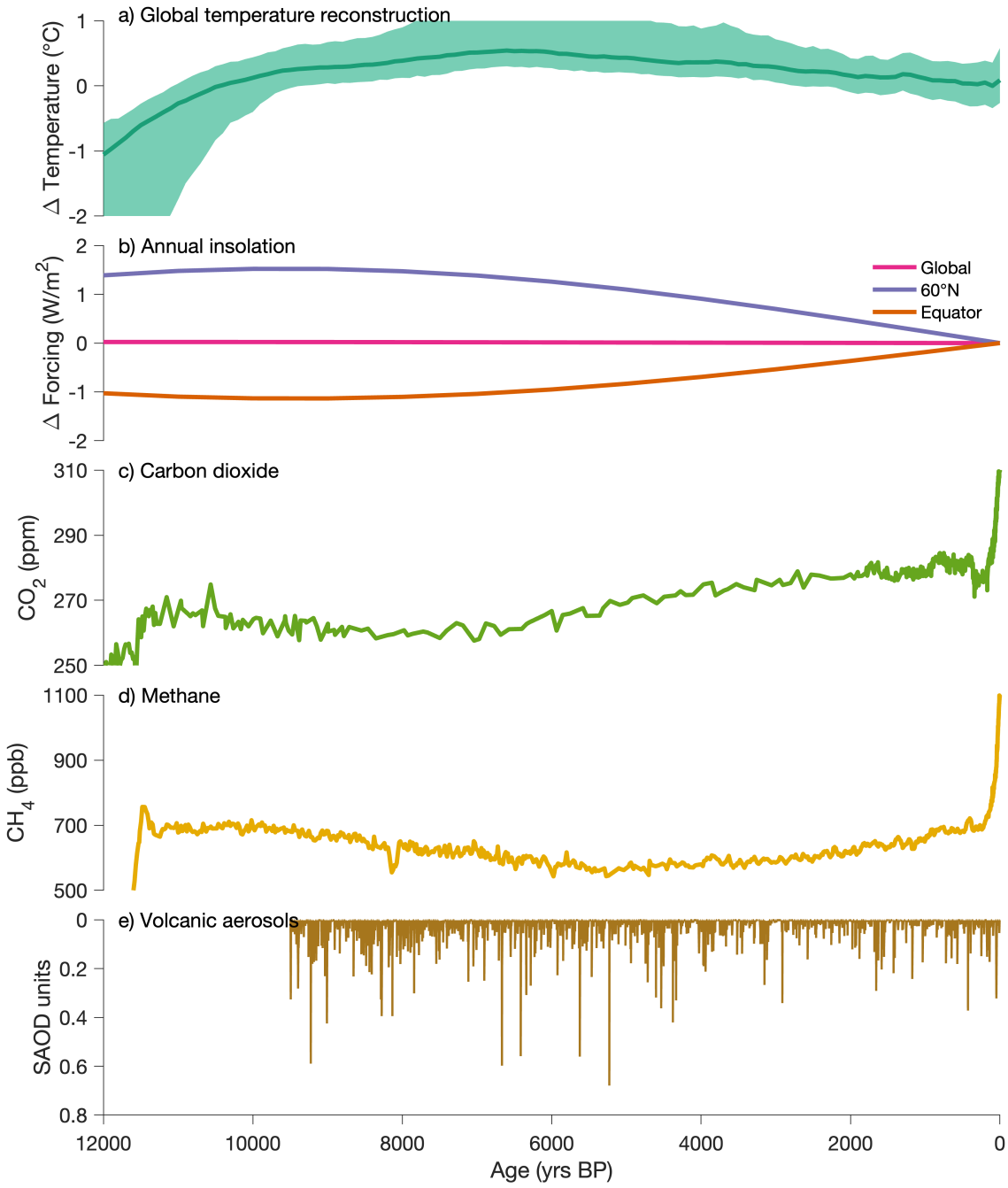

Figure 1.1: a) Global mean surface temperature reconstruction, solid line and shading are the median and 90% range of ensemble members (Kaufman, McKay, Routson, Erb, Dätwyler, et al., 2020). b) Annual insolation at 60°N, 0°, and globally. Concentrations of atmospheric c) CO_2 and d) CH_4 in Antarctic ice cores (Köhler et al., 2017). e) Volcanic Sulfur Aerosol Optical Depth (SAOD) inferred from sulfate aerosols in polar ice (Sigl et al., 2022). Δ values are relative to present.

Proxy records are the primary source used to understand climate variability during the Holocene. Although these proxies only provide indirect estimates of environmental/climate variables, they have been shown to reflect changes in their ambient environment, such as temperature, productivity, and hydroclimate. As such, proxy records have been used as 'observations' to provide a first order estimate of how the climate has changed during the Holocene. Indeed, numerous proxy records have been produced and used to understand climate changes from a proxy site to global level and across various timescales (Davis et al., 2020; Gill et al., 2017; Kaufman, McKay, Routson, Erb, Dätwyler, et al., 2020; Liefert & Shuman, 2020; Mann et al., 2008; Marcott et al., 2013; Moffa-Sanchez et al., 2019; Neukom et al., 2014; Osman et al., 2021; PAGES2k Consortium, 2013, 2019; Tierney et al., 2015).

Coupled General Circulation Models (CGCMs) have emerged as an alternative tool to understand climate change during the Holocene over the past two decades. CGCMs are numerical models that are built based on our best approximation of how the climate system works within a physically consistent framework. Unlike proxy records, CGCMs provide spatiotemporally complete climate fields and process based variables to decipher the dynamics behind changes in climate variables of interests (e.g., surface temperature). Additionally, idealized simulations can be carried out to isolate and determine the forcings that are most important for changes over the period of interests (Liu, Zhu, et al., 2014). Multiple transient simulations have been run over the past two decades using CGCMs to understand the spatiotemporal evolution of climate during the Holocene and the drivers behind these changes (Askjær et al., 2022; Bader et al., 2020; Liu et al., 2009; Smith & Gregory, 2012; Timm & Timmermann, 2007).

The increasingly abundant proxy records and the availability of transient simulations from CGCMs during the Holocene has provided opportunities to leverage both sources to further our understanding about the climate system. One way to do so is to

use CGCMs to help interpret the dynamics and determine forcings that drive changes in proxy records (Cheung et al., 2022; Liu, Lu, et al., 2014). This combined approach provides a strong physical basis to support interpretations of observed changes in proxy records and circumvent limitations that arise from the fact that proxies are indirect recorders of the climate system. A comparison between climate model simulations and proxy records also offer an 'out of sample test' opportunity to determine if CGCMs can simulate climate conditions outside of the historical period's (1850 CE - present) boundary conditions (Bova et al., 2021; Liu, Zhu, et al., 2014; Osman et al., 2021; Thompson et al., 2022). Furthermore, there have been attempts to combine proxy records and CGCMs via offline data assimilation to provide a spatiotemporally complete view of the climate system during the Holocene that are constrained by climate models (Erb et al., 2022; Osman et al., 2021).

As a result of the vast number of proxy records published and CGCM simulations carried out, we now understand more about Holocene climate change. Nonetheless, there remains challenges in inferring Holocene climate change using spatially sparse proxy records and uncertainties in understanding the dynamics and forcings driving changes observed in the proxy records. Furthermore, although there have been investigations on whether proxy records and climate models show consistent changes and variability during the Holocene, how these similarities and differences translate into contextualizing and informing modern anthropogenic warming is yet to be fully explored.

The accuracy of proxy record interpretation is a major challenge in using proxy records to understand past climate. Because proxies are indirect recorders of the climate system, there is a need to understand how the climate signal is translated into the proxy record. Furthermore, proxy records frequently record climate variables that represent changes due to multiple processes, thus making inferences of the mechanisms behind difficult. Significant progress has been made over the past decade to address

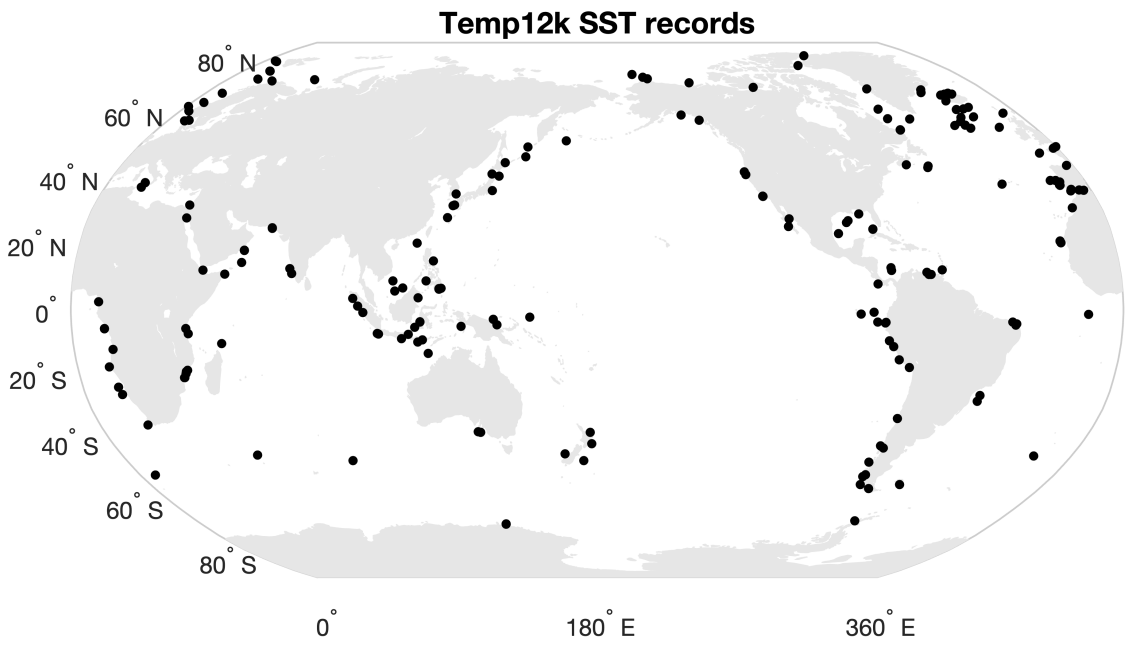

Figure 1.2: Sea surface temperature records from the Temp12k database (Kaufman, McKay, Routson, Erb, Davis, et al., 2020).

how the climate signal is recorded and translated into proxy records via constructions of proxy system models (e.g., Dee et al., 2018; Dolman & Laepple, 2018). The availability of CGCMs has also aided conceptual/simple models in inferring mechanisms driving changes observed in proxy records. However, it is still unclear if CGCMs can capture all the relevant processes that are important for interpreting proxy records and whether conceptual models are sufficient to describe the signals recorded in proxy records. This is particularly an issue for Holocene marine proxy records because they are often located along the continental margins (Figure 1.2), where CGCMs typically underperform (Richter, 2015; Small et al., 2015).

The sparse spatial coverage of proxy records also makes using proxy records to understand climate change during the Holocene more difficult. Because the location of proxy records depends on whether there is a suitable environment for a proxy archive to record changes on the timescale of interest (e.g., the Holocene), proxy records that span the Holocene are often clustered towards specific regions, such

as the continental margin for marine proxy records (Figure 1.2). Given the spatial constraint, it is therefore critical to cover as wide range of locations as possible to better understand large scale past climate change. Nevertheless, there are many regions, for instance the northeast Pacific and the Southern Hemisphere, that remain undersampled (Figure 1.2). Furthermore, many studies to date focus on a few proxy records instead of the larger existing proxy record networks to interpret large scale climate changes during the Holocene (e.g., Barron & Anderson, 2011; MacDonald et al., 2016). With recent efforts in proxy records synthesis, there are opportunities to leverage these databases to better understand the spatiotemporal evolution of the climate during the Holocene.

Although CGCMs can address shortcomings posed by proxy records, whether they can simulate the behavior and characteristics of the climate system accurately is not fully understood. A critical aspect is whether the timing, location, and magnitude of change in response towards external forcings, especially anthropogenic forcing, is consistent with observations. A large number of studies have compared CGCM simulations with proxy records to determine if they exhibit similar temporal characteristics (Bova et al., 2021; Liu, Zhu, et al., 2014; Osman et al., 2021; PAGES 2k-PMIP3 group, 2015; PAGES2k Consortium, 2019; Thompson et al., 2022). However, these similarities and differences have yet to been fully explored and quantified.

2 Outline

This dissertation aims to contribute to the discussion of Holocene climate variability by addressing the limitations mentioned above. Specifically, we focus on improving our interpretations of proxy records from eastern boundary coastal margins, reconstructing Holocene ocean conditions in the northeast Pacific, analyzing the relationship between the Pacific Ocean and western North America hydroclimate, and understanding how proxy records and CGCMs provide different information with

regards to the time of emergence of surface warming.

In chapter 2, we assess if changes in sea surface temperature and productivity recorded in marine sediment records near Baja California are consistent with Ekman upwelling, where stronger winds would lead to cooler sea surface temperature and higher productivity. By analyzing satellite observed sea surface temperature, chlorophyll, and wind stress, we find that Ekman upwelling is only the second most dominant co-varying pattern in this region, and that its importance changes across timescales. This highlights the potential of timescale dependent mechanism in driving changes along eastern boundary current regions and cautions against extrapolating mechanisms that operate on shorter timescales to paleoclimate timescales.

In chapter 3, we focus on reconstructing Holocene sea surface temperature and marine productivity changes in the Northeast Pacific, a region that lacks paleoclimate records covering the Holocene, and understanding the drivers behind these changes. By reconstructing the sea surface temperature and marine productivity in three locations and combining these results with other published records in this region, we find that sea surface temperature is more spatially and temporally variable than previously thought, and that there is no clear relationship between sea surface temperature and marine productivity. Whereas climate model simulations do not follow the pattern shown in proxy records, these simulations provide support that it is indeed possible that sea surface temperature patterns can be different between these proxy locations.

In chapter 4, we provide a synthesis view on the changes and the relationship of Pacific Ocean sea surface temperature and western North America hydroclimate during the Holocene. By compiling published proxy records on both realms, we show that Pacific Ocean sea surface temperature and western North America hydroclimate follow a similar temporal evolution, suggesting a potential relationship akin to modern El Niño teleconnections. Then, by using idealized model simulations, we find that carbon dioxide and precession appear to play a significant role in changing western

North America hydroclimate while detecting forced changes in Pacific sea surface temperature is more difficult. These results together emphasize the coupling between Pacific Ocean and western North America hydroclimate and highlights the previously underappreciated role of carbon dioxide in driving hydroclimate changes during the Holocene.

In chapter 5, we determine whether climate models and proxy records provide different spatiotemporal view of the time of emergence of surface warming. Specifically, we compare the time of emergence of warming in the last millennium reanalysis and its model prior Community Climate System Model version 4 (CCSM4). Even though they provide a similar time of emergence of warming spatial pattern, CCSM4 consistently suggests an earlier warming than the reanalysis, indicating that the there is a stronger anthropogenic warming signal and a weaker background noise in models than in proxy records. By analyzing the signal and noise separately, we suggest that this difference is caused by both a larger signal and lower noise in CCSM4 compared to proxy records. This implies that a smaller fraction of the current warming is from anthropogenic forcing, but also suggests future warming might be even larger than what we are currently experiencing.

Results from this dissertation together improve our interpretations of proxy records, advance our knowledge on the spatiotemporal evolution, dynamics, forcings associated with Pacific sea surface temperature and western North America hydroclimate changes during the Holocene, and allow us to better understand the difference in the time of emergence of warming suggested by proxy records and CGCMs.

3 Future Work

Despite these advances, there are a number of outstanding questions associated to these topics that remain to be addressed.

In particular, chapter 2 highlights the advantage and the need for more extensive

usage of satellite products to understand what marine proxies record and how to interpret them. Most efforts in understanding proxies and their interpretations rely on in situ observations, which are often costly and discontinuous (see for example Rosell-Melé & Prahl, 2013, and references therein). Satellite records can overcome these shortcomings and provide more spatiotemporally complete and continuous observations, even though they come with an expense of not recording some variables of interest. Indeed, some studies have used satellite records to understand chlorophyll seasonality and used these results to infer seasonality of alkenones (Schneider et al., 2010; Timmermann et al., 2014). However, subsequent research has shown that the phenology of satellite derived chlorophyll and coccolithophores estimates are different (Hopkins et al., 2015). Furthermore, small scale features in the ocean have shown to be important in driving phytoplankton biomass, indicating temperature driven seasonality might not be the sole major driver of phytoplankton seasonality (Keerthi et al., 2022). This can in turn influence our understanding on the seasonality of alkenone production.

Chapters 3 and 4 also demonstrate the advantage of compiling multiple proxy records across space in order to gain a more comprehensive understanding how the climate has changed in the past. In fact, there have been multiple community efforts in recent years in compiling proxy records to better understand the spatiotemporal evolution of a specific variable (e.g., temperature, hydroclimate, water isotopes, wildfire) (e.g., Harrison et al., 2022; Kaufman, McKay, Routson, Erb, Davis, et al., 2020; Konecky et al., 2020; PAGES2k Consortium, 2017). However, to date, less effort has been made to try to determine the relationship between these reconstructed variables across time and space. Hence, there remain opportunities to leverage these large scale proxy compilations to further our understanding about the climate system.

Additionally, results from chapter 3 illustrate the need to improve our understanding on the drivers of sea surface temperature across space and time. Sea surface

temperature changes have often been viewed as a direct response to changes in radiative forcing. As such, many work has relied on correlating forcing reconstructions with temperature records for interpretation. However, this is not always the case. Thus, a more nuanced view is needed to interpret sea surface temperature changes. Recent developments of climate model experiments (Gregory et al., 2016) and analysis techniques (Zika et al., 2021) offer a potential avenue to advance our knowledge on this topic. Specifically, these experiments and analyses attempt to separate the drivers of temperature change into radiative warming versus circulation effects. By computing these two terms in climate models and comparing them across simulations with different paleoclimate boundary conditions, these results can potentially improve our interpretations of proxy records.

Lastly, paleoclimate data assimiliation offers a potential new ground for proxy-model comparison. Prior proxy model comparison studies rely on climate field reconstruction techniques to combine proxy records to compare with climate models. However, the process of climate field reconstructions often introduce biases (Smerdon, 2012), which might distort the fidelity of such proxy-model comparison. On the other hand, paleoclimate data assimilation allows comparison between proxy records and climate models within the same framework. By comparing characteristics in the reanalysis product with the model prior, we can gain a better understanding of how proxy records can alter the results and thus provide clues on how proxy records and climate models differ.

References

Askjær, T. G., Zhang, Q., Schenk, F., Ljungqvist, F. C., Lu, Z., Brierley, C. M., Hopcroft, P. O., Jungclaus, J., Shi, X., Lohmann, G., Sun, W., Liu, J., Braconnot, P., Otto-Bliesner, B. L., Wu, Z., Yin, Q., Kang, Y., & Yang, H. (2022). Multi-centennial Holocene climate variability in proxy records and transient model simulations. *Quaternary Science Reviews*, *296*, 107801. https://doi.org/10.1016/j.quascirev.2022.107801

Bader, J., Jungclaus, J., Krivova, N., Lorenz, S., Maycock, A., Raddatz, T., Schmidt, H., Toohey, M., Wu, C.-J., & Claussen, M. (2020). Global temperature modes shed light on the Holocene temperature conundrum. *Nature communications*, *11*(1), 1–8.

Baggenstos, D., Häberli, M., Schmitt, J., Shackleton, S. A., Birner, B., Severinghaus, J. P., Kellerhals, T., & Fischer, H. (2019). Earth's radiative imbalance from the Last Glacial Maximum to the present. *Proceedings of the National Academy of Sciences*, *116*(30), 14881–14886. https://doi.org/10.1073/pnas.1905447116

Barron, J. A., & Anderson, L. (2011). Enhanced Late Holocene ENSO/PDO expression along the margins of the eastern North Pacific. *Quaternary International*, *235*(1-2), 3–12.

Bova, S., Rosenthal, Y., Liu, Z., Godad, S. P., & Yan, M. (2021). Seasonal origin of the thermal maxima at the Holocene and the last interglacial. *Nature*, *589*(7843), 548–553. https://doi.org/10.1038/s41586-020-03155-x

Cartapanis, O., Jonkers, L., Moffa-Sanchez, P., Jaccard, S. L., & de Vernal, A. (2022). Complex spatio-temporal structure of the holocene thermal maximum. *Nature Communications*, *13*(1). https://doi.org/10.1038/s41467-022-33362-1

Cheung, A. H., Sandwick, S., Du, X., Abella-Gutiérrez, J., Vachula, R. S., Herbert, T. D., Fox-Kemper, B., & Herguera, J. C. (2022). Middle to Late Holocene Sea Surface Temperature and Productivity Changes in the Northeast Pacific. *Paleoceanography and Paleoclimatology*, *37*(11). https://doi.org/10.1029/2021pa004399

Davis, C. V., Myhre, S. E., Deutsch, C., Caissie, B., Praetorius, S., Borreggine, M., & Thunell, R. (2020). Sea surface temperature across the Subarctic North Pacific and marginal seas through the past 20,000 years: A paleoceanographic synthesis. *Quaternary Science Reviews*, *246*, 106519. https://doi.org/10.1016/j.quascirev.2020.106519

Dee, S. G., Russell, J. M., Morrill, C., Chen, Z., & Neary, A. (2018). Prysm v2.0: A proxy system model for lacustrine archives. *Paleoceanography and Paleoclimatology*, *33*(11), 1250–1269. https://doi.org/https://doi.org/10.1029/2018PA003413

Dolman, A. M., & Laepple, T. (2018). Sedproxy: a forward model for sediment-archived climate proxies. *Climate of the Past*, *14*(12), 1851–1868. https://doi.org/10.5194/cp-14-1851-2018

Erb, M. P., McKay, N. P., Steiger, N., Dee, S., Hancock, C., Ivanovic, R. F., Gregoire, L. J., & Valdes, P. (2022). Reconstructing Holocene temperatures in time and

space using paleoclimate data assimilation. *Climate of the Past*, *18*(12), 2599–2629. https://doi.org/10.5194/cp-18-2599-2022

Gill, E. C., Rajagopalan, B., Molnar, P. H., Kushnir, Y., & Marchitto, T. M. (2017). Reconstruction of Indian summer monsoon winds and precipitation over the past 10,000 years using equatorial pacific SST proxy records. *Paleoceanography*, *32*(2), 195–216. https://doi.org/https://doi.org/10.1002/2016PA002971

Gregory, J. M., Bouttes, N., Griffies, S. M., Haak, H., Hurlin, W. J., Jungclaus, J., Kelley, M., Lee, W. G., Marshall, J., Romanou, A., Saenko, O. A., Stammer, D., & Winton, M. (2016). The flux-anomaly-forced model intercomparison project (fafmip) contribution to cmip6: Investigation of sea-level and ocean climate change in response to co_2 forcing. *Geoscientific Model Development*, *9*(11), 3993–4017. https://doi.org/10.5194/gmd-9-3993-2016

Gulev, S. K., Thorne, P. W., Ahn, J., Dentener, F. J., Domingues, C. M., Gerland, S., Gong, D., Kaufman, D. S., Nnamchi, H. C., Quaas, J., et al. (2021). Changing State of the Climate System. In Climate Change 2021: The Physical Science Basis. Contribution of Working Group I to the Sixth Assessment Report of the Intergovernmental Panel on Climate Change. *IPCC Sixth Assessment Report*.

Harrison, S. P., Villegas-Diaz, R., Cruz-Silva, E., Gallagher, D., Kesner, D., Lincoln, P., Shen, Y., Sweeney, L., Colombaroli, D., Ali, A., Barhoumi, C., Bergeron, Y., Blyakharchuk, T., Bobek, P., Bradshaw, R., Clear, J. L., Czerwiński, S., Daniau, A.-L., Dodson, J., ... Paillard, J. (2022). The reading palaeofire database: An expanded global resource to document changes in fire regimes from sedimentary charcoal records. *Earth System Science Data*, *14*(3), 1109–1124. https://doi.org/10.5194/essd-14-1109-2022

Hopkins, J., Henson, S. A., Painter, S. C., Tyrrell, T., & Poulton, A. J. (2015). Phenological characteristics of global coccolithophore blooms. *Global Biogeochemical Cycles*, *29*(2), 239–253. https://doi.org/https://doi.org/10.1002/2014GB004919

Kaufman, D., & Broadman, E. (2023). Revisiting the Holocene global temperature conundrum. *Nature*, *614*(7948), 425–435. https://doi.org/10.1038/s41586-022-05536-w

Kaufman, D., McKay, N., Routson, C., Erb, M., Dätwyler, C., Sommer, P. S., Heiri, O., & Davis, B. (2020). Holocene global mean surface temperature, a multi-method reconstruction approach. *Scientific data*, *7*(1), 1–13.

Kaufman, D., McKay, N., Routson, C., Erb, M., Davis, B., Heiri, O., Jaccard, S., Tierney, J., Dätwyler, C., Axford, Y., et al. (2020). A global database of Holocene paleotemperature records. *Scientific data*, *7*(1), 1–34.

Keerthi, M. G., Prend, C. J., Aumont, O., & Lévy, M. (2022). Annual variations in phytoplankton biomass driven by small-scale physical processes. *Nature Geoscience*, *15*(12), 1027–1033. https://doi.org/10.1038/s41561-022-01057-3

Köhler, P., Nehrbass-Ahles, C., Schmitt, J., Stocker, T. F., & Fischer, H. (2017). A 156 kyr smoothed history of the atmospheric greenhouse gases CO_2, CH_4, and N_2O and their radiative forcing. *Earth System Science Data*, *9*(1), 363–387. https://doi.org/10.5194/essd-9-363-2017

Konecky, B. L., McKay, N. P., Churakova (Sidorova), O. V., Comas-Bru, L., Dassié, E. P., DeLong, K. L., Falster, G. M., Fischer, M. J., Jones, M. D., Jonkers, L., Kaufman, D. S., Leduc, G., Managave, S. R., Martrat, B., Opel, T., Orsi, A. J., Partin, J. W., Sayani, H. R., Thomas, E. K., ... Iso2k Project Members. (2020). The iso2k database: A global compilation of paleo-$\delta^{18}O$ and $\delta^{2}H$ records to aid understanding of common era climate. *Earth System Science Data*, *12*(3), 2261–2288. https://doi.org/10.5194/essd-12-2261-2020

Kunz, T., & Laepple, T. (2021). Frequency-dependent estimation of effective spatial degrees of freedom. *Journal of Climate*, *34*(18), 7373–7388. https://doi.org/10.1175/jcli-d-20-0228.1

Liefert, D. T., & Shuman, B. N. (2020). Pervasive Desiccation of North American Lakes During the Late Quaternary. *Geophysical Research Letters*, *47*(3). https://doi.org/10.1029/2019gl086412

Liu, Z., Lu, Z., Wen, X., Otto-Bliesner, B. L., Timmermann, A., & Cobb, K. M. (2014). Evolution and forcing mechanisms of El Niño over the past 21,000 years. *Nature*, *515*(7528), 550–553.

Liu, Z., Otto-Bliesner, B., He, F., Brady, E., Tomas, R., Clark, P., Carlson, A., Lynch-Stieglitz, J., Curry, W., Brook, E., et al. (2009). Transient simulation of last deglaciation with a new mechanism for Bølling-Alleröd warming. *science*, *325*(5938), 310–314.

Liu, Z., Zhu, J., Rosenthal, Y., Zhang, X., Otto-Bliesner, B. L., Timmermann, A., Smith, R. S., Lohmann, G., Zheng, W., & Timm, O. E. (2014). The holocene temperature conundrum. *Proceedings of the National Academy of Sciences*, *111*(34). https://doi.org/10.1073/pnas.1407229111

MacDonald, G. M., Moser, K. A., Bloom, A. M., Potito, A. P., Porinchu, D. F., Holmquist, J. R., Hughes, J., & Kremenetski, K. V. (2016). Prolonged California aridity linked to climate warming and Pacific sea surface temperature. *Scientific Reports*, *6*(1). https://doi.org/10.1038/srep33325

Mann, M. E., Zhang, Z., Hughes, M. K., Bradley, R. S., Miller, S. K., Rutherford, S., & Ni, F. (2008). Proxy-based reconstructions of hemispheric and global

surface temperature variations over the past two millennia. *Proceedings of the National Academy of Sciences*, *105*(36), 13252–13257.

Marcott, S. A., Shakun, J. D., Clark, P. U., & Mix, A. C. (2013). A reconstruction of regional and global temperature for the past 11,300 years. *Science*, *339*(6124), 1198–1201.

Moffa-Sanchez, P., Rosenthal, Y., Babila, T. L., Mohtadi, M., & Zhang, X. (2019). Temperature Evolution of the Indo-Pacific Warm Pool Over the Holocene and the Last Deglaciation. *Paleoceanography and Paleoclimatology*, *34*(7), 1107–1123. https://doi.org/https://doi.org/10.1029/2018PA003455

Neukom, R., Gergis, J., Karoly, D. J., Wanner, H., Curran, M., Elbert, J., Gonzalez-Rouco, F., Linsley, B. K., Moy, A. D., Mundo, I., et al. (2014). Inter-hemispheric temperature variability over the past millennium. *Nature climate change*, *4*(5), 362–367.

Osman, M. B., Tierney, J. E., Zhu, J., Tardif, R., Hakim, G. J., King, J., & Poulsen, C. J. (2021). Globally resolved surface temperatures since the Last Glacial Maximum. *Nature*, *599*(7884), 239–244. https://doi.org/10.1038/s41586-021-03984-4

PAGES 2k-PMIP3 group. (2015). Continental-scale temperature variability in PMIP3 simulations and PAGES 2k regional temperature reconstructions over the past millennium. *Climate of the Past*, *11*(12), 1673–1699. https://doi.org/10.5194/cp-11-1673-2015

PAGES2k Consortium. (2013). Continental-scale temperature variability during the past two millennia. *Nature Geoscience*, *6*(5), 339–346.

PAGES2k Consortium. (2017). A global multiproxy database for temperature reconstructions of the Common Era. *Scientific data*, *4*.

PAGES2k Consortium. (2019). Consistent multidecadal variability in global temperature reconstructions and simulations over the Common Era. *Nature Geoscience*, *12*(8), 643–649.

Richter, I. (2015). Climate model biases in the eastern tropical oceans: Causes, impacts and ways forward. *WIREs Climate Change*, *6*(3), 345–358. https://doi.org/https://doi.org/10.1002/wcc.338

Rosell-Melé, A., & Prahl, F. G. (2013). Seasonality of $U_{37}^{K'}$ temperature estimates as inferred from sediment trap data. *Quaternary Science Reviews*, *72*, 128–136.

Schneider, B., Leduc, G., & Park, W. (2010). Disentangling seasonal signals in Holocene climate trends by satellite-model-proxy integration. *Paleoceanography*, *25*(4). https://doi.org/https://doi.org/10.1029/2009PA001893

Sigl, M., Toohey, M., McConnell, J. R., Cole-Dai, J., & Severi, M. (2022). Volcanic stratospheric sulfur injections and aerosol optical depth during the Holocene (past 11,500 years) from a bipolar ice-core array. *Earth System Science Data*, *14*(7), 3167–3196. https://doi.org/10.5194/essd-14-3167-2022

Small, R. J., Curchitser, E., Hedstrom, K., Kauffman, B., & Large, W. G. (2015). The benguela upwelling system: Quantifying the sensitivity to resolution and coastal wind representation in a global climate model∗. *Journal of Climate*, *28*(23), 9409–9432. https://doi.org/10.1175/jcli-d-15-0192.1

Smerdon, J. E. (2012). Climate models as a test bed for climate reconstruction methods: Pseudoproxy experiments. *WIREs Climate Change*, *3*(1), 63–77. https://doi.org/https://doi.org/10.1002/wcc.149

Smith, R. S., & Gregory, J. (2012). The last glacial cycle: Transient simulations with an AOGCM. *Climate Dynamics*, *38*(7-8), 1545–1559. https://doi.org/10.1007/s00382-011-1283-y

Thompson, A. J., Zhu, J., Poulsen, C. J., Tierney, J. E., & Skinner, C. B. (2022). Northern Hemisphere vegetation change drives a Holocene thermal maximum. *Science advances*, *8*(15), eabj6535. https://doi.org/10.1126/sciadv.abj6535

Tierney, J. E., Abram, N. J., Anchukaitis, K. J., Evans, M. N., Giry, C., Kilbourne, K. H., Saenger, C. P., Wu, H. C., & Zinke, J. (2015). Tropical sea surface temperatures for the past four centuries reconstructed from coral archives. *paleoceanography*, *30*(3), 226–252.

Timm, O., & Timmermann, A. (2007). Simulation of the last 21 000 years using accelerated transient boundary conditions. *Journal of Climate*, *20*(17), 4377–4401. https://doi.org/https://doi.org/10.1175/JCLI4237.1

Timmermann, A., Sachs, J., & Timm, O. E. (2014). Assessing divergent SST behavior during the last 21 ka derived from alkenones and G. ruber-Mg/Ca in the equatorial Pacific. *Paleoceanography*, *29*(6), 680–696. https://doi.org/https://doi.org/10.1002/2013PA002598

von der Heydt, A. S., Ashwin, P., Camp, C. D., Crucifix, M., Dijkstra, H. A., Ditlevsen, P., & Lenton, T. M. (2021). Quantification and interpretation of the climate variability record. *Global and Planetary Change*, *197*, 103399. https://doi.org/10.1016/j.gloplacha.2020.103399

Wanner, H., Beer, J., Bütikofer, J., Crowley, T. J., Cubasch, U., Flückiger, J., Goosse, H., Grosjean, M., Joos, F., Kaplan, J. O., et al. (2008). Mid-to Late Holocene climate change: an overview. *Quaternary Science Reviews*, *27*(19-20), 1791–1828.

Zika, J. D., Gregory, J. M., McDonagh, E. L., Marzocchi, A., & Clément, L. (2021). Recent water mass changes reveal mechanisms of ocean warming. *Journal of Climate*, *34*(9), 3461–3479. https://doi.org/10.1175/jcli-d-20-0355.1

Chapter 2

Can We Use Sea Surface Temperature and Productivity Proxy Records to Reconstruct Ekman Upwelling?

Anson Cheung[1], Baylor Fox-Kemper[1], Timothy Herbert[1]

1. Department of Earth, Environmental, and Planetary Science, Brown University, Providence, RI 02912, USA

Published: Climate of the Past (2019), 15

Abstract

Marine sediments have greatly improved our understanding of the climate system, but their interpretation often assumes that certain climate mechanisms operate consistently over all timescales of interest and that variability at one or a few sample sites is representative of an oceanographic province. In this study, we test these assumptions using modern observations in an idealized manner mimicking paleo-reconstruction to investigate whether sea surface temperature and productivity proxy records in the Southern California Current System can be used to reconstruct Ekman upwelling. The method uses extended empirical orthogonal function (EEOF) analysis of the covariation of alongshore wind stress, chlorophyll, and sea surface temperature as measured by satellites from 2002 to 2009. We find that EEOF1 does not reflect an Ekman upwelling pattern but instead much broader California Current processes. EEOF2 and 3 reflect upwelling patterns, but these patterns are timescale dependent and regional. Thus, the skill of using one site to reconstruct the large-scale dominant patterns is spatially dependent. Lastly, we show that using multiple sites and/or multiple variables generally improves field reconstruction. These results together suggest that caution is needed when attempting to extrapolate mechanisms that may be important on seasonal timescales (e.g., Ekman upwelling) to deeper time but also the advantage of having multiple proxy records.

1 Introduction

The climate system varies across multiple timescales and is driven by both stochastic processes and deterministic forcings (Huybers & Curry, 2006). Paleoclimate records help us understand mechanisms of climate variability and change over long timescales by extending instrumental records beyond the historical period. Numerous studies have used paleoclimate records to understand climate system responses to different external forcings (e.g., Shakun et al., 2012), have put recent climate change into a long-term context (e.g., Abram et al., 2016; PAGES2k Consortium, 2013), and have helped benchmark climate models (e.g., Harrison et al., 2015).

Marine sediment is one of the most widely used archives for paleoclimate studies. Using marine sediments for paleoclimate inference usually involves multiple steps, whereby one first measures multiple sensors, frequently proxies for sea surface temperature (SST) and productivity, from a single site. Then, one compares them with other nearby local records, hemispheric reconstructions, and forcing reconstructions. Lastly, one applies modern large-scale climatology to explain changes observed in paleoclimate records (e.g., Abram et al., 2016; Goni et al., 2006; Leduc, Herbert, et al., 2010; MARGO, 2009; McGregor et al., 2007; Vargas et al., 2007). While these comparisons have improved our understanding about paleoclimate significantly, uncertainties and oversimplifications may often result in overly broad interpretations and assertions. Notably, this approach typically assumes that (1) certain climate mechanisms always operate over the past at all timescales of interest, and (2) large-scale phenomena can be linked to variability at one or a few sample sites (i.e., a paleoclimate record location). In actuality, some have found a substantial difference in SST reconstruction at nearby sites (e.g., Leduc, Schneider, et al., 2010, and references therein).

This paper illustrates an approach to test commonly asserted interpretations of

SST and productivity proxy records by using observational data to analyze a region where a known mechanism drives a large fraction of the variability and with well-preserved high-resolution sedimentary records: the southern California region, an example of an eastern boundary upwelling system (EBUS). There are strong scientific and societal interests in understanding EBUSs because physical and biogeochemical changes in these regions are known to have significant impacts on regional climate (Jacox et al., 2014; Ravelo et al., 2004; Snyder et al., 2003) and the global fishery industry (Pauly & Christensen, 1995; Ryther, 1969; Ware & Thomson, 2005). Unfortunately, it remains uncertain how EBUSs will change on decadal to centennial timescales in the future (Bakun et al., 2015; Di Lorenzo, 2015; Garcia-Reyes et al., 2015, and references therein). Nevertheless, underlying sediments in these regions often accumulate rapidly and contain a wealth of paleoclimate information, in particular organic biomarkers and associated proxies. Thus, this has allowed for high-resolution (subdecadal timescale) and high-quality paleoclimate reconstructions along many EBUSs, which provide additional constraints on past and future changes in EBUSs (e.g., Leduc, Herbert, et al., 2010; McGregor et al., 2007; Vargas et al., 2007)

Variability in SST and productivity reconstructions along EBUSs are often regarded as a response to Ekman pumping (e.g., Leduc, Herbert, et al., 2010; MARGO, 2009; McGregor et al., 2007; Vargas et al., 2007). However, many other processes are also at play in EBUSs and can drive SST and productivity changes (e.g., eddies, zonal advection, surface heat flux variations, changes in nutrient sources and concentration forced by subsurface processes, and large-scale climate variability that affects the stratification) (Chhak & Di Lorenzo, 2007; Di Lorenzo et al., 2005; Gruber et al., 2011; Jacox et al., 2016; Rykaczewski & Dunne, 2010; Xiu et al., 2018). Depending on spatial and temporal timescales, these processes can overwhelm the Ekman signal in SST and productivity changes recorded by proxy records.

Here we use high-resolution modern observations available during the satellite era to probe the spatial and temporal influence of Ekman pumping on environmental parameters of interest (e.g., SST and productivity). We apply the extended empirical orthogonal function (EEOF) approach (Chen & Harr, 1993) to analyze covariation between sea surface temperature, productivity, and alongshore wind stress in the Southern California Current System using high-resolution satellite data. We test the hypotheses that (1) the dominant covarying EEOF pattern resembles regionwide Ekman upwelling, (2) Ekman upwelling patterns, and thus the wind stress magnitude, can be recovered using time averaged proxies, and (3) large-scale changes are not the dominant drivers of variability at a single paleoclimate site. We also assess the benefits of using multiple proxy records from multiple sites to better understand the climate variability of the past in EBUS regions.

2 California Current System

The availability of numerous high-resolution spatiotemporal data (e.g., repeated hydrography, gliders, satellites) and advances in modeling have allowed us to better understand the variability of the California Current System (CCS) on multiple timescales. The CCS is made up of the California Current, California Undercurrent, and upwelling zones, which interact with a variety of local topographic features and estuaries. On 1st order, the CCS as a whole is driven by large-scale climate forcing. Changes in atmospheric pressure systems (subtropical high, Aleutian low) alter wind strength and direction, which in turn affect current direction, strength,and upwelling variability. The stratification in the region is set by large-scale features and forcing of the North Pacific. Variations in topographic features, wind forcing, freshwater inputs, and submesoscale–mesoscale features across spatial scales also play important roles in determining the spatiotemporal characteristics of the CCS. Capet et al., 2008; Checkley Jr and Barth, 2009; Lynn and Simpson, 1987 provide overviews on the dynamics

of the CCS and drivers of SST, chlorophyll, and wind forcing variability.

The optimal marine sediments to reconstruct subdecadal climate variability require a high sedimentation rate with minimal bioturbation and hence anoxic depositional environments. Along the CCS, these conditions mostly occur south of 24°N with the exception of silled basins (e.g., Santa Barbara Basin) (van Geen et al., 2003). As a result, previous high-resolution (subdecadal) paleoclimate studies were mostly done in the southern part of the CCS (SCCS; Fig. 2.1) (e.g., Abella-Gutiérrez & Herguera, 2016; Goni et al., 2006; Zhao et al., 2000).

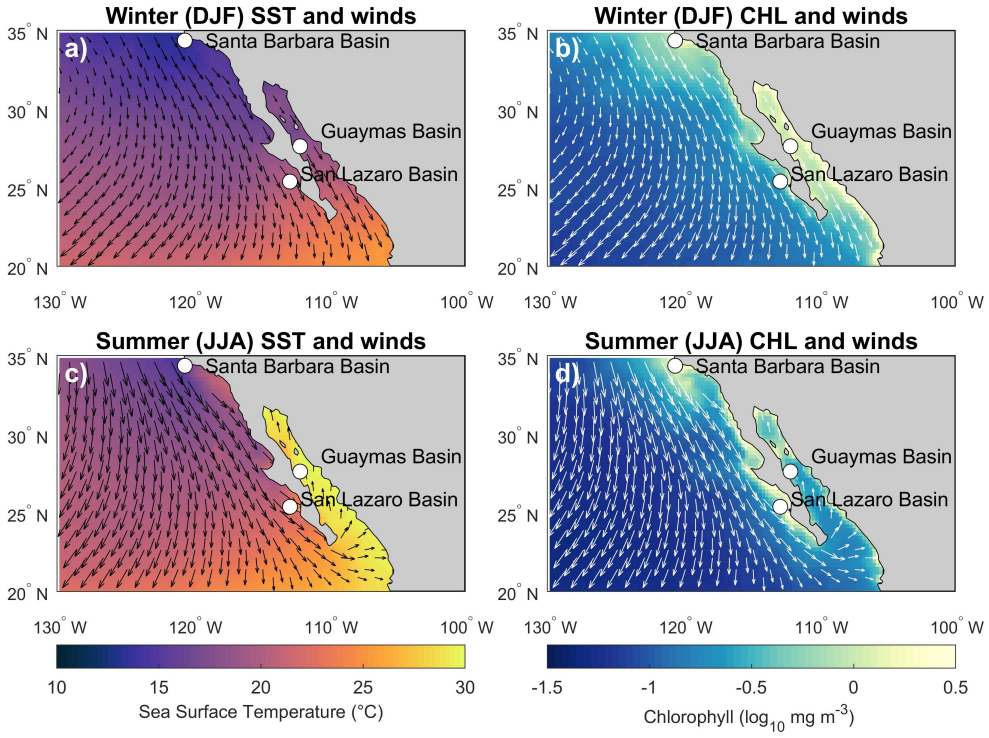

Figure 2.1: a) Winter (December, January, February) sea surface temperature average and wind pattern; b) Winter chlorophyll monthly average and wind pattern; c) Summer (June, July, August) sea surface temperature average and wind pattern; d) Summer chlorophyll monthly average and wind pattern. The basins highlighted are where high-resolution (subdecadal) sediment cores were previously retrieved and analyzed.

3 Data and Methods

This study made use of high-spatiotemporal-resolution estimates of sea surface temperature (SST), chlorophyll a (CHL), and alongshore wind stress (TAU) from satellite measurements to assess the role of Ekman pumping in driving SST and productivity changes along the SCCS. We used an extended empirical orthogonal function (EEOF) to assess the covariation between these variables because they are expected to be correlated spatially and temporally if Ekman theory is indeed the primary mechanism driving changes in the region. EEOF analysis decomposes the dataset into different covarying patterns that are orthogonal to each other. Each covarying pattern is accompanied by a time series that represents the time evolution of the covarying pattern. These patterns do not necessarily correspond to dynamical modes, but they are suggestive of physical processes that are present in the system (Monahan et al., 2009). Thus, analysis of EEOF patterns allows us to make inferences about the potential underlying dynamics. In addition, we assessed the effects of time averaging and spatial subsampling on the ability to recover dominant patterns within the spatial window analyzed. Such an assessment allows us to determine the fidelity of using proxies, which are time averaged and undersampled spatially, to understand Ekman pumping in the SCCS. Details of the data and method used can be found in Sect. 3.1 and 3.2.

3.1 Data

We used sea surface temperature (SST) from the Geostationary Environmental Satellite (GOES) system, chlorophyll a (CHL) from MODIS, and alongshore wind stress (TAU) observations from QuikSCAT that span from July 2002 to November 2009. Although CHL does not equate precisely to primary productivity and also differs from productivity inferred from proxy records, CHL provides a 1st-order esti-

mate of productivity (Henson et al., 2010). All data were derived and are available from the National Aeronautics and Space Administration Jet Propulsion Laboratory PO.DAAC and ocean color data server. We did not use the California Cooperative Oceanic Fisheries Investigations dataset because sampling resolution is low and the spatial extent is small when compared to satellite images. Reanalysis products (e.g., SODA) were also not chosen because even though they may span a longer period of time, there are many uncertainties associated with these products, for instance initial conditions, boundary forcings, model physics, and resolution (approximately 25 km horizontal) (Carton et al., 2018). Furthermore, Capet et al., 2008 show that submesoscale permitting resolution (750m horizontal) is needed in order to accurately simulate this upwelling system.

For TAU calculation, we used the descending pass of level 3 gridded Jet Propulsion Laboratory v2 QuikSCAT surface wind observations (SeaPAC, 2006). The QuikSCAT satellite is equipped with the SeaWinds scatterometer, a microwave radar that measures ocean radar backscatter over a cross section, which varies with satellite parameters and surface geometry (Chelton & Freilich, 2005; Freilich et al., 1994). Surface wind vectors can be estimated using model functions to estimate the relationship between wind and radar backscatter over the cross section. Level 3 data were derived using the direction interval retrieval with threshold nudging wind vector solutions based on level 2B data, which used the QSCAT-1B geophysical model function (Perry, 2001). Level 3 QuikSCAT data provide $0.25^\circ \times 0.25^\circ$ spatial resolution on a daily timescale. The QuikSCAT accuracy is about 0.75 ms^{-1} in the along-wind component and about 1.5 ms^{-1} in the crosswind component (Chelton & Freilich, 2005).

We utilized SST observations from the Geostationary Environmental Satellite (GOES) system. GOES provides neartime SST measurements along the west coast of North America. We used level 3 gridded GOES 6 km near-real-time SST daily

data after 12 May 2003 (NOAA/NESDIS, 2003b) and averaged hourly SST data to daily mean resolution prior to 12 May 2003 (NOAA/NESDIS, 2003a). Level 3 GOES SST data provide $0.05° \times 0.05°$ spatial resolution with better than 1K SST accuracy (Wick et al., 2002).

For CHL concentrations, we used ocean color from the Moderate Resolution Imaging Spectroradiometer on the Aqua satellite (MODIS-Aqua) (Hu et al., 2012). MODIS-Aqua is sun synchronous and measures 36 spectral bands. We used level 3 standard mapped image CHL measurements from MODIS-Aqua v2018.0 (O.B.G.P., 2015). Level 3 CHL data provides $0.041° \times 0.041°$ spatial resolution on near daily timescale with an accuracy of approximately $\pm 35\%$ (Dall'Olmo et al., 2005).

3.2 Method

3.2.1 Observation preprocessing

To allow comparison between SST, CHL, and TAU, CHL and SST were regridded to $0.25° \times 0.25°$ spatial resolution. This was done by bounding the datasets to $15° - 45°N, 130° - 100°W$, then calculating the area weighted CHL and SST value over each new grid cell. We further restricted our latitudinal extent to $15° - 35°N$ to make the analysis more computationally efficient. Repeated analysis using different spatial domains (case 1: only east of $125°W$; case 2: only north of $20°N$) suggests our conclusions are insensitive to the spatial extent selected for analysis (not shown).

Since the primary interest is Ekman driven upwelling along the coast, we computed the TAU by using (2.1):

$$\tau = \rho C_D U |\vec{U}| \tag{2.1}$$

where τ = alongshore wind stress, ρ = air density, C_D = drag coefficient, U = wind speed, $|\vec{U}|$ = alongshore wind vector. $|\vec{U}|$ was calculated by summing the alongshore component of zonal and meridional wind vectors such that $-|\vec{U}|$ and $|\vec{U}|$ represent

equatorward and poleward wind stress respectively. We used constant values for the coefficients, where $\rho = 1.2kg/m^3$ and $C_D = 1.2 \times 10^{-3}$ (Large & Pond, 1981).

Linear interpolation of all of the near-daily datasets temporally ensured uniform daily sampling rate data at each grid cell. The logarithm of CHL data was taken after regridding but before EEOF analysis because CHL exhibits a nearly log-normal distribution (Campbell, 1995). Before EEOF analysis, each variable was normalized by dividing the dataset by its domain-wide and all-time standard deviation, which makes the anomaly variations in each variable comparable to each other in terms of occurrence likelihood (assuming approximately Gaussian distributions).

To follow the logic of analyzing fields that would resemble proxy records, no removal of mean or climatological states or seasonality from the satellite records was performed. Thus, the EEOF analysis is performed on the total fields, rather than the anomaly fields.

3.2.2 Extended Empirical Orthogonal Function

Extended Empirical Orthogonal Function (EEOF) decomposition analysis was used to extract dominant patterns with covariation in SST, CHL, and TAU. EEOF is a variant of Empirical Orthogonal Function (EOF) analysis, a method that extracts coherent, orthogonal patterns by optimizing variance into multiple orthogonal functions in time and space. Multiple variants of the EOF exist, which all involve taking into account temporal correlations of a variable or correlations between variables (e.g. Bretherton et al., 1992; Hannachi et al., 2007, and reference therin). Examining multiple time snapshots as a single field allows EOF-based analysis to extract propagating patterns (e.g., Chen & Harr, 1993) and covarying patterns (Kutzbach, 1967). Figures 2.2 and 2.3 show examples of three different EOF based methods that are fundamental to the analysis herein (EOF, EEOF (temporal correlation), EEOF (multiple variables)).

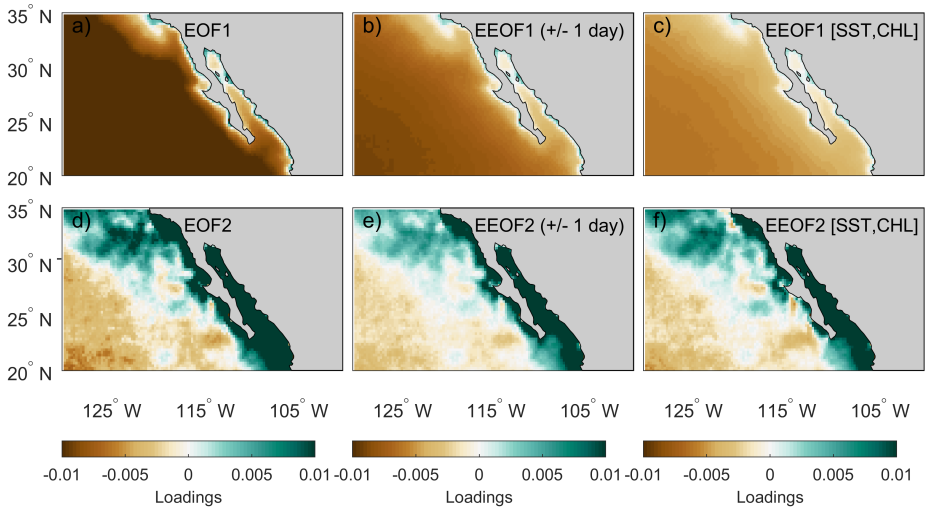

Figure 2.2: Example of decomposing chlorophyll into different modes by using an (a, d) empirical orthogonal function, (b, e) an extended empirical orthogonal function with 1 day lead and lag, and (c, f) an extended empirical orthogonal function with chlorophyll included.

The EEOF method used in this study involved extracting dominant covarying patterns by taking into account both temporal correlation within the same variable (symmetric lead-lag relationships) and correlation between variables. We employed the singular value decomposition (SVD) method (Bretherton et al., 1992) to decompose the covarying pattern of SST, CHL, and TAU into the relevant EEOF objects.

To consider time correlation of a variable X for EEOF analysis, we form the following data matrix:

$$X = \begin{pmatrix} x_{1,1} & \cdots & x_{1,j} & x_{1+k,1} & \cdots & x_{1+k,j} & x_{1+2k,1} & \cdots & x_{1+2k,j} \\ \vdots & \ddots & \vdots & \vdots & \ddots & \vdots & \vdots & \ddots & \vdots \\ x_{m-2k,1} & \cdots & x_{m-2k,j} & x_{m-2k+1,j} & \cdots & x_{m-2k+1,j} & x_{m,1} & \cdots & x_{m,j} \end{pmatrix} \tag{2.2}$$

Where $x_{t,i}$ is a data point at a certain time snapshot t and space gridpoint i, $t = 1, 2, ..., m$, $i = 1, 2, ..., j$, $k =$ time unit of lead and lag included, $m =$ temporal length of the dataset, and $j =$ total spatial grid points covered. Thus, X is the concatenation

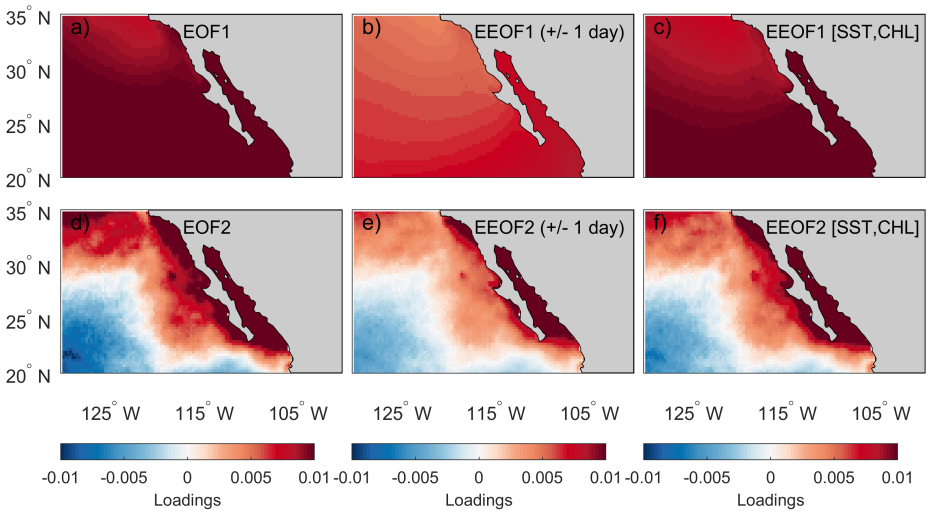

Figure 2.3: Example of decomposing temperature into different modes by using an (a, d) empirical orthogonal function, (b, e) an extended empirical orthogonal function with 1 day lead and lag, and (c, f) an extended empirical orthogonal function with sea surface temperature included.

of multiple reproductions of $x_{t,i}$, with each column featuring x evaluated at sequential times, and each row representing every spatial value of x, concatenated with spatial maps that are displaced in time to provide lead and lag information. Similarly, the data matrix, M, with three variables can be written as follow:

$$\mathrm{M} = \Big(\mathrm{SST} \quad | \quad \mathrm{CHL} \quad | \quad \mathrm{TAU} \Big) \tag{2.3}$$

Where SST, CHL, and TAU are submatrices with structure similar to matrix X. Note that each row of M is a complete spatiotemporal set of each variable, including every spatial location and lead and lag times for each variable, so that M is effectively the concatenation of three X matrices, one for each variable. Then, using SVD, we can decompose (2.3) into:

$$M = USV^T \tag{2.4}$$

where U = a matrix of left orthogonal, singular vectors as columns with temporal

information of the M matrix (Principal Components (PCs)), S = singular values, and V = a matrix of right orthogonal, singular vectors as columns with spatial information (Extended Empirical Orthogonal Functions (EEOFs)) of the M matrix. Note that the SVD method arrives at a basis of eigenvectors of the covariance matrices $M^T M$, i.e., $M^T MV = S^2 V$, and MM^T, i.e., $MM^T U = S^2 U$, so this approach is equivalent (although slightly different algorithmically) to generating EEOFs by eigenvalue decomposition.

Since proxy records reflect time averaged environmental information (usually monthly or longer), daily satellite information for analysis does not accurately depict the temporal smoothing characteristics in proxies. Hence, we performed EEOF analysis independently on daily data after averaging it into 30 days ($\sim$ monthly), and 365 days ($\sim$ annual) with non-overlapping means. The relatively short span of satellite observations does not allow us to extend our analysis to longer time periods that might also be of interest.

3.2.3 Determining the significance of modes and lead-lag

Based on singular values, EEOF1 explains $\sim$ 85% of the total variance, EEOF2 and 3 each explains $\sim$ 5% of the total variance. Instead of using singular values to determine the significance of each mode, we selected the number of modes and lead-lags to retain by evaluating the skill to reconstruct TAU. This approach was motivated by the interest of this study to detect Ekman upwelling, which involves covariation of SST, CHL, and TAU, and our inability to reconstruct TAU directly using proxies. Reconstruction of TAU (TAU_{rec}) was carried out as follow:

$$M_0 = \Big(\text{SST} \quad | \quad \text{CHL} \quad | \quad \text{TAU}(0) \Big) \tag{2.5}$$

where $TAU(0)$ = the columns for TAU in the original data matrix were replaced with zeros. Then,

$$M_{rec} = rM_0V_nV_n^T \tag{2.6}$$

$$M_{rec} = \left(SST_{rec} \quad | \quad CHL_{rec} \quad | \quad TAU_{rec} \right) \tag{2.7}$$

where r = rescaling factor calculated by $\frac{std(SST|CHL)}{std(SST_{rec}|CHL_{rec})}$, V_n = spatial information obtained from decomposing M (Eq. 2.4) with n numbers of mode retained, where n=1...5. Note that as n is much smaller than the rank of M_{rec}, $V_nV_n^T$ is not the identity matrix, but is better thought of as the projection of M_0 onto the leading modes of M. As zero wind stress is inconsistent with any of the modes V_n, multiplying M_0 by this factor adds TAU variability back into the zeroed values that is more consistent with the observed SST and CHL, which is M_{rec}.

We used Root Mean Square Error (RMSE) as a metric to measure agreement between reconstructed TAU and actual TAU:

$$RMSE = \sqrt{\overline{\overline{(TAU_{rec} - TAU)^2}}} \tag{2.8}$$

where $\overline{[\cdot]}$ represents mean of the data.

Our analysis shows that reconstruction using three modes with no lead-lag information included provides the most stable result in predicting TAU from SST and CHL regardless of averaging timescale (Fig. 2.4). This result, and similar results of convergence accuracy by adding more modes, suggest that the first three modes ($n = 3$) are reliable in this and other analyses, which will be used for the remainder of this paper.

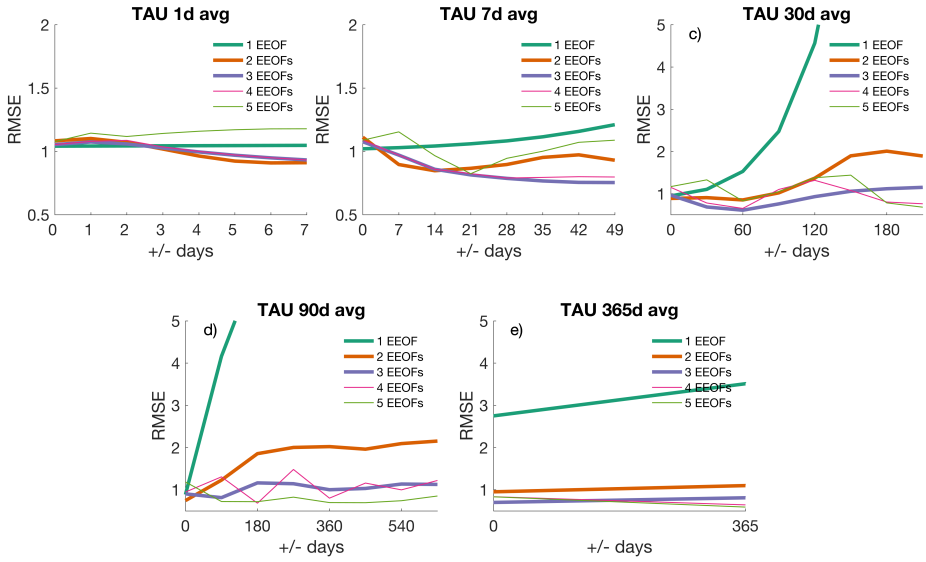

Figure 2.4: Root Mean Square Error of reconstructed wind stress with respect to actual wind stress using a) daily data; b) 7-day averaged data; c) 30-day averaged data; d) 90-day averaged data; e) 365-day averaged data.

3.2.4 Reconstruction of Principal Components

We determined how well proxy records could represent large scale circulation patterns by means of signal reconstruction. We focused specifically on three sites with previously published high-resolution paleoclimate records – Santa Barbara Basin, San Lazaro Basin, and Guaymas Basin – and two environmental variables, SST and productivity (Abella-Gutiérrez & Herguera, 2016; Goni et al., 2006; Zhao et al., 2000). We carried out three different kinds of reconstructions to address (1) how well does a single site/proxy record represent large scale circulation? (2) Does increasing the number of proxy records and/or sites improve the skill to represent modes extracted from EEOF analysis? and (3) Does increasing proxy records and/or sites improve the skill to reconstruct the original dataset? This was achieved by first only retaining the target time series (i.e., those proxy records that are to be included) from the location in M_{tar}:

$$M_{tar} = \begin{pmatrix} 0 & \cdots & \cdots & tar_{1,j} & \cdots & 0 \\ \vdots & \ddots & \vdots & \vdots & \ddots & \vdots \\ 0 & \cdots & \cdots & tar_{m,j} & \cdots & 0 \end{pmatrix} \tag{2.9}$$

We reconstructed the temporal evolution of each mode by (2.10), using only the targeted proxy records and n EEOF modes:

$$U_{rec} = r_s M_{tar}(S_n V_n^T)^{-1} \tag{2.10}$$

We reconstructed the dataset by (2.11):

$$M_{rec} = r_s M_{tar} V_n V_n^T = U_{rec} S_n V_n^T V_n V_n^T \tag{2.11}$$

where U_{rec} = reconstructed PCs, r_s = ratio between the standard deviation of time-series from target site(s) and the standard deviation of the reconstructed timeseries from target site(s), S_n and V_n were derived from (2.4) and n = modes retained for analyses. In this scenario, only the parts of V_n associated with the target location were retained for reconstruction. The pseudo-inversion of the matrix $S_n V_n^T$ was done using Moore-Penrose pseudo-inverse, which amounts to inverting only the non-singular degrees of freedom, while zeroing out the remaining modes. Similarly, the multiplication of M_{tar} by $V_n V_n^T$ considers only the projection of M_{tar} onto the n retained modes (VV^T is the identity matrix, but if only some modes are retained, then only $V_n^T V_n$ is an identity, but over the smaller dimensional space spanned by the retained modes). By retaining 1 mode ($n = 1$) and limiting the proxy record used in M_{tar} to 1, equations 2.10 and 2.11 can be used to addressed the ability of using a proxy record at a single location to represent large scale circulation, which is represented by EEOF1. Similarly, by retaining 3 modes ($n = 3$), equations 2.10 and 2.11 can be used to evaluate the effects of increasing proxy records to reconstruct modes extracted

from EEOF analysis and the original dataset.

4 Results and discussion

4.1 Does the dominant covarying pattern reflect Ekman upwelling?

EEOF analysis of daily-resolution data displays spatial patterns that are distinct from what would be expected from Ekman upwelling. By computing cross-shore (the difference divided by its arc length at locations 25.375° N, 112.875° W and 22.875° N, 120.625° W) and meridional gradients (the difference divided by its arc length at locations 34.375° N, 120.625° W and 22.875° N, 120.625° W) and comparing them, we find the TAU and CHL display a weak cross-shore gradient compared to their own respective meridional gradient. On the other hand, SST exhibits a meridional gradient that is stronger than its cross-shore gradient (Fig. 2.5). These patterns remain dominant when 30 and 365 d averaged data were used.

The fact that EEOF1 does not resemble an Ekman upwelling pattern has two major implications. First, this implies that wind stress is not the only forcing that drives CHL and SST changes along EBUSs. Previous studies have reported different mechanisms that could control changes in CHL or SST along EBUSs on various timescales. For instance, changes in subsurface nutrient concentration and sources have been shown to alter primary productivity (Chhak & Di Lorenzo, 2007; Rykaczewski & Dunne, 2010), whereas surface heat flux has been shown to exert a dominant control on sea surface temperature in the California Current System Di Lorenzo et al., 2005. Our study confirms these results and further iterates the importance of considering different factors that could affect CHL and SST along EBUSs, which are often used as indicators for changes in Ekman-driven upwelling. Second, paleoclimate reconstructions in the SCCS will be unlikely to reflect Ekman upwelling, in contrast to the common paradigm in the field, and couplings observed between proxy reconstructions of SST and productivity likely capture other processes

4.2 Can time-averaged proxies be used to reconstruct Ekman upwelling?

Even though the dominant covarying pattern does not reflect Ekman upwelling, the EEOF method allows us to decompose multiple covarying patterns for analysis. Our results suggest that EEOF2 and EEOF3 resemble an Ekman upwelling pattern on daily timescales, but they reflect upwelling at different locations (Figs. 2.6-2.7). Specifically, EEOF2 depicts upwelling conditions off Baja California, whereas EEOF3 reflects upwelling or other rapid changes in conditions at the Sea of Cortez. This presents an opportunity to understand whether time-averaged proxies can be used to reconstruct Ekman upwelling given optimal site selection.

Visual comparison of EEOF2 and EEOF3 patterns across different averaging windows suggests that these patterns change with respect to the averaging window. For both EEOFs, their patterns resemble Ekman upwelling when data with daily resolution are used. These Ekman-upwelling-like patterns disappear when 365 d averaged data are used instead and only spatially incoherent structures are retained (bottom rows in Figs. 2.6i–l and 2.7i–l). The disappearance of an Ekman upwelling pattern suggests that either Ekman upwelling is a subannual process and/or that this process is not a dominant feature on an annual timescale. We further analyze the changes in temporal scale by comparing 30 and 365 d averages of the principal component derived using daily data with principal components derived from 30 and 365 d average data. The averages of the principal component derived using daily data represent the assumption that the same dynamical process happen at all timescales, whereas the principal components derived from averaged data represent the actual covarying pattern on the timescale of interest. Our results show that the 30 and 365 d means of PC2 and PC3 derived from daily data do not always track the principal components derived from time-averaged data (Figs. 2.6h, l and 2.7h, l). While it is not possible to diagnose the underlying cause using our method, these results imply that marine sedimentary records, which generally integrate over the annual cycle, cannot cap-

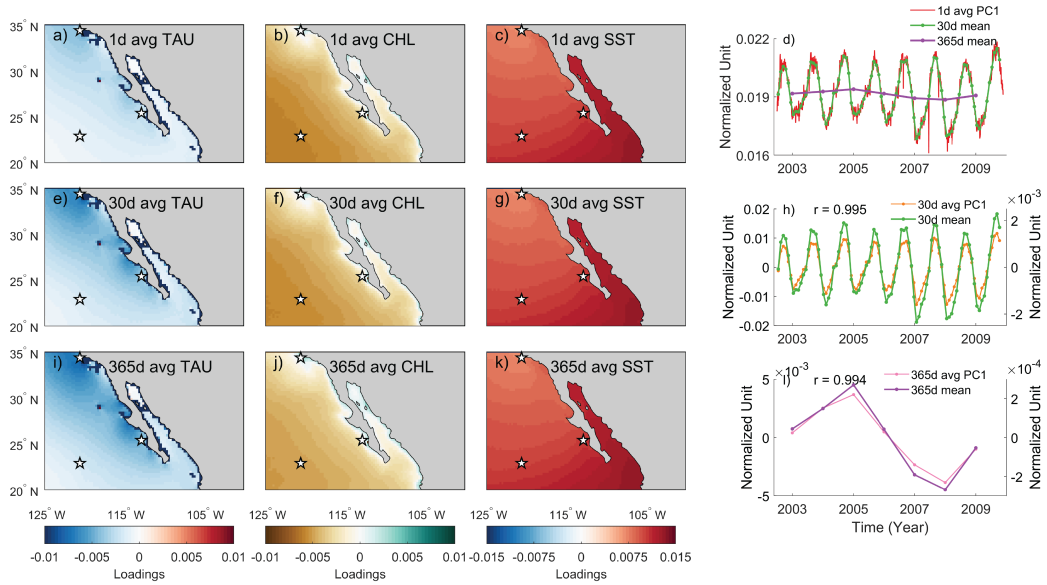

Figure 2.5: EEOF1 spatial and temporal patterns of TAU, CHL, and SST using a–d) daily; e–h) 30 day averaged; i–l) 365 day averaged data. Stars in spatial pattern plots indicate locations where the differences were taken to compute crossshore and meridional gradients. 30 day mean (green) and 365 day mean (purple) timeseries were derived from averaging 1d avg PC1. Correlation coefficient indicates how well does time mean of 1d avg PC track PC of time averaged data.

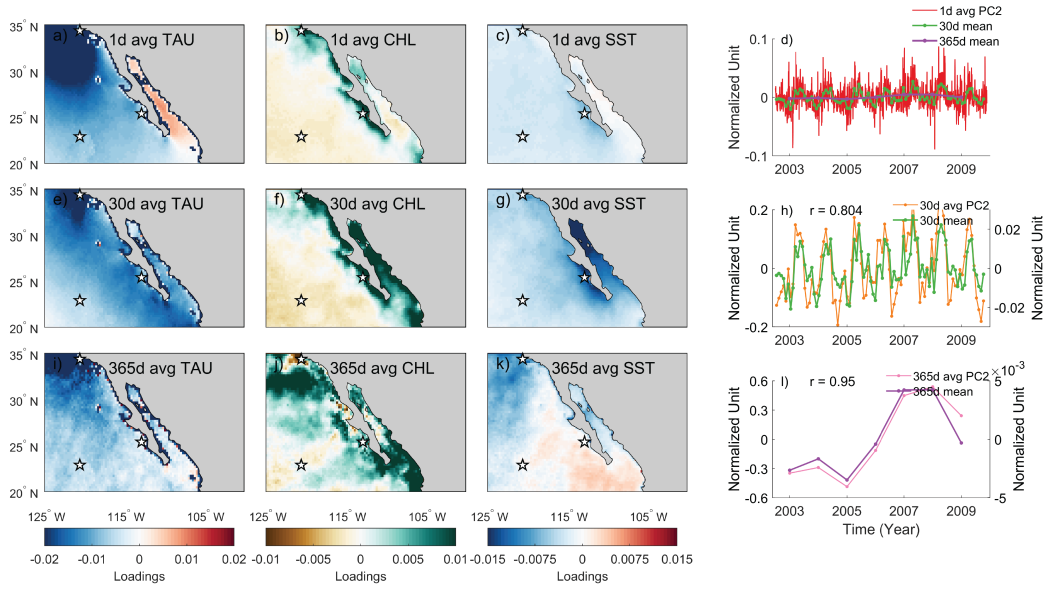

Figure 2.6: EEOF2 spatial and temporal patterns of TAU, CHL, and SST using a–d) daily; e–h) 30 day averaged; i–l) 365 day averaged data. Stars in spatial pattern plots indicate locations where the differences were taken to compute crossshore and meridional gradients. 30 day mean (green) and 365 day mean (purple) timeseries were derived from averaging 1d avg PC2. Correlation coefficient indicates how well does time mean of 1d avg PC track PC of time averaged data.

ture Ekman upwelling variations in this region. Furthermore, these results highlight the importance of considering what timescales are reflected in the proxy record. On the assumption that some proxies are seasonally biased (e.g., "integrated production temperature" applied to the interpretation of alkenone paleotemperature estimates by Conte et al., 1992) we add a sine-weighting function (maximum in March and minimum in September) to the 30 d averaged dataset and reanalyze the resulting EEOF pattern.We find that the pattern is similar to the one without weighting (not shown). This suggests that the seasonal cycle does not dominate the resulting EEOF patterns over this spatial and temporal domain.

4.3 Are there benefits to analyzing records from multiple sites?

Since an upwelling pattern is only observed in the analysis using daily and 30 d averaged data, we focus on assessing the potential benefits of analyzing records from multiple sites on 30 d ($\sim$ monthly) data. We acknowledge that most sedimentary records integrate over an annual cycle. However, since we cannot recover the upwelling pattern in the first three modes when using 365 d averaged data, we consider an idealized situation instead in which proxy records integrate climate information on an approximately monthly timescale.

With only a single proxy-type measurement from one site, one can only assume it reflects the dominant large-scale circulation pattern of that area (represented by EEOF1–PC1 in this case). However, comparisons between PC1 and reconstructed PC1s based on a variable from one site show that the ability to recover the dominant pattern depends on the location and variable (Fig. 2.8). This varying relationship suggests that small-scale processes can drive variability at a proxy site, which can lead to behavior that is different from large-scale circulation. Therefore, caution is needed when trying to extrapolate variability in a single proxy record from one paleoclimate site to infer large-scale circulation changes. Nevertheless, in the absence of additional

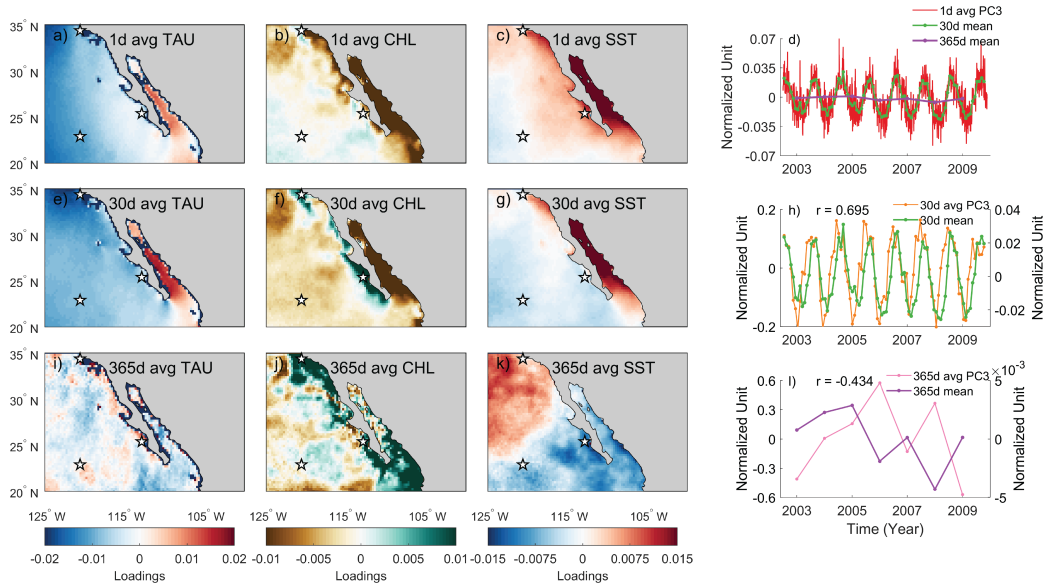

Figure 2.7: EEOF3 spatial and temporal patterns of TAU, CHL, and SST using a–d) daily; e–h) 30 day averaged; i–l) 365 day averaged data. Stars in spatial pattern plots indicate locations where the differences were taken to compute crossshore and meridional gradients. 30 day mean (green) and 365 day mean (purple) timeseries were derived from averaging 1d avg PC3. Correlation coefficient indicates how well does time mean of 1d avg PC track PC of time averaged data.

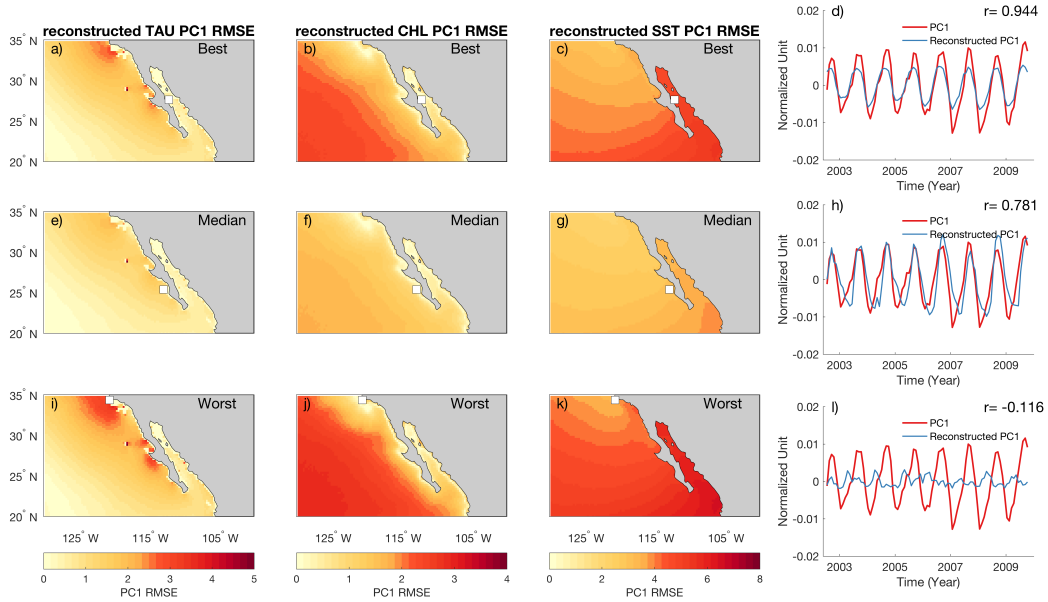

Figure 2.8: (a–d) Best, (e–h) Median, and (i–l) Worst PC1 reconstruction spatial RMSE and timeseries using only 1 variable from 1 site. White marker indicates the site used in that reconstruction, with circle indicating SST and square indicating CHL. The mean of both timeseries were removed for visualization purpose.

sites available to recover sediment cores, we find that measuring multiple variables often leads to better constraint of large-scale climate variability (Fig. 2.9a).

Multiple drilling expeditions in the SCCS have recovered cores from different locations, which allows us to determine whether there are benefits to analyzing records from multiple sites.With multiple sites available, we can potentially reconstruct different patterns of large-scale variability (Figs. 2.5–2.7). In the case of 30 d averaged data, a multiple-site-based reconstruction allows us to reconstruct spatiotemporal patterns that are associated with Ekman-driven upwelling (Fig. 2.9). There is also a tendency of increasing reconstruction skill when more sites and proxies are used. Therefore, there is potential to recover multiple covarying patterns that are driven by different dynamics.

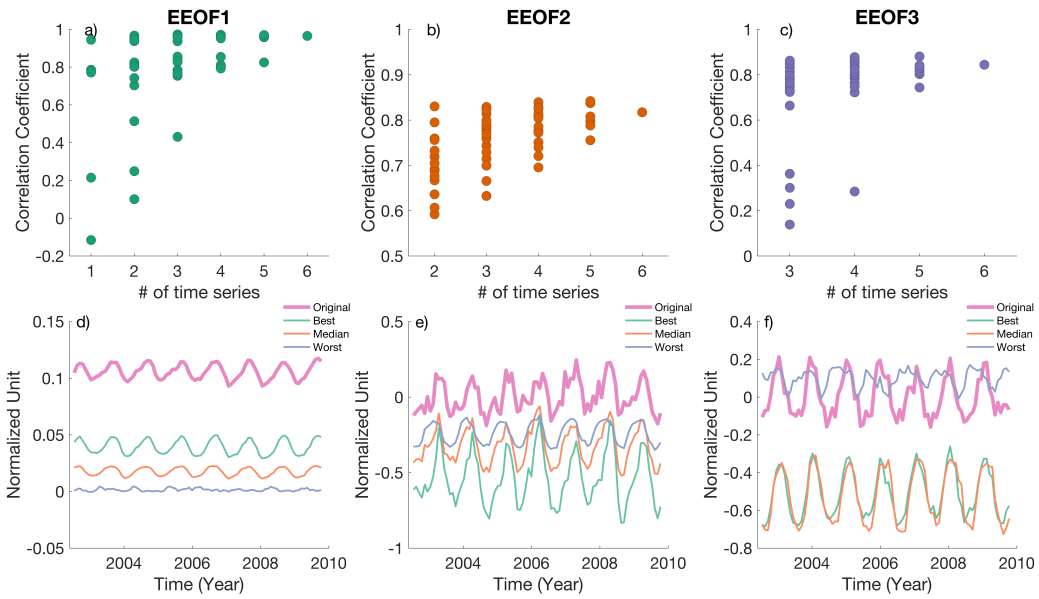

Figure 2.9: Correlation coefficient between reconstructed and actual a) PC1, b) PC2, c) PC3 temporal pattern using 30 day averaged data with varying numbers of time series from the target sites. Also shown are best, median, worst and original temporal pattern reconstructions (ranked by correlation with original PC) of d) PC1, e) PC2, and f) PC3.

Adding reconstruction sites and variables analyzed can also potentially improve the ability to reconstruct spatiotemporal variability in the spatial domain analyzed.

This has been shown in other pseudo-proxy experiments that concern hemispheric reconstruction (e.g., Wang et al., 2014). Although our reconstruction technique is rather simple compared to commonly used climate field reconstruction techniques in pseudo-proxy experiments and other reconstructions (e.g., Wang et al., 2014), we show that similar results emerge, wherein an increasing number of sites and/or variables can help better reconstruct full field data that contain multiple variables (Fig. 2.10; Eq. 2.3). Therefore, these results together argue for the notion of using multiple sites and proxies for paleoclimate reconstruction.

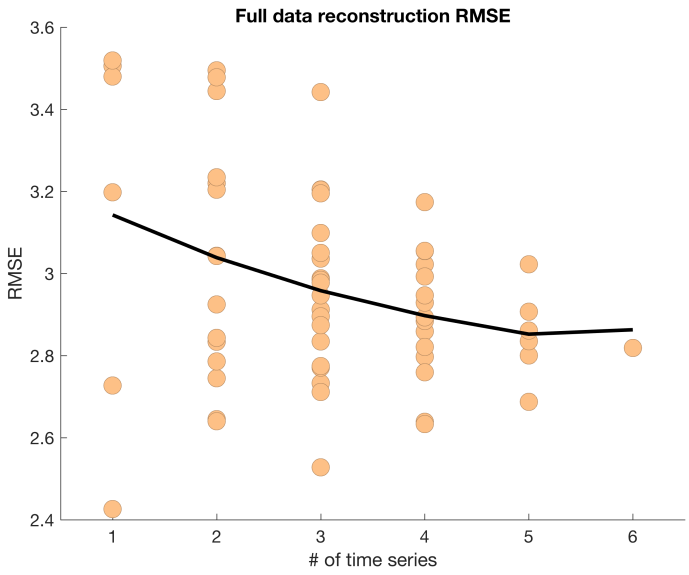

Figure 2.10: Full data reconstruction RMSE using different numbers of timeseries as input for reconstruction.

4.4 Implications

While this study only focuses on the case of Ekman upwelling in the SCCS, it has general implications for paleoclimate studies. First, our analysis provides empirical evidence that it is important to consider the spatial representativeness of a proxy record. This calls for careful interpretation in each proxy record developed in order to avoid over simplification and over-interpretation of the climate system. Second, we demonstrate that depending on time averaging and the timescale of interest,

mechanisms such as Ekman upwelling might or might not be an important process that drives variability in proxy records. Therefore, it is also important to understand whether the proxies applied and the record are able to resolve the timescales at which the mechanism of interest dominates (e.g., El Niño–Southern Oscillation on interannual timescale). Third, we show that analyzing different proxy records from multiple sites can help us reconstruct multiple covarying patterns and improve climate field reconstruction. Last, we propose and demonstrate a multivariate method that allows us to test the assumptions regarding spatial and temporal sampling. We expect that this method can also be easily applied to other regions to provide a 1st-order constraint on how the proxy records can be interpreted.

4.5 Limitations

There are multiple limitations that have to be taken into account when applying the results from this analysis to a paleoclimate context. Firstly, our analysis is only based on 7 years of instrumental data. It is possible that the patterns established in this study are only applicable to the years analyzed due to potential nonstationary covarying relationships between the variables analyzed. Furthermore, the short length of the instrumental records does not allow us to assess the impacts of basin-scale low-frequency climate variability.

Secondly, our analysis assumes that signals from proxy records can capture surface ocean conditions perfectly and are free from other noise. This assumption is certainly violated, with multiple studies pointing to different sources of uncertainties in sedimentary records (e.g., Dolman & Laepple, 2018). Nevertheless, our analysis provides an idealized scenario to understand assumptions associated with spatial and temporal sampling and marks an important step toward better interpreting paleoclimate records.

Thirdly, the utilization of a chlorophyll satellite product assumes that chlorophyll

is related to primary productivity, which in turn is related to export productivity, a variable that is believed to be captured by proxies. While the first assumption that chlorophyll and primary productivity are related is probably accurate on 1st order (Henson et al., 2010), the relationship between primary productivity and export productivity is less trivial. Previous studies have identified a general relationship between export productivity, marine productivity, and sea surface temperature (Dunne et al., 2005; Laws et al., 2011). Sediment trap studies done in the Santa Barbara and Guaymas basins generally show a similar pattern (Thunell, 1998; Thunell et al., 1994), with export production correlated positively with primary productivity (organic carbon and opal in the Santa Barbara Basin; opal in the Guaymas Basin). However, a discontinuous sediment trap study done in the San Lazaro Basin suggested productivity driven by remineralization during El Niño, which resulted low export productivity despite high productivity (Silverberg et al., 2004). This highlights the potential complexity in plankton communities along a continental margin, which can experience both eutrophic and oligotrophic conditions. In fact, (Dunne et al., 2005) examined the proposed parameterization by synthesizing different sediment trap sites and showed that the positive relationship between primary productivity and export productivity works in a global sense but not small scales. Furthermore, many studies have highlighted other factors to consider when considering export production, for instance particle size, ballasting effects, remineralization, eddy subduction, and mixed layer pumping (Boyd et al., 2019; Lam & Marchal, 2015, and references therein). Hence, more dedicated experiments are needed in order to establish a quantitative relationship between the chlorophyll data used here and paleo-productivity records.

Fourthly, we assume that each statistical mode retrieved in this study is tied to a dynamical mechanism. However, previous studies have cautioned against such interpretations (e.g., Hannachi et al., 2007). Nevertheless, our study does not aim

to diagnose Ekman upwelling processes but simply aims to determine whether it is possible to recover Ekman upwelling-related patterns in proxy records. Hence, we argue that the distinction between a dynamical mode and statistical mode does not undermine our results.

Lastly, our multiple-record analysis assumes that proxy records contain perfect age models. In most cases, this assumption is also invalid. It is inevitable that each sedimentary record contains absolute age uncertainties. Therefore, using marine sedimentary records for a multi-site proxy reconstruction with a high temporal resolution is more challenging and might yield a different conclusion than ours.

5 Summary and Conclusion

This study aimed to evaluate assumptions commonly made in paleoclimate studies: (1) a certain mechanism operates in the past on all timescales of interest, and (2) large-scale phenomena can explain the most variance in a small location (i.e., a paleoclimate site). We tested these assumptions by focusing on the Southern California Current System and used observational records to understand whether it is possible to reconstruct Ekman upwelling using multiple sedimentary records. We introduced an extended empirical orthogonal function framework and applied it to satellite records to make inferences about paleoclimate records. Our results indicate that the dominant TAU, CHL, and SST covarying pattern does not resemble Ekman upwelling. In addition, the relationship between these variables appears to depend on timescales and spatial scales. A positive result is that our analysis suggests that a few sediment sites can monitor large-scale fields associated with the Southern California Current. Lastly, we highlight the potential benefits of using multiple proxy records to understand different large-scale covarying patterns. Our study suggests that instrumental records are helpful for testing assumptions in paleoclimatology and the associated spatial- and temporal-scale extrapolations made based on paleoclimate reconstruc-

tions. Testing these assumptions might help us better interpret proxy records and understand past climate changes.

Acknowledgements

The Geostationary Environmental Satellites SST, QuikSCAT surface wind data were obtained from the NASA EOSDIS Physical Oceanography Distributed Active Archive Center (PO.DAAC) at the Jet Propulsion Laboratory, Pasadena, CA. MODIS chlorophyll-a data were obtained from NASA Goddard Space Flight Center, Ocean Ecology Laboratory, Ocean Biology Processing Group. We thank R. Vachula, N. Richter, S. Garelick for helpful comments, suggestions and discussions. AHC was supported by the Brown University Presidential Fellowship. BFK was supported by ONR N00014-17-1-2393.

References

Abella-Gutiérrez, J., & Herguera, J. C. (2016). Sensitivity of carbon paleoproductivity in the Southern California Current System on different time scales for the last 2ka. *Paleoceanography*, *31*(7), 953–970. https://doi.org/https://doi.org/10.1002/2015PA002872

Abram, N. J., Mcgregor, H. V., Tierney, J. E., Evans, M. N., Mckay, N. P., & Kaufman, D. S. (2016). Early onset of industrial-era warming across the oceans and continents. *Nature*, *536*(7617), 411–418. https://doi.org/10.1038/nature19082

Bakun, A., Black, B. A., Bograd, S. J., Garcia-Reyes, M., Miller, A. J., Rykaczewski, R. R., & Sydeman, W. J. (2015). Anticipated Effects of Climate Change on Coastal Upwelling Ecosystems. *Curr. Clim. Change. Rep.*, *1*, 85–93. https://doi.org/10.1007/s40641-015-0008-4

Boyd, P. W., Claustre, H., Levy, M., Siegel, D. A., & Weber, T. (2019). Multi-faceted particle pumps drive carbon sequestration in the ocean. *Nature*, *568*(7752), 327.

Bretherton, C., Smith, C., & Wallace, J. (1992). An Intercomparison of Methods for Finding Coupled Patterns in Climate Data. *J. Climate*, *5*, 541–560.

Campbell, J. W. (1995). The lognormal distribution as a model for bio-optical variability in the sea. *J Geophys Res Oceans*, *100*(C7), 13237–13254.

Capet, X., McWilliams, J. C., Molemaker, M. J., & Shchepetkin, A. (2008). Mesoscale to submesoscale transition in the California Current System. Part I: Flow structure, eddy flux, and observational tests. *Journal of physical oceanography*, *38*(1), 29–43.

Carton, J. A., Chepurin, G. A., & Chen, L. (2018). SODA3: A New Ocean Climate Reanalysis. *Journal of Climate*, *31*(17), 6967–6983. https://doi.org/10.1175/JCLI-D-18-0149.1

Checkley Jr, D. M., & Barth, J. A. (2009). Patterns and processes in the California Current System. *Progress in Oceanography*, *83*(1–4), 49–64. https://doi.org/10.1016/j.pocean.2009.07.028

Chelton, D., & Freilich, M. (2005). Scatterometer-Based Assessment of 10-m Wind Analyses from the Operational ECMWF and NCEP Numerical Weather Prediction Models. *Mon. Wea. Rev.*, *133*, 409–429. https://doi.org/10.1175/MWR-2861.1

Chen, J.-M., & Harr, P. A. (1993). Interpretation of Extended Empirical Orthogonal Function (EEOF) Analysis. *Mon. Wea. Rev.*, *121*, 2631–2636.

Chhak, K., & Di Lorenzo, E. (2007). Decadal variations in the California Current upwelling cells. *Geophys. Res. Lett.*, *34*, L14604. https://doi.org/10.1029/2007GL030203

Conte, M. H., Eglinton, G., & Madureira, L. A. (1992). Long-chain alkenones and alkyl alkenoates as palaeotemperature indicators: Their production, flux and early sedimentary diagenesis in the eastern north atlantic. *Organic Geochemistry*, *19*(1), 287–298. https://doi.org/https://doi.org/10.1016/0146-6380(92)90044-X

Dall'Olmo, G., Gitelson, A. A., Rundquist, D. C., Leavitt, B., Barrow, T., & Holz, J. C. (2005). Assessing the potential of SeaWiFS and MODIS for estimating chlorophyll concentration in turbid productive waters using red and near-infrared bands. *Remote Sensing of Environment*, *96*(2), 176–187.

Di Lorenzo, E. (2015). Climate science: The future of coastal ocean upwelling. *Nature*, *518*(7539), 310.

Di Lorenzo, E., Miller, A. J., Schneider, N., & McWilliams, J. C. (2005). The Warming of the California Current System: Dynamics and Ecosystem Implications. *Journal of Physical Oceanography*, *35*(3), 336–362. https://doi.org/10.1175/JPO-2690.1

Dolman, A. M., & Laepple, T. (2018). Sedproxy: a forward model for sediment-archived climate proxies. *Climate of the Past*, *14*(12), 1851–1868. https://doi.org/10.5194/cp-14-1851-2018

Dunne, J. P., Armstrong, R. A., Gnanadesikan, A., & Sarmiento, J. L. (2005). Empirical and mechanistic models for the particle export ratio. *Global Biogeochemical Cycles*, *19*(4).

Freilich, M. H., Long, D. G., & Spencer, M. W. (1994). SeaWinds: a scanning scatterometer for ADEOS-II-science overview. *Proceedings of IGARSS '94 - 1994 IEEE International Geoscience and Remote Sensing Symposium, Pasadena, CA, USA*, *2*, 960–963.

Garcia-Reyes, M., Sydeman, W. J., Schoeman, D. S., Rykaczewski, R. R., Black, B. A., Smit, A. J., & Bograd, S. J. (2015). Under Pressure: Climate Change, Upwelling, and Eastern Boundary Upwelling Ecosystems. *Front. Mar. Sci.*, *2*, 109. https://doi.org/10.3389/fmars.2015.00109

Goni, M. A., Thunell, R. C., Woodwort, M. P., & Müller-Karger, F. E. (2006). Changes in wind-driven upwelling during the last three centuries: Interocean teleconnections. *Geophys. Res. Lett.*, *33*, L15604. https://doi.org/10.1029/2006GL026415

Gruber, N., Lachkar, Z., Frenzel, H., Marchesiello, P., Münnich, M., McWilliams, J. C., Nagai, T., & Plattner, G.-K. (2011). Eddy-induced reduction of biological production in eastern boundary upwelling systems. *Nat. Geosci.*, *4*, 787–792. https://doi.org/10.1038/NGEO1273

Hannachi, A., Jolliffe, I. T., & Stephenson, D. B. (2007). Empirical orthogonal functions and related techniques in atmospheric science: A review. *Int. J. Climatol.*, *27*, 1119–1152. https://doi.org/10.1002/joc.1499

Harrison, S. P., Bartlein, P. J., Izumi, K., Li, G., Annan, J., Hargreaves, J., Braconnot, P., & Kageyama, M. (2015). Evaluation of CMIP5 palaeo-simulations to improve climate projections. *Nat. Clim. Change*, *5*, 735–743. https://doi.org/10.1038/NCLIMATE2649

Henson, S., Sarmiento, J., Dunne, J., Bopp, L., Lima, I., Doney, S., John, J., & Beaulieu, C. (2010). Detection of anthropogenic climate change in satellite records of ocean chlorophyll and productivity. *Biogeosciences*, *7*, 621–640.

Hu, C., Lee, Z., & Franz, B. (2012). Chlorophyll-a algorithms for oligotrophic oceans: A novel approach based on three-band reflectance difference. *J Geophys Res Oceans*, *117*(C01011). https://doi.org/10.1029/2011JC007395

Huybers, P., & Curry, W. (2006). Links between annual, Milankovitch and continuum temperature variability. *Nature*, *441*, 329–332. https://doi.org/10.1038/nature04745

Jacox, M. G., Hazen, E. L., & Bograd, S. J. (2016). Optimal Environmental Conditions and Anomalous Ecosystem Responses: Constraining Bottom-up Controls of Phytoplankton Biomass in the California Current System. *Sci. Rep.*, *6*, 27612. https://doi.org/10.1038/srep27612

Jacox, M., Moore, A., Edwards, C., & Fiechter, J. (2014). Spatially resolved upwelling in the California Current System and its connections to climate variability. *Geophysical Research Letters*, *41*(9), 3189–3196.

Kutzbach, J. (1967). Empirical Eigenvectors of Sea-Level Pressure, Surface Temperature and Precipitation Complexes over North America. *J. Appl. Meteor.*, *6*, 791–802.

Lam, P. J., & Marchal, O. (2015). Insights into particle cycling from thorium and particle data. *Annual review of marine science*, *7*, 159–184.

Large, W., & Pond, S. (1981). Open Ocean Momentum Flux Measurements in Moderate to Strong Winds. *J. Phys. Oceanogr.*, *11*, 324–336. https://doi.org/https://doi.org/10.1175/1520-0485(1981)011⟨0324:OOMFMI⟩2.0.CO;2

Laws, E. A., D'Sa, E., & Naik, P. (2011). Simple equations to estimate ratios of new or export production to total production from satellite-derived estimates of sea surface temperature and primary production. *Limnology and Oceanography: Methods*, *9*(12), 593–601.

Leduc, G., Schneider, R., Kim, J.-H., & Lohmann, G. (2010). Holocene and eemian sea surface temperature trends as revealed by alkenone and mg/ca paleothermometry. *Quaternary Science Reviews*, *29*(7), 989–1004. https://doi.org/https://doi.org/10.1016/j.quascirev.2010.01.004

Leduc, G., Herbert, C. T., Blanz, T., Martinez, P., & Schneider, R. (2010). Contrasting evolution of sea surface temperature in the Benguela upwelling system under natural and anthropogenic climate forcings. *Geophys. Res. Lett.*, *37*, L20705. https://doi.org/10.1029/2010GL044353

Lynn, R. J., & Simpson, J. J. (1987). The California Current system: The seasonal variability of its physical characteristics. *J. Geophys. Res.*, *92*(C12), 12947–12966. https://doi.org/10.1029/JC092iC12p12947

MARGO. (2009). Constraints on the magnitude and patterns of ocean cooling at the Last Glacial Maximum. *Nat. Geosci.*, *2*, 127–132. https://doi.org/10.1038/NGEO411

McGregor, H. V., Dima, M., Fischer, H. W., & Mulitza, S. (2007). Rapid 20th-Century Increase in Coastal Upwelling off Northwest Africa. *Science*, *315*(5812), 637–639. https://doi.org/10.1126/science.1134839

Monahan, A. H., Fyfe, J. C., Ambaum, M. H. P., Stephenson, D. B., & North, G. R. (2009). Empirical Orthogonal Functions: The Medium is the Message. *Journal of Climate*, *22*(24), 6501–6514. https://doi.org/10.1175/2009JCLI3062.1

NOAA/NESDIS. (2003a). GOES Level 3 6km Near Real Time SST 1 Hour. Ver. 1. PO.DAAC, CA, USA. https://doi.org/10.5067/GOES3-1HOUR

NOAA/NESDIS. (2003b). GOES Level 3 6km Near Real Time SST 24 Hour. Ver. 1. PO.DAAC, CA, USA. https://doi.org/10.5067/GOES3-24HOUR

O.B.G.P. (2015). MODIS Aqua level 3 global daily mapped 4 km chlorophyll a v2014.0. ver. 2014.0. po.daac, ca, usa. *Dataset accessed [2018-07-26].*

PAGES2k Consortium. (2013). Continental-scale temperature variability during the past two millennia. *Nat. Geosci.*, *6*, 339–346. https://doi.org/10.1038/NGEO1797

Pauly, D., & Christensen, V. (1995). Primary production required to sustain global fisheries. *Nature*, *374*, 255–257.

Perry, K. L. (2001). SeaWinds on QuikSCAT Level 3 Daily, Gridded Ocean Wind Vectors (JPL SeaWinds Project). *Version 1.1, JPL Document D-20335, Jet Propulsion Laboratory, Pasadena, CA*.

Ravelo, A. C., Andreasen, D. H., Lyle, M., Lyle, A. O., & Wara, M. W. (2004). Regional climate shifts caused by gradual global cooling in the Pliocene epoch. *Nature*, *429*(6989), 263.

Rykaczewski, R. R., & Dunne, J. P. (2010). Enhanced nutrient supply to the California Current Ecosystem with global warming and increased stratification in an earth system model. *Geophys. Res. Lett.*, *37*, L21606. https://doi.org/10.1029/2010GL045019

Ryther, J. H. (1969). Photosynthesis and Fish Production in the Sea. *Science*, *166*, 72–76. https://doi.org/10.1126/science.166.3901.72

SeaPAC. (2006). SeaWinds on QuikSCAT Level 3 Daily Gridded Ocean Wind Vectors (JPL Version 2). Ver. 2. PO.DAAC, CA, USA. *Dataset accessed [2018-07-27] at http://dx.doi.org/10.5067/QSXXX-L3002.*

Shakun, J. D., Clark, P. U., He, F., Marcott, S. A., Mix, A. C., Liu, Z., Otto-Bliesner, B., Schmittner, A., & Bard, E. (2012). Global warming preceded by increasing

carbon dioxide concentrations during the last deglaciation. *Nature*, *484*, 49–54. https://doi.org/10.1038/nature10915

Silverberg, N., Martínez, A., Aguíñiga, S., Carriquiry, J. D., Romero, N., Shumilin, E., & Cota, S. (2004). Contrasts in sedimentation flux below the southern california current in late 1996 and during the el niño event of 1997–1998. *Estuarine, Coastal and Shelf Science*, *59*(4), 575–587. https://doi.org/https://doi.org/10.1016/j.ecss.2003.11.003

Snyder, M. A., Sloan, L. C., Diffenbaugh, N. S., & Bell, J. L. (2003). Future climate change and upwelling in the California Current. *Geophysical Research Letters*, *30*(15).

Thunell, R. C. (1998). Particle fluxes in a coastal upwelling zone: sediment trap results from Santa Barbara Basin, California. *Deep Sea Research Part II: Topical Studies in Oceanography*, *45*(8-9), 1863–1884.

Thunell, R. C., Pride, C. J., Tappa, E., & Muller-Karger, F. E. (1994). Biogenic silica fluxes and accumulation rates in the Gulf of California. *Geology*, *22*(4), 303–306.

van Geen, A., Zheng, Y., Bernhard, J. M., Cannariato, K. G., Carriquiry, J., Dean, W. E., Eakins, B. W., Ortiz, J. D., & Pike, J. (2003). On the preservation of laminated sediments along the western margin of North America. *Paleoceanography*, *18*(4), 1098. https://doi.org/10.1029/2003PA000911

Vargas, G., Pantoja, S., Rutllant, J. A., Lange, C. B., & Ortlieb, L. (2007). Enhancement of coastal upwelling and interdecadal ENSO-like variability in the Peru-Chile Current since late 19th century. *Geophys. Res. Lett.*, *34*, L13607. https://doi.org/10.1029/2006GL028812

Wang, J., Emile-Geay, J., Guillot, D., Smerdon, J. E., & Rajaratnam, B. (2014). Evaluating climate field reconstruction techniques using improved emulations of real-world conditions. *Climate of the Past*, *10*(1), 1–19. https://doi.org/10.5194/cp-10-1-2014

Ware, D. M., & Thomson, R. E. (2005). Bottom-Up Ecosystem Trophic Dynamics Determine Fish Production in the Northeast Pacific. *Science*, *308*, 1280–1284. https://doi.org/10.1126/science.1109049

Wick, G. A., Bates, J. J., & Scott, D. J. (2002). Satellite and skin-layer effects on the accuracy of sea surface temperature measurements from the GOES satellites. *Journal of Atmospheric and Oceanic Technology*, *19*(11), 1834–1848.

Xiu, P., Chai, F., Curchitser, E. N., & Castruccio, F. S. (2018). Future changes in coastal upwelling ecosystems with global warming: The case of the California

Current System. *Sci. Rep.*, *8*, 2866. https://doi.org/10.1038/s41598-018-21247-7

Zhao, M., Eglinton, G., Read, G., & Schimmelmann, A. (2000). An alkenone ($U_{37}^{K'}$) quasi-annual sea surface temperature record (AD 1440 to 1940) using varved sediments from the Santa Barbara Basin. *Organic Geochemistry*, *31*(9), 903–917. https://doi.org/10.1016/S0146-6380(00)00034-6

Chapter 3

Middle to Late Holocene Sea Surface Temperature and Productivity Changes in the Northeast Pacific

Anson H. Cheung[1,2], Samantha Sandwick[1], Xiaojing Du[1,2], Jose Abella-Gutiérrez[3,4], Richard S. Vachula[5], Timothy D. Herbert[1,2], Baylor Fox-Kemper[1,2], Juan Carlos Herguera[3]

1. Department of Earth, Environmental, and Planetary Sciences, Brown University, Providence, RI, USA

2. Institute at Brown for Environment and Society, Brown University, Providence, RI, USA

3. Centro de Investigacion Científica y de Educación Superior de Ensenada, Baja California, Mexico

4. Now at Department of Geological Sciences, Environmental Science Institute, Jackson School of Geosciences, The University of Texas at Austin, Austin, TX, USA

5. Department of Geosciences, Auburn University, Auburn, AL, USA

Published: Paleoceanography and Paleoclimatology (2022), 37

Abstract

Variations of the sea surface temperature (SST) and primary productivity in the northeast Pacific have far-reaching implications. In addition to influencing the regional and global temperature and hydroclimate, these conditions also control marine ecosystems and their services, which subsequently impact regional economies. Yet, our understanding of the variability and controls of northeast Pacific SST and productivity on timescales exceeding observational records remains limited. Here, we use marine sediment records from seven locations, spanning 25.2°N–59.6°N, in the northeast Pacific to characterize the millennial-scale variability of SST and productivity from 9,000 to 1,000 years BP. We explore the dynamics of their spatiotemporal evolution and compare these data with transient climate model outputs to identify potential drivers. Through a heat budget analysis and optimal fingerprinting analysis, we characterize the spatial pattern of forcings. We find that SST varied spatially in the northeast Pacific, with higher latitudes exhibiting greater magnitude changes than lower latitudes, which differs from previous work suggesting regional synchronicity and coherence during the Holocene. Our analysis did not find evidence for coherent variability of primary producer community nor carbon export, highlighting the difficulty of identifying the complex interactions between environmental conditions, producers, and carbon export. Model-proxy disagreement demonstrates the need for higher resolution model frameworks, but shows nonetheless that observed variability in the proxy records can be explained by a combination of greenhouse gas and orbital forcing. We suggest that the complex SST variations and marine ecosystem responses to forced changes are important factors that can drive disagreements in model projections.

1 Introduction

Sea surface temperature (SST) and primary productivity variations in the northeast (NE) Pacific have significant impacts on global and regional climate, marine ecosystems, and the economy of nearby regions. Within the NE Pacific, average SST controls the abundance of low level stratocumulus clouds, which in turn affects the global radiative balance (Wood, 2012). SST also interacts with the atmosphere and influences the hydroclimate and temperature of the western North America (Johnstone & Dawson, 2010; Swain et al., 2016). Furthermore, SST influences the distribution of marine ecosystems, species habitat and their abundances. Such influence have important implications on regional economy (Bond et al., 2015; Cavole et al., 2016). Aside from SST, the amount of primary productivity in this region also affects the marine ecosystem and have significant consequences because of the ecosystem services they provide (Ware & Thomson, 2005). Additionally, the amount and composition of primary producers in this region influences the amount of carbon exported to the deep ocean (DeVries & Weber, 2017). All in all, these observations highlight the importance of understanding variability of SST and primary productivity in the NE Pacific.

Whereas seasonal to decadal (short term) SST and primary productivity in the NE Pacific are relatively well studied, changes on multidecadal and longer timescales that are beyond instrumental records (long term) in this region are less clear. Modern observations and modeling studies have allowed us to identify processes responsible for SST and primary productivity variations in this region and distinguish spatiotemporal patterns that correspond to these processes (e.g.., Bograd et al., 2015; Di Lorenzo et al., 2008; Jacox et al., 2015; Jacox et al., 2014; Johnstone & Mantua, 2014; Kahru et al., 2012; Pozo Buil & Di Lorenzo, 2017). However, the importance of each process on SST and primary productivity evolution have shown to be dependent on spatial

and temporal scales (Cheung et al., 2019; Kahru et al., 2012; Long et al., 2014; Moore et al., 2018; Rykaczewski & Dunne, 2010; Xie et al., 2010). Therefore, we cannot infer future changes based solely upon our understanding of short term processes (e.g., Bakun, 1990; Sydeman et al., 2014). Although long climate model simulations can circumvent this discrepancy and provide a pathway to investigate long term changes of these variables (e.g., Alexander et al., 2018; Lotze et al., 2019), the robustness of these models remain unclear due to significant model structural uncertainty (Schlunegger et al., 2020). Specifically, they are unable to resolve mesoscale, submesoscale, boundary layer mixing, other processes important for upwelling (Capet et al., 2008; Renault et al., 2016; Xiu et al., 2018). There is also disagreement among parameterization of unresolved processes (Li et al., 2019), the different plankton functional groups represented, and nutrient transport dynamics (Fu et al., 2016). Alternatively, paleoclimate records can provide insights as to how SST and primary productivity in the NE Pacific could change on timescales that are not resolved by instrumental records, even though their spatial coverage is more limited.

The Holocene is an optimal time period to understand how SST and primary productivity in NE Pacific change on long timescales. Studying past climate intervals can help provide additional insights on how these variables change in response to external forcings (Harrison et al., 2015). Analyzing transient changes during the Holocene is particularly advantageous because of the abundance in proxy records (e.g., Kaufman, McKay, Routson, Erb, Davis, et al., 2020) , relatively well constrained chronology (Reimer et al., 2020), a good understanding of the dominant external forcings that are changing (primarily greenhouse gases and orbital), and the computational ability to simulate transient changes using general circulation models (e.g., Bader et al., 2020; Z. Liu et al., 2009). These benefits allow us to quantify SST and primary productivity changes in the NE Pacific on long timescales, identify processes that could be responsible behind these changes, and determine the external forcings that caused

these changes.

Multiple empirical studies have investigated how and why Holocene SST and primary productivity in the NE Pacific have changed over millennial timescales. Syntheses of SST records in the NE Pacific generally suggested an increase in SST since ca. 7,000 years BP (Barron & Anderson, 2011; Davis et al., 2020; Kim et al., 2004). Primary productivity was also suggested to have increased at the same time (Addison et al., 2018; Barron et al., 2019; Barron et al., 2018; Barron et al., 2003). These studies suggest that the increase in SST could be related to shifts in atmospheric patterns (i.e., Pacific North American pattern; Wallace and Gutzler (1981)), whereas the primary productivity increase was driven by changes in the length of upwelling season (Diffenbaugh & Ashfaq, 2007). Ultimately, all these changes were proposed to be related to changes in orbital forcing.

Even though these studies painted a relatively consistent image of how and why SSTs in the NE Pacific change, whether these observed patterns and proposed mechanisms are accurate remain debatable. Specifically, many temperature proxy records included in previous studies either do not have reliable age constraints and temporal resolution (e.g., the record with the highest resolution and best age constraints in Kim et al., 2004 contained only 3 14C dates with an average sampling resolution of $\sim$132 years) or are qualitative (e.g., Barron & Anderson, 2011; Routson et al., 2021). In addition, the uniform increase in SST in the NE Pacific contradicts temperature changes inferred from hemispheric-scale compilations and the proposed insolation gradient change mechanism (Kaufman, McKay, Routson, Erb, Davis, et al., 2020; Routson et al., 2019). Hence, to characterize SST evolution in the NE Pacific accurately and to identify self-consistent mechanisms/drivers behind these changes, it is important to analyze reliable SST records with high temporal resolution and good chronological constraints in tandem with transient climate model simulations.

The primary productivity patterns observed, mechanisms proposed to explain

those changes, and the implications of these changes are also contentious. In particular, the primary productivity records analyzed in those studies are dependent on spatial calibration with modern observations (Lopes & Mix, 2018; Ren et al., 2014) or are subject to sediment dilution (Gardner et al., 1997) and diagenesis (Ragueneau et al., 2000). Although the proposed mechanism to explain observed primary productivity changes, upwelling season length, is supported by simulations from an atmospheric regional model (Diffenbaugh & Ashfaq, 2007), it is unclear whether changes driven by this mechanism are detectable in proxy records. More importantly, recent modeling studies have suggested changes in higher trophic level marine species could be larger than primary producers in some regions due to alterations of food web dynamics (Lotze et al., 2019; Stock et al., 2014; Stock et al., 2017), and that carbon export efficiency of a specific region depends on the type of primary producer present (Fu et al., 2016; Jin et al., 2006). These results imply that impacts of primary productivity on marine ecosystems (via energy transfer) and the carbon cycle (via export production) may be better understood by characterizing changes in primary producer composition and each primary producer's contribution to carbon export.

In this study, we aim to understand the millennial-scale evolution of SST and productivity in the NE Pacific during the Holocene, as well as the process and the external forcing behind the changes observed in the proxy records. Specifically, we address the following questions: (a) Do we observe similar temporal evolution of SST, primary producer composition, and each primary producer's contribution to carbon export at these locations? (b) Do we expect similar dynamics to drive SST at these locations? and (c) Can we attribute changes observed in proxy records to specific forcings?

To address these questions, we present three new centennial-scale resolved alkenone-based SST and productivity records from Saanich Inlet at Vancouver Island, British Columbia (ODP1034), Santa Barbara Basin in Southern California Bight (MV0508-

32JC), and Soledad Basin (Baja California) (a.k.a. San Lazaro Basin; MD02-2505/MD02-2506C 2) in the NE Pacific. We complement these records with a number of published SST and productivity records. These proxies together cover the majority of the NE Pacific, where coarse resolution model simulations suggest a nearly uniform decrease in SST during the Holocene (Z. Liu, Zhu, et al., 2014; Lohmann et al., 2013). We also supplement proxy records with outputs from transient climate model simulations to investigate physical processes and external forcing fingerprints. Furthermore, we revisit published productivity records to understand changes in the primary producer community (siliceous vs. alkenone synthesizing haptophytes) and their contributions toward carbon export (represented by total organic carbon).

2 Data and Methods

2.1 Proxy Records

We analyzed geochemical measurements in sediment cores collected from 7 different locations to infer changes in SST and phytoplankton productivity (Figure 1, Table 1). For convenience, we will refer PCM00-78, MD02-2505, MD02-2506C 2, and GC41/PC14 as Soledad Basin, and MV0508-32JC, ODP 893 as Santa Barbara Basin, as these cores were collected from these respective basins. Most measurements have been presented in previous studies (Addison et al., 2018; Addison et al., 2012; Arellano-Torres et al., 2019; Barron et al., 2003; A. S. Chang et al., 2008; Dean et al., 2006; Gardner & Dartnell, 1995; O'Mara et al., 2019; Praetorius et al., 2015; Stein & Rack, 1995). Readers are referred to those studies for detailed methodology. Here, we supplemented these published records with new alkenone measurements from three locations.

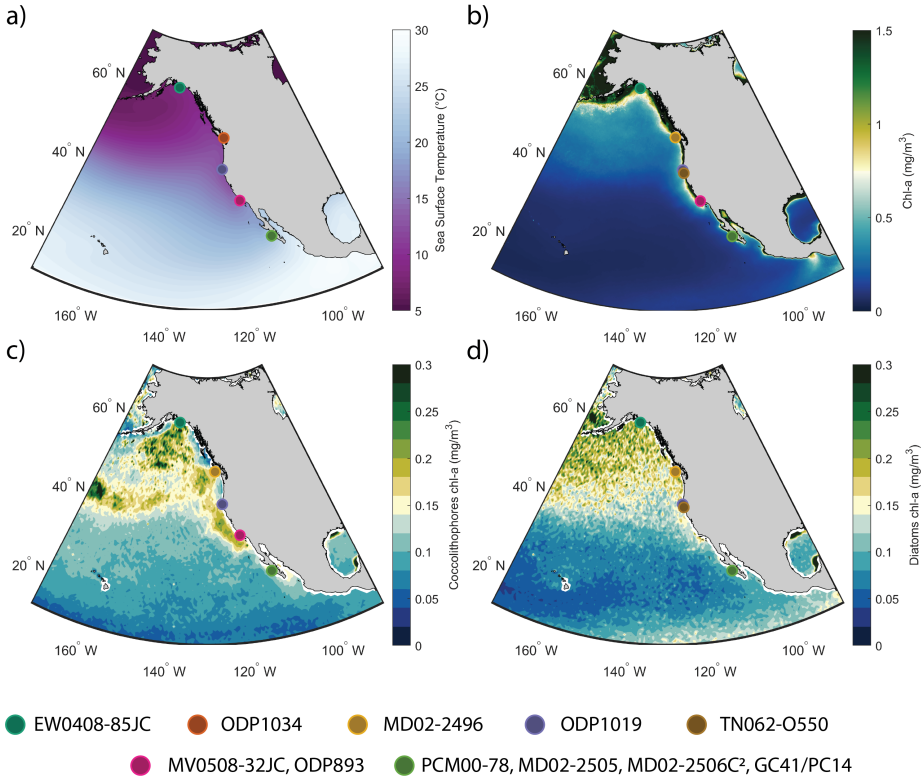

Figure 3.1: Observations and proxy locations. Observed averaged mean annual a) sea surface temperature in 1981-2020 (Reynolds et al., 2002), b) chlorophyll-a in 2003-2020 (O.B.G.P., 2015), c) coccolithophores in 2003-2020 (Bracher et al., 2017; Losa et al., 2017), and d) diatoms in 2003-2020 (Bracher et al., 2017; Losa et al., 2017). Circles represent locations of a) SST, b) C_{org}, c) $C_{37total}$, and d) Si proxy records (indicated by core names) analyzed in this study.

2.1.1 SST and Productivity Proxies

SST was inferred using the alkenone paleothermometer method based on the Müller et al. (1998) calibration. Alkenones are long chain ketones that are produced by *E. huxleyi* and *G. oceanica* in the open ocean. The unsaturation ratio of C_{37} alkenones ($U^{k'}_{37}$) has been shown to correlate with temperature and has been applied extensively to reconstruct past SSTs (see Herbert, 2014, and references therein). Based on calibration studies, variations of $U^{k'}_{37}$ downcore are often interpreted to best reflect mean annual SST change (e.g., Conte et al., 2006; Müller et al., 1998). However, some studies have argued that $U^{k'}_{37}$ preferentially records warm season temperature, especially in high latitudes (e.g., Max et al., 2020; Prahl et al., 2010; Tierney & Tingley, 2018a) or when $U^{k'}_{37}$ disagrees with other paleothermometers (Schneider et al., 2010; Timmermann et al., 2014) and climate model simulation (e.g. Z. Liu, Zhu, et al., 2014; Lohmann et al., 2013). While there is merit to consider seasonal bias in regions where coccolithophores are only produced during a limited period (e.g., Seki et al., 2007; Tsutsui et al., 2016), a synthesis of global sediment trap records does not show any systemic seasonality with flux weighted alkenone-based SST and observed mean annual SST in good agreement (Rosell-Melé & Prahl, 2013). In addition, a transect of core top samples from the California margin suggests $U^{k'}_{37}$ is well correlated to mean annual SST and does not show the influence of the seasonal progression of upwelling (Herbert et al., 1998). Hence, we interpreted variations of $U^{k'}_{37}$ in all records (including EW0408-85JC, where Praetorius et al. (2015) interpreted their record as summer SST changes) analyzed in this paper to reflect mean annual SST changes.

To infer changes in productivity, we focused on C_{37} alkenone concentration ($C_{37\text{total}}$), biogenic silica (Si), and total organic carbon (C_{org}) measurements and calculated the ratios between these variables to infer changes in productivity. All these proxies have been shown to be related to primary productivity (Ragueneau et al., 2000; Raja &

Rosell-Melé, 2021; Schoepfer et al., 2015) and have been applied to reconstruct past primary productivity (e.g., Addison et al., 2018; Addison et al., 2012; Barron et al., 2003; Bolton et al., 2010; Gardner et al., 1997; Schubert et al., 1998). However, these proxies can also be influenced by diagenesis (Anderson et al., 2019; Ragueneau et al., 2000) and sediment dilution (e.g., Gardner et al., 1997). Even though diagenesis is not a primary concern here because of relatively high sedimentation rate and thus low oxygen exposure, concentrations of these biological measurements can be biased by changes in inputs of non-biogenic sediments. In this study, we instead focused on $C_{37total}/C_{org}$, Si/C_{org}, and $Si/C_{37total}$ ratios, where we do not need to consider the effects of changes in sedimentation rate, and thus can avoid the effects of sediment dilution. More importantly, we can understand how primary producers are changing, specifically changes in contributions of alkenone synthesizing haptophytes to total organic carbon ($C_{37total}/C_{org}$), siliceous primary producers to total organic carbon (Si/C_{org}), and the relative abundance of siliceous primary producers and alkenone synthesizing haptophytes ($Si/C_{37total}$). These metrics, albeit different from primary productivity, are critical because the amount of carbon exported from the ocean surface depends on the type of primary producer (e.g., Fu et al., 2016; Jin et al., 2006), and each type of primary producer may respond differently to environmental changes (e.g., Xiu et al., 2018). We further compared $Si/C_{37total}$ with satellite estimates of diatoms and coccolithophores (Bracher et al., 2017; Losa et al., 2017) to determine if proxy records resemble patterns in observations qualitatively.

2.1.2 Chronology

The chronology of EW0408-85JC, MD02-2496, ODP1019, TN062-O550, GC41/PC14, PCM00-78C/PCM00-78K was based on 14C dates. Details of 14C ages used in these published records can be found in (Barron et al., 2018; Barron et al., 2003; Cosma et al., 2008; Davies-Walczak et al., 2014; Marchitto et al., 2010; O'Mara et al., 2019).

Table 3.1: Information of sediment cores analyzed in this study. Check mark indicates the proxy is included in this study

Site Name	Lat (°)	Lon (°)	avg. sed. rate (mm/yr)	avg. SST resolution (yr/sample)	no. of 14C dates over 10 kyr BP	$U^{k'}_{37}$	$C_{37total}$	C_{org}	Si	References
EW0408-85JC	59.6	-144.2	0.62	166	15	✓	✓	✓	✓	Addison et al. (2012), Praetorius et al. (2015)
MD02-2496	49.0	-127.0	1.19	—	6	—	—	✓	✓	A. S. Chang et al. (2008)
ODP1034	48.6	-123.5	9.11	76	42	✓	—	—	—	This study
ODP1019	41.6	-124.9	0.52	134	7	✓	✓	✓	✓	Barron et al. (2003)
TN062-O550	40.9	-124.6	0.99	—	10	—	—	✓	✓	Addison et al. (2018)
MV0508-32JC	34.3	-120.0	1.00	57	—	✓	✓	—	—	This study
ODP893	34.3	-120.0	0.94	—	—	—	—	✓	—	Gardner and Dartnell (1995), Stein and Rack (1995)
MD02-2505/MD02-2506C[2]	25.2	-112.7	3.16	45	4	✓	✓	—	—	This study
GC41/PC14	25.2	-112.7	1.09	—	18	—	—	✓	✓	Dean et al. (2006), Arellano-Torres et al. (2019)
PCM00-78C/PCM00-78K	25.2	-112.7	1.12	1.80	8	✓	✓	—	—	O'Mara et al. (2019)

We re-calibrated all these 14C ages using the latest radiocarbon age calibration curves (Table S3.2 in Supplementary Information; Heaton et al. (2020) and Reimer et al. (2020) and constructed the age-depth model using BACON (Blaauw & Christen, 2011). The chronology for ODP 893 used in this study is generated by stratigraphic correlation with an adjacent core MV0811-14JC in Santa Barbara Basin (Du et al., 2018). The chronology for MV0811-14JC is based on high-resolution 14C dates and variable reservoir age, so the latest radiocarbon age calibration curve would not alter it significantly.

The chronologies of sediment cores analyzed in this study (ODP1034, MV0508-32JC, MD02-2505 and MD02-2506C 2) were based on a combination of 14C dates and stratigraphic correlation. For ODP1034, we first spliced cores from different holes into a composite depth following Bornhold et al. (1998). Then, we used 14C dates provided in Bornhold et al. (1998) and Blais-Stevens et al. (2001) to construct

the age-depth model using BACON. Massive layers were treated as instantaneous events and were removed in BACON (Blaauw & Christen, 2011). For MV0508-32JC, we identified gray layers using core images and used these layers as tie points to correlate with the stratigraphy presented in Du et al. (2018). For MD02-2506C 2, we correlated the core with PCM00-78K using Ca X-ray fluorescence measurements. We then extrapolated the PCM00-78 age model to estimate ages in MD02-2506C 2. For MD02-2505, we relied on 14C measurements from Rodríguez-Sanz et al. (2013), which were only available for the early Holocene portion, and extrapolated the age-depth relationship toward the core-top using BACON (Blaauw & Christen, 2011) .

The number of radiocarbon dates, sedimentation rate, and sampling resolution of these cores provide a good basis to analyze millennial scale variability (Table 3.1). In a Bayesian age-depth model framework, the number of radiocarbon dates included strongly influences the uncertainty in the age-depth model (Blaauw et al., 2018). Even though the density of radiocarbon dates in some sediment cores used in this study remains low (e.g., 4 in MD02-2505/MD02-2506C 2), which results in large uncertainty (max. 95% confidence interval range = 2,157 years), BACON tends to overestimate the age uncertainty (Trachsel & Telford, 2017) . Nevertheless, the number of radiocarbon dates available in each core and the Bayesian age-depth model approach represent an improvement in chronological constraint compared to previous synthesis studies (e.g., Kim et al., 2004; Leduc, Schneider, et al., 2010). The sampling resolution of these cores (∼200 years) should also minimize millennial-scale aliasing, so our results should provide an accurate representation of how SST has changed in the NE Pacific on millennial timescales.

2.1.3 Laboratory Method

Sediments were freeze dried and lipids from ∼0.1–1.5 g of sediments were extracted using Dionex 200 or 350 Accelerated Solvent Extractor with 100% Methylene Chlo-

ride (DCM). Then, total lipid extracts of sediments from ODP1034 and MV0508-32JC were separated by silica gel column chromatography into non-polar, ketone, and polar fractions using Hexane, DCM, and Methanol as eluents, respectively. The ketone fraction of ODP1034 was further separated by silver nitrate column chromatography using DCM and ethyl acetate as eluents separately. Afterward, ketone fractions from MV0508-32JC and fractions obtained using ethyl acetate from ODP1034 were dried and reconstituted with toulene and n-hexatriacontane (C36) and n-heptatriacontane (C37) alkane standards. These samples were analyzed on an Agilent 6890 Gas Chromatograph coupled with a flame ionization detector (GC-FID) and a poly (trifluoropropylmethylsiloxane) stationary phase column (VF200-ms; Longo et al., 2013). We also analyzed an internal standard to determine reproducibility of our results. We defined analytical uncertainty as 1 standard deviation of replicate internal standards measurements, and found that analytical uncertainty for $U_{37}^{K'}$ was $\sim$0.002 units, whereas the relative standard deviation for C37 concentration to be $\sim$5%.

2.1.4 Data Analysis

We calculated the $U_{37}^{K'}$ index of each sample and inferred the temperature using the calibration in Müller et al. (1998). We inferred the C37 alkenone concentration (C37:3 + C37:2) by normalizing the peak areas of C37:3 and C37:2 alkenone peaks against the C36 and C37 spikes that were co-analyzed in each sample.

To facilitate proxy-model comparison and to account for analytical and chronological uncertainties, we computed an ensemble of 200 years binned composites for each proxy record from 9,000 to 1,000 years before present (yrs BP) using a Monte Carlo approach. The 200 years window was selected to minimize the extrapolation needed to estimate SST changes ($U_{37}^{K'}$ temporal resolution: <200 years; Table 1). We focused on changes between 9,000 and 1,000 years BP because some proxy records do not have measurements for the last millennium and/or prior to ca. 9,000 years

BP. To create a 200 years composite of a proxy record, we first estimated the proxy value, determined from a normal distribution (with mean = measured value, standard deviation = analytical uncertainty). Second, we selected an age-depth relationship from the posterior distribution derived from BACON. Third, we averaged the values within each 200 years bin. This was repeated 1,000 times to obtain an ensemble. The analytical uncertainties of published records were obtained from the original study (Table 1). In cases where the analytical uncertainty was not reported, we used the most conservative estimate of uncertainty reported in other records.

We compared the five SST records that we focused on in this study with Holocene SST latitudinal bands computed using SST records that were synthesized in Kaufman, McKay, Routson, Erb, Davis, et al. (2020) (Temp12K) to determine if these five records follow large scale changes. These synthesized records include inferred SSTs from δ^{18}O, alkenone, and Mg/Ca (Andrews et al., 1999; Antonarakou et al., 2015; Arz et al., 2003; Bard et al., 2000; Barron et al., 2003; Benway et al., 2006; Bolliet et al., 2011; Cacho et al., 2001; Cacho et al., 1999; Came et al., 2007; Castañeda et al., 2010; Castañeda et al., 2004; F. Chang et al., 2015; Doose-Rolinski et al., 2001; Elmore et al., 2015; Emeis & Dawson, 2003; Emeis et al., 2003; Eynaud et al., 2009; Fan et al., 2018; Farmer et al., 2008; Flower et al., 2004; Fraser et al., 2014; Harada et al., 2006; Herbert & Schuffert, 2000; Hill et al., 2006; Hillaire-Marcel et al., 1994; Huguet et al., 2006; Ijiri et al., 2005; Isono et al., 2009; Keigwin & Jones, 1995; Keigwin et al., 2005; Kennett et al., 2007; Kienast & McKay, 2001; Kim et al., 2007; Kim et al., 2004; Kristjánsdóttir et al., 2017; Kubota et al., 2010; Lea et al., 2003; Marchitto et al., 2010; Martrat et al., 2007; Martrat et al., 2003; Martrat et al., 2014; McClymont et al., 2012; Minoshima et al., 2007; Mohtadi et al., 2014; Moossen et al., 2015; Overpeck et al., 1996; Pelejero et al., 1999; Praetorius et al., 2015; Riethdorf et al., 2013; Rigual-Hernández et al., 2017; Rodrigo-Gámiz et al., 2014; Rodrigues et al., 2010; Rosenthal et al., 2003; Rühlemann et al., 1999; Sachs, 2007; Saraswat et al.,

2013; Schmidt, Chang, et al., 2012; Schmidt & Lynch-Stieglitz, 2011; Schmidt et al., 2004; Schmidt, Weinlein, et al., 2012; Schwab et al., 2012; Sejrup et al., 2011; Shintani et al., 2011; Staubwasser et al., 2003; Steinke et al., 2008; Stott et al., 2007; Sun et al., 2005; Thornalley et al., 2010; Tierney et al., 2016; Tiwari et al., 2015; Weldeab et al., 2007; Weldeab et al., 2005; Werner et al., 2013; Yamamoto et al., 2013; Zhao et al., 1995; Ziegler et al., 2008). We followed the approach in Routson et al. (2019) and calculated the bootstrapped zonal average SST over four latitudinal bands: 60°N - 80°N, 40°N - 60°N, 20°N - 40°N, and 0°N - 20°N. Additionally, we calculated the Pacific and Atlantic only zonal average SST to determine if the temporal patterns are synchronous between the two basins.

2.2 Transient Climate Model Simulations

We analyzed 9,000–1,000 years BP interval of outputs from the Transient Climate Evolution of the last 21,000 years (TraCE21ka; Z. Liu et al. (2009)) experiments to understand potential drivers of SST evolution shown in proxy records. TraCE21ka simulations were run using the Community Climate System Model version 3 (W. D. Collins et al., 2006). In the fully coupled experiment, greenhouse gases, orbital parameters, ice sheets, and meltwater were set as boundary forcings and varied from last glacial maximum (LGM) to present. In single forcing experiments, only the target forcing was allowed to evolve while the remaining forcings were set constant at LGM conditions. Even though CCSM3 is known to have an average $\sim$ 1.5°C SST bias in ocean eastern boundaries (Large & Danabasoglu, 2006), previous studies focusing on the Pacific have found consistency between proxies from the tropical Pacific and TraCE21ka in recording the evolution of El Niño Southern Oscillation variability (Z. Liu, Lu, et al., 2014) and also have used TraCE21ka to investigate the impacts of Pacific Meridional Overturning Circulation on intertropical convergence zone shift during last deglaciation (W. Liu & Hu, 2015).

We carried out a heat budget analysis to determine the drivers of SST variation and an optimal fingerprinting analysis to understand spatial fingerprints of each forcing on SST. All analyses were done using decadally averaged annual mean data since outputs with higher temporal resolution were not available. Further, since proxy records were unevenly sampled over time, unless otherwise specified, we averaged and/or integrated model results over 200 years to yield more direct comparison with proxy records. Additionally, we focused on model simulation results between 9,000 and 1,000 years BP, the same time window analyzed in proxy records.

2.2.1 Heat Budget Analysis

Assuming a well mixed surface ocean, SST variations can be understood through a mixed layer heat budget. This budget can be written as:

$$\underbrace{\frac{\partial T}{\partial t}}_{\text{temperature tendency}} = \underbrace{\frac{Q_{net}}{\rho c_p H}}_{\text{net surface heat flux}} - \underbrace{\nabla \cdot uT}_{\text{horizontal advection}} - \underbrace{w\frac{\partial T}{\partial z}}_{\text{vertical advection}} + \text{residual} \quad (3.1)$$

where T = potential temperature, t = time, Q_{net} = net air sea heat flux, ρ = seawater density, c_p = specific heat capacity, H = pre-defined depth of the mixed layer, ∇ = horizontal divergence operator, u = horizontal velocity, w = vertical velocity, z = vertical depth, and residual = temperature tendency that could not be explained by the other three terms. Q_{net} is further estimated following:

$$Q_{net} = Q_{shf} - Q_{sw}\left[R\exp\left(\frac{-H}{\gamma_1}\right) + (1-R)\exp\left(\frac{-H}{\gamma_2}\right)\right] \quad (3.2)$$

where Q_{shf} = surface heat flux, Q_{sw} = shortwave heat flux, H = pre-defined depth of the upper ocean, R, γ_1, γ_2 = are constants for type I water following (Paulson & Simpson, 1977).

Two additional steps were taken to better compare our heat budget results with

proxy records. First, since proxy records are in $^{\circ}C$ and results from heat budget analysis are in temperature tendency ($^{\circ}C/s$), we integrated the heat budget over time with a 200 year timestep and estimated the temperature change relative to 1000 yrs BP. Second, instead of comparing each proxy record with the heat budget of one grid cell, we compared each proxy record with the heat budget of a region. A grid cell was included in the region if the correlation between its SST and the grid cell nearest to the proxy record was > 0.85. We labelled these regions using the latitude of the grid cell nearest to the proxy record as opposed to the site name because grid cells and core sites are not identically collocated (see Table 1).

We carried out a singular value decomposition (SVD) on all the heat budget terms (see Eq. 3.1) across the five locations (H). This allowed us to determine if the heat budget was balanced similarly at each location for a given temporal pattern. This was accomplished following:

$$H = U \cdot S \cdot V^T \tag{3.3}$$

where U = principal components, S = singular values, and V = eigenvectors (or EOFs) of the data matrix H with all the heat budget terms from the five target locations.

2.2.2 Optimal Fingerprinting Analysis

To understand the spatial fingerprint of each forcing onto SST fields, we carried out an optimal fingerprinting analysis on TraCE21ka simulations. Identification of spatial fingerprints from an external forcing is generally posed as:

$$Y = Xa + u \tag{3.4}$$

where in our study, Y = SST from full forcing simulation, X = SST from each single forcing experiment, a = scaling factors of each forcing, and u = internal variability.

Since SSTs from single forcing experiments contain both forced signals and internal variability, the true forced signal is not known exactly. To account for error in variables due to internal variability, a total least squares (TLS) regression approach was adopted for this analysis to solve Eq. 3.4. This method has been widely adopted in modern climate change detection and attribution studies (e.g. Allen & Stott, 2003; Hegerl & Zwiers, 2011, and references therein).

We followed Allen and Stott (2003) to obtain the scaling factor of each forcing, which represents the contribution of the specific forcing to total change during the analyzed time period (a in Eq. 3.4). First, we defined a data matrix Z where it includes mean centered and pre-whitened X, Y:

$$Z = \left[\frac{X_{anom}}{\sqrt{var(X_{anom})}} \; \frac{Y_{anom}}{\sqrt{var(Y_{anom})}} \right] \tag{3.5}$$

where X_{anom}, Y_{anom} = mean centered X, Y respectively and $var(\cdot)$ = variance.

Next, we decomposed Z from Eq. 3.5 using SVD. Since we seek to obtain the most distinct pattern of each forcing from full forcing simulations, we identified the singular vector (V) that corresponds to the smallest singular value (thus eigenvalues) in Eq. 3.3, and re-scaled the eigenvector such that the element that corresponds to Y = -1. The remaining elements of the vector correspond to the scaling factor of each forcing. We estimated the statistical significance of each scaling factor to 95% confidence level using a bootstrap method following DelSole et al. (2019).

3 Results

Our SST records are interpreted to reflect mean annual SST. In all the alkenone based SST records, the most recent estimates are in close agreement with modern observed mean annual SST ($\sim$ 1°C difference), with all but EW0408-85JC showing a slightly cooler estimate in proxies (Figure 3.2). If alkenones-based SST were to

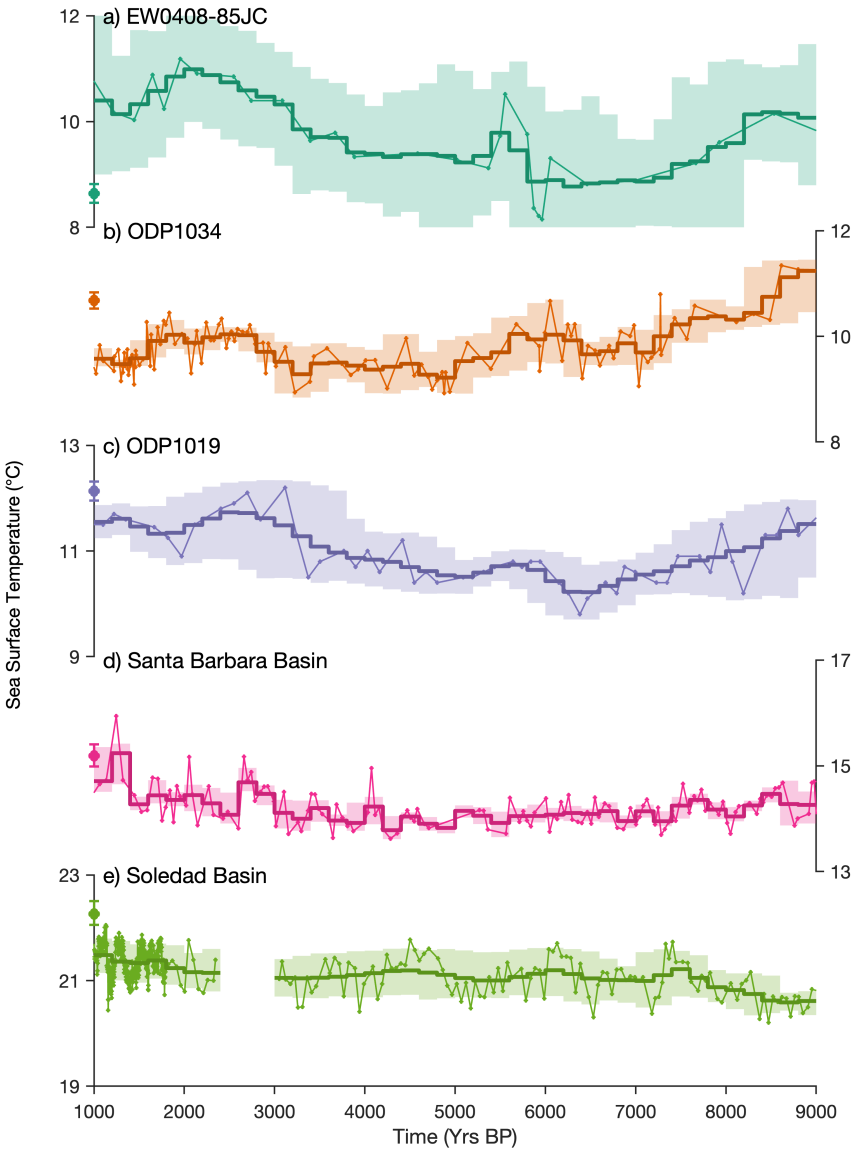

Figure 3.2: $U^{k'}_{37}$ based SST reconstruction. $U^{k'}_{37}$ based SST estimates from a) EW0408-85JC, b) ODP1034, c) ODP1019, d) Santa Barbara Basin, e) Soledad Basin. Lines with circles represent the dataset at original resolution, thick lines represent 200-year binned composites, and shaded areas represent 95% confidence interval of each 200-year composites, which accounts for chronological and analytical uncertainties. The circle indicates modern mean annual SST estimate based on OISST, and the error bar indicates 95% confidence interval based on bootstrap averaging.

primarily reflect warm season temperature, all of our records would be warmer than modern observation. But this is not the case. Furthermore, a comparison between core top $U_{37}^{k'}$ SST and observed mean annual SST suggests that the temperature bias does not increase monotonically with an increase in latitude (Figure S3.1 in Supplementary Information) (Tierney & Tingley, 2018a). These results together suggest that it is unlikely that our proxy records show a systematic warm season bias. As for EW0408-85JC, even though previous studies interpreted alkenone based SST to primarily reflect summer temperature (Praetorius et al., 2015; Prahl et al., 2010), the observed summer SST is still warmer than the alkenone SST estimate that is based on a calibration model that accounts for seasonal bias in the North Pacific (Figure 7b in Tierney and Tingley (2018a)). This suggests that summer season temperature might not be the only possible explanation to such difference. Hence, even though seasonal bias remains possible in EW0408-85JC, given the large positive residual between observed SST and alkenone SST, we interpret the proxy record as mean annual SST.

The five 200 years averaged $U_{37}^{k'}$ SST composite records display varying temporal patterns with different magnitudes of changes (Figure 3.2). The variability of Soledad Basin and MV0508-32JC records is small over the analysis period and show a small increase in SST from early to mid-Holocene to late Holocene (~ 0.89°C for Soledad Basin and ~ 1.46°C for MV0508-32JC). On the other hand, EW0408-85JC, ODP1034, and ODP1019 all showed an initial decrease in SST (~ 1.4°C) between 9,000 years BP and mid Holocene (ca. 7,000–4,000 years BP) before a recovery with similar magnitude toward the present (with the exception of ODP1034, where the SST change since the mid-Holocene was < 1°C). A comparison with Pacific only, Atlantic only, and all basin zonally averaged SST suggests that these five proxy records from the NE Pacific generally follow patterns of Pacific zonal averaged SST. However, these records diverge from the all basin and Atlantic zonal average SST in 40°N-60°N and

20°N-40°N (Figure 3.3).

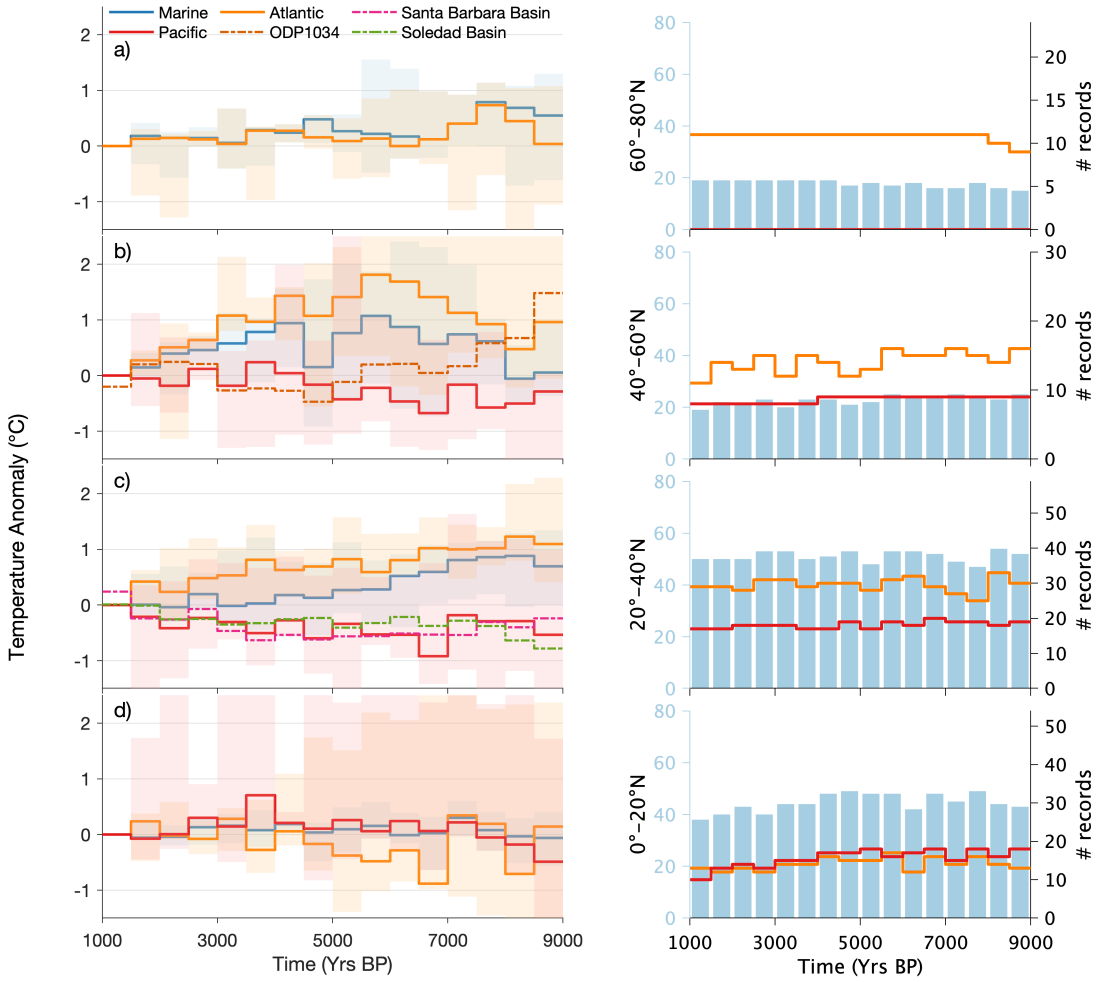

Figure 3.3: Zonally averaged SST anomaly. Zonally averaged SST anomaly (with mean SST 9000-1000 yrs BP removed) at a) $60-80°$ N, b) $40-60°$ N, c) $20-40°$ N, and d) $0-20°$ N. Left panel shows temporal evolution of SST in all ocean basins (blue), Pacific (red), Atlantic (orange), and in the three new study sites. Records that are included in these stacks are listed in Table S3.1 Shaded areas are uncertainties related to sampling. Right panel shows the number of marine records available (blue bars) and the number of records available in the Pacific (red) and Atlantic (orange).

Although the ratio between productivity indicators is qualitatively consistent with modern observations, the magnitude of changes in the productivity records vary by location. Observation suggests elevated diatom productivity in high latitudes relative to low latitude and high coccolithophore productivity along the western north America coast (Figures 3.1c–3.1d). The most recent Si/C37total values from the five

sediment records provide a consistent image – the ratio is highest in high latitude and lowest in low latitude (Figure 3.4). We also observe small Si/Corg temporal variations at all of our study sites. The absolute value of Si/Corg appears to be highest in high latitudes and lowest in low latitudes (Figure 3.5). Similarly, we find small C37total/Corg temporal variations at all of our study sites. The absolute value of C37total/Corg is highest in low latitudes and decrease toward high latitude (Figure 3.6). These results suggest siliceous productivity contributes most to carbon export at high latitudes whereas calcareous productivity contributes most to carbon export at low latitudes, and that their contributions did not change significantly throughout the Holocene.

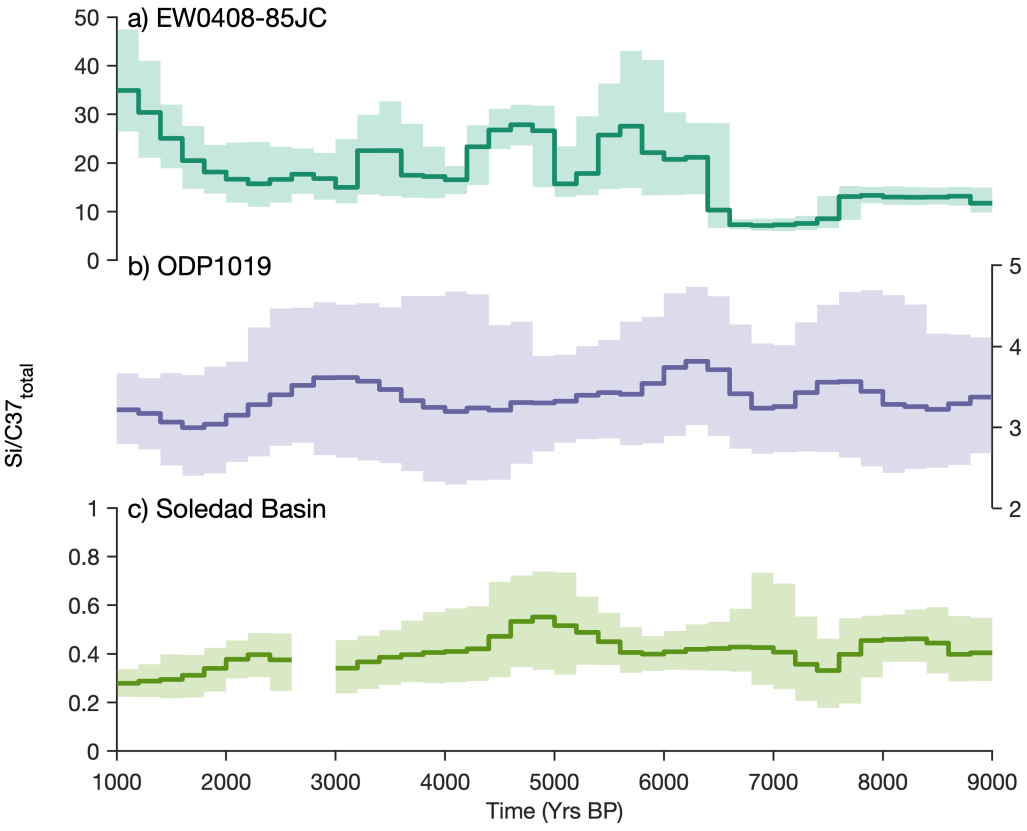

Figure 3.4: $Si/C_{37total}$ ratio. 200 year composites of ratio between Si and $C_{37total}$ at a) EW0408-85JC, b) ODP1019, and c) Soledad Basin. Shaded areas represent 95% confidence interval of each 200-year composite, which accounts for chronological and analytical uncertainties.

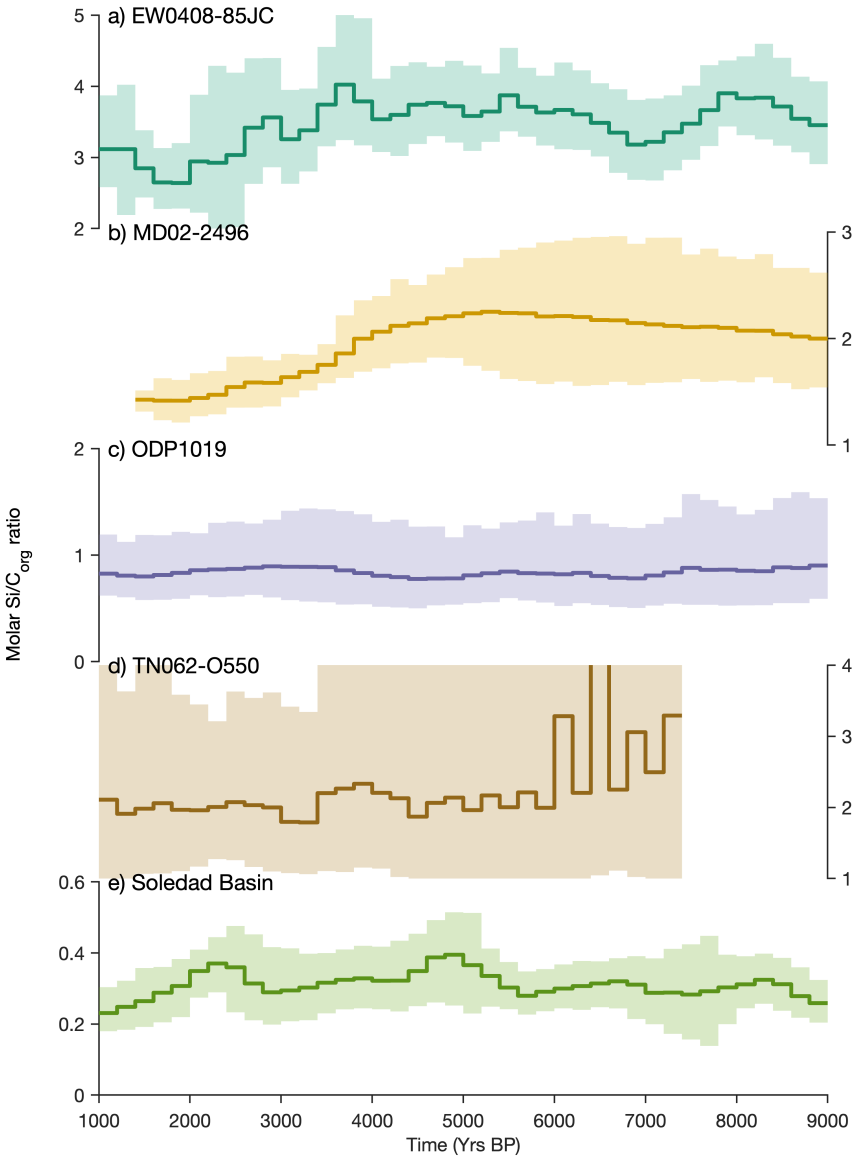

Figure 3.5: Molar Si/C_{org} ratio. 200 year composites of molar ratio between Si and C_{org} at a) EW0408-85JC, b) MD02-2496, c) ODP1019, d) TN062-O550, and e) Soledad Basin. Shaded areas represent 95% confidence interval of each 200-year composite, which accounts for chronological and analytical uncertainties.

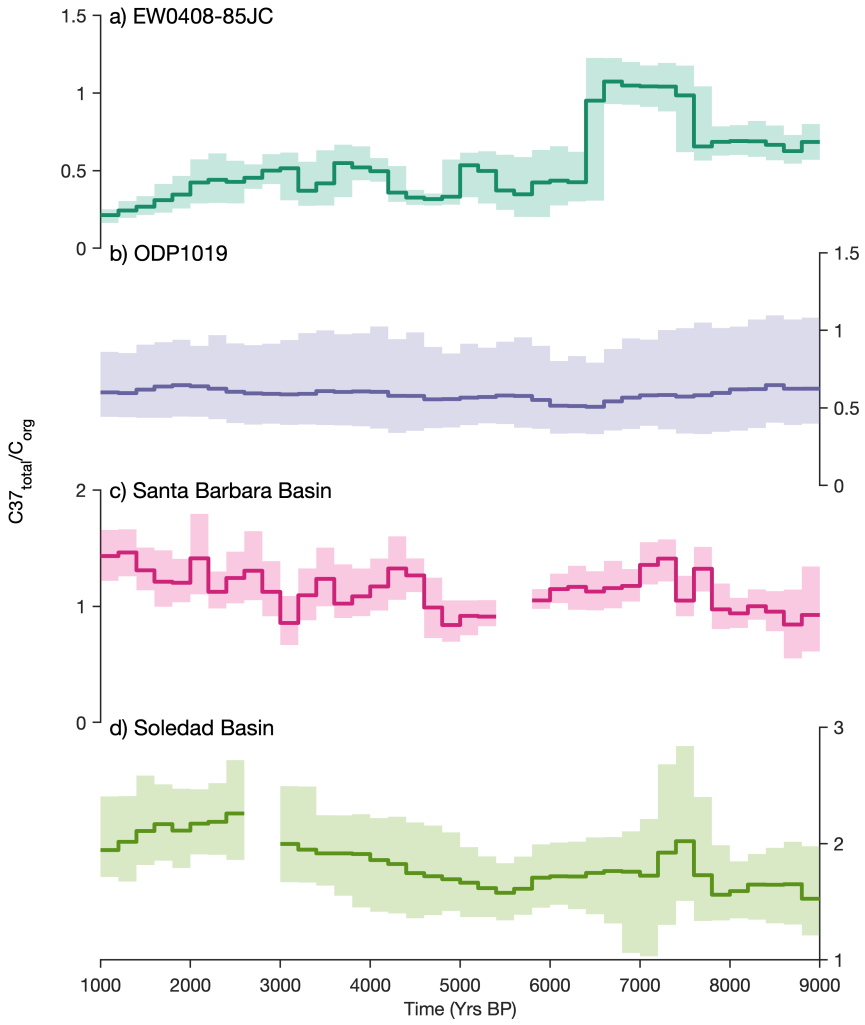

Figure 3.6: $C_{37total}/C_{org}$ ratio. 200 year composites of ratio between $C_{37total}$ and C_{org} at a) EW0408-85JC, b) ODP1019, c) Santa Barbara Basin, and d) Soledad Basin. Shaded areas represent 95% confidence interval of each 200-year composite, which accounts for chronological and analytical uncertainties.

SST evolution in TraCE21ka simulations exhibit different temporal patterns from proxy records, which impedes our ability to make direct inference about mechanisms that drive SST changes shown in proxy records. Specifically, 200 years TraCE21ka based SST composites all show smaller ($< 1°C$) changes during the analysis window (Figure 3.7) compared to proxy records (Figure 3.2). Nevertheless, we analyzed 3 EOFs of the heat budgets to determine if different processes are responsible for driving SST variability at each location (Figure 3.8). Although the first EOF explains most of the variance across all of the heat budget components ($\sim 99\%$ variance), including more EOFs improves the representation of variations shown in the heat budget (Figure S3.2 in Supplementary Information).

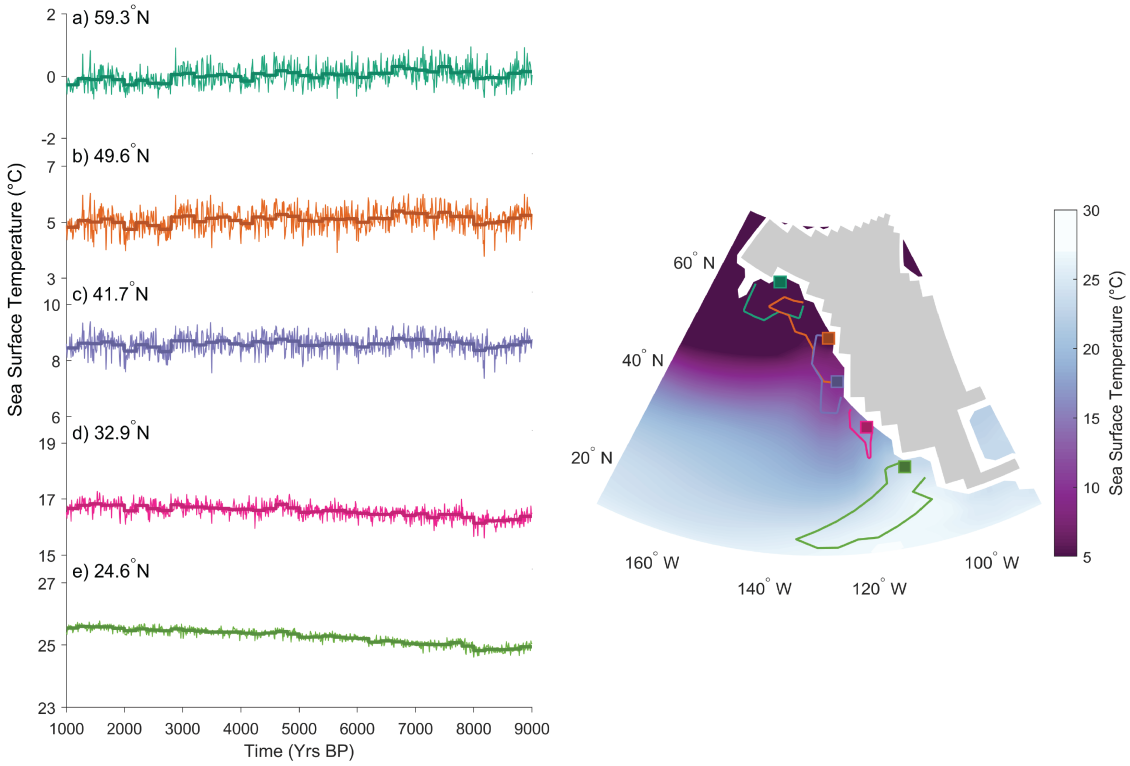

Figure 3.7: SST in TraCE21ka. a-e) timeseries of averaged SST of the grid nearest to the proxy site and neighboring grids with correlation > 0.85 with the nearest grid. Thick lines are 200 year composites. Right panel shows the map with the grid cell nearest to the proxy site (square) and the grids with correlation > 0.85 with that grid (contours). Background color of the map represents average of mean annual SST between 9,000-1,000 yrs BP.

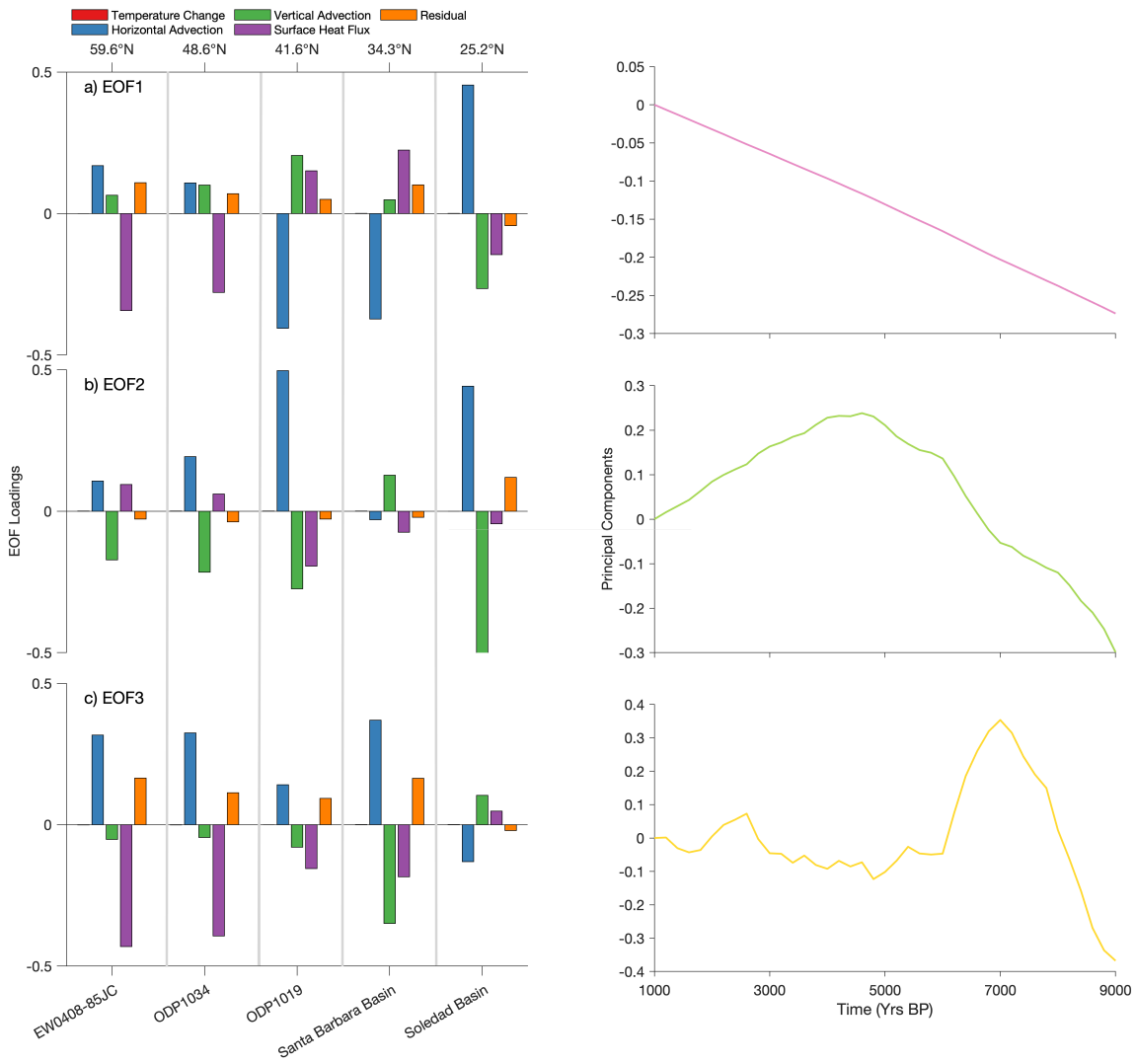

Figure 3.8: EOFs of heat budget at proxy locations. Shown are EOF loadings of each component at the proxy locations for a) EOF1, b) EOF2, and c) EOF3. Also shown are the principal components representing the temporal evolution of these EOFs.

Optimal fingerprinting analysis on TraCE21ka simulations suggests the fingerprint of each external forcing on SST is spatially heterogeneous. Specifically, greenhouse gas forcing has a positive imprint throughout the NE Pacific, but a negative one in lower latitudes, though with less certainty, as indicated by the insignificant scaling factors (Figure 3.9a). On the other hand, orbital forcing, primarily from precession and obliquity, is negatively related to SST at all sites in the NE Pacific, but positively related in low latitudes. The fingerprint is somewhat uncertain between 20°N-40°N

(Figure 3.9b). Only small regions display significant fingerprints of ice sheet and freshwater forcings (Figures 3.9c–3.9d).

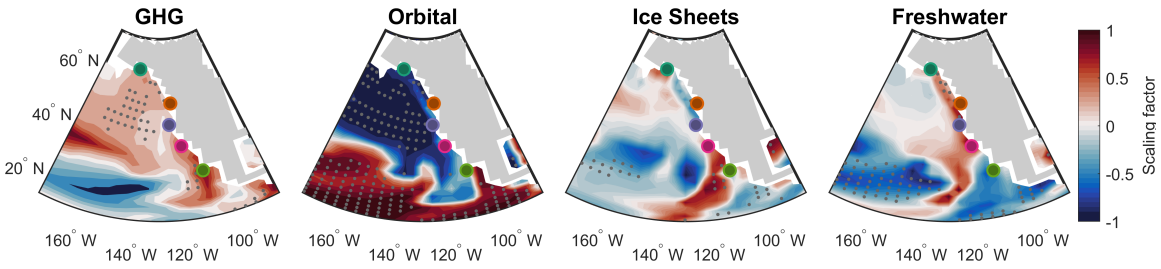

Figure 3.9: Optimal fingerprinting analysis. Spatial fingerprints (scaling factors) of each forcing on SST fields on 200 year timescales derived from TLS regression. Gray stipplings represent statistically significant fingerprint at 95% confidence level based on bootstrapping.

4 Discussion

4.1 Changes in Proxy Records

The five SST records presented in this study provide new insights on the evolution of SST in the NE Pacific during the Holocene. Whereas previous studies focused on linear changes in the NE Pacific during the Holocene (e.g., Kim et al., 2004; Leduc, Schneider, et al., 2010), our results highlight the additional complexity in the temporal evolution of SST in the NE Pacific, especially in mid-latitudes. These records together suggest a dynamic NE Pacific (e.g., Cheung et al., 2019) instead of a region where changes are expected to be linear and with amplitudes scale with latitude. The three new records in this study also provide better constraints on changes in SST than previously published records which are either subject to age uncertainty (Kienast & McKay, 2001), or have proxies which are influenced by other environmental factors (Kennett et al., 2007), or seasonal bias (Marchitto et al., 2010).

The temporal evolution of the SST records shown in this study also challenges previous attempts to reconcile proxy-model and proxy-proxy disagreements. Previous studies used the strong correlation between alkenone based SST records and

winter/summer insolation as the primary evidence to support the idea that alkenone records exhibit a dominant seasonal bias (Bova et al., 2021; Leduc, Schneider, et al., 2010; Z. Liu, Zhu, et al., 2014; Schneider et al., 2010). As such, alkenone records had to be seasonally adjusted before comparing with climate models or other proxy records. Given that maximum vertical transport and temperature occurs during warm season in the NE Pacific (e.g., Jacox et al., 2018), the evidence used in previous studies would suggest that our records are likely to be biased to summer, and that they should show a negative temperature trend (with higher amplitude in higher latitude) that corresponds to summer insolation. Yet, this is not the case. With the exception of ODP1034, which shows a $\sim 1^{\circ}$C cooling, none of the records examined here exhibit a cooling trend (Figure 3.2), in contrast to many alkenone-based reconstructions from the North Atlantic (Figure 3.3). These results indicate that it is insufficient to use the correlation between proxy records and insolation as evidence that proxies are seasonally biased and that it may not be appropriate to correct proxy records based on their correlation with insolation in hope to reconcile proxy-model and proxy-proxy disagreements.

Our SST records further highlight the shortcomings in current synthesis and compilation studies. When compared to studies of Holocene zonally averaged temperature trends, which suggest an increasing meridional temperature gradient toward the present, our records show the opposite trend (Figure 3.3; Davis et al. (2020), Kaufman, McKay, Routson, Erb, Davis, et al. (2020), and Routson et al. (2019)). Additionally, our records further confirm the contrasting temperature trends between the Pacific and the Atlantic mid latitudes (orange vs. red in Figure 3.3). These results together point to a sampling bias toward the Atlantic in hemispheric scale temperature compilations and reconstructions, and that an increase in proxy network spatial density is needed (Judd et al., 2020).

In contrast to SST, our productivity records suggest little to no consistent changes

in primary producer community and their contributions to export productivity. Even though modern studies suggest that changes in primary producer community would pose significant impact on higher trophic level species (Stock et al., 2014), our Si/C37total records do not display any coherent changes over time (Figure 3.4). There are also no coherent patterns in the contributions of alkenone synthesizing haptophytes and diatoms to carbon export (Figures 3.5 and 3.6). Hence, although there are suggestions of an increased coastal upwelling and thus primary productivity since the mid Holocene based on microfossil assemblages (diatoms and silicoflagellates) (Addison et al., 2018; Barron et al., 2019; Barron et al., 2018; Barron et al., 2003), we do not see a change in primary producer community composition and export productivity.

4.2 Mechanisms Behind Changes in Proxy Records

Although proxy records allow us to capture the spatiotemporal evolution of past climates and ecosystems, climate model simulations are needed to help infer physical mechanisms behind these observed changes. Unfortunately, SST from TraCE21ka simulations do not capture the SST temporal patterns in the NE Pacific, nor is CCSM3 capable of simulating ocean biogeochemistry. Therefore, we cannot make direct inferences regarding the mechanisms driving SST and productivity changes. Nevertheless, TraCE21ka simulations remain useful in hypothesis testing.

The spatially variable SST temporal patterns shown in our records raise the question of whether similar physical processes govern the whole NE Pacific. Previous studies have suggested that changes in the persistence of Pacific North American pattern are responsible for SST changes in the NE Pacific (Barron & Anderson, 2011; Kim et al., 2004). Regardless of the cause of such a change, these studies implied a geographically uniform change in NE Pacific SST is expected. However, our EOF analysis on TraCE21ka heat budget suggest that different physical processes are responsible for different heat budget temporal patterns, and that different physical

processes can be responsible even when each proxy site in the NE Pacific shows similar temporal patterns. For instance, northern site variability is dominated by changes in surface forcing and southern site variations are driven by changes in horizontal and vertical advection (Figure 3.8). Together, these results paint a complex picture of SST dynamics in the NE Pacific.

While interpretations based on TraCE21ka cannot be directly applied to interpreting our proxy records, two inferences can be made based on these results. First, common interpretations of SST records in eastern boundary currents are not necessarily accurate. Many studies infer changes in SST records from eastern boundary currents to be dominated by wind driven upwelling (e.g., Abram et al., 2016; Goni et al., 2006; Leduc, Herbert, et al., 2010; MARGO, 2009; McGregor et al., 2007; Vargas et al., 2007). However, our study provides proxy (different SST patterns) and modeling (different heat balance in TraCE21ka) evidence that this upwelling-only rationale is incomplete, which further confirms analysis based on decade long satellite observations (Cheung et al., 2019). Therefore, processes aside from Ekman upwelling must be responsible for the SST variations in northeast Pacific. This highlights the need for physical nuance in proxy interpretations along coastal regions. Second, the temporal disagreement between our proxy records and climate model simulations highlight the model's inability to simulate variations shown in SST proxy records. Whereas previous studies primarily highlighted proxy seasonal bias as the cause of proxy-model disagreement (Bova et al., 2021; Marsicek et al., 2018; Schneider et al., 2010), some also noted that this bias cannot fully account for proxy-model disagreement (Laepple & Huybers, 2014; Z. Liu, Zhu, et al., 2014; Osman et al., 2021). In our case, a large magnitude and spatially varying changes in proxy records could simply be a result of seasonal bias. However, our heat budget analysis indicates that there were changes in process level at each proxy location, even though they were balanced out, and that the dominant process that changed is location dependent. This suggests that changes

observed in proxy records are indeed possible, albeit not simulated by models, and that seasonal bias is not the only explanation that can be invoked. This lends support to the idea that errors in climate models undermine their ability to match with proxy records. Unfortunately, the cause remains disputed. Nonetheless, some studies have suggested misrepresentation of boundary forcings during the Holocene as the cause of proxy-model disagreement (Y. Liu et al., 2018; Thompson et al., 2022), whereas other studies have highlighted biases introduced due to models' inability to simulate sub-grid scale variability (Constantinou & Hogg, 2021; Jüling et al., 2021; Laepple & Huybers, 2014).

4.3 External Forcings

Besides identifying processes, it is also important to understand which forcings are driving changes observed in proxy records. Precession, obliquity, and greenhouse gas content have all changed throughout the Holocene. Traditionally, precession has been considered to be the external forcing that has undergone the most significant change and so, many studies have examined the relationship between proxy records and precession (Wanner et al., 2008). However, the influence of greenhouse gases and combined orbital forcing (precession and obliquity) on the climate system have also been suggested (Bova et al., 2021; Kaufman, McKay, Routson, Erb, Dätwyler, et al., 2020; Routson et al., 2019).

The primary empirical evidence for an externally forced climate signal comes from the comparison between spatiotemporal patterns of proxy records and the temporal evolution of external forcings. Our records suggest that SST in the NE Pacific does not follow a simple linear trend, in contrast to the trend in precession. Our proxy records also showed an increase in SST toward the present instead of a decrease in mid-high latitudes, which exhibits the opposite temporal behavior compared to the zonally average temperature trend and insolation gradient (Figure 3.3). Furthermore,

although the direction and amplitude of SST change in proxy records are consistent with greenhouse gas forcing, where there is larger amplitude change in high latitude due to polar amplification (M. Collins et al., 2013), the timing of the SST increase in mid-high latitude in the NE Pacific is inconsistent with a linear increase in greenhouse gas forcing over the Holocene. Overall, the lack of correspondence between forcing and SST proxy records suggest no single forcing dominates SST in the NE Pacific, and that the external forcing responsible is unlikely to impose a direct effect (local top of the atmosphere change) on SST, as opposed to what is commonly assumed (Bova et al., 2021; Routson et al., 2019; Wanner et al., 2008).

Although proxy records provide the most direct evidence of whether externally forcing drives changes, model simulations allow us to determine the expected fingerprints from external forcings. As noted before, results based on TraCE21ka may not be directly applicable in the real world due to discrepancies in SST variability when compared to proxy records. Nonetheless, TraCE21ka offers an environment to test hypotheses with regards to spatial fingerprint of external forcings within a physically constrained world. The detection and attribution analysis of TraCE21ka simulations suggest a spatially heterogeneous fingerprint from each forcing. For instance, in contrast to an expected uniform positive fingerprint, greenhouse gases impose a positive fingerprint in mid to high latitude in the NE Pacific, but a negative fingerprint in low latitudes. Orbital forcing (precession and obliquity), on the other hand, imposes a negative fingerprint in mid-high latitude but a positive fingerprint in low latitude in the NE Pacific, in contrast with what would be expected from the change in insolation gradient. The fingerprint of each forcing (greenhouse gases and orbital) is also significant in the NE Pacific. Together, these results highlight that externally driven SST does not necessarily follow external forcing time series, and that it is likely that multiple forcings have a role in driving SST changes in the NE Pacific during the Holocene. Since TraCE21ka simulations do not include biogeochemistry, we can-

not make inferences about productivity proxies analyzed here. However, newer and planned paleoclimate simulations that include ocean biogeochemistry(e.g., Segschneider et al., 2018) should help us better understand how external forcings have influenced productivity in this region.

5 Summary and Conclusion

In this study, we investigated how SST and productivity in the NE Pacific changed from 9,000 to 1,000 years BP and the processes and forcings behind these observed changes. We find that SST changes in the NE Pacific are spatially variable, with higher latitudes showing larger changes than lower latitudes. On the other hand, we do not find significant and coherent changes in primary producer community, nor each primary producer's contribution to carbon export. While model-proxy disagreement impedes our ability to directly identify processes driving changes observed in proxies, we show that it is possible that different processes are responsible for the observed changes. Furthermore, we suggest that it is likely multiple external forcings are responsible for the changes observed in proxy records.

Our results have led to new insights on changes in the NE Pacific and more broadly interpretations of Holocene climate change. First, our new SST records and analysis of model simulations highlight the variability and the different temporal evolution of SST in the NE Pacific, as opposed to synchronous changes proposed in previous studies (Kim et al., 2004). Second, our productivity records underscore the difficulty of detecting changes that have cascading effects to the food web and carbon export during the Holocene. Third, we highlight the pitfalls in directly tying external forcing time series to Holocene proxy records, wherein external forcing fingerprints could be complex due to radiative feedbacks and atmospheric-oceanic processes.

More broadly, inferences can be made about future climate change in the NE Pacific. Although there are ample evidence from proxy records and climate model simu-

lations that SST, primary producer composition and export productivity will change under large greenhouse gas forcings (e.g., anthropogenic warming and deglaciation) (Fu et al., 2016; Lopes et al., 2015; Praetorius et al., 2015; Schlunegger et al., 2020), our results indicate that these changes might not be substantial and can be more complex spatially under smaller forced changes. The difference in magnitude and spatial structure of forced changes implies that the SST and ecosystem changes shown in our records might not be directly analogous to the future. Nonetheless, we believe that these complex changes are still important to consider and might be responsible for the difference (and uncertainties) between model projections of SST and ecosystem responses (Fu et al., 2016; Schlunegger et al., 2020). Lastly, the model's inability to simulate observed SST changes underscores the need to improve the model resolution of local and subgrid scale processes to improve future projections of local climate change.

Acknowledgements

MV0508-32JPC was archived at Marine and Geology Repository, College of Earth, Ocean, and Atmospheric Sciences, Oregon State University (OSU-MGR NSF Grant OCE-1558679). Samples from ODP1034 were provided by the International Ocean Discovery Program (IODP) Gulf Coast Repository. TraCE-21ka was made possible by the DOE INCITE computing program, and supported by NCAR, the NSF P2C2 program, and the DOE Abrupt Change and EaSM programs. This work was supported by Henry L. Doherty Oceanography Fund at Brown University, IAI grant UCAR97-73970, CONAYCT grants SEP04-C01-46152 and CB-2009-01-130095, Brown University Graduate School Presidential Fellowship to A. H. Cheung, the Voss Postdoctoral Fellowship at Brown University, Institute at Brown for Environment and Society to X. Du, and NSF #2148945 to B. Fox-Kemper. We thank Ingrid Hendy for making us aware of the availability of MV0508-32JPC for alkenone analysis, Steve Yeager for

assistance in the heat budget analysis, and Kristin Kimble for helpful comments and suggestions.

References

Abram, N. J., Mcgregor, H. V., Tierney, J. E., Evans, M. N., Mckay, N. P., & Kaufman, D. S. (2016). Early onset of industrial-era warming across the oceans and continents. *Nature*, *536*(7617), 411–418. https://doi.org/10.1038/nature19082

Addison, J. A., Barron, J., Finney, B., Kusler, J., Bukry, D., Heusser, L. E., & Alexander, C. R. (2018). A Holocene record of ocean productivity and upwelling from the northern California continental slope. *Quaternary International*, *469*, 96–108.

Addison, J. A., Finney, B. P., Dean, W. E., Davies, M. H., Mix, A. C., Stoner, J. S., & Jaeger, J. M. (2012). Productivity and sedimentary δ^{15}N variability for the last 17,000 years along the northern Gulf of Alaska continental slope. *Paleoceanography*, *27*(1). https://doi.org/https://doi.org/10.1029/2011PA002161

Alexander, M. A., Scott, J. D., Friedland, K. D., Mills, K. E., Nye, J. A., Pershing, A. J., Thomas, A. C., & Carmack, E. C. (2018). Projected sea surface temperatures over the 21st century: Changes in the mean, variability and extremes for large marine ecosystem regions of Northern Oceans. *Elementa: Science of the Anthropocene*, *6*.

Allen, M. R., & Stott, P. A. (2003). Estimating signal amplitudes in optimal fingerprinting, Part I: Theory. *Climate Dynamics*, *21*(5-6), 477–491.

Anderson, R. F., Sachs, J. P., Fleisher, M. Q., Allen, K. A., Yu, J., Koutavas, A., & Jaccard, S. L. (2019). Deep-Sea Oxygen Depletion and Ocean Carbon Sequestration During the Last Ice Age. *Global Biogeochemical Cycles*, *33*(3), 301–317. https://doi.org/https://doi.org/10.1029/2018GB006049

Andrews, J. T., Keigwin, L., Hall, F., & Jennings, A. E. (1999). Abrupt deglaciation events and Holocene palaeoceanography from high-resolution cores, Cartwright Saddle, Labrador Shelf, Canada. *Journal of Quaternary Science: Published for the Quaternary Research Association*, *14*(5), 383–397.

Antonarakou, A., Kontakiotis, G., Mortyn, P., Drinia, H., Sprovieri, M., Besiou, E., & Tripsanas, E. (2015). Biotic and geochemical (δ18O, δ13C, Mg/Ca, Ba/Ca) responses of Globigerinoides ruber morphotypes to upper water column variations during the last deglaciation, Gulf of Mexico. *Geochimica et Cosmochimica Acta*, *170*, 69–93.

Arellano-Torres, E., Álvarez-Covelli, C., Kasper-Zubillaga, J. J., & Lozano-García, M. d. S. (2019). A 14-ka Record of Dust Input and Phytoplankton Regime Changes in the Subtropical NE Pacific: Oceanic and Terrestrial Processes Linked by Teleconnections at Suborbital Scales. *Paleoceanography and Paleoclimatology*, *34*(1), 35–53. https://doi.org/https://doi.org/10.1029/2018PA003479

Arz, H. W., Pätzold, J., Müller, P. J., & Moammar, M. O. (2003). Influence of Northern Hemisphere climate and global sea level rise on the restricted Red Sea marine environment during termination I. *Paleoceanography*, *18*(2).

Bader, J., Jungclaus, J., Krivova, N., Lorenz, S., Maycock, A., Raddatz, T., Schmidt, H., Toohey, M., Wu, C.-J., & Claussen, M. (2020). Global temperature modes shed light on the Holocene temperature conundrum. *Nature communications*, *11*(1), 1–8.

Bakun, A. (1990). Global climate change and intensification of coastal ocean upwelling. *Science*, *247*(4939), 198–201.

Bard, E., Rostek, F., Turon, J.-L., & Gendreau, S. (2000). Hydrological impact of Heinrich events in the subtropical northeast Atlantic. *Science*, *289*(5483), 1321–1324.

Barron, J. A., Addison, J. A., Heusser, L. E., Bukry, D., Schwartz, V., & Wagner, A. (2019). An 11,300 yr record of paleoclimatology and paleoceanography of the central California coast in a gravity core from Pioneer Seamount. *Quaternary International*.

Barron, J. A., & Anderson, L. (2011). Enhanced Late Holocene ENSO/PDO expression along the margins of the eastern North Pacific. *Quaternary International*, *235*(1-2), 3–12.

Barron, J. A., Bukry, D., Heusser, L. E., Addison, J. A., & Alexander, C. R. (2018). High-resolution climate of the past 7300 years of coastal northernmost California: Results from diatoms, silicoflagellates, and pollen. *Quaternary International*, *469*, 109–119.

Barron, J. A., Heusser, L., Herbert, T., & Lyle, M. (2003). High-resolution climatic evolution of coastal northern California during the past 16,000 years. *Paleoceanography*, *18*(1). https://doi.org/https://doi.org/10.1029/2002PA000768

Benway, H. M., Mix, A. C., Haley, B. A., & Klinkhammer, G. P. (2006). Eastern Pacific Warm Pool paleosalinity and climate variability: 0–30 kyr. *Paleoceanography*, *21*(3). https://doi.org/10.1029/2005pa001208

Blaauw, M., & Christen, J. A. (2011). Flexible paleoclimate age-depth models using an autoregressive gamma process. *Bayesian analysis*, *6*(3), 457–474. https://doi.org/10.1214/11-ba618

Blaauw, M., Christen, J. A., Bennett, K., & Reimer, P. J. (2018). Double the dates and go for Bayes—Impacts of model choice, dating density and quality on chronologies. *Quaternary Science Reviews*, *188*, 58–66.

Blais-Stevens, A., Bornhold, B., Kemp, A., Dean, J., & Vaan, A. (2001). Overview of late quaternary stratigraphy in Saanich Inlet, British Columbia: Results of ocean drilling program leg 169S. *Marine Geology*, *174*(1-4), 3–26.

Bograd, S. J., Buil, M. P., Di Lorenzo, E., Castro, C. G., Schroeder, I. D., Goericke, R., Anderson, C. R., Benitez-Nelson, C., & Whitney, F. A. (2015). Changes in source waters to the Southern California Bight. *Deep Sea Research Part II: Topical Studies in Oceanography*, *112*, 42–52.

Bolliet, T., Holbourn, A., Kuhnt, W., Laj, C., Kissel, C., Beaufort, L., Kienast, M., Andersen, N., & Garbe-Schönberg, D. (2011). Mindanao Dome variability over the last 160 kyr: Episodic glacial cooling of the West Pacific Warm Pool. *Paleoceanography*, *26*(1).

Bolton, C. T., Lawrence, K. T., Gibbs, S. J., Wilson, P. A., Cleaveland, L. C., & Herbert, T. D. (2010). Glacial–interglacial productivity changes recorded by alkenones and microfossils in late Pliocene eastern equatorial Pacific and Atlantic upwelling zones. *Earth and Planetary Science Letters*, *295*(3-4), 401–411.

Bond, N. A., Cronin, M. F., Freeland, H., & Mantua, N. (2015). Causes and impacts of the 2014 warm anomaly in the NE Pacific. *Geophysical Research Letters*, *42*(9), 3414–3420. https://doi.org/https://doi.org/10.1002/2015GL063306

Bornhold, B., Firth, J., & 14 others. (1998). Proceedings of the Ocean Drilling Program, Vol. 169S, Initial Reports, Saanich Inlet. https://doi.org/10.2973/odp.proc.ir.169s.1998

Bova, S., Rosenthal, Y., Liu, Z., Godad, S. P., & Yan, M. (2021). Seasonal origin of the thermal maxima at the Holocene and the last interglacial. *Nature*, *589*(7843), 548–553. https://doi.org/10.1038/s41586-020-03155-x

Bracher, A., Dinter, T., Wolanin, A., Rozanov, V. V., Losa, S. N., & Soppa, M. A. (2017). Global monthly mean chlorophyll a surface concentrations from August 2002 to April 2012 for diatoms, coccolithophores and cyanobacteria from PhytoDOAS algorithm version 3.3 applied to SCIAMACHY data. PANGAEA. https://doi.org/10.1594/PANGAEA.870486

Cacho, I., Grimalt, J. O., Canals, M., Sbaffi, L., Shackleton, N. J., Schönfeld, J., & Zahn, R. (2001). Variability of the western Mediterranean Sea surface temperature during the last 25,000 years and its connection with the Northern Hemisphere climatic changes. *Paleoceanography*, *16*(1), 40–52.

Cacho, I., Grimalt, J. O., Pelejero, C., Canals, M., Sierro, F. J., Flores, J. A., & Shackleton, N. (1999). Dansgaard-Oeschger and Heinrich event imprints in Alboran Sea paleotemperatures. *Paleoceanography*, *14*(6), 698–705.

Came, R., Oppo, D., & McManus, J. (2007). Amplitude and timing of salinity and temperature variability in the high-latitude North Atlantic. *Geology*, *35*, 315–318.

Capet, X., McWilliams, J. C., Molemaker, M. J., & Shchepetkin, A. F. (2008). Mesoscale to submesoscale transition in the California Current System. Part I: Flow structure, eddy flux, and observational tests. *Journal of physical oceanography*, *38*(1), 29–43.

Castañeda, I. S., Schefuß, E., Pätzold, J., Sinninghe Damsté, J. S., Weldeab, S., & Schouten, S. (2010). Millennial-scale sea surface temperature changes in the eastern Mediterranean (Nile River Delta region) over the last 27,000 years. *Paleoceanography*, *25*(1).

Castañeda, I. S., Smith, L. M., Kristjánsdóttir, G. B., & Andrews, J. T. (2004). Temporal changes in Holocene δ18O records from the northwest and central North Iceland Shelf. *Journal of Quaternary Science*, *19*(4), 321–334.

Cavole, L. M., Demko, A. M., Diner, R. E., Giddings, A., Koester, I., Pagniello, C. M., Paulsen, M.-L., Ramirez-Valdez, A., Schwenck, S. M., Yen, N. K., et al. (2016). Biological impacts of the 2013–2015 warm-water anomaly in the Northeast Pacific: winners, losers, and the future. *Oceanography*, *29*(2), 273–285.

Chang, A. S., Pedersen, T. F., & Hendy, I. L. (2008). Late Quaternary paleoproductivity history on the Vancouver Island margin, western Canada: a multiproxy geochemical study. *Canadian Journal of Earth Sciences*, *45*(11), 1283–1297.

Chang, F., Li, T., Xiong, Z., & Xu, Z. (2015). Evidence for sea level and monsoonally driven variations in terrigenous input to the northern East China Sea during the last 24.3 ka. *Paleoceanography*, *30*(6), 642–658.

Cheung, A. H., Fox-Kemper, B., & Herbert, T. (2019). Can we use sea surface temperature and productivity proxy records to reconstruct Ekman upwelling? *Climate of the Past*, *15*(6), 1985–1998. https://doi.org/10.5194/cp-15-1985-2019

Collins, M., Knutti, R., Arblaster, J., Dufresne, J.-L., Fichefet, T., Friedlingstein, P., Gao, X., Gutowski, W. J., Johns, T., Krinner, G., et al. (2013). Long-term climate change: projections, commitments and irreversibility. In *Climate Change 2013-The Physical Science Basis: Contribution of Working Group I to the Fifth Assessment Report of the Intergovernmental Panel on Climate Change* (pp. 1029–1136). Cambridge University Press.

Collins, W. D., Bitz, C. M., Blackmon, M. L., Bonan, G. B., Bretherton, C. S., Carton, J. A., Chang, P., Doney, S. C., Hack, J. J., Henderson, T. B., Kiehl, J. T., Large, W. G., McKenna, D. S., Santer, B. D., & Smith, R. D. (2006). The community climate system model version 3 (ccsm3). *Journal of Climate*, *19*(11), 2122–2143. https://doi.org/10.1175/JCLI3761.1

Constantinou, N. C., & Hogg, A. M. (2021). Intrinsic oceanic decadal variability of upper-ocean heat content. *Journal of Climate*, *34*(15), 6175–6189.

Conte, M. H., Sicre, M.-A., Rühlemann, C., Weber, J. C., Schulte, S., Schulz-Bull, D., & Blanz, T. (2006). Global temperature calibration of the alkenone unsaturation index ($u^{K'}_{37}$) in surface waters and comparison with surface sediments. *Geochemistry, Geophysics, Geosystems*, *7*(2). https://doi.org/https://doi.org/10.1029/2005GC001054

Cosma, T. N., Hendy, I. L., & Chang, A. S. (2008). Chronological constraints on Cordilleran Ice Sheet glaciomarine sedimentation from core MD02-2496 off Vancouver Island (western Canada). *Quaternary Science Reviews*, *27*(9-10), 941–955.

Davies-Walczak, M., Mix, A. C., Stoner, J. S., Southon, J., Cheseby, M., & Xuan, C. (2014). Late Glacial to Holocene radiocarbon constraints on North Pacific Intermediate Water ventilation and deglacial atmospheric CO2 sources. *Earth and Planetary Science Letters*, *397*, 57–66.

Davis, C. V., Myhre, S. E., Deutsch, C., Caissie, B., Praetorius, S., Borreggine, M., & Thunell, R. (2020). Sea surface temperature across the Subarctic North Pacific and marginal seas through the past 20,000 years: A paleoceanographic synthesis. *Quaternary Science Reviews*, *246*, 106519. https://doi.org/10.1016/j.quascirev.2020.106519

Dean, W. E., Zheng, Y., Ortiz, J. D., & van Geen, A. (2006). Sediment Cd and Mo accumulation in the oxygen-minimum zone off western Baja California linked to global climate over the past 52 kyr. *Paleoceanography*, *21*(4). https://doi.org/https://doi.org/10.1029/2005PA001239

DelSole, T., Trenary, L., Yan, X., & Tippett, M. K. (2019). Confidence intervals in optimal fingerprinting. *Climate Dynamics*, *52*(7), 4111–4126.

DeVries, T., & Weber, T. (2017). The export and fate of organic matter in the ocean: New constraints from combining satellite and oceanographic tracer observations. *Global Biogeochemical Cycles*, *31*(3), 535–555. https://doi.org/https://doi.org/10.1002/2016GB005551

Di Lorenzo, E., Schneider, N., Cobb, K. M., Franks, P., Chhak, K., Miller, A. J., McWilliams, J. C., Bograd, S. J., Arango, H., Curchitser, E., et al. (2008). North Pacific Gyre Oscillation links ocean climate and ecosystem change. *Geophysical Research Letters*, *35*(8).

Diffenbaugh, N. S., & Ashfaq, M. (2007). Response of California Current forcing to mid-Holocene insolation and sea surface temperatures. *Paleoceanography*, *22*(3). https://doi.org/https://doi.org/10.1029/2006PA001382

Doose-Rolinski, H., Rogalla, U., Scheeder, G., Lückge, A., & von Rad, U. (2001). High-resolution temperature and evaporation changes during the late Holocene in the northeastern Arabian Sea. *Paleoceanography*, *16*(4), 358–367.

Du, X., Hendy, I., & Schimmelmann, A. (2018). A 9000-year flood history for Southern California: A revised stratigraphy of varved sediments in Santa Barbara Basin. *Marine Geology*, *397*, 29–42. https://doi.org/10.1016/j.margeo.2017.11.014

Elmore, A., Wright, J. D., & Southon, J. (2015). Continued meltwater influence on North Atlantic Deep Water instabilities during the early Holocene. *Marine Geology*, *360*, 17–24.

Emeis, K.-C., & Dawson, A. G. (2003). Holocene palaeoclimate records over Europe and the North Atlantic. *The Holocene*, *13*(3), 305–309.

Emeis, K.-C., Struck, U., Blanz, T., Kohly, A., & Voβ, M. (2003). Salinity changes in the central Baltic Sea (NW Europe) over the last 10000 years. *The Holocene*, *13*(3), 411–421.

Eynaud, F., De Abreu, L., Voelker, A., Schönfeld, J., Salgueiro, E., Turon, J.-L., Penaud, A., Toucanne, S., Naughton, F., Goñi, M. F. S., et al. (2009). Position of the Polar Front along the western Iberian margin during key cold episodes of the last 45 ka. *Geochemistry, Geophysics, Geosystems*, *10*(7).

Fan, W., Jian, Z., Chu, Z., Dang, H., Wang, Y., Bassinot, F., Han, X., & Bian, Y. (2018). Variability of the Indonesian throughflow in the Makassar Strait over the last 30 ka. *Scientific reports*, *8*(1), 1–8.

Farmer, E. J., Chapman, M. R., & Andrews, J. E. (2008). Centennial-scale Holocene North Atlantic surface temperatures from Mg/Ca ratios in Globigerina bulloides. *Geochemistry, Geophysics, Geosystems*, *9*(12).

Flower, B. P., Hastings, D. W., Hill, H. W., & Quinn, T. M. (2004). Phasing of deglacial warming and Laurentide Ice Sheet meltwater in the Gulf of Mexico. *Geology*, *32*(7), 597–600.

Fraser, N., Kuhnt, W., Holbourn, A., Bolliet, T., Andersen, N., Blanz, T., & Beaufort, L. (2014). Precipitation variability within the West Pacific Warm Pool over the past 120 ka: Evidence from the Davao Gulf, southern Philippines. *Paleoceanography*, *29*(11), 1094–1110.

Fu, W., Randerson, J. T., & Moore, J. K. (2016). Climate change impacts on net primary production (NPP) and export production (EP) regulated by increasing stratification and phytoplankton community structure in the CMIP5 models. *Biogeosciences*, *13*(18), 5151–5170. https://doi.org/10.5194/bg-13-5151-2016

Gardner, J. V., & Dartnell, P. (1995). Centennial-Scale Late Quaternary Stratigraphies of Carbonate and Organic Carbon from Santa Barbara BAsin, Hole 893A, and their Paleoceanographic Significance. *Proceedings of the Ocean Drilling Program, Scientific Results*, *146*(Pt 2).

Gardner, J. V., Dean, W. E., & Dartnell, P. (1997). Biogenic sedimentation beneath the California Current System for the past 30 kyr and its paleoceanographic significance. *Paleoceanography*, *12*(2), 207–225. https://doi.org/https://doi.org/10.1029/96PA03567

Goni, M. A., Thunell, R. C., Woodwort, M. P., & Müller-Karger, F. E. (2006). Changes in wind-driven upwelling during the last three centuries: Interocean teleconnections. *Geophys. Res. Lett.*, *33*, L15604. https://doi.org/10.1029/2006GL026415

Harada, N., Ahagon, N., Sakamoto, T., Uchida, M., Ikehara, M., & Shibata, Y. (2006). Rapid fluctuation of alkenone temperature in the southwestern Okhotsk Sea during the past 120 ky. *Global and Planetary Change*, *53*(1-2), 29–46. https://doi.org/10.1016/j.gloplacha.2006.01.010

Harrison, S. P., Bartlein, P., Izumi, K., Li, G., Annan, J., Hargreaves, J., Braconnot, P., & Kageyama, M. (2015). Evaluation of CMIP5 palaeo-simulations to improve climate projections. *Nature Climate Change*, *5*(8), 735–743.

Heaton, T. J., Köhler, P., Butzin, M., Bard, E., Reimer, R. W., Austin, W. E., Ramsey, C. B., Grootes, P. M., Hughen, K. A., Kromer, B., et al. (2020). Marine20—the marine radiocarbon age calibration curve (0–55,000 cal BP). *Radiocarbon*, *62*(4), 779–820.

Hegerl, G., & Zwiers, F. (2011). Use of models in detection and attribution of climate change. *WIREs Climate Change*, *2*(4), 570–591. https://doi.org/https://doi.org/10.1002/wcc.121

Herbert, T. D. (2014). 8.15 - alkenone paleotemperature determinations. In H. D. Holland & K. K. Turekian (Eds.), *Treatise on geochemistry (second edition)* (Second Edition, pp. 399–433). Elsevier. https://doi.org/https://doi.org/10.1016/B978-0-08-095975-7.00615-X

Herbert, T. D., & Schuffert, J. D. (2000). Alkenone unsaturation estimates of sea-surface temperatures at Site 1002 over a full glacial cycle. In *Proceedings of the ocean drilling program, 165 scientific results*. Ocean Drilling Program. https://doi.org/10.2973/odp.proc.sr.165.030.2000

Herbert, T. D., Schuffert, J. D., Thomas, D., Lange, C., Weinheimer, A., Peleo-Alampay, A., & Herguera, J.-C. (1998). Depth and seasonality of alkenone production along the California Margin inferred from a core top transect. *Paleoceanography*, *13*(3), 263–271. https://doi.org/https://doi.org/10.1029/98PA00069

Hill, T., Kennett, J. P., Pak, D., Behl, R., Robert, C., & Beaufort, L. (2006). Pre-Bölling warming in Santa Barbara Basin, California: surface and intermediate water records of early deglacial warmth. *Quaternary Science Reviews*, *25*(21-22), 2835–2845.

Hillaire-Marcel, C., Vernal, A. d., Bilodeau, G., & Wu, G. (1994). Isotope stratigraphy, sedimentation rates, deep circulation, and carbonate events in the Labrador Sea during the last $\sim$ 200 ka. *Canadian Journal of Earth Sciences*, *31*(1), 63–89.

Huguet, C., Kim, J.-H., Sinninghe Damste, J. S., & Schouten, S. (2006). Reconstruction of sea surface temperature variations in the Arabian Sea over the last 23 kyr using organic proxies (TEX86 and $U_{37}^{K'}$). *Paleoceanography*, *21*(3).

Ijiri, A., Wang, L., Oba, T., Kawahata, H., Huang, C.-Y., & Huang, C.-Y. (2005). Paleoenvironmental changes in the northern area of the East China Sea during the past 42,000 years. *Palaeogeography, Palaeoclimatology, Palaeoecology*, *219*(3-4), 239–261. https://doi.org/10.1016/j.palaeo.2004.12.028

Isono, D., Yamamoto, M., Irino, T., Oba, T., Murayama, M., Nakamura, T., & Kawahata, H. (2009). The 1500-year climate oscillation in the midlatitude North Pacific during the Holocene. *Geology*, *37*(7), 591–594.

Jacox, M. G., Edwards, C. A., Hazen, E. L., & Bograd, S. J. (2018). Coastal Upwelling Revisited: Ekman, Bakun, and Improved Upwelling Indices for the U.S. West Coast. *Journal of Geophysical Research: Oceans*, *123*(10), 7332–7350. https://doi.org/https://doi.org/10.1029/2018JC014187

Jacox, M. G., Fiechter, J., Moore, A. M., & Edwards, C. A. (2015). ENSO and the California Current coastal upwelling response. *Journal of Geophysical Research: Oceans*, *120*(3), 1691–1702.

Jacox, M. G., Moore, A., Edwards, C., & Fiechter, J. (2014). Spatially resolved upwelling in the California Current System and its connections to climate variability. *Geophysical Research Letters*, *41*(9), 3189–3196.

Jin, X., Gruber, N., Dunne, J., Sarmiento, J. L., & Armstrong, R. (2006). Diagnosing the contribution of phytoplankton functional groups to the production and export of particulate organic carbon, CaCO3, and opal from global nutrient and alkalinity distributions. *Global Biogeochemical Cycles*, *20*(2).

Johnstone, J. A., & Dawson, T. E. (2010). Climatic context and ecological implications of summer fog decline in the coast redwood region. *Proceedings of the National Academy of Sciences*, *107*(10), 4533–4538.

Johnstone, J. A., & Mantua, N. J. (2014). Atmospheric controls on northeast Pacific temperature variability and change, 1900–2012. *Proceedings of the National Academy of Sciences*, *111*(40), 14360–14365.

Judd, E. J., Bhattacharya, T., & Ivany, L. C. (2020). A Dynamical Framework for Interpreting Ancient Sea Surface Temperatures. *Geophysical Research Letters*, *47*(15), e2020GL089044. https://doi.org/https://doi.org/10.1029/2020GL089044

Jüling, A., Von Der Heydt, A., & Dijkstra, H. A. (2021). Effects of strongly eddying oceans on multidecadal climate variability in the Community Earth System Model. *Ocean Science*, *17*(5), 1251–1271.

Jung, S. J. (1996). *Wassermassenaustausch zwischen NE-Atlantik und Nordmeer während der letzten 300.000/80.000 Jahre im Abbild stabiler O-und C-lsotope* (Doctoral dissertation). Christian-Albrechts-Universität Kiel.

Kahru, M., Di Lorenzo, E., Manzano-Sarabia, M., & Mitchell, B. G. (2012). Spatial and temporal statistics of sea surface temperature and chlorophyll fronts in the California Current. *Journal of plankton research*, *34*(9), 749–760.

Kaufman, D., McKay, N., Routson, C., Erb, M., Dätwyler, C., Sommer, P. S., Heiri, O., & Davis, B. (2020). Holocene global mean surface temperature, a multi-method reconstruction approach. *Scientific data*, *7*(1), 1–13.

Kaufman, D., McKay, N., Routson, C., Erb, M., Davis, B., Heiri, O., Jaccard, S., Tierney, J., Dätwyler, C., Axford, Y., et al. (2020). A global database of Holocene paleotemperature records. *Scientific data*, *7*(1), 1–34.

Kawahata, H., Yamamoto, H., Ohkushi, K., Yokoyama, Y., Kimoto, K., Ohshima, H., & Matsuzaki, H. (2009). Changes of environments and human activity at the Sannai-Maruyama ruins in Japan during the mid-Holocene Hypsithermal climatic interval. *Quaternary Science Reviews*, *28*(9-10), 964–974. https://doi.org/10.1016/j.quascirev.2008.12.009

Keigwin, L., & Jones, G. A. (1995). The marine record of deglaciation from the continental margin off Nova Scotia. *Paleoceanography*, *10*(6), 973–985.

Keigwin, L., Sachs, J., Rosenthal, Y., & Boyle, E. (2005). The 8200 year BP event in the slope water system, western subpolar North Atlantic. *Paleoceanography*, *20*(2).

Kennett, D. J., Kennett, J. P., Erlandson, J. M., & Cannariato, K. G. (2007). Human responses to Middle Holocene climate change on California's Channel Islands. *Quaternary Science Reviews*, *26*(3-4), 351–367.

Kienast, S. S., & McKay, J. L. (2001). Sea surface temperatures in the subarctic northeast Pacific reflect millennial-scale climate oscillations during the last 16 kyrs. *Geophysical Research Letters*, *28*(8), 1563–1566.

Kim, J.-H., Meggers, H., Rimbu, N., Lohmann, G., Freudenthal, T., Müller, P. J., & Schneider, R. R. (2007). Impacts of the North Atlantic gyre circulation on Holocene climate off northwest Africa. *Geology*, *35*(5), 387–390.

Kim, J.-H., Rimbu, N., Lorenz, S. J., Lohmann, G., Nam, S.-I., Schouten, S., Rühlemann, C., & Schneider, R. R. (2004). North Pacific and North Atlantic sea-surface temperature variability during the Holocene. *Quaternary Science Reviews*, *23*(20-22), 2141–2154.

Kim, J.-H., Romero, O. E., Lohmann, G., Donner, B., Laepple, T., Haam, E., & Damste, J. S. S. (2012). Pronounced subsurface cooling of North Atlantic waters off Northwest Africa during Dansgaard–Oeschger interstadials. *Earth and Planetary Science Letters*, *339*, 95–102.

Kristjánsdóttir, G. B., Moros, M., Andrews, J. T., & Jennings, A. E. (2017). Holocene Mg/Ca, alkenones, and light stable isotope measurements on the outer North Iceland shelf (MD99-2269): A comparison with other multi-proxy data and sub-division of the Holocene. *The Holocene*, *27*(1), 52–62.

Kubota, Y., Kimoto, K., Tada, R., Oda, H., Yokoyama, Y., & Matsuzaki, H. (2010). Variations of East Asian summer monsoon since the last deglaciation based on Mg/Ca and oxygen isotope of planktic foraminifera in the northern East China Sea. *Paleoceanography*, *25*(4), n/a–n/a. https://doi.org/10.1029/2009pa001891

Laepple, T., & Huybers, P. (2014). Ocean surface temperature variability: Large model–data differences at decadal and longer periods. *Proceedings of the National Academy of Sciences*, *111*(47), 16682–16687.

Large, W. G., & Danabasoglu, G. (2006). Attribution and impacts of upper-ocean biases in ccsm3. *Journal of Climate*, *19*(11), 2325–2346. https://doi.org/10.1175/JCLI3740.1

Lea, D. W., Pak, D. K., Peterson, L. C., & Hughen, K. A. (2003). Synchroneity of tropical and high-latitude Atlantic temperatures over the last glacial termination. *Science*, *301*(5638), 1361–1364.

Leduc, G., Herbert, C. T., Blanz, T., Martinez, P., & Schneider, R. (2010). Contrasting evolution of sea surface temperature in the Benguela upwelling system under natural and anthropogenic climate forcings. *Geophys. Res. Lett.*, *37*, L20705. https://doi.org/10.1029/2010GL044353

Leduc, G., Schneider, R., Kim, J.-H., & Lohmann, G. (2010). Holocene and Eemian sea surface temperature trends as revealed by alkenone and Mg/Ca paleothermometry. *Quaternary Science Reviews*, *29*(7-8), 989–1004.

Li, Q., Reichl, B. G., Fox-Kemper, B., Adcroft, A. J., Belcher, S. E., Danabasoglu, G., Grant, A. L. M., Griffies, S. M., Hallberg, R., Hara, T., Harcourt, R. R., Kukulka, T., Large, W. G., McWilliams, J. C., Pearson, B., Sullivan, P. P., Van Roekel, L., Wang, P., & Zheng, Z. (2019). Comparing Ocean Surface Boundary Vertical Mixing Schemes Including Langmuir Turbulence. *Journal of Advances in Modeling Earth Systems*, *11*(11), 3545–3592. https://doi.org/https://doi.org/10.1029/2019MS001810

Liu, W., & Hu, A. (2015). The role of the PMOC in modulating the deglacial shift of the ITCZ. *Climate dynamics*, *45*(11), 3019–3034.

Liu, Y., Zhang, M., Liu, Z., Xia, Y., Huang, Y., Peng, Y., & Zhu, J. (2018). A possible role of dust in resolving the holocene temperature conundrum. *Scientific reports*, *8*(1), 1–9. https://doi.org/10.1038/s41598-018-22841-5

Liu, Z., Lu, Z., Wen, X., Otto-Bliesner, B. L., Timmermann, A., & Cobb, K. M. (2014). Evolution and forcing mechanisms of El Niño over the past 21,000 years. *Nature*, *515*(7528), 550–553.

Liu, Z., Otto-Bliesner, B., He, F., Brady, E., Tomas, R., Clark, P., Carlson, A., Lynch-Stieglitz, J., Curry, W., Brook, E., et al. (2009). Transient simulation of last deglaciation with a new mechanism for Bølling-Alleröd warming. *science*, *325*(5938), 310–314.

Liu, Z., Zhu, J., Rosenthal, Y., Zhang, X., Otto-Bliesner, B. L., Timmermann, A., Smith, R. S., Lohmann, G., Zheng, W., & Timm, O. E. (2014). The Holocene temperature conundrum. *Proceedings of the National Academy of Sciences*, *111*(34), E3501–E3505.

Lohmann, G., Pfeiffer, M., Laepple, T., Leduc, G., & Kim, J.-H. (2013). A model–data comparison of the Holocene global sea surface temperature evolution. *Climate of the Past*, *9*(4), 1807–1839. https://doi.org/10.5194/cp-9-1807-2013

Long, S.-M., Xie, S.-P., Zheng, X.-T., & Liu, Q. (2014). Fast and slow responses to global warming: Sea surface temperature and precipitation patterns. *Journal of Climate*, *27*(1), 285–299.

Longo, W. M., Dillon, J. T., Tarozo, R., Salacup, J. M., & Huang, Y. (2013). Unprecedented separation of long chain alkenones from gas chromatography with a poly (trifluoropropylmethylsiloxane) stationary phase. *Organic Geochemistry*, *65*, 94–102.

Lopes, C., & Mix, A. C. (2018). North Pacific Paleotemperature and Paleoproductivity Reconstructions Based on Diatom Species. *Paleoceanography and Paleoclimatology*, *33*(7), 703–715. https://doi.org/https://doi.org/10.1029/2018PA003352

Lopes, C., Kucera, M., & Mix, A. C. (2015). Climate change decouples oceanic primary and export productivity and organic carbon burial. *Proceedings of the National Academy of Sciences*, *112*(2), 332–335.

Losa, S. N., Soppa, M. A., Dinter, T., Wolanin, A., Brewin, R. J., Bricaud, A., Oelker, J., Peeken, I., Gentili, B., Rozanov, V., et al. (2017). Synergistic exploitation of hyper-and multi-spectral precursor sentinel measurements to determine phytoplankton functional types (SynSenPFT). *Frontiers in Marine Science*, *4*, 203.

Lotze, H. K., Tittensor, D. P., Bryndum-Buchholz, A., Eddy, T. D., Cheung, W. W., Galbraith, E. D., Barange, M., Barrier, N., Bianchi, D., Blanchard, J. L., et al. (2019). Global ensemble projections reveal trophic amplification of ocean biomass declines with climate change. *Proceedings of the National Academy of Sciences*, *116*(26), 12907–12912.

Marchitto, T. M., Muscheler, R., Ortiz, J. D., Carriquiry, J. D., & van Geen, A. (2010). Dynamical response of the tropical Pacific Ocean to solar forcing during the early Holocene. *Science*, *330*(6009), 1378–1381.

MARGO. (2009). Constraints on the magnitude and patterns of ocean cooling at the Last Glacial Maximum. *Nat. Geosci.*, *2*, 127–132. https://doi.org/10.1038/NGEO411

Marsicek, J., Shuman, B. N., Bartlein, P. J., Shafer, S. L., & Brewer, S. (2018). Reconciling divergent trends and millennial variations in Holocene temperatures. *Nature*, *554*(7690), 92–96.

Martrat, B., Grimalt, J. O., Shackleton, N. J., de Abreu, L., Hutterli, M. A., & Stocker, T. F. (2007). Four climate cycles of recurring deep and surface water destabilizations on the Iberian margin. *Science*, *317*(5837), 502–507.

Martrat, B., Grimalt, J. O., Villanueva, J., van Kreveld, S., & Sarnthein, M. (2003). Climatic dependence of the organic matter contributions in the north eastern Norwegian Sea over the last 15,000 years. *Organic geochemistry*, *34*(8), 1057–1070.

Martrat, B., Jimenez-Amat, P., Zahn, R., & Grimalt, J. O. (2014). Similarities and dissimilarities between the last two deglaciations and interglaciations in the North Atlantic region. *Quaternary Science Reviews*, *99*, 122–134.

Max, L., Lembke-Jene, L., Zou, J., Shi, X., & Tiedemann, R. (2020). Evaluation of reconstructed sea surface temperatures based on $U_{37}^{K'}$ from sediment surface samples of the North Pacific. *Quaternary Science Reviews*, *243*, 106496.

McClymont, E. L., Ganeshram, R. S., Pichevin, L. E., Talbot, H. M., Van Dongen, B. E., Thunell, R. C., Haywood, A. M., Singarayer, J. S., & Valdes, P. J. (2012). Sea-surface temperature records of Termination 1 in the Gulf of California: Challenges for seasonal and interannual analogues of tropical Pacific climate change. *Paleoceanography*, *27*(2).

McGregor, H. V., Dima, M., Fischer, H. W., & Mulitza, S. (2007). Rapid 20th-Century Increase in Coastal Upwelling off Northwest Africa. *Science*, *315*(5812), 637–639. https://doi.org/10.1126/science.1134839

Minoshima, K., Kawahata, H., & Ikehara, K. (2007). Changes in biological production in the mixed water region (MWR) of the northwestern North Pacific during the last 27 kyr. *Palaeogeography, Palaeoclimatology, Palaeoecology*, *254*(3-4), 430–447.

Mohtadi, M., Prange, M., Oppo, D. W., Pol-Holz, D., Merkel, U., Zhang, X., Steinke, S., Lückge, A., et al. (2014). North Atlantic forcing of tropical Indian Ocean climate. *Nature*, *509*(7498), 76–80.

Moore, J. K., Fu, W., Primeau, F., Britten, G. L., Lindsay, K., Long, M., Doney, S. C., Mahowald, N., Hoffman, F., & Randerson, J. T. (2018). Sustained climate warming drives declining marine biological productivity. *Science*, *359*(6380), 1139–1143.

Moossen, H., Bendle, J., Seki, O., Quillmann, U., & Kawamura, K. (2015). North Atlantic Holocene climate evolution recorded by high-resolution terrestrial and marine biomarker records. *Quaternary Science Reviews*, *129*, 111–127.

Müller, P. J., Kirst, G., Ruhland, G., Von Storch, I., & Rosell-Melé, A. (1998). Calibration of the alkenone paleotemperature index $U_{37}^{K'}$ based on core-tops from the eastern South Atlantic and the global ocean (60° N-60° S). *Geochimica et Cosmochimica Acta*, *62*(10), 1757–1772.

O.B.G.P. (2015). MODIS Aqua level 3 global daily mapped 4 km chlorophyll a v2014.0. ver. 2014.0. po.daac, ca, usa. *Dataset accessed [2018-07-26]*.

O'Mara, N. A., Cheung, A. H., Kelly, C. S., Sandwick, S., Herbert, T. D., Russell, J. M., Abella-Gutiérrez, J., Dee, S. G., Swarzenski, P. W., & Herguera, J. C. (2019). Subtropical Pacific Ocean Temperature Fluctuations in the Common Era: Multidecadal Variability and Its Relationship With Southwestern North American Megadroughts. *Geophysical Research Letters*, *46*(24), 14662–14673. https://doi.org/https://doi.org/10.1029/2019GL084828

Osman, M. B., Tierney, J. E., Zhu, J., Tardif, R., Hakim, G. J., King, J., & Poulsen, C. J. (2021). Globally resolved surface temperatures since the Last Glacial Maximum. *Nature*, *599*(7884), 239–244. https://doi.org/10.1038/s41586-021-03984-4

Overpeck, J., Anderson, D., Trumbore, S., & Prell, W. (1996). The southwest Indian Monsoon over the last 18 000 years. *Climate Dynamics*, *12*(3), 213–225.

Paulson, C. A., & Simpson, J. J. (1977). Irradiance measurements in the upper ocean. *Journal of Physical Oceanography*, *7*(6), 952–956. https://doi.org/10.1175/1520-0485(1977)007⟨0952:IMITUO⟩2.0.CO;2

Pelejero, C., Grimalt, J. O., Heilig, S., Kienast, M., & Wang, L. (1999). High-resolution $U_{37}^{K'}$ temperature reconstructions in the South China Sea over the past 220 kyr. *Paleoceanography*, *14*(2), 224–231. https://doi.org/https://doi.org/10.1029/1998PA900015

Pozo Buil, M., & Di Lorenzo, E. (2017). Decadal dynamics and predictability of oxygen and subsurface tracers in the California Current System. *Geophysical Research Letters*, *44*(9), 4204–4213.

Praetorius, S. K., Mix, A. C., Walczak, M., Wolhowe, M. D., Addison, J. A., & Prahl, F. G. (2015). North Pacific deglacial hypoxic events linked to abrupt ocean warming. *Nature*, *527*(7578), 362–366.

Prahl, F. G., Rontani, J.-F., Zabeti, N., Walinsky, S., & Sparrow, M. (2010). Systematic pattern in $U_{37}^{K'}$ –Temperature residuals for surface sediments from high

latitude and other oceanographic settings. *Geochimica et Cosmochimica Acta*, *74*(1), 131–143.

Ragueneau, O., Tréguer, P., Leynaert, A., Anderson, R., Brzezinski, M., DeMaster, D., Dugdale, R., Dymond, J., Fischer, G., Francois, R., et al. (2000). A review of the Si cycle in the modern ocean: recent progress and missing gaps in the application of biogenic opal as a paleoproductivity proxy. *Global and Planetary Change*, *26*(4), 317–365.

Raja, M., & Rosell-Melé, A. (2021). Appraisal of sedimentary alkenones for the quantitative reconstruction of phytoplankton biomass. *Proceedings of the National Academy of Sciences*, *118*(2).

Reimer, P. J., Austin, W. E., Bard, E., Bayliss, A., Blackwell, P. G., Ramsey, C. B., Butzin, M., Cheng, H., Edwards, R. L., Friedrich, M., et al. (2020). The IntCal20 Northern Hemisphere radiocarbon age calibration curve (0–55 cal kBP). *Radiocarbon*, *62*(4), 725–757.

Ren, J., Gersonde, R., Esper, O., & Sancetta, C. (2014). Diatom distributions in northern North Pacific surface sediments and their relationship to modern environmental variables. *Palaeogeography, Palaeoclimatology, Palaeoecology*, *402*, 81–103.

Renault, L., Deutsch, C., McWilliams, J. C., Frenzel, H., Liang, J.-H., & Colas, F. (2016). Partial decoupling of primary productivity from upwelling in the California Current system. *Nature Geoscience*, *9*(7), 505–508.

Reynolds, R. W., Rayner, N. A., Smith, T. M., Stokes, D. C., & Wang, W. (2002). An improved in situ and satellite SST analysis for climate. *Journal of climate*, *15*(13), 1609–1625.

Riethdorf, J.-R., Max, L., Nürnberg, D., Lembke-Jene, L., & Tiedemann, R. (2013). Deglacial development of (sub) sea surface temperature and salinity in the subarctic northwest Pacific: Implications for upper-ocean stratification. *Paleoceanography*, *28*(1), 91–104. https://doi.org/https://doi.org/10.1002/palo.20014

Rigual-Hernández, A., Colmenero-Hidalgo, E., Martrat, B., Bárcena, M., de Vernal, A., Sierro, F., Flores, J., Grimalt, J., Henry, M., & Lucchi, R. (2017). Svalbard ice-sheet decay after the Last Glacial Maximum: New insights from micropalaeontological and organic biomarker paleoceanographical reconstructions. *Palaeogeography, Palaeoclimatology, Palaeoecology*, *465*, 225–236.

Risebrobakken, B., Jansen, E., Andersson, C., Mjelde, E., & Hevrøy, K. (2003). A high-resolution study of Holocene paleoclimatic and paleoceanographic changes

in the Nordic Seas. *Paleoceanography*, *18*(1). https://doi.org/https://doi.org/10.1029/2002PA000764

Rodrigo-Gámiz, M., Martínez-Ruiz, F., Rampen, S., Schouten, S., & Sinninghe Damsté, J. (2014). Sea surface temperature variations in the western Mediterranean Sea over the last 20 kyr: A dual-organic proxy ($U_{37}^{K'}$ and LDI) approach. *Paleoceanography*, *29*(2), 87–98.

Rodrigues, T., Grimalt, J. O., Abrantes, F., Naughton, F., & Flores, J.-A. (2010). The last glacial–interglacial transition (LGIT) in the western mid-latitudes of the North Atlantic: Abrupt sea surface temperature change and sea level implications. *Quaternary Science Reviews*, *29*(15-16), 1853–1862.

Rodríguez-Sanz, L., Mortyn, P. G., Herguera, J. C., & Zahn, R. (2013). Hydrographic changes in the tropical and extratropical Pacific during the last deglaciation. *Paleoceanography*, *28*(3), 529–538.

Rosell-Melé, A., & Prahl, F. G. (2013). Seasonality of $U_{37}^{K'}$ temperature estimates as inferred from sediment trap data. *Quaternary Science Reviews*, *72*, 128–136.

Rosenthal, Y., Oppo, D. W., & Linsley, B. K. (2003). The amplitude and phasing of climate change during the last deglaciation in the Sulu Sea, western equatorial Pacific. *Geophysical Research Letters*, *30*(8).

Routson, C. C., Kaufman, D. S., McKay, N. P., Erb, M. P., Arcusa, S. H., Brown, K. J., Kirby, M. E., Marsicek, J. P., Anderson, R. S., Jiménez-Moreno, G., Rodysill, J. R., Lachniet, M. S., Fritz, S. C., Bennet, J. R., Goman, M. F., Metcalfe, S. E., Galloway, J. M., Schoups, G., Wahl, D. B., … Gavin, D. G. (2021). A multiproxy database of western North American Holocene paleoclimate records. *Earth System Science Data*, *13*(4), 1613–1632. https://doi.org/10.5194/essd-2020-215

Routson, C. C., McKay, N. P., Kaufman, D. S., Erb, M. P., Goosse, H., Shuman, B. N., Rodysill, J. R., & Ault, T. (2019). Mid-latitude net precipitation decreased with Arctic warming during the Holocene. *Nature*, *568*(7750), 83–87.

Rühlemann, C., Mulitza, S., Müller, P. J., Wefer, G., & Zahn, R. (1999). Warming of the tropical Atlantic Ocean and slowdown of thermohaline circulation during the last deglaciation. *Nature*, *402*(6761), 511–514.

Rykaczewski, R. R., & Dunne, J. P. (2010). Enhanced nutrient supply to the California Current Ecosystem with global warming and increased stratification in an earth system model. *Geophysical Research Letters*, *37*(21). https://doi.org/https://doi.org/10.1029/2010GL045019

Sachs, J. P. (2007). Cooling of Northwest Atlantic slope waters during the Holocene. *Geophysical research letters*, *34*(3).

Saraswat, R., Lea, D. W., Nigam, R., Mackensen, A., & Naik, D. K. (2013). Deglaciation in the tropical Indian Ocean driven by interplay between the regional monsoon and global teleconnections. *Earth and Planetary Science Letters*, *375*, 166–175.

Schlunegger, S., Rodgers, K. B., Sarmiento, J. L., Ilyina, T., Dunne, J. P., Takano, Y., Christian, J. R., Long, M. C., Frölicher, T. L., Slater, R., & Lehner, F. (2020). Time of Emergence and Large Ensemble Intercomparison for Ocean Biogeochemical Trends. *Global Biogeochemical Cycles*, *34*(8), e2019GB006453. https://doi.org/https://doi.org/10.1029/2019GB006453

Schmidt, M. W., Chang, P., Hertzberg, J. E., Them, T. R., Ji, L., & Otto-Bliesner, B. L. (2012). Impact of abrupt deglacial climate change on tropical Atlantic subsurface temperatures. *Proceedings of the National Academy of Sciences*, *109*(36), 14348–14352.

Schmidt, M. W., & Lynch-Stieglitz, J. (2011). Florida Straits deglacial temperature and salinity change: Implications for tropical hydrologic cycle variability during the Younger Dryas. *Paleoceanography*, *26*(4).

Schmidt, M. W., Spero, H. J., & Lea, D. W. (2004). Links between salinity variation in the Caribbean and North Atlantic thermohaline circulation. *Nature*, *428*(6979), 160–163.

Schmidt, M. W., Weinlein, W. A., Marcantonio, F., & Lynch-Stieglitz, J. (2012). Solar forcing of Florida Straits surface salinity during the early Holocene. *Paleoceanography*, *27*(3).

Schneider, B., Leduc, G., & Park, W. (2010). Disentangling seasonal signals in Holocene climate trends by satellite-model-proxy integration. *Paleoceanography*, *25*(4). https://doi.org/https://doi.org/10.1029/2009PA001893

Schoepfer, S. D., Shen, J., Wei, H., Tyson, R. V., Ingall, E., & Algeo, T. J. (2015). Total organic carbon, organic phosphorus, and biogenic barium fluxes as proxies for paleomarine productivity. *Earth-Science Reviews*, *149*, 23–52.

Schubert, C., Villanueva, J., Calvert, S., Cowie, G., Von Rad, U., Schulz, H., Berner, U., & Erlenkeuser, H. (1998). Stable phytoplankton community structure in the Arabian Sea over the past 200,000 years. *Nature*, *394*(6693), 563–566.

Schwab, C., Kinkel, H., Weinelt, M., & Repschläger, J. (2012). Coccolithophore paleoproductivity and ecology response to deglacial and Holocene changes in the Azores Current System. *Paleoceanography*, *27*(3).

Segschneider, J., Schneider, B., & Khon, V. (2018). Climate and marine biogeochemistry during the Holocene from transient model simulations. *Biogeosciences*, *15*(10), 3243–3266. https://doi.org/10.5194/bg-15-3243-2018

Sejrup, H., Haflidason, H., & Andrews, J. (2011). A Holocene North Atlantic SST record and regional climate variability. *Quaternary Science Reviews*, *30*(21-22), 3181–3195.

Seki, O., Nakatsuka, T., Kawamura, K., Saitoh, S.-I., & Wakatsuchi, M. (2007). Time-series sediment trap record of alkenones from the western Sea of Okhotsk. *Marine Chemistry*, *104*(3-4), 253–265.

Shintani, T., Yamamoto, M., & Chen, M.-T. (2011). Paleoenvironmental changes in the northern South China Sea over the past 28,000 years: A study of TEX86-derived sea surface temperatures and terrestrial biomarkers. *Journal of Asian Earth Sciences*, *40*(6), 1221–1229. https://doi.org/10.1016/j.jseaes.2010.09.013

Staubwasser, M., Sirocko, F., Grootes, P. M., & Segl, M. (2003). Climate change at the 4.2 ka BP termination of the Indus valley civilization and Holocene south Asian monsoon variability. *Geophysical Research Letters*, *30*(8).

Stein, R., & Rack, F. R. (1995). A 160,000-Year High-Resolution Record of Quantity and Composition of Organic Carbon in the Santa Barbara Basin (Site 893). *Proceedings of the Ocean Drilling Program, Scientific Results*, *146*(Pt 2).

Steinke, S., Kienast, M., Groeneveld, J., Lin, L.-C., Chen, M.-T., & Rendle-Bühring, R. (2008). Proxy dependence of the temporal pattern of deglacial warming in the tropical South China Sea: toward resolving seasonality. *Quaternary Science Reviews*, *27*(7-8), 688–700.

Stock, C. A., Dunne, J., & John, J. (2014). Drivers of trophic amplification of ocean productivity trends in a changing climate. *Biogeosciences*, *11*(24), 7125–7135.

Stock, C. A., John, J. G., Rykaczewski, R. R., Asch, R. G., Cheung, W. W., Dunne, J. P., Friedland, K. D., Lam, V. W., Sarmiento, J. L., & Watson, R. A. (2017). Reconciling fisheries catch and ocean productivity. *Proceedings of the National Academy of Sciences*, *114*(8), E1441–E1449.

Stott, L., Timmermann, A., & Thunell, R. (2007). Southern Hemisphere and deep-sea warming led deglacial atmospheric CO2 rise and tropical warming. *science*, *318*(5849), 435–438.

Sun, Y., Oppo, D. W., Xiang, R., Liu, W., & Gao, S. (2005). Last deglaciation in the Okinawa Trough: Subtropical northwest Pacific link to Northern Hemisphere

and tropical climate. *Paleoceanography*, *20*(4). https://doi.org/https://doi.org/10.1029/2004PA001061

Swain, D. L., Horton, D. E., Singh, D., & Diffenbaugh, N. S. (2016). Trends in atmospheric patterns conducive to seasonal precipitation and temperature extremes in California. *Science Advances*, *2*(4), e1501344.

Sydeman, W., García-Reyes, M., Schoeman, D., Rykaczewski, R., Thompson, S., Black, B., & Bograd, S. (2014). Climate change and wind intensification in coastal upwelling ecosystems. *Science*, *345*(6192), 77–80.

Thompson, A. J., Zhu, J., Poulsen, C. J., Tierney, J. E., & Skinner, C. B. (2022). Northern Hemisphere vegetation change drives a Holocene thermal maximum. *Science advances*, *8*(15), eabj6535. https://doi.org/10.1126/sciadv.abj6535

Thornalley, D. J., Elderfield, H., & McCave, I. N. (2010). Intermediate and deep water paleoceanography of the northern North Atlantic over the past 21,000 years. *Paleoceanography*, *25*(1).

Tierney, J. E., Pausata, F. S., & Demenocal, P. (2016). Deglacial Indian monsoon failure and North Atlantic stadials linked by Indian Ocean surface cooling. *Nature Geoscience*, *9*(1), 46–50.

Tierney, J. E., & Tingley, M. P. (2018a). BAYSPLINE: A New Calibration for the Alkenone Paleothermometer. *Paleoceanography and Paleoclimatology*, *33*(3), 281–301. https://doi.org/https://doi.org/10.1002/2017PA003201

Tierney, J. E., & Tingley, M. P. (2018b). BAYSPLINE: A New Calibration for the Alkenone Paleothermometer. *Paleoceanography and Paleoclimatology*, *33*(3), 281–301. https://doi.org/https://doi.org/10.1002/2017PA003201

Timmermann, A., Sachs, J., & Timm, O. E. (2014). Assessing divergent SST behavior during the last 21 ka derived from alkenones and G. ruber-Mg/Ca in the equatorial Pacific. *Paleoceanography*, *29*(6), 680–696. https://doi.org/https://doi.org/10.1002/2013PA002598

Tiwari, M., Nagoji, S. S., & Ganeshram, R. S. (2015). Multi-centennial scale SST and Indian summer monsoon precipitation variability since the mid-Holocene and its nonlinear response to solar activity. *The Holocene*, *25*(9), 1415–1424.

Trachsel, M., & Telford, R. J. (2017). All age–depth models are wrong, but are getting better. *The Holocene*, *27*(6), 860–869.

Tsutsui, H., Takahashi, K., Asahi, H., Jordan, R. W., Nishida, S., Nishiwaki, N., & Yamamoto, S. (2016). Nineteen-year time-series sediment trap study of Coccolithus pelagicus and Emiliania huxleyi (calcareous nannoplankton) fluxes in

the Bering Sea and subarctic Pacific Ocean. *Deep Sea Research Part II: Topical Studies in Oceanography*, *125*, 227–239.

Vargas, G., Pantoja, S., Rutllant, J. A., Lange, C. B., & Ortlieb, L. (2007). Enhancement of coastal upwelling and interdecadal ENSO-like variability in the Peru-Chile Current since late 19th century. *Geophys. Res. Lett.*, *34*, L13607. https://doi.org/10.1029/2006GL028812

Wallace, J. M., & Gutzler, D. S. (1981). Teleconnections in the geopotential height field during the Northern Hemisphere winter. *Monthly weather review*, *109*(4), 784–812.

Wanner, H., Beer, J., Bütikofer, J., Crowley, T. J., Cubasch, U., Flückiger, J., Goosse, H., Grosjean, M., Joos, F., Kaplan, J. O., et al. (2008). Mid-to Late Holocene climate change: an overview. *Quaternary Science Reviews*, *27*(19-20), 1791–1828.

Ware, D. M., & Thomson, R. E. (2005). Bottom-Up Ecosystem Trophic Dynamics Determine Fish Production in the Northeast Pacific. *Science*, *308*(5726), 1280–1284. https://doi.org/10.1126/science.1109049

Weldeab, S., Lea, D. W., Schneider, R. R., & Andersen, N. (2007). 155,000 years of West African monsoon and ocean thermal evolution. *science*, *316*(5829), 1303–1307.

Weldeab, S., Schneider, R. R., Kölling, M., & Wefer, G. (2005). Holocene African droughts relate to eastern equatorial Atlantic cooling. *Geology*, *33*(12), 981–984.

Werner, K., Spielhagen, R. F., Bauch, D., Hass, H. C., & Kandiano, E. (2013). Atlantic Water advection versus sea-ice advances in the eastern Fram Strait during the last 9 ka: Multiproxy evidence for a two-phase Holocene. *Paleoceanography*, *28*(2), 283–295. https://doi.org/https://doi.org/10.1002/palo.20028

Wood, R. (2012). Stratocumulus clouds. *Monthly Weather Review*, *140*(8), 2373–2423.

Xie, S.-P., Deser, C., Vecchi, G. A., Ma, J., Teng, H., & Wittenberg, A. T. (2010). Global warming pattern formation: Sea surface temperature and rainfall. *Journal of Climate*, *23*(4), 966–986.

Xiu, P., Chai, F., Curchitser, E. N., & Castruccio, F. S. (2018). Future changes in coastal upwelling ecosystems with global warming: The case of the California Current System. *Scientific reports*, *8*(1), 1–9.

Yamamoto, M., Sai, H., Chen, M.-T., & Zhao, M. (2013). The East Asian winter monsoon variability in response to precession during the past 150 000 yr. *Climate of the Past*, *9*(6), 2777–2788.

Zhao, M., Beveridge, N., Shackleton, N., Sarnthein, M., & Eglinton, G. (1995). Molecular stratigraphy of cores off northwest Africa: Sea surface temperature history over the last 80 ka. *Paleoceanography*, *10*(3), 661–675.

Ziegler, M., Nürnberg, D., Karas, C., Tiedemann, R., & Lourens, L. J. (2008). Persistent summer expansion of the Atlantic Warm Pool during glacial abrupt cold events. *Nature Geoscience*, *1*(9), 601–605.

Supplementary Information

Introduction

The supporting information contains two tables and three figures. Table S3.1 includes information on which SST records were included in creating SST latitudinal bands. Table S3.2 provides information about the reservoir age corrections used for each site. Figure S3.1 shows a comparison between core top Uk'37 SST using the calibration from Müller et al. (1998) and observed mean annual SST. Figure S3.2 shows the root mean square error (RMSE) between the EOF and the original model output. Figures S3.3-S3.4 show characteristics and information of the SST latitudinal bands in timeseries format.

Site Name	Lat (°N)	Lon (°E)	Proxy	Ocean	Reference
			60-80°N		
MSM05-5-712-2	78.92	6.77	Mg/Ca, δ^{18}O	Arctic	Werner et al. (2013)
GIK3258-2	75.00	13.97	$U_{37}^{K'}$, δ^{18}O	Atlantic	Martrat et al. (2003)
SV04	74.96	13.90	$U_{37}^{K'}$	Atlantic	Rigual-Hernández et al. (2017)
MD95-2011	66.97	7.64	$U_{37}^{K'}$, δ^{18}O	Atlantic	Risebrobakken et al. (2003)
B997-321	66.89	-18.97	δ^{18}O	Arctic	Castañeda et al. (2004)
B997-327	66.64	-20.86	δ^{18}O	Arctic	Castañeda et al. (2004)
MD99-2269	66.64	-20.86	Mg/Ca, δ^{18}O	Arctic	Kristjánsdóttir et al. (2017)
B997-324	66.52	-21.14	δ^{18}O	Arctic	Castañeda et al. (2004)
MD99-2266	66.23	-23.27	$U_{37}^{K'}$	Arctic	Moossen et al. (2015)
P1003	63.76	5.26	δ^{18}O	Atlantic	Sejrup et al. (2011)
RAPiD-12-1K	62.09	-17.82	Mg/Ca, δ^{18}O	Atlantic	Thornalley et al. (2010)
ODP984	61.43	-24.08	Mg/Ca, δ^{18}O	Atlantic	Came et al. (2007)
			40-60°N		
EW0408-85JC	59.56	-144.15	δ^{18}O	Pacific	Praetorius et al. (2015)
HU90-013-013	58.21	-48.37	δ^{18}O	Atlantic	Hillaire-Marcel et al. (1994)

Site Name	Lat (°N)	Lon (°E)	Proxy	Ocean	Reference
EW0408-66JC	57.87	-137.10	δ^{18}O	Pacific	Praetorius et al. (2015)
IOW225514	57.83	8.70	$U^{K'}_{37}$	Atlantic	Emeis et al. (2003)
IOW225517	57.66	7.09	$U^{K'}_{37}$	Atlantic	Emeis et al. (2003)
MD99-2251	57.45	-27.91	Mg/Ca	Atlantic	Farmer et al. (2008)
KNR166-14-11JPC	56.23	-27.65	δ^{18}O	Atlantic	Elmore et al. (2015)
GIK17051-3	56.16	-31.99	δ^{18}O	Atlantic	Jung (1996)
GIK17049-6	55.26	-26.73	δ^{18}O	Atlantic	Jung (1996)
HU87033-87018PC	54.80	-56.06	δ^{18}O	Atlantic	Andrews et al. (1999)
HU87033-87017PC	54.62	-56.18	δ^{18}O	Atlantic	Andrews et al. (1999)
LV29-114-3	49.38	152.88	Mg/Ca, $U^{K'}_{37}$	Pacific	Riethdorf et al. (2013)
MD01-2412	44.53	145.00	$U^{K'}_{37}$	Pacific	Harada et al. (2006)
OCE326-GGC30	43.89	-62.80	$U^{K'}_{37}$	Atlantic	Sachs (2007)
OCE326-GGC26	43.48	-54.87	$U^{K'}_{37}$, δ^{18}O	Atlantic	Keigwin et al. (2005)
HU73-031-7	42.98	-55.5	δ^{18}O	Atlantic	Keigwin and Jones (1995)
ODP1019C	41.68	-124.93	$U^{K'}_{37}$	Pacific	Barron et al. (2003)
KT05-6-PC-02	41.00	140.77	$U^{K'}_{37}$	Pacific	Kawahata et al. (2009)
PC6	40.40	143.50	$U^{K'}_{37}$	Pacific	Minoshima et al. (2007)
			20-40°N		
MD03-2699	39.04	-10.66	$U^{K'}_{37}$	Atlantic	Rodrigues et al. (2010)
D13882	38.63	-9.45	$U^{K'}_{37}$	Atlantic	Rodrigues et al. (2010)
BS79-38	38.40	13.60	$U^{K'}_{37}$	Atlantic	Cacho et al. (2001)
GEOFAR-KF16	38.00	-31.13	Mg/Ca	Atlantic	Schwab et al. (2012)
SU81-18	37.77	-10.18	$U^{K'}_{37}$	Atlantic	Bard et al. (2000)
MD01-2444	37.57	-10.13	$U^{K'}_{37}$	Atlantic	Martrat et al. (2007)
M40-4-SL78	37.04	13.19	$U^{K'}_{37}$	Atlantic	Emeis and Dawson (2003)
MD99-2341	36.39	-7.07	δ^{18}O	Atlantic	Eynaud et al. (2009)
GeoB5901-2	36.38	-7.07	$U^{K'}_{37}$	Atlantic	Kim et al. (2004)

Site Name	Lat (°N)	Lon (°E)	Proxy	Ocean	Reference
M39008-3	36.38	-7.07	$U^{K'}_{37}$, $\delta^{18}O$	Atlantic	Eynaud et al. (2009)
ODP976	36.21	-4.31	$U^{K'}_{37}$, Mg/Ca	Atlantic	Martrat et al. (2014)
TTR17-434G	36.21	-4.31	LDI, $U^{K'}_{37}$	Atlantic	Rodrigo-Gámiz et al. (2014)
MD95-2043	36.14	-2.62	Mg/Ca, $\delta^{18}O$	Atlantic	Cacho et al. (1999)
MD01-2421	36.03	141.78	$U^{K'}_{37}$, $\delta^{18}O$	Pacific	Isono et al. (2009)
MD99-2339	35.89	-7.53	$\delta^{18}O$	Atlantic	Eynaud et al. (2009)
SSDP-102	34.95	128.88	$U^{K'}_{37}$	Pacific	Kim et al. (2004)
MD02-2503	34.39	-120.04	$\delta^{18}O$	Pacific	Hill et al. (2006)
ODP893A	34.29	-120.04	$\delta^{18}O$	Pacific	Kennett et al. (2007)
GeoB7702-3	31.65	34.07	TEX_{86}	Atlantic	Castañeda et al. (2010)
MD98-2195	31.64	128.94	$U^{K'}_{37}$, TEX_{86}	Pacific	Ijiri et al. (2005)
KY07-04-PC1	31.63	128.95	Mg/Ca	Pacific	Kubota et al. (2010)
PC1	31.46	128.41	$\delta^{18}O$	Pacific	F. Chang et al. (2015)
Cape Ghir	30.85	-10.27	$U^{K'}_{37}$	Atlantic	Kim et al. (2007)
MD02-2575	29.00	-87.12	Mg/Ca, $\delta^{18}O$	Atlantic	Ziegler et al. (2008)
A7	27.82	126.98	Mg/Ca	Pacific	Sun et al. (2005)
GeoB5844-2	27.71	34.68	$U^{K'}_{37}$, $\delta^{18}O$	Indian	Arz et al. (2003)
MD02-2515	27.48	-112.07	$U^{K'}_{37}$, TEX_{86}	Pacific	McClymont et al. (2012)
EN43-PC6	26.95	-91.35	Mg/Ca, $\delta^{18}O$	Atlantic	Flower et al. (2004)
KNR159-JPC26	26.37	-92.03	Mg/Ca, $\delta^{18}O$	Atlantic	Antonarakou et al. (2015)
MV99-PC14	25.20	-112.72	Mg/Ca	Pacific	Marchitto et al. (2010)
SO90-56KA	24.61	65.92	$U^{K'}_{37}$	Indian	Doose-Rolinski et al. (2001)
SO90-63KA	24.61	65.98	$\delta^{18}O$	Indian	Staubwasser et al. (2003)
KNR166-JPC51	24.41	-83.22	Mg/Ca, $\delta^{18}O$	Atlantic	Schmidt, Weinlein, et al. (2012)
KNR166-JPC26	24.33	-83.25	Mg/Ca, $\delta^{18}O$	Atlantic	Schmidt and Lynch-Stieglitz (2011)
ODP658C	20.75	-18.58	$U^{K'}_{37}$	Atlantic	Zhao et al. (1995)
GeoB7926-2	20.21	-18.45	$U^{K'}_{37}$, TEX_{86}	Atlantic	Kim et al. (2012)
GIK17940-2	20.12	119.36	$U^{K'}_{37}$	Pacific	Pelejero et al. (1999)
MD97-2146	20.12	117.38	TEX_{86}, $U^{K'}_{37}$	Pacific	Shintani et al. (2011)

Site Name	Lat (°N)	Lon (°E)	Proxy	Ocean	Reference
			0-20°N		
RC27-23	17.99	57.59	$\delta^{18}O$	Indian	Overpeck et al. (1996)
RC27-28	17.90	57.59	$\delta^{18}O$	Indian	Overpeck et al. (1996)
SO42-74KL	14.32	57.35	$U^{K'}_{37}$, TEX_{86}, $\delta^{18}O$	Indian	Huguet et al. (2006)
ODP999A	12.74	-78.74	Mg/Ca, $\delta^{18}O$	Atlantic	Schmidt et al. (2004)
SN-6	12.49	74.13	Mg/Ca	Indian	Tiwari et al. (2015)
M35003-4	12.09	-61.24	$U^{K'}_{37}$, $\delta^{18}O$	Atlantic	Rühlemann et al. (1999)
P178-15P	11.96	44.30	$U^{K'}_{37}$, TEX_{86}, Mg/Ca, $\delta^{18}O$	Indian	Tierney et al. (2016)
VM28-122	11.93	-78.68	Mg/Ca, $\delta^{18}O$	Atlantic	Schmidt et al. (2004)
VM12-107	11.33	-66.63	Mg/Ca, $\delta^{18}O$	Atlantic	Schmidt, Chang, et al. (2012)
SK237-GC04	10.98	75.00	Mg/Ca, $\delta^{18}O$	Indian	Saraswat et al. (2013)
NIOP-C2-905-PC	10.78	51.93	$U^{K'}_{37}$, TEX_{86}	Indian	Huguet et al. (2006)
ODP1002C	10.71	-65.17	$U^{K'}_{37}$	Atlantic	Herbert and Schuffert (2000)
PL07-39PC	10.70	-65.94	Mg/Ca, $\delta^{18}O$	Atlantic	Lea et al. (2003)
MD97-2141	8.80	121.30	Mg/Ca, $\delta^{18}O$	Pacific	Rosenthal et al. (2003)
MD97-2151	8.73	109.87	$U^{K'}_{37}$, TEX_{86}	Pacific	Yamamoto et al. (2013)
ME0005A-43JC	7.86	-83.61	$U^{K'}_{37}$, Mg/Ca, $\delta^{18}O$	Pacific	Benway et al. (2006)
MD01-2390	6.64	113.41	Mg/Ca, $\delta^{18}O$	Pacific	Steinke et al. (2008)
MD06-3067	6.48	125.83	Mg/Ca	Pacific	Bolliet et al. (2011)
MD06-3075	6.48	125.83	$U^{K'}_{37}$, $\delta^{18}O$	Pacific	Fraser et al. (2014)
MD98-2181	6.30	125.82	Mg/Ca	Pacific	Stott et al. (2007)
GIK18287-3	5.66	110.66	$U^{K'}_{37}$, $\delta^{18}O$	Pacific	Kienast and McKay (2001)
MD98-2178	3.62	118.70	Mg/Ca, $\delta^{18}O$	Pacific	Fan et al. (2018)
SO189-119KL	3.52	96.32	Mg/Ca, $\delta^{18}O$	Indian	Mohtadi et al. (2014)
MD03-2707	2.50	9.39	Mg/Ca, $\delta^{18}O$	Atlantic	Weldeab et al. (2007)
GeoB4905-4	2.50	9.37	Mg/Ca, $\delta^{18}O$	Atlantic	Weldeab et al. (2005)

SO189-144KL	1.16	98.07	δ^{18}O	Indian	Mohtadi et al. (2014)

Table S3.1: List of SST and hydroclimate proxy records used.

Table S3.2: Regional radiocarbon marine reservoir correction (ΔR) and standard error (σ) at each site

Site Name	Δ R	σ
EW0408-85JC	287	40
MD02-2496	247	71
ODP1034	251	45
ODP1019[1]	1198 (248)	31 (31)
TN062-O550	174	92
MD02-2505	106	119
GC41/PC14[2]	106 (306)	119
PCM00-78C/PCM00-78K	106	119

1. numbers in parenthesis indicate ΔR and σ used for radiocarbon ages taken from depths $\geq$4.17m. See Barron et al. (2003) for details.

2. numbers in parenthesis indicate ΔR used for radiocarbon ages in benthic foraminifera. See Marchitto et al. (2010) for details.

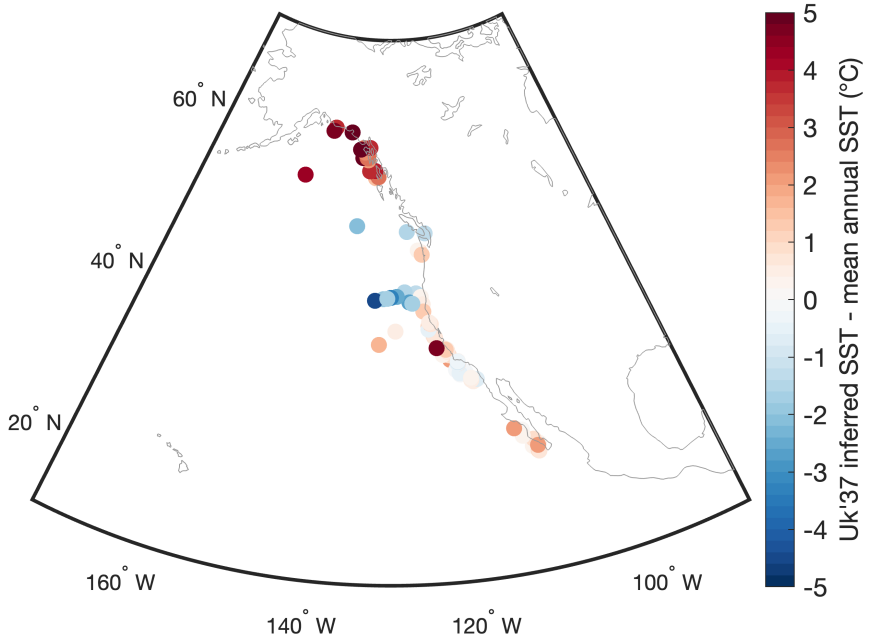

Figure S3.1: Comparison between core top $U_{37}^{k'}$ SST and observed mean annual SST. Core top data were taken from Tierney and Tingley (2018b).

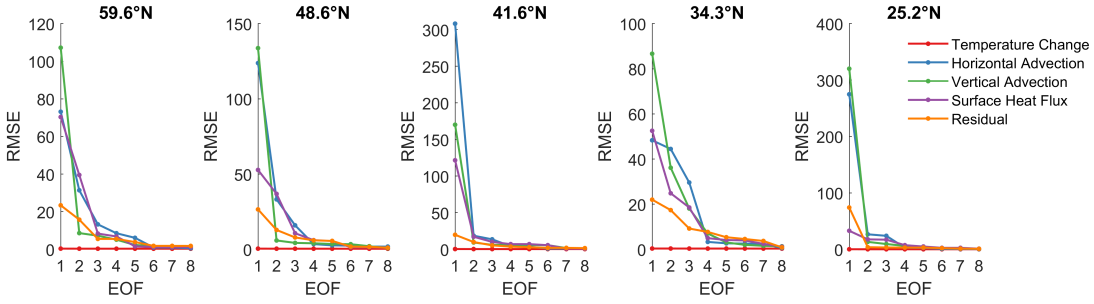

Figure S3.2: Root Mean Square Error of heat budget terms based on the number of EOF retained at each proxy location.

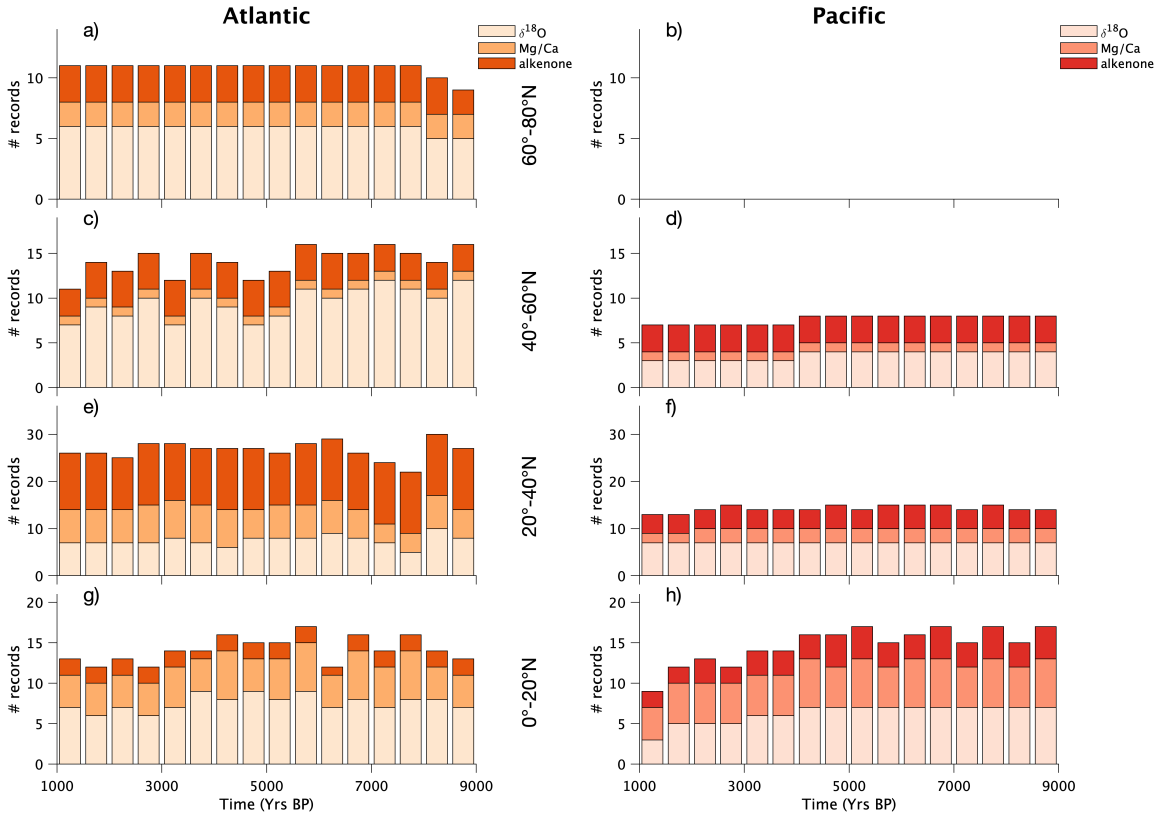

Figure S3.3: Number of proxy records (by proxies) at each time slice in the Atlantic and the Pacific.

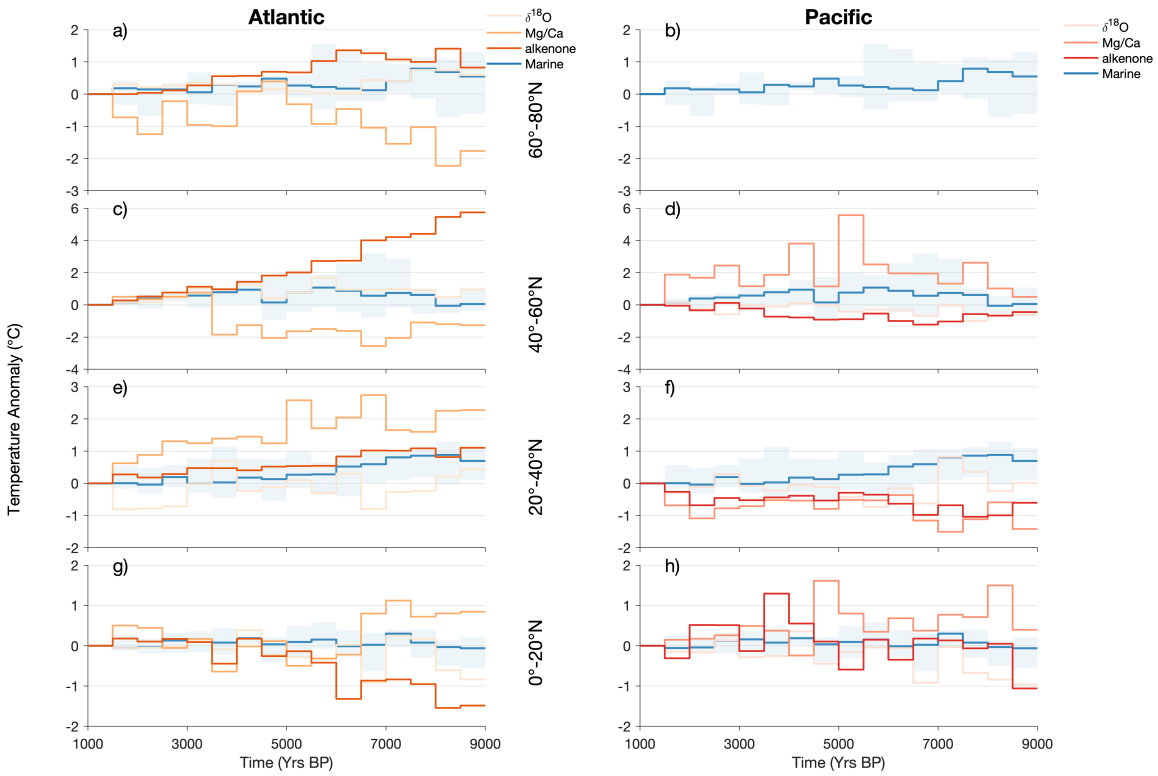

Figure S3.4: Averaged timeseries based on the ocean basin and proxy type compared to the averaged timeseries of all SST proxies.

Chapter 4

Spatiotemporal Evolution and Drivers of Western North America Hydroclimate and Pacific Sea Surface Temperature during the Holocene

Anson H. Cheung[1,2], Xiaojing Du[1,2], Meredith C. Parish[1,2], Richard S. Vachula[3], Baylor Fox-Kemper[1,2], Timothy D. Herbert[1,2]

1. Department of Earth, Environmental, and Planetary Sciences, Brown University, Providence, RI 02912, USA

2. Institute at Brown for Environment and Society, Brown University, Providence, RI 02912, USA

3. Department of Geosciences, Auburn University, Auburn, AL 36849, USA

Abstract

Hydroclimate variations in western North America (wNA) have significant impacts on agriculture, water resources, ecosystems, and the economy, but how wNA hydroclimate, especially precipitation, will change in the future remains unclear. Modeling evidence suggests part of this uncertainty arises from the dependence of precipitation on changes in the Pacific Ocean sea surface temperature (SST). However, the fidelity of projected Pacific SST patterns remains debated, which hinders our ability to understand future wNA hydroclimate. Here, we investigate changes in wNA hydroclimate and its relationship with Pacific SST over the Holocene by analyzing a compilation of proxy records from both regions. Monte Carlo empirical orthogonal function analyses suggest a coherent temporal evolution between wNA hydroclimate and Pacific SST, with spatial patterns consistent with our current understanding between these two regions. By projecting model based idealized forcing fingerprints onto proxy records, we also highlight the importance of precession and the previously underappreciated role of carbon dioxide in driving wNA hydroclimate change. These results together emphasize the importance to consider the coupling between wNA hydroclimate and Pacific SST when understanding climate system responds to external forcings, highlight the need to improve model representation of ocean process, and clarify the role precession and carbon dioxide play in driving Pacific SST and wNA hydroclimate changes during the Holocene.

1 Introduction

Hydroclimate variations in western North America (wNA) have significant impacts on agriculture, water resources, ecosystems, and the economy, but how wNA hydroclimate will change in the future remains unclear. The impacts of hydroclimate changes in the wNA are well exemplified by the ongoing 21st century drought, which has caused substantial crop loss (Howitt et al., 2014), a significant reduction in Colorado River flow which drove a decrease in reservoir levels (Udall & Overpeck, 2017), and unprecedented wildfires (Higuera et al., 2021; Parks & Abatzoglou, 2020). Although there is an increasing consensus that future anthropogenic climate change will cause long-term aridification in wNA due to increasing temperature (Ault et al., 2016; Udall & Overpeck, 2017; Williams et al., 2020), the sign, amplitude, and the driver of future precipitation changes in this region remain uncertain (Cook et al., 2020). Recent analyses of climate model simulations suggest that future precipitation changes in wNA is ultimately determined by changes in the Pacific Ocean sea surface temperature (SST) (Allen & Luptowitz, 2017; Dong & Leung, 2021; Dong et al., 2021; Zappa et al., 2020). Hence, constraining Pacific SST changes is conducive to reducing uncertainty in wNA hydroclimate. However, whether projected Pacific SST patterns from models are accurate remain debated (Heede et al., 2020; Lee et al., 2022; Seager et al., 2019), which hampers our ability to understand future wNA hydroclimate. As such, there is a need to constrain the relationship between Pacific SST and wNA hydroclimate from the longer temporal perspective provided by paleoclimate reconstructions.

The Holocene (past $\sim 11,000$ years) provides an ample time window to understand how wNA hydroclimate and Pacific SST change and co-evolve on timescales exceeding the observational record, and how they respond to external forcings (e.g., orbital, greenhouse gases). Numerous studies have been carried out to reconstruct

wNA hydroclimate and Pacific SST changes (e.g., L. Anderson, 2011; Barron et al., 2003; Fraser et al., 2014; Jiménez-Moreno & Anderson, 2012; Kirby et al., 2012; MacDonald et al., 2016; Parish et al., 2022; Ruan et al., 2015; Sun et al., 2005) and their relationship to external forcings (e.g., Barron & Anderson, 2011; Routson et al., 2019; Shuman & Marsicek, 2016). However, we still do not have good constraints on the spatiotemporal evolution of wNA hydroclimate and Pacific SST during the Holocene and the forcings driving these changes.

A major shortcoming of previous studies is that they have often relied on a single or few proxy records to understand the temporal evolution of Holocene wNA hydroclimate (e.g., L. Anderson, 2011; Jiménez-Moreno & Anderson, 2012; Kirby et al., 2012; MacDonald et al., 2016; Parish et al., 2022) and Pacific SST (e.g., Barron et al., 2003; Fraser et al., 2014; Ruan et al., 2015; Sun et al., 2005). As a result, it is difficult to assess the spatial pattern of these changes. Proxy syntheses and proxy-model comparisons, on the other hand, have often focused on changes in specific periods (e.g., middle Holocene) relative to the present as opposed to analyzing the entire Holocene (Bartlein et al., 2010; Hermann et al., 2018; Palmer et al., 2023). These limitations together have undermined the ability to assess spatiotemporal changes of wNA hydroclimate and Pacific SST during the Holocene. Further, they have led to ambiguous views regarding the role of the atmosphere and ocean in driving wNA hydroclimate changes. Some studies focus solely on the role of changing atmospheric moisture pathway and strength due to orbital forcing on wNA hydroclimate (e.g., Liefert & Shuman, 2020; Routson et al., 2019; Skinner et al., 2020) whereas others explored the how changes in atmosphere-ocean interaction due to orbital forcing influenced the teleconnection strength and consequently wNA hydroclimate (Barron & Anderson, 2011).

Additionally, the potential forcings and mechanisms that drive wNA hydroclimate and Pacific SST changes during the Holocene also remain unclear. Hydroclimate re-

constructions of wNA based on various proxies (e.g., pollen, isotopes, stratigraphy) in lake sediments (e.g., Jiménez-Moreno & Anderson, 2012; Kirby et al., 2012; MacDonald et al., 2016; Parish et al., 2022; Steinman et al., 2016), marine sediments (e.g., Barron et al., 2003; Du et al., 2021; Du et al., 2018), and speleothems (e.g., Asmerom et al., 2007; Ersek et al., 2012; Lachniet et al., 2020) have recorded substantial changes during the Holocene, with the timing of changes corresponding to the evolution of boreal summer insolation driven by orbital forcing. Although similar temporal evolution is also found in many marine sediment based SST reconstructions in the Pacific, Pacific SST changes are more spatially variable, hindering our understanding of the associated climate forcings (Cheung et al., 2022; Davis et al., 2020). In addition, although orbital forcing is often invoked to explain these hydroclimate changes, the relative role of precession and obliquity is unclear.

These uncertainties and shortcomings in previous studies underscores the need for new approaches to constrain the spatiotemporal evolution of wNA hydroclimate and Pacific during the Holocene, their relationship, and the forcings underlying these changes. Here, we compiled existing wNA hydroclimate and Pacific SST proxy records and applied Monte Carlo Empirical Orthogonal Function Analysis (MCEOF) to understand their spatiotemporal evolution and relationship. Then, we applied idealized climate model experiments to determine the forcings driving these changes.

2 Methods

2.1 Proxy Synthesis

We compiled 55 marine SST records (Cheung et al., 2022; Kaufman et al., 2020; Zhang et al., 2021) and 90 terrestrial hydroclimate records (Routson et al., 2021) and selected 35 marine SST records and 38 terrestrial hydroclimate records for analyses. We identified and selected alkenone $U^{K'}_{37}$, TEX_{86}, and planktic foraminifera Mg/Ca records from the Pacific Ocean (based on NASA GCMD convention), covering 9000-

2000 years before present (yrs BP) based on their published age model. Hydroclimate conditions were inferred from pollen, diatoms, oxygen isotopes, carbon isotopes, particle size, lake level, total organic carbon, carbon to nitrogen ratio, and macrofossils in lake sediments. Similar to marine proxy records, we only selected records that are within the wNA area using the IPCC reference regions definition (Iturbide et al., 2020), cover 9000-2000 yrs BP, and are interpreted to reflect precipitation or precipitation minus evaporation. This period was chosen to balance the number of records available and the length of the analysis window, as many records do not cover the last 2000 years (Kaufman et al., 2020)

We estimated the chronological and calibration uncertainties in each record. For chronological uncertainty, we recalibrated the age-depth model of each proxy record to IntCal20 (Reimer et al., 2020) and Marine20 (Heaton et al., 2020) using BACON (Blaauw & Christen, 2011), and extracted 1000 iterations of the age-depth model from the posterior distribution. We estimated calibration uncertainty of SST proxy records by recalibrating each SST record with Bayesian based calibrations (Tierney et al., 2019; Tierney & Tingley, 2015, 2018) and assumed a prior of 5°C. Although the prior value is larger than error estimates from other calibrations (e.g., Müller et al., 1998), the focus on anomaly rather than absolute temperature in our analyses reduces the influence from calibration uncertainty on our results. For hydroclimate proxy records, we assumed the uncertainty follows a normal distribution and we assigned a 10% relative standard deviation uncertainty for each measurement. We then generated 1000 iterations of each proxy record based on the posterior distribution for SST records and repeated sampling of the uncertainty distribution for hydroclimate records.

We aligned all the proxy records into a common timestep to carry out our analysis. Specifically, we binned each proxy record into 250-year bins from 2000 yrs BP to 9000 yrs BP. This bin width was chosen to minimize the effects of chronological uncertainty

and the extrapolation needed, given that the median resolution for records from both databases are < 200 years, while still resolving sub-millennial timescale variability (Kaufman et al., 2020; Routson et al., 2021). This approach was repeated using the 1000 iterations of the age-depth model and calibrated timeseries. We only retained proxy records where, on average, 60% or greater of the bins contained data. 11 SST records and 11 hydroclimate records were removed because of this threshold. This resulted in 35 SST records and 38 hydroclimate records (Figure 4.1, Table 4.1). Then, we linearly interpolated the selected binned records to ensure there were no empty values in time bins. Afterwards, we normalized each proxy record by centering the data towards the mean value of 3000-2000 yrs BP so that changes in each record are relative to the most recent 1000 years of the analysis period, and dividing by the standard deviation of the data.

Site Name	Lat (°N)	Lon (°E)	Proxy	Reference
		SST		
A7	27.82	126.98	Mg/Ca	Sun et al. (2005)
BJ8-03-13GGC	-7.40	115.20	Mg/Ca	Linsley et al. (2010)
BJ8-03-70GGC	-3.57	119.38	Mg/Ca	Linsley et al. (2010)
B-3GC	31.48	128.52	$U_{37}^{K'}$	X. Huang et al. (2009)
DGKS9604	28.28	127.02	$U_{37}^{K'}$	Yu et al. (2009)
GIK17940-2	20.12	119.36	$U_{37}^{K'}$	Pelejero et al. (1999)
GeoB10069-3	-9.01	120.02	Mg/Ca	Gibbons et al. (2014)
GIK18515-3	-3.63	119.36	Mg/Ca	Schoder et al. (2016)
KT05-6-PC-02	41.00	140.77	$U_{37}^{K'}$	Kawahata et al. (2009)
KY07-04-PC1	31.63	128.95	Mg/Ca	Kubota et al. (2010)
LV29-114-3	49.38	152.88	Mg/Ca, $U_{37}^{K'}$	Riethdorf et al. (2013)
M135-004-3	-17.41	-71.74	$U_{37}^{K'}$	Salvatteci et al. (2019)
M135-005-3	-17.42	-71.77	$U_{37}^{K'}$	Salvatteci et al. (2019)
M77-2-003-2	-15.10	-75.69	$U_{37}^{K'}$	Salvatteci et al. (2019)

Site Name	Lat (°N)	Lon (°E)	Proxy	Reference
M77-2-024-5	-11.08	-78.02	$U^{K'}_{37}$	Salvatteci et al. (2019)
M77-2-029-3	-9.30	-79.62	$U^{K'}_{37}$	Salvatteci et al. (2019)
M77-2-059-1	-3.95	-81.32	$U^{K'}_{37}$	Nürnberg et al. (2015)
MD01-2412	44.53	145.00	$U^{K'}_{37}$	Harada et al. (2006)
MD02-2505	25.20	-112.70	$U^{K'}_{37}$	Cheung et al. (2022)
MD06-3075	6.48	125.83	$U^{K'}_{37}$	Fraser et al. (2014)
MD97-2146	20.12	117.38	TEX_{86}, $U^{K'}_{37}$	Shintani et al. (2011)
MD98-2161	-5.21	117.48	Mg/Ca	Fan et al. (2018)
MD98-2178	3.62	118.70	Mg/Ca	Fan et al. (2018)
MD98-2181	6.30	125.82	Mg/Ca	Stott et al. (2007)
MD98-2195	31.64	128.94	$U^{K'}_{37}$	Ijiri et al. (2005)
ME0005A-43JC	7.86	-83.61	Mg/Ca	Benway et al. (2006)
MR003-K03-PC01	46.32	152.53	$U^{K'}_{37}$	Harada et al. (2004)
MV0508-32JC	34.25	-120.04	$U^{K'}_{37}$	Cheung et al. (2022)
ODP1034	48.63	-123.50	$U^{K'}_{37}$	Cheung et al. (2022)
ODP1202	24.80	122.50	$U^{K'}_{37}$	Ruan et al. (2015)
ODP1019C	41.68	-124.93	$U^{K'}_{37}$	Barron et al. (2003)
Oki2	26.07	125.20	$U^{K'}_{37}$	Zhang et al. (2021)
PC6	40.40	143.50	$U^{K'}_{37}$	Minoshima et al. (2007)
		Hydroclimate		
Begbie Lake	48.59	-123.68	pollen	Brown et al. (2019)
Bison Lake	39.76	-107.35	$\delta^{18}O$	L. Anderson (2011)
Boomerang Lake	49.18	-124.16	pollen	Brown et al. (2006)
Carp	45.92	-120.88	pollen	Barnosky (1985)
Copley	38.87	-107.08	pollen	Fall (1997)
Cottonwood Pass Pond	38.83	-106.41	pollen	Fall (1997)
Cumbres Bog	37.02	-106.45	pollen	Johnson et al. (2013)
Emerald	39.15	-106.41	stratigraphy, pollen	Jiménez-Moreno et al. (2019), Shuman et al. (2014)
Enos Lake	49.28	-124.15	pollen	Brown et al. (2006)

Site Name	Lat (°N)	Lon (°E)	Proxy	Reference
Foy Lake	48.20	-114.40	diatom	Stone and Fritz (2006)
Heal Lake	48.54	-123.46	pollen	Brown et al. (2006)
Hermit Lake	38.09	-105.63	pollen	R. S. Anderson et al. (2019)
Jones	47.05	-113.14	δ^{18}O	Shapley et al. (2009)
Keystone Iron Bog	38.87	-107.03	pollen	Fall (1985)
Kite Lake	39.33	-106.13	pollen	Jiménez-Moreno and Anderson (2012)
Koksilah River Discharge	48.76	-123.68	pollen	Brown and Schoups (2015)
Lake of the Woods	43.48	-109.89	stratigraphy	Pribyl and Shuman (2014)
Little Windy	41.43	-106.33	stratigraphy	Minckley et al. (2012)
Lower Bear Lake	34.20	-116.90	C/N	Kirby et al. (2012)
Marion	49.31	-122.55	pollen	Mathewes (1973)
Midden Cluster	34.15	-116.00	macrofossils	Harbert and Nixon (2018)
Owens Lake	36.44	-117.97	δ^{18}O	Benson et al. (2002)
Pixie	48.60	-124.20	pollen	Brown and Hebda (2002), Brown et al. (2006)
Rainbow Lake	44.94	-109.50	stratigraphy	Shuman and Marsicek (2016)
Rapid	42.73	-109.19	pollen	Fall (1988)
Red Rock	40.08	-105.54	pollen	Maher (1972)
Rhamnus Lake	48.63	-123.72	pollen	Brown et al. (2006)
San Juan River Discharge	48.58	-124.31	pollen	Brown and Schoups (2015)
Stewart Bog	35.83	-105.72	pollen	Jiménez-Moreno et al. (2008)
Tiago Lake	40.58	-106.61	pollen	Jiménez-Moreno and Anderson (2012)
Upper Big Creek	40.91	-106.62	stratigraphy	Shuman et al. (2015)

Table 4.1: List of SST and hydroclimate proxy records used.

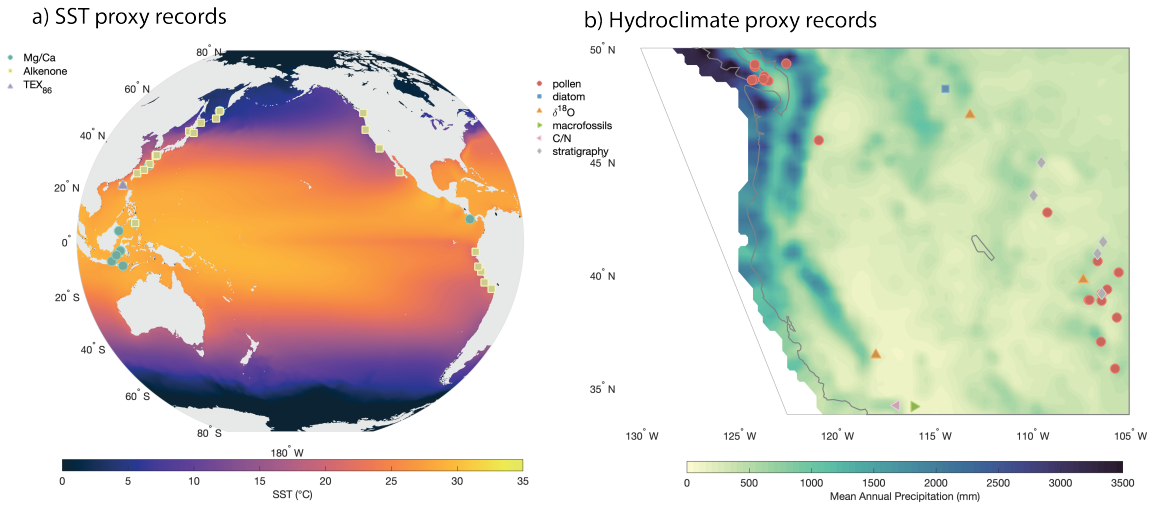

Figure 4.1: Maps showing a) SST proxy records and b) hydroclimate proxy records synthesized in this study. Background color represents a) average mean annual SST over 1991-2020 based on OISST v2 (B. Huang et al., 2021) and b) mean annual precipitation over 1981-2010 based on GPCC v2020 (Schneider et al., 2017).

2.2 Monte Carlo Empirical Orthogonal Function

We extracted dominant patterns of Pacific SST and wNA hydroclimate using a modified version of Monte Carlo Empirical Orthogonal Function (MCEOF) (Anchukaitis & Tierney, 2012). MCEOF is a procedure that accounts for chronological uncertainty in proxy records by iteratively sampling different combinations of age-depth models from each proxy record and carrying out EOF analysis. There are several differences between the original MCEOF and the one we applied. First, we applied an EOF instead of a rotated EOF. Second, we binned our data instead of interpolating them, and accounted for both chronological and calibration uncertainties. Third, to avoid allowing regions with multiple proxy records to dominate the EOF results, we put our proxy records into 1x1 degree grids and averaged records within the same grid. Lastly, we weighted each grid with its cosine latitude prior to EOF to prevent high latitude grid cells, which represent smaller areas than those in low latitudes, from dominating the results. We selected the numbers of modes to retain based on a scree test (Figure S4.1), wherein we identified the principal component

when the slope of the eigenvalues/singular values level off (Wilks, 2011)

2.3 Climate Model Simulations

We used model simulation outputs from Erb, Jackson, and Broccoli (2015) and Erb et al. (2018) for our analysis. Nine idealized simulations were carried out using the Community Earth System Model version 1.2 (CESM) and Geophysical Fluid Dynamics Laboratory Climate Model 2.1 (GFDL). These simulations include half carbon dioxide (CO_2), high obliquity, low obliquity, perihelion at the Northern Hemisphere autumnal equinox, winter solstice, vernal equinox, summer solstice, zero eccentricity, and a preindustrial control run. Details can be found in Erb, Jackson, and Broccoli (2015) and Erb et al. (2018) Each simulation was run for 500 years. We extracted annual mean sea surface temperature and total precipitation from the last 200 years from CESM and the last 100 years from GFDL for analysis. These simulations were used, as opposed to transient simulations (Z. Liu et al., 2009; Smith & Gregory, 2012; Timm & Timmermann, 2007), because these models have improved/better representation of the climate system such as the atmosphere e.g., Hurrell et al., 2013, they allow separation of the effects of each orbital parameter, and they allow more appropriate external forcing conditions to be used.

2.4 Detection and Attribution

We used an EOF based technique (Marvel & Bonfils, 2013; Marvel et al., 2019; Santer et al., 2012) to detect and attribute the spatiotemporal patterns observed in proxy records to external forcings. This approach assumes that climate models can simulate the climate system's response towards a specific forcing accurately, and that the corresponding spatiotemporal pattern can be represented by the leading EOF of this simulation. By projecting this model-based spatial fingerprint onto proxy records, we can obtain a temporal signal which results from a specific forcing. Then,

by comparing the temporal signal with the temporal fingerprint derived from the models using correlation coefficient, we can determine which forcing(s) is most likely responsible for changes observed in proxy records. A high positive correlation coefficient will indicate that forcing is an important factor whereas a low positive or negative correlation coefficient will mean the forcing is less likely to be important. Because we included calibration and chronological uncertainties in our proxy records, this analysis results in 1000 correlation coefficient estimates for each forcing.

To determine the forcing fingerprints of obliquity, precession, CO_2, and CH_4, and their contributions to driving observed changes, we relied on pseudo transient single forcing simulations by using the linear reconstruction technique outlined in Erb, Jackson, and Broccoli (2015) The boundary conditions we used in our reconstruction differed from previous studies (Erb, Jackson, & Broccoli, 2015; Erb et al., 2018) as we used calculations from Berger and Loutre (1991) for orbital parameters, which has a 1000 year temporal resolution, and reconstructions from Köhler et al. (2017) for greenhouse gases, which has 1 year temporal resolution. Even though global CH_4 reconstructions are available (e.g., Joos & Spahni, 2008), we used the reconstruction from Köhler et al. (2017), which only represents the Southern Hemisphere, because there are mismatches in timing between ice cores from both hemispheres (Baumgartner et al., 2014). As a result, this represents a lower bound of absolute values of global CH_4. The orbital parameters were interpolated into 250-year timesteps given their resolution is less than 250 year, whereas greenhouse gas reconstructions were binned into 250-year timesteps. After reconstructing changes due to each forcing, we selected the grids with proxy records, and then used data from those grids to calculate the first EOF from each reconstruction to define the fingerprint of each forcing. Then, we projected each spatial fingerprint onto the proxy dataset. To facilitate this projection, we put our proxy records into the model native grids and averaged the proxy records that are within the same grid. Afterwards, we compared the resulting

temporal signal to the temporal fingerprint defined from the model using Pearson correlation coefficient.

Here, we focused on the relative roles of obliquity, precession, atmospheric greenhouse gas concentrations (CO_2 and CH_4) on driving wNA hydroclimate (Figure 4.2) and SST (Figure 4.3) fingerprints based on simulations using the Community Earth System Model 1.2 (CESM) and Geophysical Fluid Dynamics Lab Climate Model 2.1 (GFDL). Although the Laurentide Ice Sheet did not fully deglaciate until c.a. 6.7 ka (Ullman et al., 2016), the largest dome is located in the Northeastern North America, which makes it unlikely to influence the atmospheric circulation and hydroclimate in wNA. Therefore, we did not analyze the influence of ice sheets on Pacific SST and wNA hydroclimate.

3 Results and Discussion

3.1 Spatiotemporal Evolution of WNA Hydroclimate and Pacific SST

Changes in wNA hydroclimate and Pacific SST can be described by two distinct spatiotemporal patterns (Figures 4.4-4.5). The first principal component (PC1) associated with wNA hydroclimate and Pacific SST both indicate a monotonic increase throughout the analysis period. The associated spatial pattern (EOF1) of wNA hydroclimate suggests an increase in moisture throughout the Holocene across broad spatial scales, with the strongest positive expression inland portion of wNA, whereas the EOF1 of Pacific SST is a zonal dipole in the tropics, characterized by a Holocene-length increase SSTs in the eastern equatorial pacific and decrease in the Indo Pacific Warm Pool, and a near uniform warming in the North Pacific. The second principal component (PC2) shows an initial increase until ca. 5000 yrs BP and then a small decrease afterwards. The associated spatial patterns (EOF2) indicate that most of the wNA was increasingly wet in the early Holocene until $\sim$ 5000 yrs BP, and trends towards drying in the latter part of the Holocene. Furthermore, the western Pacific

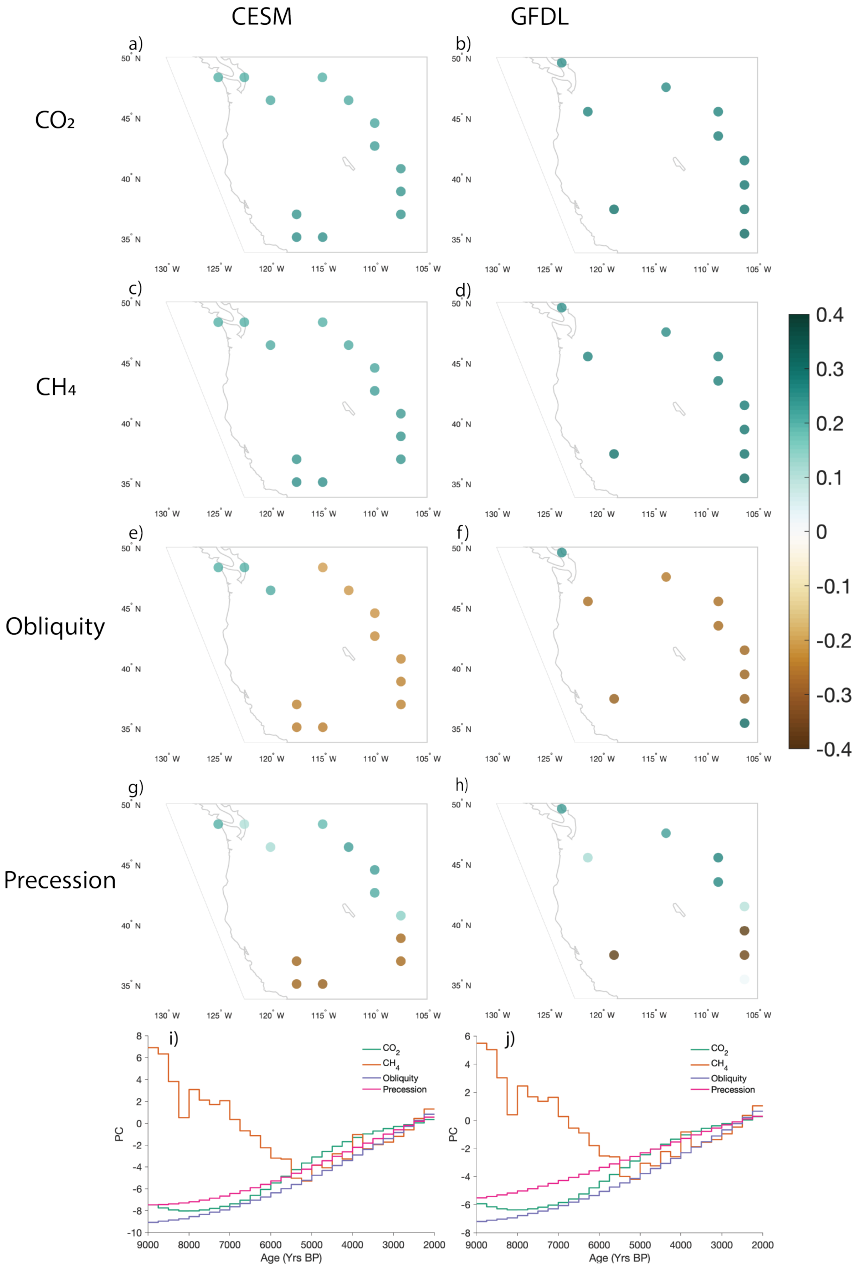

Figure 4.2: Expected spatial fingerprints on hydroclimate due to a-b) CO_2, c-d) CH_4, e-f) obliquity, and g-h) precession. i-j) The timeseries associated with each fingerprint. The left hand side are based on CESM and the right hand side are based on GFDL. Each circle represents a grid cell where proxy records are present.

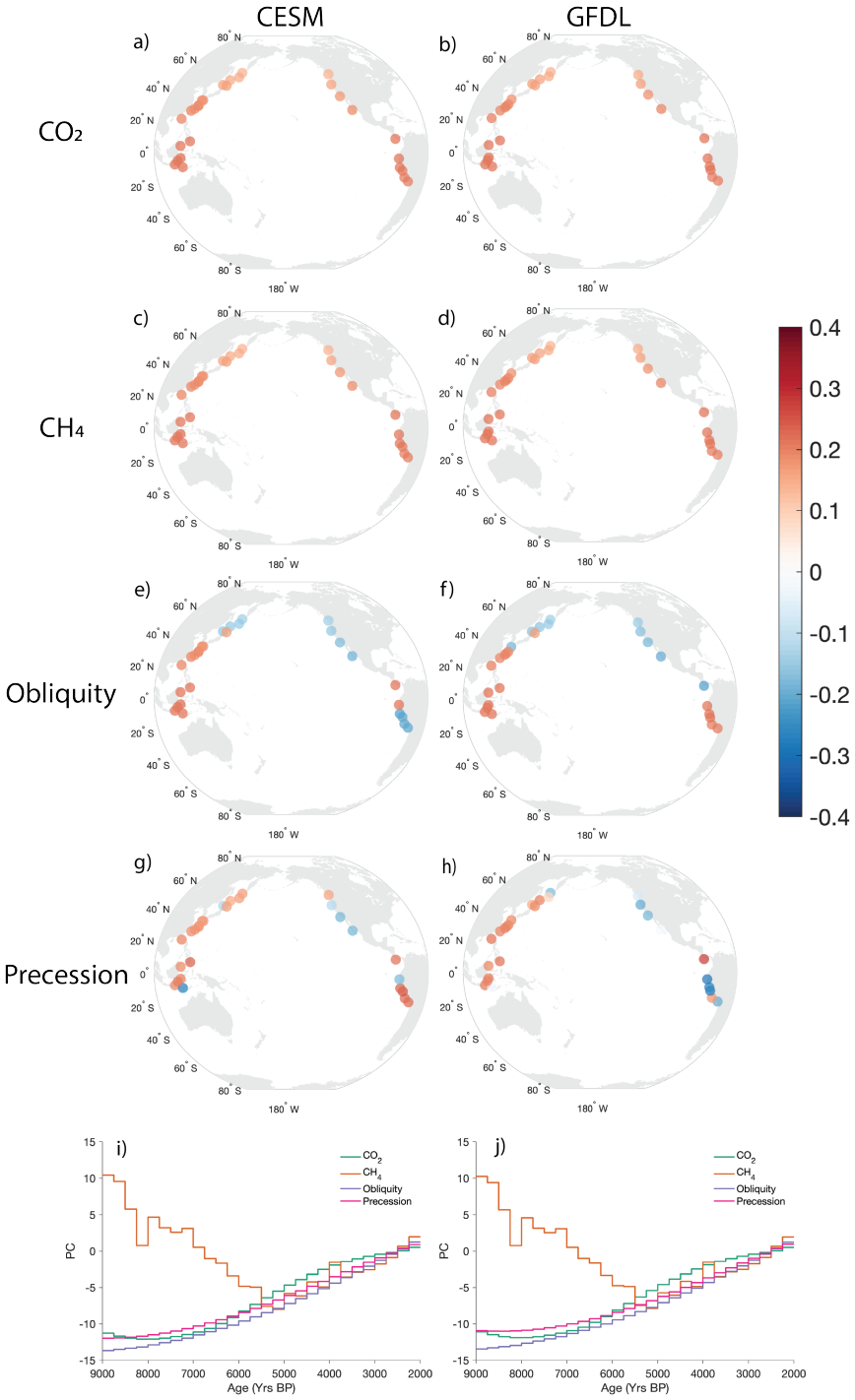

Figure 4.3: Expected spatial fingerprints on SST due to a-b) CO_2, c-d) CH_4, e-f) obliquity, and g-h) precession. i-j) The timeseries associated with each fingerprint. The left panel is based on CESM and the right panel is based on GFDL. Each circle represents a grid cell where proxy records are present.

was getting warmer and the Northeast Pacific was cooling until ca. 5000 yrs BP before the trend reversed.

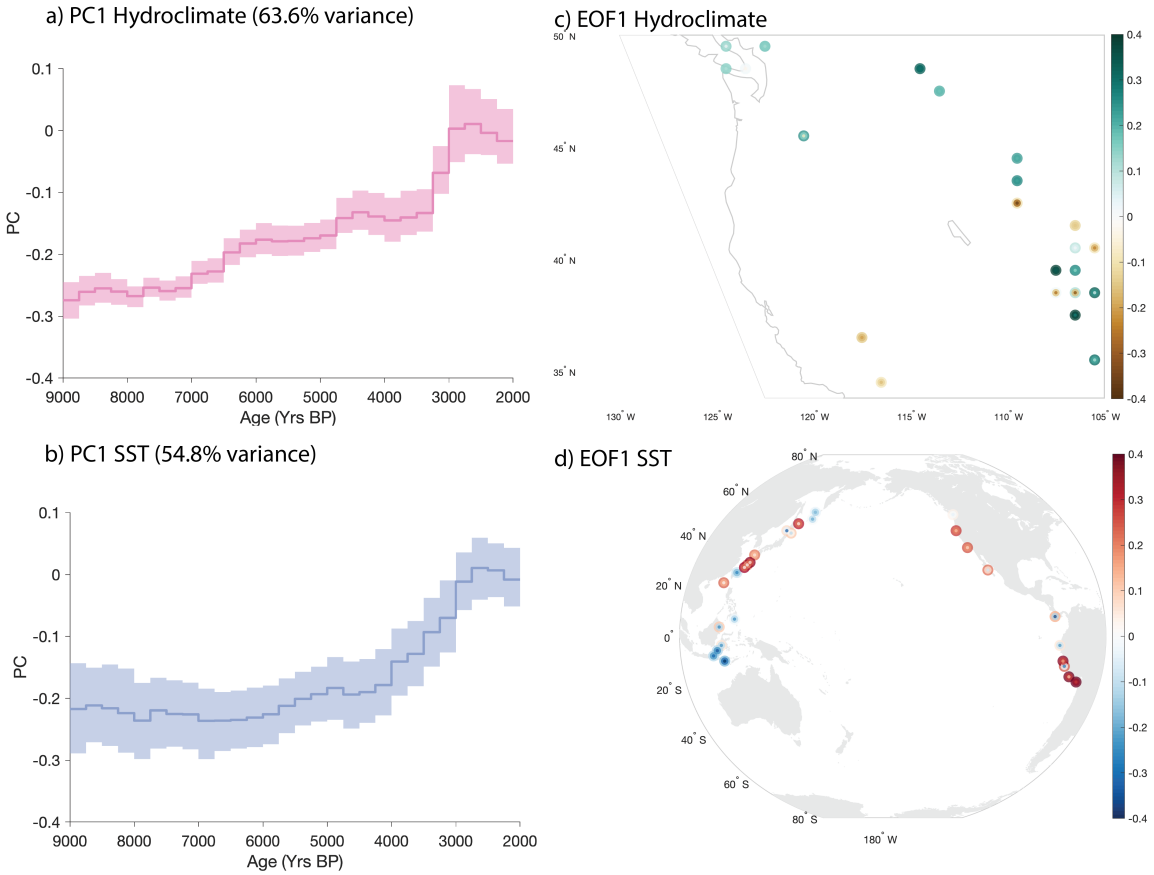

Figure 4.4: The temporal component of EOF1 in a) hydroclimate records and b) SST records, and the spatial components of EOF1 in c) hydroclimate records and d) SST records. Shadings in timeseries indicate the 95% confidence interval of each PC1 due to chronological and calibration uncertainties. The outer ring, inner ring, and central colors represent 97.5th, 2.5th, and 50th (median) percentile of loading values respectively. The median variance explained is denoted in the timeseries title.

The similar temporal evolution of wNA hydroclimate and Pacific SST revealed by the MCEOF analysis (Figure S4.2) suggests that wNA hydroclimate changes during the Holocene could be related to Pacific SST, or they are driven by some of the same climate forcings. Additionally, similar spatiotemporal patterns are obtained when applying MCEOF to the combined wNA hydroclimate and Pacific SST proxy records, suggesting the patterns obtained separately covary with each other (Figure S4.2). These results indicate an increasingly wet wNA is accompanied by an increasingly

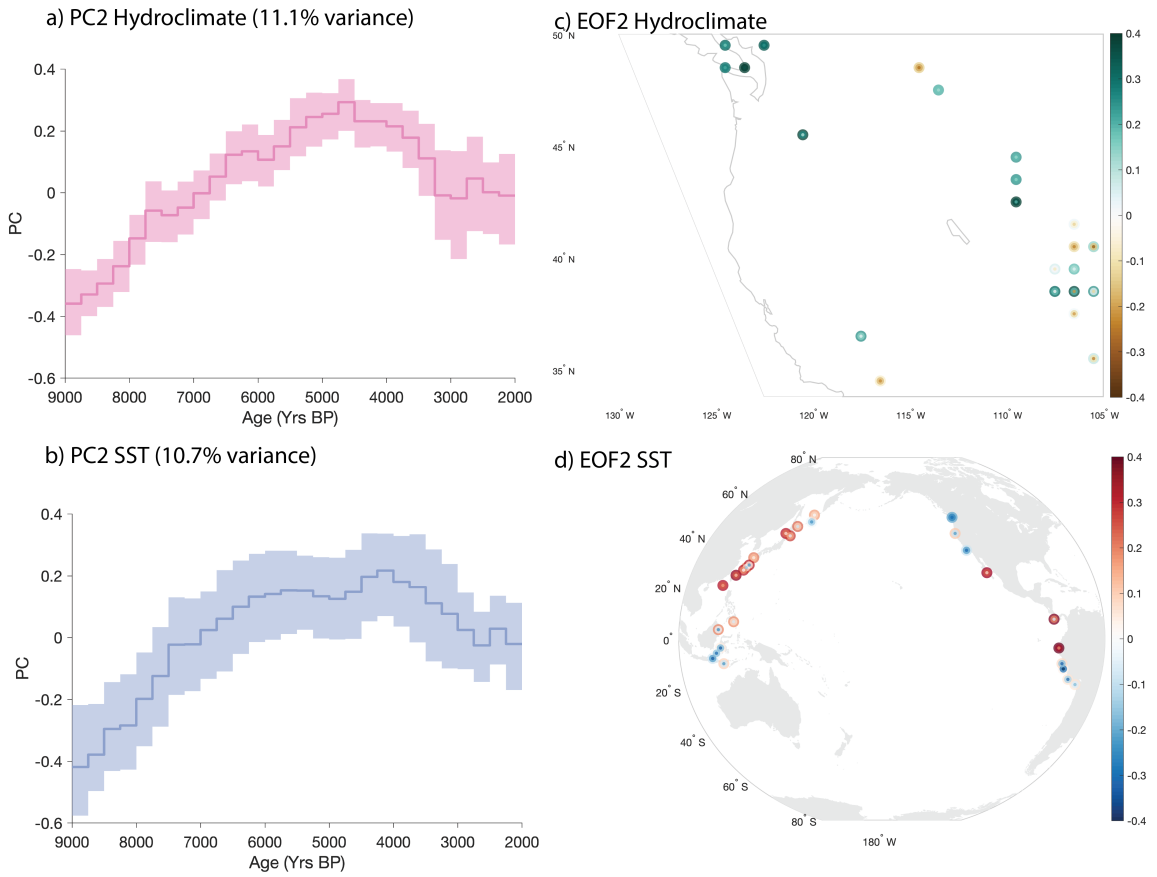

Figure 4.5: The temporal component of EOF1 in a) hydroclimate records and b) SST records, and the spatial components of EOF1 in c) hydroclimate records and d) SST records. Shadings in timeseries indicate the 95% confidence interval of each PC1 due to chronological and calibration uncertainties. The outer ring, inner ring, and central colors represent 97.5th, 2.5th, and 50th (median) percentile of loading values respectively. The median variance explained is denoted in the timeseries title.

warm North Pacific and reduced tropical Pacific zonal temperature gradient (El Niño-like condition) from early to late Holocene. Such relationship between the wNA hydroclimate and Pacific SST is consistent with the interannual-scale atmospheric and oceanic teleconnections between tropical Pacific and wNA reported based on instrumental observation and modern climate simulations (Hoskins & Karoly, 1981; X. Liu et al., 2021; Ma et al., 2015; Trenberth et al., 1998; Yeh et al., 2018).

3.2 Drivers of WNA Hydroclimate and Pacific SST Change

CO_2 and precession stand out as the most important forcings in driving wNA hydroclimate and Pacific SST change (Figure 4.6). The fingerprint of these forcings are clearly identified in wNA hydroclimate using two different climate models, as indicated by the positive correlation coefficient between the temporal fingerprint and signal. On the other hand, the driver of Pacific SST is less clear – the position of each correlation coefficient distribution change when a different climate model fingerprint is used and that most distributions overlap with zero. This suggests that model uncertainty and proxy calibration and chronological uncertainties are large relative to the fingerprint signal. Nonetheless, fingerprints based on CESM suggest CO_2 and precession are important factors to consider for Pacific SST. When combined wNA hydroclimate and Pacific SST fields, we find that CO_2 and precession are important factors to consider, even though their relative importance depends on the model used. Obliquity and CH_4 do not seem to play a major role in driving changes in wNA hydroclimate and Pacific SST because of the negative correlation coefficients between the temporal fingerprint and the signal.

The importance of CO_2 in driving wNA hydroclimate changes during the Holocene in addition to precession is somewhat surprising because of the small changes in greenhouse gases concentrations. Because orbital forcing is presumably the dominant forcing during the Holocene (Otto-Bliesner et al., 2017), previous studies have primarily attributed wNA hydroclimate changes to changes in either obliquity and/or precession (Hermann et al., 2018; Skinner et al., 2020; R. S. Thompson et al., 1993). The role of CO_2 on wNA hydroclimate has been postulated to be minor since the change is small ($\sim$ 20 ppm; Köhler et al., 2017). Yet, our results suggest that the impacts of CO_2 are significant. This corroborates with a previous comparison between proxy records and insolation forced climate simulations that suggest insolation was not the sole driver of wNA hydroclimate changes between the middle Holocene and present

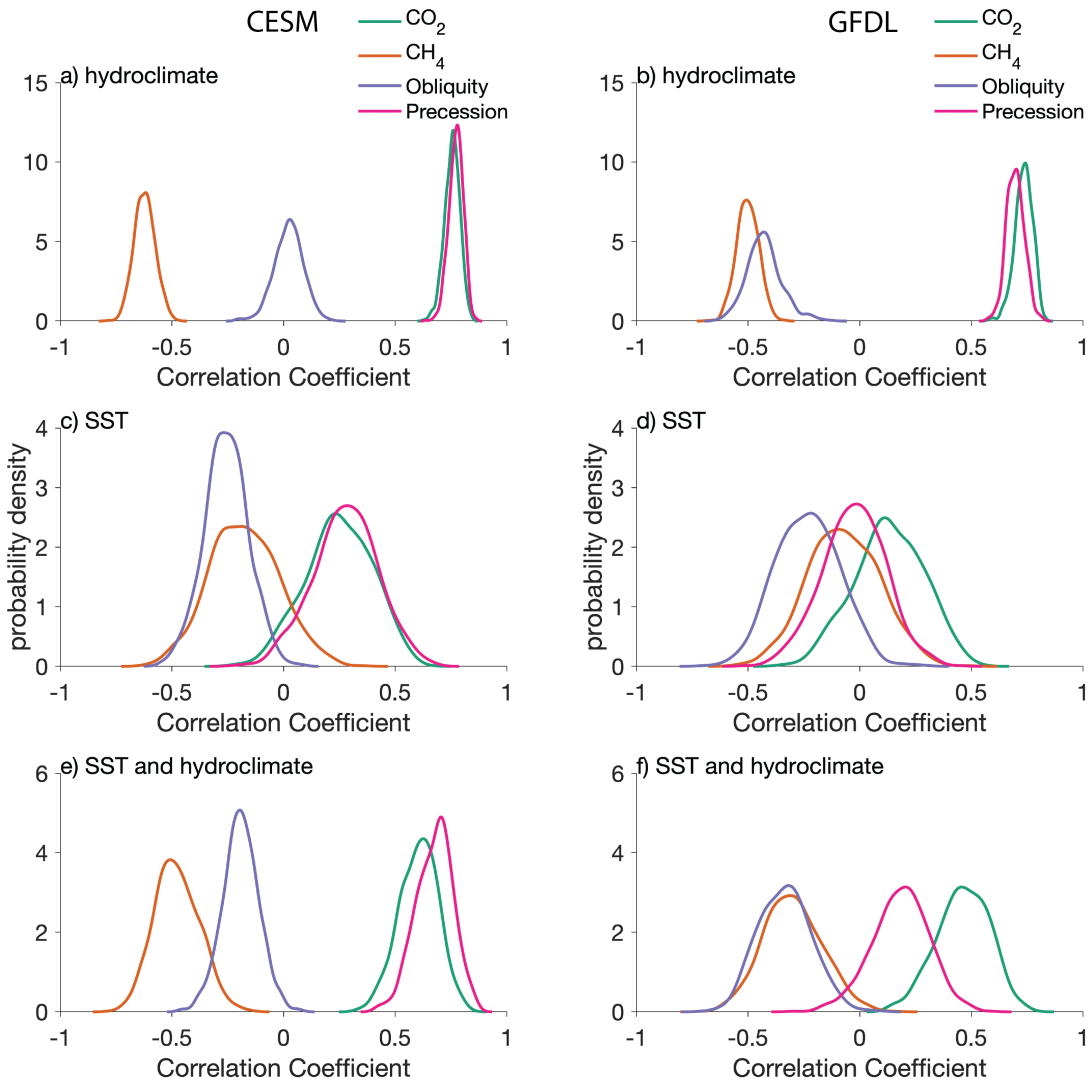

Figure 4.6: Correlation coefficients between fingerprints and CO2 (teal), CH4 (orange), obliquity (purple), and precession (pink) signals based on (left) CESM and (right) GFDL for (a-b) hydroclimate records, (c-d) SST records, and (e-f) combined SST and hydroclimate records.

(Diffenbaugh & Sloan, 2004). Future model projections provide some clues on how CO_2 could influence wNA hydroclimate. A moisture budget analysis based on near term future change projection in wNA hydroclimate suggests that elevated CO_2 will lead to an increase in precipitation because of a combination of enhanced moisture convergence during winter and transient eddy convergence and surface climate during summer (Seager et al., 2014). Indeed, evidence from both proxies (L. Anderson, 2011; Bailey et al., 2018; Nagashima et al., 2022) and models (Hermann et al., 2018) suggested a shift in the Aleutian low in mid-Holocene relative to present, which altered the moisture strength and pathway towards the wNA. This indicates that CO_2 driven atmospheric circulation changes highlighted in Seager et al. (2014) could have been responsible for changes observed in the Holocene. Unlike local radiative warming perturbations, consequences of shifts in the Aleutian low are unlikely to follow simple relationships with most quantification of the magnitude of each forcing.

In addition to CO_2, our results also emphasize the role of precession over obliquity in driving wNA hydroclimate. Because obliquity controls the meridional insolation gradient, prior analysis has suggested that the weaker insolation gradient drives a weaker temperature gradient, which subsequently leads less moisture convergence to wNA, and thus causes drier conditions during the mid-Holocene (Routson et al., 2019). However, our analysis suggests that an opposite temporal pattern (drying trend towards the present) would have occurred in wNA if obliquity was the dominant driver. Instead, the spatiotemporal evolution of wNA hydroclimate is more consistent with precession changes. There are two possible mechanisms that can explain the impacts of precession on wNA hydroclimate. First, changes in precession influence the seasonal distribution of insolation in each hemisphere. Compared to the present, the Northern Hemisphere was characterized by warmer, shorter summers and cooler, longer winters during the early- and mid-Holocene. The increased summer temperature during summer could have led to a strengthening subtropical anticyclone

and subsequently drier conditions (Seager et al., 2014; R. S. Thompson et al., 1993). Second, precession has been suggested to influence the tropical Pacific. On seasonal timescales, changes in precession induce dynamical changes in the tropical Pacific through coupled atmosphere-ocean dynamics and shifts in the position of the Walker Circulation (Chiang et al., 2022; Erb, Broccoli, et al., 2015) Consequently, this affects the strength and position of teleconnection patterns, which play a role in governing wNA hydroclimate. On interannual timescales, changes in precession have also been suggested to influence the amplitude (Grothe et al., 2020; White et al., 2018) and/or the spatial expression of SST (Karamperidou & DiNezio, 2022). Similar to seasonal cycle changes, the change in either the amplitude or the spatial expression of SST can subsequently alter the teleconnection patterns and wNA hydroclimate. The ability to disentangle the relative role of obliquity and precession advances our knowledge on how different orbital parameters affect wNA hydroclimate and clarifies their relative roles during the Holocene.

In contrast to wNA hydroclimate, we are unable to attribute changes in Pacific SST to one or two specific forcings confidently. Since the radiative forcing changes due to precession and obliquity averages out on annual timescales and greenhouse gasses are small during the Holocene, it is possible that these forcings did not leave any substantially distinct spatial fingerprints on Pacific SST. As a result, proxy records are unable to detect these changes. However, both proxy records and climate model experiments have shown that there is detectable temperature change between the middle Holocene to present (Brierley et al., 2020; Kaufman et al., 2020; Z. Liu et al., 2014; Lohmann et al., 2013). Hence, the small magnitude of forcing during the Holocene is unlikely to be the only explanation for the lack of forced signal detected. Alternatively, the method and the models used can be inadequate to detect forced signals in proxy records. Our method hinges on the assumption that the model's responses to forcings are accurate and that the climate system's response to forcing

can be approximated linearly. While accurate on first order (Erb, Jackson, & Broccoli, 2015), the difference in correlation coefficient distributions based on CESM and GFDL suggest that the forcing fingerprint is model dependent (cf. Figure 7c,d). Indeed, an analysis on the latest generation of climate models suggests large discrepancies between their SST response to middle Holocene conditions (Brierley et al., 2020) Furthermore, more recent studies have indicated the importance of land surface and vegetation changes in altering Holocene climate (Y. Liu et al., 2018; A. J. Thompson et al., 2022), which are not considered in our analysis. Thus, our method might be insufficient to detect and attribute changes in SST records. Lastly, the spatial distribution of proxy records could also hinder our ability to detect forced changes. Since the climate state and sensitivity to external forcings are dependent on location, the fact that our SST records are unevenly distributed and are along the coast outside of the tropics can obscure the true climate signal and make detection difficult (Judd et al., 2020; Osman et al., 2021). All in all, we suggest that the weak forced signal during the Holocene and the limitations in our method and proxy network leads to a difficulty in detecting and attributing Pacific SST changes recorded in proxy records.

4 Conclusion

Our study sheds new insights on the evolution of Pacific SST and wNA hydroclimate and the drivers behind them. During the Holocene, wNA hydroclimate and Pacific SST are shown to have co-evolved temporally. The two distinct temporal, but spatially coherent patterns in wNA hydroclimate are associated with two different Pacific SST patterns, with both patterns indicating a warming Pacific would lead to a wetter wNA. These results provide empirical evidence supporting a fundamental coupling between Pacific SST and wNA hydroclimate on Holocene timescales. Changes in wNA hydroclimate appears to be driven primarily by CO_2 and precession, which is a major paradigm shift for our understanding of the controls of wNA during the

Holocene.

Although the rate of change considered in this study are slower than current anthropogenic climate change, our results highlight the role of atmospheric greenhouse gases change in driving hydroclimate changes in wNA. Further, our results emphasize the importance of considering the coupling between wNA hydroclimate and Pacific SST to understand how the climate system responds to external forcings. The inconsistent attribution of Pacific SST using two different models suggest that there is a need to further improve the representation of Pacific SST in general circulation models to narrow down the uncertainty of wNA hydroclimate response to forced changes. The difference in forced fingerprints between models also suggest a need to better characterize how different climate forcings affect the climate system and whether models are showing consistent and accurate response to external forcings.

References

Allen, R. J., & Luptowitz, R. (2017). El Niño-like teleconnection increases California precipitation in response to warming. *Nature Communications*, *8*(1). https://doi.org/10.1038/ncomms16055

Anchukaitis, K. J., & Tierney, J. E. (2012). Identifying coherent spatiotemporal modes in time-uncertain proxy paleoclimate records. *Climate Dynamics*, *41*(5-6), 1291–1306. https://doi.org/10.1007/s00382-012-1483-0

Anderson, L. (2011). Holocene record of precipitation seasonality from lake calcite δ^{18}O in the central Rocky Mountains, United States. *Geology*, *39*(3), 211–214. https://doi.org/10.1130/g31575.1

Anderson, R. S., Soltow, H. R., & Jiménez-Moreno, G. (2019). Postglacial environmental change of a high-elevation forest, Sangre de Cristo Mountains of south-central Colorado. In *From saline to freshwater: The diversity of western lakes in space and time* (pp. 221–239). Geological Society of America. https://doi.org/10.1130/2018.2536(13)

Asmerom, Y., Polyak, V., Burns, S., & Rassmussen, J. (2007). Solar forcing of Holocene climate: New insights from a speleothem record, southwestern United States. *Geology*, *35*(1), 1. https://doi.org/10.1130/g22865a.1

Ault, T. R., Mankin, J. S., Cook, B. I., & Smerdon, J. E. (2016). Relative impacts of mitigation, temperature, and precipitation on 21st-century megadrought risk in the American Southwest. *Science Advances*, *2*(10). https://doi.org/10.1126/sciadv.1600873

Bailey, H. L., Kaufman, D. S., Sloane, H. J., Hubbard, A. L., Henderson, A. C., Leng, M. J., Meyer, H., & Welker, J. M. (2018). Holocene atmospheric circulation in the central North Pacific: A new terrestrial diatom and δ^{18}O dataset from the Aleutian Islands. *Quaternary Science Reviews*, *194*, 27–38. https://doi.org/10.1016/j.quascirev.2018.06.027

Barnosky, C. W. (1985). Late Quaternary vegetation in the southwestern Columbia basin, Washington. *Quaternary Research*, *23*(1), 109–122.

Barron, J. A., & Anderson, L. (2011). Enhanced Late Holocene ENSO/PDO expression along the margins of the eastern North Pacific. *Quaternary International*, *235*(1-2), 3–12.

Barron, J. A., Heusser, L., Herbert, T., & Lyle, M. (2003). High-resolution climatic evolution of coastal northern California during the past 16,000 years. *Paleoceanography*, *18*(1). https://doi.org/https://doi.org/10.1029/2002PA000768

Bartlein, P. J., Harrison, S. P., Brewer, S., Connor, S., Davis, B. A. S., Gajewski, K., Guiot, J., Harrison-Prentice, T. I., Henderson, A., Peyron, O., Prentice, I. C., Scholze, M., Seppä, H., Shuman, B., Sugita, S., Thompson, R. S., Viau, A. E., Williams, J., & Wu, H. (2010). Pollen-based continental climate reconstructions at 6 and 21 ka: A global synthesis. *Climate Dynamics*, *37*(3-4), 775–802. https://doi.org/10.1007/s00382-010-0904-1

Baumgartner, M., Kindler, P., Eicher, O., Floch, G., Schilt, A., Schwander, J., Spahni, R., Capron, E., Chappellaz, J., Leuenberger, M., Fischer, H., & Stocker, T. F. (2014). NGRIP CH_4 concentration from 120 to 10 kyr before present and its relation to a δ^{15}N temperature reconstruction from the same ice core. *Climate of the Past*, *10*(2), 903–920. https://doi.org/10.5194/cp-10-903-2014

Benson, L., Kashgarian, M., Rye, R., Lund, S., Paillet, F., Smoot, J., Kester, C., Mensing, S., Meko, D., & Lindström, S. (2002). Holocene multidecadal and multicentennial droughts affecting Northern California and Nevada. *Quaternary Science Reviews*, *21*(4-6), 659–682. https://doi.org/10.1016/s0277-3791(01)00048-8

Benway, H. M., Mix, A. C., Haley, B. A., & Klinkhammer, G. P. (2006). Eastern Pacific Warm Pool paleosalinity and climate variability: 0–30 kyr. *Paleoceanography*, *21*(3). https://doi.org/10.1029/2005pa001208

Berger, A., & Loutre, M. (1991). Insolation values for the climate of the last 10 million years. *Quaternary Science Reviews*, *10*(4), 297–317. https://doi.org/10.1016/0277-3791(91)90033-q

Blaauw, M., & Christen, J. A. (2011). Flexible paleoclimate age-depth models using an autoregressive gamma process. *Bayesian analysis*, *6*(3), 457–474. https://doi.org/10.1214/11-ba618

Brierley, C. M., Zhao, A., Harrison, S. P., Braconnot, P., Williams, C. J. R., Thornalley, D. J. R., Shi, X., Peterschmitt, J.-Y., Ohgaito, R., Kaufman, D. S., Kageyama, M., Hargreaves, J. C., Erb, M. P., Emile-Geay, J., D'Agostino, R., Chandan, D., Carré, M., Bartlein, P. J., Zheng, W., … Abe-Ouchi, A. (2020). Large-scale features and evaluation of the PMIP4-CMIP6 *midHolocene* simulations. *Climate of the Past*, *16*(5), 1847–1872. https://doi.org/10.5194/cp-16-1847-2020

Brown, K. J., Hebda, N., Schoups, G., Conder, N., Smith, K., & Trofymow, J. (2019). Long-term climate, vegetation and fire regime change in a managed municipal water supply area, British Columbia, Canada. *The Holocene*, *29*(9), 1411–1424. https://doi.org/10.1177/0959683619854523

Brown, K. J., & Hebda, R. J. (2002). Origin, development, and dynamics of coastal temperate conifer rainforests of southern Vancouver Island, Canada. *Canadian Journal of Forest Research*, *32*(2), 353–372. https://doi.org/10.1139/x01-197

Brown, K. J., & Schoups, G. (2015). Multi-millennial streamflow dynamics in two forested watersheds on Vancouver Island, Canada. *Quaternary Research*, *83*(3), 415–426. https://doi.org/10.1016/j.yqres.2015.03.003

Brown, K., Fitton, R., Schoups, G., Allen, G., Wahl, K., & Hebda, R. (2006). Holocene precipitation in the coastal temperate rainforest complex of southern British Columbia, Canada. *Quaternary Science Reviews*, *25*(21-22), 2762–2779. https://doi.org/10.1016/j.quascirev.2006.02.020

Cheung, A. H., Sandwick, S., Du, X., Abella-Gutiérrez, J., Vachula, R. S., Herbert, T. D., Fox-Kemper, B., & Herguera, J. C. (2022). Middle to Late Holocene Sea Surface Temperature and Productivity Changes in the Northeast Pacific. *Paleoceanography and Paleoclimatology*, *37*(11). https://doi.org/10.1029/2021pa004399

Chiang, J. C. H., Atwood, A. R., Vimont, D. J., Nicknish, P. A., Roberts, W. H. G., Tabor, C. R., & Broccoli, A. J. (2022). Two annual cycles of the Pacific cold tongue under orbital precession. *Nature*, *611*(7935), 295–300. https://doi.org/10.1038/s41586-022-05240-9

Cook, B. I., Mankin, J. S., Marvel, K., Williams, A. P., Smerdon, J. E., & Anchukaitis, K. J. (2020). Twenty-First Century Drought Projections in the CMIP6 Forcing Scenarios. *Earth's Future*, *8*(6). https://doi.org/10.1029/2019ef001461

Davis, C. V., Myhre, S. E., Deutsch, C., Caissie, B., Praetorius, S., Borreggine, M., & Thunell, R. (2020). Sea surface temperature across the Subarctic North Pacific and marginal seas through the past 20,000 years: A paleoceanographic synthesis. *Quaternary Science Reviews*, *246*, 106519. https://doi.org/10.1016/j.quascirev.2020.106519

Diffenbaugh, N. S., & Sloan, L. C. (2004). Mid-Holocene Orbital Forcing of Regional-Scale Climate: A Case Study of Western North America Using a High-Resolution RCM. *Journal of Climate*, *17*(15), 2927–2937. https://doi.org/10.1175/1520-0442(2004)017⟨2927:moforc⟩2.0.co;2

Dong, L., & Leung, L. R. (2021). Winter Precipitation Changes in California Under Global Warming: Contributions of CO_2, Uniform SST Warming, and SST Change Patterns. *Geophysical Research Letters*, *48*(5). https://doi.org/10.1029/2020gl091736

Dong, L., Leung, L. R., Song, F., & Lu, J. (2021). Uncertainty in El Niño-like warming and California precipitation changes linked by the Interdecadal Pacific Oscillation. *Nature Communications*, *12*(1). https://doi.org/10.1038/s41467-021-26797-5

Du, X., Hendy, I., Hinnov, L., Brown, E., Zhu, J., & Poulsen, C. J. (2021). High-resolution interannual precipitation reconstruction of Southern California: Implications for Holocene ENSO evolution. *Earth and Planetary Science Letters*, *554*, 116670. https://doi.org/10.1016/j.epsl.2020.116670

Du, X., Hendy, I., & Schimmelmann, A. (2018). A 9000-year flood history for Southern California: A revised stratigraphy of varved sediments in Santa Barbara Basin. *Marine Geology*, *397*, 29–42. https://doi.org/10.1016/j.margeo.2017.11.014

Erb, M. P., Broccoli, A. J., Graham, N. T., Clement, A. C., Wittenberg, A. T., & Vecchi, G. A. (2015). Response of the Equatorial Pacific Seasonal Cycle to Orbital Forcing. *Journal of Climate*, *28*(23), 9258–9276. https://doi.org/10.1175/jcli-d-15-0242.1

Erb, M. P., Jackson, C. S., & Broccoli, A. J. (2015). Using Single-Forcing GCM Simulations to Reconstruct and Interpret Quaternary Climate Change. *Journal of Climate*, *28*(24), 9746–9767. https://doi.org/10.1175/jcli-d-15-0329.1

Erb, M. P., Jackson, C. S., Broccoli, A. J., Lea, D. W., Valdes, P. J., Crucifix, M., & DiNezio, P. N. (2018). Model evidence for a seasonal bias in Antarctic ice cores. *Nature Communications*, *9*(1). https://doi.org/10.1038/s41467-018-03800-0

Ersek, V., Clark, P. U., Mix, A. C., Cheng, H., & Edwards, R. L. (2012). Holocene winter climate variability in mid-latitude western North America. *Nature Communications*, *3*(1). https://doi.org/10.1038/ncomms2222

Fall, P. L. (1985). Holocene dynamics of the subalpine forest in central Colorado. *American Association of Stratigraphic Palynologists Contribution Series*, *16*, 31–46.

Fall, P. L. (1997). Timberline fluctuations and late Quaternary paleoclimates in the Southern Rocky Mountains, Colorado. *Geological Society of America Bulletin*, *109*(10), 1306–1320. https://doi.org/10.1130/0016-7606(1997)109⟨1306:tfalqp⟩2.3.co;2

Fall, P. L. (1988). *Vegetation dynamics in the southern Rocky Mountains: Late Pleistocene and Holocene timberline fluctuations*. The University of Arizona.

Fan, W., Jian, Z., Chu, Z., Dang, H., Wang, Y., Bassinot, F., Han, X., & Bian, Y. (2018). Variability of the Indonesian throughflow in the Makassar Strait over the last 30 ka. *Scientific reports*, *8*(1), 1–8.

Fraser, N., Kuhnt, W., Holbourn, A., Bolliet, T., Andersen, N., Blanz, T., & Beaufort, L. (2014). Precipitation variability within the West Pacific Warm Pool over the past 120 ka: Evidence from the Davao Gulf, southern Philippines. *Paleoceanography*, *29*(11), 1094–1110.

Gibbons, F. T., Oppo, D. W., Mohtadi, M., Rosenthal, Y., Cheng, J., Liu, Z., & Linsley, B. K. (2014). Deglacial δ^{18}O and hydrologic variability in the tropical Pacific and Indian Oceans. *Earth and Planetary Science Letters*, *387*, 240–251. https://doi.org/10.1016/j.epsl.2013.11.032

Grothe, P. R., Cobb, K. M., Liguori, G., Lorenzo, E. D., Capotondi, A., Lu, Y., Cheng, H., Edwards, R. L., Southon, J. R., Santos, G. M., Deocampo, D. M., Lynch-Stieglitz, J., Chen, T., Sayani, H. R., Thompson, D. M., Conroy, J. L., Moore, A. L., Townsend, K., Hagos, M., … Toth, L. T. (2020). Enhanced El Niño-Southern Oscillation Variability in Recent Decades. *Geophysical Research Letters*, *47*(7). https://doi.org/10.1029/2019gl083906

Harada, N., Ahagon, N., Sakamoto, T., Uchida, M., Ikehara, M., & Shibata, Y. (2006). Rapid fluctuation of alkenone temperature in the southwestern Okhotsk Sea during the past 120 ky. *Global and Planetary Change*, *53*(1-2), 29–46. https://doi.org/10.1016/j.gloplacha.2006.01.010

Harada, N., Ahagon, N., Uchida, M., & Murayama, M. (2004). Northward and southward migrations of frontal zones during the past 40 kyr in the Kuroshio-Oyashio transition area. *Geochemistry, Geophysics, Geosystems*, *5*(9), n/a–n/a. https://doi.org/10.1029/2004gc000740

Harbert, R. S., & Nixon, K. C. (2018). Quantitative Late Quaternary Climate Reconstruction from Plant Macrofossil Communities in Western North America. *Open Quaternary*, *4*(1), 8. https://doi.org/10.5334/oq.46

Heaton, T. J., Köhler, P., Butzin, M., Bard, E., Reimer, R. W., Austin, W. E. N., Ramsey, C. B., Grootes, P. M., Hughen, K. A., Kromer, B., Reimer, P. J., Adkins, J., Burke, A., Cook, M. S., Olsen, J., & Skinner, L. C. (2020). Marine20–The Marine Radiocarbon Age Calibration Curve (0–55,000 cal BP). *Radiocarbon*, *62*(4), 779–820. https://doi.org/10.1017/rdc.2020.68

Heede, U. K., Fedorov, A. V., & Burls, N. J. (2020). Time Scales and Mechanisms for the Tropical Pacific Response to Global Warming: A Tug of War between the Ocean Thermostat and Weaker Walker. *Journal of Climate*, *33*(14), 6101–6118. https://doi.org/10.1175/jcli-d-19-0690.1

Hermann, N. W., Oster, J. L., & Ibarra, D. E. (2018). Spatial patterns and driving mechanisms of mid-Holocene hydroclimate in western North America. *Journal of Quaternary Science*, *33*(4), 421–434. https://doi.org/10.1002/jqs.3023

Higuera, P. E., Shuman, B. N., & Wolf, K. D. (2021). Rocky Mountain subalpine forests now burning more than any time in recent millennia. *Proceedings of the National Academy of Sciences*, *118*(25). https://doi.org/10.1073/pnas.2103135118

Hoskins, B. J., & Karoly, D. J. (1981). The Steady Linear Response of a Spherical Atmosphere to Thermal and Orographic Forcing. *Journal of the Atmospheric Sciences*, *38*(6), 1179–1196. https://doi.org/10.1175/1520-0469(1981)038⟨1179:tslroa⟩2.0.co;2

Howitt, R., Medellín-Azuara, J., MacEwan, D., Lund, J. R., & Sumner, D. (2014). *Economic analysis of the 2014 drought for California agriculture*. Center for Watershed Sciences University of California, Davis, CA.

Huang, B., Liu, C., Banzon, V., Freeman, E., Graham, G., Hankins, B., Smith, T., & Zhang, H.-M. (2021). Improvements of the Daily Optimum Interpolation Sea Surface Temperature (DOISST) Version 2.1. *Journal of Climate*, *34*(8), 2923–2939. https://doi.org/10.1175/jcli-d-20-0166.1

Huang, X., Wang, R., Jian, Z., & Wang, J. (2009). Responses of sea surface temperature and productivity to the changes of the Kuroshio Current in the northern Okinawa Trough during the Holocene. *Advances in Earth Science*, *24*(6), 652.

Hurrell, J. W., Holland, M. M., Gent, P. R., Ghan, S., Kay, J. E., Kushner, P. J., Lamarque, J.-F., Large, W. G., Lawrence, D., Lindsay, K., Lipscomb, W. H., Long, M. C., Mahowald, N., Marsh, D. R., Neale, R. B., Rasch, P., Vavrus, S., Vertenstein, M., Bader, D., … Marshall, S. (2013). The community earth sys-

tem model: A framework for collaborative research. *Bulletin of the American Meteorological Society*, *94*(9), 1339–1360. https://doi.org/10.1175/bams-d-12-00121.1

Ijiri, A., Wang, L., Oba, T., Kawahata, H., Huang, C.-Y., & Huang, C.-Y. (2005). Paleoenvironmental changes in the northern area of the East China Sea during the past 42,000 years. *Palaeogeography, Palaeoclimatology, Palaeoecology*, *219*(3-4), 239–261. https://doi.org/10.1016/j.palaeo.2004.12.028

Iturbide, M., Gutiérrez, J. M., Alves, L. M., Bedia, J., Cerezo-Mota, R., Cimadevilla, E., Cofiño, A. S., Luca, A. D., Faria, S. H., Gorodetskaya, I. V., Hauser, M., Herrera, S., Hennessy, K., Hewitt, H. T., Jones, R. G., Krakovska, S., Manzanas, R., Martínez-Castro, D., Narisma, G. T., ... Vera, C. S. (2020). An update of IPCC climate reference regions for subcontinental analysis of climate model data: definition and aggregated datasets. *Earth System Science Data*, *12*(4), 2959–2970. https://doi.org/10.5194/essd-12-2959-2020

Jiménez-Moreno, G., & Anderson, R. S. (2012). Pollen and macrofossil evidence of Late Pleistocene and Holocene treeline fluctuations from an alpine lake in Colorado, USA. *The Holocene*, *23*(1), 68–77. https://doi.org/10.1177/0959683612450199

Jiménez-Moreno, G., Anderson, R. S., Shuman, B. N., & Yackulic, E. (2019). Forest and lake dynamics in response to temperature, North American monsoon and ENSO variability during the Holocene in Colorado (USA). *Quaternary Science Reviews*, *211*, 59–72. https://doi.org/10.1016/j.quascirev.2019.03.013

Jiménez-Moreno, G., Fawcett, P. J., & Anderson, R. S. (2008). Millennial- and centennial-scale vegetation and climate changes during the late Pleistocene and Holocene from northern New Mexico (USA). *Quaternary Science Reviews*, *27*(13-14), 1442–1452. https://doi.org/10.1016/j.quascirev.2008.04.004

Johnson, B. G., Jiménez-Moreno, G., Eppes, M. C., Diemer, J. A., & Stone, J. R. (2013). A multiproxy record of postglacial climate variability from a shallowing, 12-m deep sub-alpine bog in the southeastern San Juan Mountains of Colorado, USA. *The Holocene*, *23*(7), 1028–1038. https://doi.org/10.1177/0959683613479682

Joos, F., & Spahni, R. (2008). Rates of change in natural and anthropogenic radiative forcing over the past 20,000 years. *Proceedings of the National Academy of Sciences*, *105*(5), 1425–1430. https://doi.org/10.1073/pnas.0707386105

Judd, E. J., Bhattacharya, T., & Ivany, L. C. (2020). A Dynamical Framework for Interpreting Ancient Sea Surface Temperatures. *Geophysical Research Letters*, *47*(15), e2020GL089044. https://doi.org/https://doi.org/10.1029/2020GL089044

Karamperidou, C., & DiNezio, P. N. (2022). Holocene hydroclimatic variability in the tropical Pacific explained by changing ENSO diversity. *Nature Communications*, *13*(1). https://doi.org/10.1038/s41467-022-34880-8

Kaufman, D., McKay, N., Routson, C., Erb, M., Davis, B., Heiri, O., Jaccard, S., Tierney, J., Dätwyler, C., Axford, Y., et al. (2020). A global database of Holocene paleotemperature records. *Scientific data*, *7*(1), 1–34.

Kawahata, H., Yamamoto, H., Ohkushi, K., Yokoyama, Y., Kimoto, K., Ohshima, H., & Matsuzaki, H. (2009). Changes of environments and human activity at the Sannai-Maruyama ruins in Japan during the mid-Holocene Hypsithermal climatic interval. *Quaternary Science Reviews*, *28*(9-10), 964–974. https://doi.org/10.1016/j.quascirev.2008.12.009

Kirby, M. E., Zimmerman, S. R., Patterson, W. P., & Rivera, J. J. (2012). A 9170-year record of decadal-to-multi-centennial scale pluvial episodes from the coastal Southwest United States: a role for atmospheric rivers? *Quaternary Science Reviews*, *46*, 57–65. https://doi.org/10.1016/j.quascirev.2012.05.008

Köhler, P., Nehrbass-Ahles, C., Schmitt, J., Stocker, T. F., & Fischer, H. (2017). A 156 kyr smoothed history of the atmospheric greenhouse gases CO_2, CH_4, and N_2O and their radiative forcing. *Earth System Science Data*, *9*(1), 363–387. https://doi.org/10.5194/essd-9-363-2017

Kubota, Y., Kimoto, K., Tada, R., Oda, H., Yokoyama, Y., & Matsuzaki, H. (2010). Variations of East Asian summer monsoon since the last deglaciation based on Mg/Ca and oxygen isotope of planktic foraminifera in the northern East China Sea. *Paleoceanography*, *25*(4), n/a–n/a. https://doi.org/10.1029/2009pa001891

Lachniet, M. S., Asmerom, Y., Polyak, V., & Denniston, R. (2020). Great basin paleoclimate and aridity linked to arctic warming and tropical pacific sea surface temperatures. *Paleoceanography and Paleoclimatology*, *35*(7). https://doi.org/10.1029/2019pa003785

Lee, S., L'Heureux, M., Wittenberg, A. T., Seager, R., O'Gorman, P. A., & Johnson, N. C. (2022). On the future zonal contrasts of equatorial Pacific climate: Perspectives from Observations, Simulations, and Theories. *npj Climate and Atmospheric Science*, *5*(1). https://doi.org/10.1038/s41612-022-00301-2

Liefert, D. T., & Shuman, B. N. (2020). Pervasive Desiccation of North American Lakes During the Late Quaternary. *Geophysical Research Letters*, *47*(3). https://doi.org/10.1029/2019gl086412

Linsley, B. K., Rosenthal, Y., & Oppo, D. W. (2010). Holocene evolution of the Indonesian throughflow and the western Pacific warm pool. *Nature Geoscience*, *3*(8), 578–583. https://doi.org/10.1038/ngeo920

Liu, X., Ma, X., Chang, P., Jia, Y., Fu, D., Xu, G., Wu, L., Saravanan, R., & Patricola, C. M. (2021). Ocean fronts and eddies force atmospheric rivers and heavy precipitation in western North America. *Nature Communications*, *12*(1). https://doi.org/10.1038/s41467-021-21504-w

Liu, Y., Zhang, M., Liu, Z., Xia, Y., Huang, Y., Peng, Y., & Zhu, J. (2018). A possible role of dust in resolving the holocene temperature conundrum. *Scientific reports*, *8*(1), 1–9. https://doi.org/10.1038/s41598-018-22841-5

Liu, Z., Otto-Bliesner, B., He, F., Brady, E., Tomas, R., Clark, P., Carlson, A., Lynch-Stieglitz, J., Curry, W., Brook, E., et al. (2009). Transient simulation of last deglaciation with a new mechanism for Bølling-Alleröd warming. *science*, *325*(5938), 310–314.

Liu, Z., Zhu, J., Rosenthal, Y., Zhang, X., Otto-Bliesner, B. L., Timmermann, A., Smith, R. S., Lohmann, G., Zheng, W., & Timm, O. E. (2014). The holocene temperature conundrum. *Proceedings of the National Academy of Sciences*, *111*(34). https://doi.org/10.1073/pnas.1407229111

Lohmann, G., Pfeiffer, M., Laepple, T., Leduc, G., & Kim, J.-H. (2013). A model–data comparison of the Holocene global sea surface temperature evolution. *Climate of the Past*, *9*(4), 1807–1839. https://doi.org/10.5194/cp-9-1807-2013

Ma, X., Chang, P., Saravanan, R., Montuoro, R., Hsieh, J.-S., Wu, D., Lin, X., Wu, L., & Jing, Z. (2015). Distant Influence of Kuroshio Eddies on North Pacific Weather Patterns? *Scientific Reports*, *5*(1). https://doi.org/10.1038/srep17785

MacDonald, G. M., Moser, K. A., Bloom, A. M., Potito, A. P., Porinchu, D. F., Holmquist, J. R., Hughes, J., & Kremenetski, K. V. (2016). Prolonged California aridity linked to climate warming and Pacific sea surface temperature. *Scientific Reports*, *6*(1). https://doi.org/10.1038/srep33325

Maher, L. J. (1972). Absolute Pollen Diagram of Redrock Lake, Boulder County, Colorado. *Quaternary Research*, *2*(4), 531–553. https://doi.org/10.1016/0033-5894(72)90090-7

Marvel, K., & Bonfils, C. (2013). Identifying external influences on global precipitation. *Proceedings of the National Academy of Sciences*, *110*(48), 19301–19306. https://doi.org/10.1073/pnas.1314382110

Marvel, K., Cook, B. I., Bonfils, C. J. W., Durack, P. J., Smerdon, J. E., & Williams, A. P. (2019). Twentieth-century hydroclimate changes consistent with human influence. *Nature*, *569*(7754), 59–65. https://doi.org/10.1038/s41586-019-1149-8

Mathewes, R. W. (1973). A palynological study of postglacial vegetation changes in the University Research Forest, southwestern British Columbia. *Canadian Journal of Botany*, *51*(11), 2085–2103. https://doi.org/10.1139/b73-271

Minckley, T. A., Shriver, R. K., & Shuman, B. (2012). Resilience and regime change in a southern Rocky Mountain ecosystem during the past 17000 years. *Ecological Monographs*, *82*(1), 49–68. https://doi.org/https://doi.org/10.1890/11-0283.1

Minoshima, K., Kawahata, H., & Ikehara, K. (2007). Changes in biological production in the mixed water region (MWR) of the northwestern North Pacific during the last 27 kyr. *Palaeogeography, Palaeoclimatology, Palaeoecology*, *254*(3-4), 430–447.

Müller, P. J., Kirst, G., Ruhland, G., Von Storch, I., & Rosell-Melé, A. (1998). Calibration of the alkenone paleotemperature index $U^{K'}_{37}$ based on core-tops from the eastern South Atlantic and the global ocean (60° N-60° S). *Geochimica et Cosmochimica Acta*, *62*(10), 1757–1772.

Nagashima, K., Addison, J., Irino, T., Omori, T., Yoshimura, K., & Harada, N. (2022). Aleutian Low variability for the last 7500 years and its relation to the Westerly Jet. *Quaternary Research*, *108*, 161–179. https://doi.org/10.1017/qua.2020.116

Nürnberg, D., Böschen, T., Doering, K., Mollier-Vogel, E., Raddatz, J., & Schneider, R. (2015). Sea surface and subsurface circulation dynamics off equatorial Peru during the last $\sim$ 17kyr. *Paleoceanography*, *30*(7), 984–999. https://doi.org/https://doi.org/10.1002/2014PA002706

Osman, M. B., Tierney, J. E., Zhu, J., Tardif, R., Hakim, G. J., King, J., & Poulsen, C. J. (2021). Globally resolved surface temperatures since the Last Glacial Maximum. *Nature*, *599*(7884), 239–244. https://doi.org/10.1038/s41586-021-03984-4

Otto-Bliesner, B. L., Braconnot, P., Harrison, S. P., Lunt, D. J., Abe-Ouchi, A., Albani, S., Bartlein, P. J., Capron, E., Carlson, A. E., Dutton, A., Fischer, H., Goelzer, H., Govin, A., Haywood, A., Joos, F., LeGrande, A. N., Lipscomb, W. H., Lohmann, G., Mahowald, N., ... Zhang, Q. (2017). The PMIP4 contribution to CMIP6 – Part 2: Two interglacials, scientific objective and experimental design for Holocene and Last Interglacial simulations. *Geoscientific Model Development*, *10*(11), 3979–4003. https://doi.org/10.5194/gmd-10-3979-2017

Palmer, H. M., Vriesman, V. P., Livsey, C. M., Fish, C. R., & Hill, T. M. (2023). Holocene climate and oceanography of the coastal Western United States and California Current System. *Climate of the Past*, *19*(1), 199–232. https://doi.org/10.5194/cp-19-199-2023

Parish, M. C., Wolf, K. D., Higuera, P. E., & Shuman, B. N. (2022). Holocene water levels of Silver Lake, Montana, and the hydroclimate history of the Inland Northwest. *Quaternary Research*, *110*, 54–66. https://doi.org/10.1017/qua.2022.17

Parks, S. A., & Abatzoglou, J. T. (2020). Warmer and Drier Fire Seasons Contribute to Increases in Area Burned at High Severity in Western US Forests From 1985 to 2017. *Geophysical Research Letters*, *47*(22). https://doi.org/10.1029/2020gl089858

Pelejero, C., Grimalt, J. O., Heilig, S., Kienast, M., & Wang, L. (1999). High-resolution $U_{37}^{K'}$ temperature reconstructions in the South China Sea over the past 220 kyr. *Paleoceanography*, *14*(2), 224–231. https://doi.org/https://doi.org/10.1029/1998PA900015

Pribyl, P., & Shuman, B. N. (2014). A computational approach to Quaternary lake-level reconstruction applied in the central Rocky Mountains, Wyoming, USA. *Quaternary Research*, *82*(1), 249–259. https://doi.org/10.1016/j.yqres.2014.01.012

Reimer, P. J., Austin, W. E. N., Bard, E., Bayliss, A., Blackwell, P. G., Ramsey, C. B., Butzin, M., Cheng, H., Edwards, R. L., Friedrich, M., Grootes, P. M., Guilderson, T. P., Hajdas, I., Heaton, T. J., Hogg, A. G., Hughen, K. A., Kromer, B., Manning, S. W., Muscheler, R., … Talamo, S. (2020). The IntCal20 Northern Hemisphere Radiocarbon Age Calibration Curve (0–55 cal kBP). *Radiocarbon*, *62*(4), 725–757. https://doi.org/10.1017/rdc.2020.41

Riethdorf, J.-R., Max, L., Nürnberg, D., Lembke-Jene, L., & Tiedemann, R. (2013). Deglacial development of (sub) sea surface temperature and salinity in the subarctic northwest Pacific: Implications for upper-ocean stratification. *Paleoceanography*, *28*(1), 91–104. https://doi.org/https://doi.org/10.1002/palo.20014

Routson, C. C., Kaufman, D. S., McKay, N. P., Erb, M. P., Arcusa, S. H., Brown, K. J., Kirby, M. E., Marsicek, J. P., Anderson, R. S., Jiménez-Moreno, G., Rodysill, J. R., Lachniet, M. S., Fritz, S. C., Bennet, J. R., Goman, M. F., Metcalfe, S. E., Galloway, J. M., Schoups, G., Wahl, D. B., … Gavin, D. G. (2021). A multiproxy database of western North American Holocene paleoclimate records. *Earth System Science Data*, *13*(4), 1613–1632. https://doi.org/10.5194/essd-2020-215

Routson, C. C., McKay, N. P., Kaufman, D. S., Erb, M. P., Goosse, H., Shuman, B. N., Rodysill, J. R., & Ault, T. (2019). Mid-latitude net precipitation decreased with Arctic warming during the Holocene. *Nature*, *568*(7750), 83–87.

Ruan, J., Xu, Y., Ding, S., Wang, Y., & Zhang, X. (2015). A high resolution record of sea surface temperature in southern Okinawa Trough for the past 15,000 years. *Palaeogeography, Palaeoclimatology, Palaeoecology*, *426*, 209–215. https://doi.org/10.1016/j.palaeo.2015.03.007

Salvatteci, R., Schneider, R. R., Blanz, T., & Mollier-Vogel, E. (2019). Deglacial to Holocene Ocean Temperatures in the Humboldt Current System as Indicated by Alkenone Paleothermometry. *Geophysical Research Letters*, *46*(1), 281–292. https://doi.org/10.1029/2018gl080634

Santer, B. D., Painter, J. F., Mears, C. A., Doutriaux, C., Caldwell, P., Arblaster, J. M., Cameron-Smith, P. J., Gillett, N. P., Gleckler, P. J., Lanzante, J., Perlwitz, J., Solomon, S., Stott, P. A., Taylor, K. E., Terray, L., Thorne, P. W., Wehner, M. F., Wentz, F. J., Wigley, T. M. L., ... Zou, C.-Z. (2012). Identifying human influences on atmospheric temperature. *Proceedings of the National Academy of Sciences*, *110*(1), 26–33. https://doi.org/10.1073/pnas.1210514109

Schneider, U., Finger, P., Meyer-Christoffer, A., Rustemeier, E., Ziese, M., & Becker, A. (2017). Evaluating the Hydrological Cycle over Land Using the Newly-Corrected Precipitation Climatology from the Global Precipitation Climatology Centre (GPCC). *Atmosphere*, *8*(3), 52. https://doi.org/10.3390/atmos8030052

Schoder, J. F., Holbourn, A., Kuhnt, W., & Küssner, K. (2016). Variations in sea surface hydrology in the southern Makassar Strait over the past 26 kyr. *Quaternary Science Reviews*, *154*, 143–156. https://doi.org/10.1016/j.quascirev.2016.10.018

Seager, R., Cane, M., Henderson, N., Lee, D.-E., Abernathey, R., & Zhang, H. (2019). Strengthening tropical Pacific zonal sea surface temperature gradient consistent with rising greenhouse gases. *Nature Climate Change*, *9*(7), 517–522. https://doi.org/10.1038/s41558-019-0505-x

Seager, R., Neelin, D., Simpson, I., Liu, H., Henderson, N., Shaw, T., Kushnir, Y., Ting, M., & Cook, B. (2014). Dynamical and Thermodynamical Causes of Large-Scale Changes in the Hydrological Cycle over North America in Response to Global Warming. *Journal of Climate*, *27*(20), 7921–7948. https://doi.org/10.1175/jcli-d-14-00153.1

Shapley, M., Ito, E., & Donovan, J. (2009). Late glacial and Holocene hydroclimate inferred from a groundwater flow-through lake, Northern Rocky Mountains, USA. *The Holocene*, *19*(4), 523–535. https://doi.org/10.1177/0959683609104029

Shintani, T., Yamamoto, M., & Chen, M.-T. (2011). Paleoenvironmental changes in the northern South China Sea over the past 28,000 years: A study of TEX86-derived sea surface temperatures and terrestrial biomarkers. *Journal of Asian Earth Sciences*, *40*(6), 1221–1229. https://doi.org/10.1016/j.jseaes.2010.09.013

Shuman, B. N., Carter, G. E., Hougardy, D. D., Powers, K., & Shinker, J. J. (2014). A north-south moisture dipole at multi-century scales in the Central and Southern Rocky Mountains, U.S.A., during the late Holocene. *Rocky Mountain Geology*, *49*(1), 33–49. https://doi.org/10.2113/gsrocky.49.1.33

Shuman, B. N., & Marsicek, J. (2016). The structure of Holocene climate change in mid-latitude North America. *Quaternary Science Reviews*, *141*, 38–51. https://doi.org/10.1016/j.quascirev.2016.03.009

Shuman, B. N., Pribyl, P., & Buettner, J. (2015). Hydrologic changes in Colorado during the mid-Holocene and Younger Dryas. *Quaternary Research*, *84*(2), 187–199. https://doi.org/10.1016/j.yqres.2015.07.004

Skinner, C. B., Lora, J. M., Payne, A. E., & Poulsen, C. J. (2020). Atmospheric river changes shaped mid-latitude hydroclimate since the mid-Holocene. *Earth and Planetary Science Letters*, *541*, 116293. https://doi.org/10.1016/j.epsl.2020.116293

Smith, R. S., & Gregory, J. (2012). The last glacial cycle: Transient simulations with an AOGCM. *Climate Dynamics*, *38*(7-8), 1545–1559. https://doi.org/10.1007/s00382-011-1283-y

Steinman, B. A., Pompeani, D. P., Abbott, M. B., Ortiz, J. D., Stansell, N. D., Finkenbinder, M. S., Mihindukulasooriya, L. N., & Hillman, A. L. (2016). Oxygen isotope records of Holocene climate variability in the Pacific Northwest. *Quaternary Science Reviews*, *142*, 40–60. https://doi.org/10.1016/j.quascirev.2016.04.012

Stone, J. R., & Fritz, S. C. (2006). Multidecadal drought and Holocene climate instability in the Rocky Mountains. *Geology*, *34*(5), 409. https://doi.org/10.1130/g22225.1

Stott, L., Timmermann, A., & Thunell, R. (2007). Southern Hemisphere and deep-sea warming led deglacial atmospheric CO2 rise and tropical warming. *science*, *318*(5849), 435–438.

Sun, Y., Oppo, D. W., Xiang, R., Liu, W., & Gao, S. (2005). Last deglaciation in the Okinawa Trough: Subtropical northwest Pacific link to Northern Hemisphere and tropical climate. *Paleoceanography*, *20*(4). https://doi.org/https://doi.org/10.1029/2004PA001061

Thompson, A. J., Zhu, J., Poulsen, C. J., Tierney, J. E., & Skinner, C. B. (2022). Northern Hemisphere vegetation change drives a Holocene thermal maximum. *Science advances*, *8*(15), eabj6535. https://doi.org/10.1126/sciadv.abj6535

Thompson, R. S., Whitlock, C., Bartlein, P. J., Harrison, S. P., Spaulding, W. G., Wright, H., Kutzbach, J., Webb, T., Ruddiman, W., & Street-Perrott, F. (1993). Climatic changes in the western united states since 18,000 yr bp. *Global climates since the last glacial maximum*, 468–513.

Tierney, J. E., Malevich, S. B., Gray, W., Vetter, L., & Thirumalai, K. (2019). Bayesian Calibration of the Mg/Ca Paleothermometer in Planktic Foraminifera. *Paleoceanography and Paleoclimatology*, *34*(12), 2005–2030. https://doi.org/https://doi.org/10.1029/2019PA003744

Tierney, J. E., & Tingley, M. P. (2015). A TEX86 surface sediment database and extended Bayesian calibration. *Scientific Data*, *2*(1). https://doi.org/10.1038/sdata.2015.29

Tierney, J. E., & Tingley, M. P. (2018). BAYSPLINE: A New Calibration for the Alkenone Paleothermometer. *Paleoceanography and Paleoclimatology*, *33*(3), 281–301. https://doi.org/https://doi.org/10.1002/2017PA003201

Timm, O., & Timmermann, A. (2007). Simulation of the last 21 000 years using accelerated transient boundary conditions. *Journal of Climate*, *20*(17), 4377–4401. https://doi.org/https://doi.org/10.1175/JCLI4237.1

Trenberth, K. E., Branstator, G. W., Karoly, D., Kumar, A., Lau, N.-C., & Ropelewski, C. (1998). Progress during TOGA in understanding and modeling global teleconnections associated with tropical sea surface temperatures. *Journal of Geophysical Research: Oceans*, *103*(C7), 14291–14324. https://doi.org/https://doi.org/10.1029/97JC01444

Udall, B., & Overpeck, J. (2017). The twenty-first century colorado river hot drought and implications for the future. *Water Resources Research*, *53*(3), 2404–2418. https://doi.org/10.1002/2016wr019638

Ullman, D. J., Carlson, A. E., Hostetler, S. W., Clark, P. U., Cuzzone, J., Milne, G. A., Winsor, K., & Caffee, M. (2016). Final Laurentide ice-sheet deglaciation and Holocene climate-sea level change. *Quaternary Science Reviews*, *152*, 49–59. https://doi.org/https://doi.org/10.1016/j.quascirev.2016.09.014

White, S. M., Ravelo, A. C., & Polissar, P. J. (2018). Dampened El Niño in the Early and Mid-Holocene Due To Insolation-Forced Warming/Deepening of the Thermocline. *Geophysical Research Letters*, *45*(1), 316–326. https://doi.org/https://doi.org/10.1002/2017GL075433

Wilks, D. S. (2011). *Statistical methods in the atmospheric sciences* (Vol. 100). Academic press.

Williams, A. P., Cook, E. R., Smerdon, J. E., Cook, B. I., Abatzoglou, J. T., Bolles, K., Baek, S. H., Badger, A. M., & Livneh, B. (2020). Large contribution from anthropogenic warming to an emerging North American megadrought. *Science*, *368*(6488), 314–318. https://doi.org/10.1126/science.aaz9600

Yeh, S.-W., Cai, W., Min, S.-K., McPhaden, M. J., Dommenget, D., Dewitte, B., Collins, M., Ashok, K., An, S.-I., Yim, B.-Y., & Kug, J.-S. (2018). ENSO Atmospheric Teleconnections and Their Response to Greenhouse Gas Forcing. *Reviews of Geophysics*, *56*(1), 185–206. https://doi.org/https://doi.org/10.1002/2017RG000568

Yu, H., Liu, Z., Berné, S., Jia, G., Xiong, Y., Dickens, G. R., Wei, G., Shi, X., Liu, J., & Chen, F. (2009). Variations in temperature and salinity of the surface water above the middle Okinawa Trough during the past 37kyr. *Palaeogeography, Palaeoclimatology, Palaeoecology*, *281*(1-2), 154–164. https://doi.org/10.1016/j.palaeo.2009.08.002

Zappa, G., Ceppi, P., & Shepherd, T. G. (2020). Time-evolving sea-surface warming patterns modulate the climate change response of subtropical precipitation over land. *Proceedings of the National Academy of Sciences*, *117*(9), 4539–4545. https://doi.org/10.1073/pnas.1911015117

Zhang, Y., Zheng, X., Kong, D., Yan, H., & Liu, Z. (2021). Enhanced North Pacific subtropical gyre circulation during the late Holocene. *Nature Communications*, *12*(1). https://doi.org/10.1038/s41467-021-26218-7

Supplementary Information

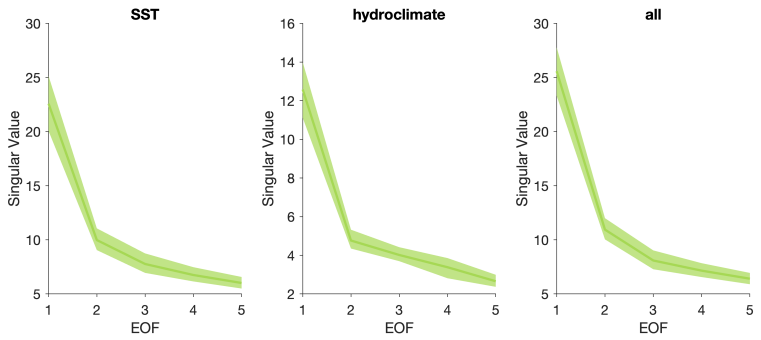

Figure S4.1: Singular values of (left) SST, (center) hydroclimate, and (right) combined SST and hydroclimate proxy records. Shading indicates the 95% confidence interval of singular values that accounts for chronological and calibration uncertainties. The solid green line indicates the median singular value.

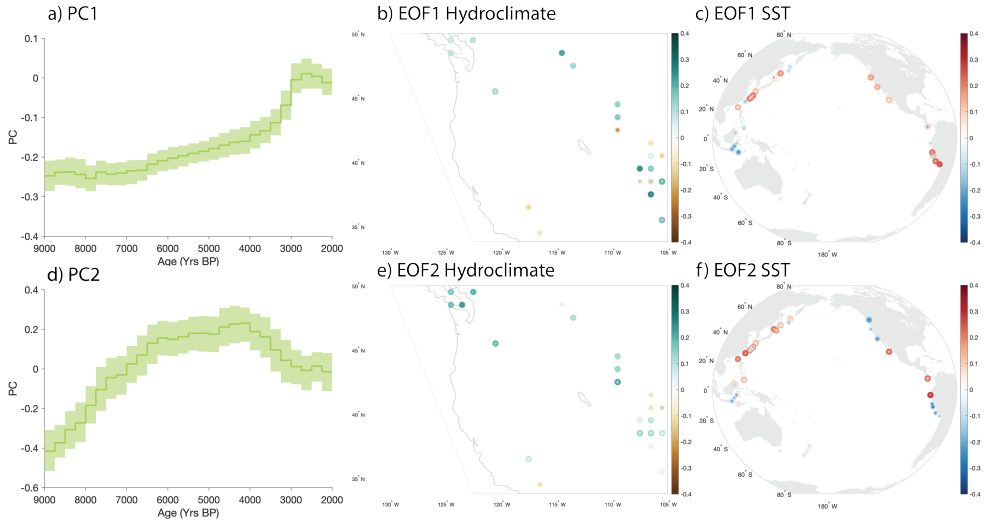

Figure S4.2: Spatiotemporal patterns of a-c) EOF1/PC1 and b) EOF2/PC2 on the combined SST and hydroclimate dataset. Shadings in timeseries indicate the 95% confidence interval of each PC1 due to chronological and calibration uncertainties. The outer ring, inner ring, and central colors represent 97.5^{th} , 2.5^{th} , and 50^{th} (median) percentile of loading values respectively.

Chapter 5

The Time of Emergence of Surface Warming in the Last Millennium Reanalysis and CCSM4

Anson H. Cheung[1], Luke A. Parsons[2], Baylor Fox-Kemper[1]

1. Department of Earth, Environmental, and Planetary Sciences, Brown University, Providence, RI 02912, USA

2. Nicholas School of the Environment, Duke University, Durham, NC 27710, USA

Abstract

Understanding climate variability of the last millennium allows us to better contextualize the recent warming that has occurred since the industrial period. Proxy records and climate models are two major sources of information to determine the location, magnitude of anthropogenic warming and the timing when the warming signal emerges from the last millennium baseline. However, whether the information and context they provide on anthropogenic warming are consistent remain unclear. Here, we compute the time of emergence of surface warming in the Community Climate System Model version 4 (CCSM4) and compare it with results from the Last Millennium Reanalysis (LMR) product, which combines proxy records and climate models, to address this question. Even though they show a similar time of emergence of warming spatial pattern, surface warming in CCSM4 emerges earlier than in LMR, particularly in the low latitudes. Our analysis indicates that CCSM4 simulates a stronger forced response than those recorded by proxy records, and that variability on decadal to longer timescales in CCSM4 is weaker than those in proxy records. This implies that CCSM4 overestimates the contribution of forced climate change in recent decades, but suggests that future climate change might be even larger than what we currently experiencing. These results together underscore the importance to better understand and quantify climate variability, the urgency to reduce anthropogenic greenhouse gases emissions, and the need to revisit climate risk assessments that rely on climate models.

1 Introduction

Understanding climate variability of the last millennium provides a context for how the climate system evolves in the absence of large anthropogenic greenhouse gas emissions. Studying the climate of this period allows us to better contextualize the recent warming that has occurred since the industrial period (e.g, Abram et al., 2016; Mann et al., 2008; PAGES2k Consortium, 2019). Specifically, we can gain a better understanding in the magnitude and location of where anthropogenic warming is occurring and the timing when the warming signal exceeds the background noise. These information sources are useful for detecting anthropogenic climate change (Doblas-Reyes et al., 2021) and for adaptation planning (Ranasinghe et al., 2021).

Proxy records and climate models are two major sources of information for understanding climate of the last millennium and providing context on the location, magnitude of anthropogenic warming, and the timing when the warming signal emerges from background. Although proxy records capture past temperature changes indirectly and have incomplete spatiotemporal coverage, they have been widely used to reconstruct global (e.g., PAGES2k Consortium, 2019), hemispheric (e.g., Mann et al., 2008; Neukom et al., 2014), continental and basin scale (PAGES2k Consortium, 2013; Tierney et al., 2015) temperatures, and different modes of climate variability (e.g., Abram et al., 2014; Emile-Geay et al., 2013; Trouet et al., 2009), which can be then used to detect the emergence of anthropogenically forced warming/change (Abram et al., 2016). Last millennium climate model simulations, on the other hand, have been largely used in conjunction with proxy reconstructions to understand the forcings responsible for driving the changes reconstructed by paleoclimate records (e.g., PAGES2k Consortium, 2019; Schurer et al., 2013). The use of climate models to determine location, magnitude of anthropogenic warming, and the timing when the warming signal emerges from background has largely been restricted to historical

(1850-present) simulations (Giorgi & Bi, 2009; Hawkins & Sutton, 2012; Mahlstein et al., 2011).

The critical role proxy records and climate models play in determining the characteristics of the emergence of warming highlights the need to ensure they provide consistent information. However, proxy-model comparison studies thus far have mostly focused on determining if there is a consistent forced response from volcanic forcing (Dee et al., 2020; Zhu et al., 2022), comparable variability across timescale (Dee et al., 2017; Laepple & Huybers, 2014; Parsons et al., 2017; Zhu et al., 2019), and agreement in representing regional and continental scale temperature changes (PAGES 2k-PMIP3 group, 2015). Even though these studies offer clues on whether proxy records and climate models will paint a consistent picture of the emergence of anthropogenic warming, to date, this has not been explicitly addressed.

Here, we determine the 'Time of Emergence' (TOE) (Hawkins & Sutton, 2012) of surface warming in the Community Climate Sytem Model version 4 (CCSM4) and compare it with TOE of surface warming in the Last Millennium Reanalysis (LMR) product (Hakim et al., 2016; Tardif et al., 2019), which combines data from proxy records and outputs of CCSM4 last millennium simulation. By comparing the TOE of warming between these two datasets, we can determine if proxy records and climate models offer similar estimates of the TOE of anthropogenic warming and the associated spatial pattern.

2 Data and Method

2.1 Data

This study used outputs from the Last Millennium Reanalysis version 2.1 (LMRv2.1) (see Hakim et al., 2016; Tardif et al., 2019, for a full description). The LMR is an offline data assimilation framework that randomly draws 100 time-averaged states from the CCSM4 last millennium simulation (Landrum et al., 2013) to form a fixed prior

and assimilates proxy records from the PAGES2k Consortium database (PAGES2k Consortium, 2017) at each time step using an ensemble Kalman filter. This results in annually resolved reconstruction of climate fields. To probe the error due to proxy records incorporated and the climate states used, a Monte Carlo approach is used to generate multiple iterations, where each iteration has a different set of climate states chosen from the climate model and a different 75% of the proxy records assimilated. LMRv2.1 spans 0-2000 CE and has 20 iterations available.

We compared the LMRv2.1 with different versions of the LMR to determine the robustness of the TOE of warming features. We first compared results from LMRv2.1 with LMRv2.0, which assimilates proxy records from the LMR database (Anderson et al., 2019) instead of PAGES2k Consortium database (PAGES2k Consortium, 2017). The LMR database contains an extended amount of proxy records (up to a 4-fold increase during the 19^{th} to 20^{th} century) that are not included in the PAGES2k database (PAGES2k Consortium, 2017). Since outputs from LMR can be influenced by the prior model (Amrhein et al., 2020), we supplemented LMRv2.1 with two reanalysis products from Parsons and Hakim (2019). These reanalysis products also followed the LMR framework, but used the LMR database (Anderson et al., 2019), carried out 11 Monte Carlo iterations, and used a different climate model prior in one of the reanalysis products. We specifically focused on the reanalysis products from Parsons and Hakim (2019) that used CCSM4 (henceforth known as LMR CCSM4) and MPI-ESM-P (henceforth known as LMR MPI-ESM-P) as model priors.

We analyzed last millennium simulations from two fully-coupled climate models, CCSM4 and MPI-ESM-P, that were used as a prior in the reanalysis products. Last millennium simulations from these two climate models follow the PMIP3 protocol (Schmidt et al., 2011) and run 850-1849 CE. We extended these simulations with historical simulations that span 1850-2005 CE. To make direct comparison with reanalysis products, we interpolated the data into $2^{\circ} \times 2^{\circ}$ resolution using bilinear

interpolation prior to analysis.

2.2 Method

We calculated the time of emergence (TOE) based on a modified method in Hawkins and Sutton (2012). Calculation of TOE requires estimates of the climate change signal and variability (noise) relative to a baseline. Hawkins and Sutton (2012) used 1986-2005 as the baseline and defined the signal of each grid box by first regressing its temperature onto global mean temperature that was smoothed with a fourth order polynomial, then using the regression relationship as the signal estimate. The signal was estimated by taking the standard deviation of seasonal or annual means. We opted for an alternate baseline and definitions of signal and noise. Specifically, we used 850-1799 CE as the baseline and focused on 20 year or longer variability to minimize the impacts from internal variability on TOE estimates. The 850-1799 CE baseline also better represents pre-industrial condition than shorter baselines that were used in previous studies (e.g., Hawkins & Sutton, 2012). Prior to calculations, we applied a 20 year fourth order Butterworth filter to all data. We defined the noise as the standard deviation of the baseline and the signal as the low pass filtered temperature between 1800 - 2000 CE. The TOE is defined as the time where the signal permanently exceeds two times the noise within the time window (i.e., 850-2000 CE). Because TOE is sensitive to the definition of signal, noise and the reference period (Doblas-Reyes et al., 2021), we tested the sensitivity of our results by generating four alternative calculations: (1) a 10 year Butterworth filter was used, (2) a 50 year Butterworth filter was used, (3) the Medieval Warm Period (950-1250 CE) was used as the reference period, and (4) the Little Ice Age (1450-1750 CE) was used as the reference period (Figures S5.1-S5.2).

To understand the differences in TOE between reanalysis and climate models, it is necessary to compare their noise and signal estimates. However, estimating the

noise in LMR is not trivial. The variance in LMR is shown to be dependent on the number of proxies assimilated, which varies across time, aside from climate (Tardif et al., 2019). Hence, we cannot determine if LMR and climate model offer similar noise estimates based on the data used in this study. We focused on comparing the signal estimate instead by computing the 20^{th} century trend in reanalysis and climate models, when changes are primarily dominated by greenhouse gases emissions and there are abundant proxy records available. Specifically, we calculated the linear trend of 20^{th} century temperature in LMRv2.1 and CCSM4 using ordinary least squares. Because the magnitude of the linear trend can be influenced by internal variability, we calculated the trend in six other CCSM4 historical simulation members. We then compared the slopes from all CCSM4 members with the slopes from all the LMRv2.1 iterations using a Kolmogorov-Smirnov test to determine if they are from the same distribution. If the resulting spatial pattern is similar to the difference in TOE of warming between LMR and CCSM4, then that would suggest the difference in signal estimate is responsible for the different TOE of warming estimates. Alternatively, if the slope difference and TOE of warming spatial patterns do not match each other, then that would suggest the difference in noise estimate in LMR and CCSM4 plays a role in driving the different TOE of warming estimates.

3 Results and Discussion

The spatial patterns of the TOE in the LMR and CCSM4 are similar and consistent with prior studies (Hawkins & Sutton, 2012; Mahlstein et al., 2011). On a global scale, the warming emerges notably earlier in the low latitudes, specifically regions with atmospheric deep convection (Parsons et al., 2020), than the high latitudes in both the LMR and CCSM4 (Figure 5.1a-c). In LMRv2.1, warming in the Indian Ocean, the Southwest Pacific and subtropical North Pacific emerge earlier than the rest of the tropics and the world. Though, warming in the eastern equatorial Pacific

emerges noticeably later than the rest of the tropics. On the other hand, the warming emerges at a similar time in most of the tropics in CCSM4, with the exception of equatorial Atlantic and subtropical Northeast Pacific. Overall, these results capture the TOE of warming pattern that is consistent with our current understanding of the climate system – the warming in the tropics emerge from the background earlier than the extratropics owing to the comparatively small internal variability in the tropics (Hawkins & Sutton, 2012), with the exception of eastern equatorial Pacific owing to the substantially larger internal variability compared to the rest of the tropics (Parsons et al., 2020).

These patterns appear to be strongly dependent on the length of filter an to a lesser extent the baseline used (Figure S5.1-S5.2). Nevertheless, these results are not surprising and are consistent with our understanding on TOE calculations (Doblas-Reyes et al., 2021). Ultimately, the selection of the length of filter and the baseline depends on the framing question (Doblas-Reyes et al., 2021; Ranasinghe et al., 2021). In our case, the 20 year filter is appropriate because it smooths out the majority of the subdecadal to decadal variability, which are often not associated with anthropogenic influences, whereas the baseline (850 - 1799 CE) selected most accurately reflects background conditions when compared to other shorter baseline periods that could be influenced by anomalous changes in boundary conditions (e.g., a long period of anomalously low total solar irradiance) .

Although the overall spatial TOE pattern in LMR and CCSM4 are similar, there is a substantial difference in the TOE (Figure 5.1d). Notably, the warming in LMR emerges later than the warming in CCSM4 in most of the tropics by ~ 50 years. The difference in TOE between LMR and CCSM4, on the other hand, is less clear outside of the tropics. Because estimates of TOE of warming in the LMR can be influenced by the number and location proxy records that are assimilated and the prior model, we investigate whether these factors can affect our results.

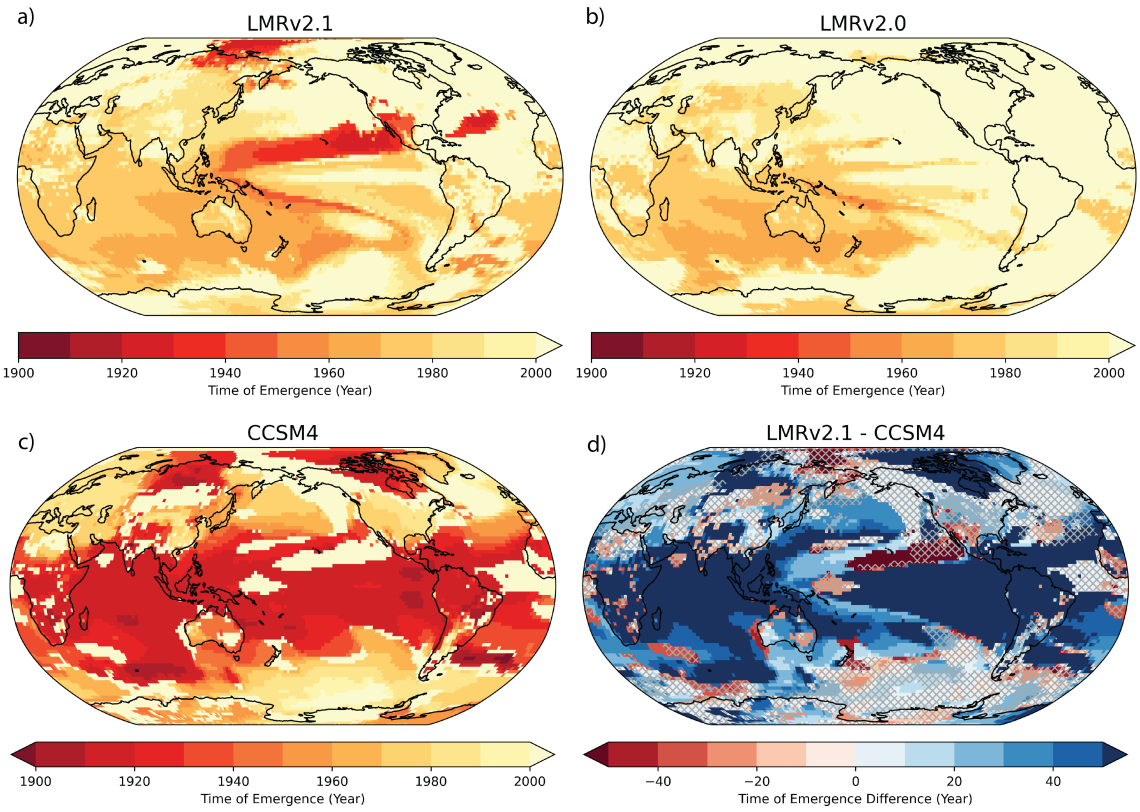

Figure 5.1: Time of emergence of warming in a) LMRv2.1 (median), b) LMRv2.0 (median), c) CCSM4 last millennium run. d) The difference in the time of emergence between LMRv2.1 and CCSM4. Hatching indicates less than 18 out of 20 iterations of the LMR has a time of emergence of warming fall in the same direction when compared to the CCSM4 last millennium run.

The overall TOE of warming pattern does not depend on the proxy database used. Previous analysis suggests that differing the total number of proxy records used in assimilation by a large amount can change how well these reanalysis products can capture the climate system (Tardif et al., 2019). Indeed, we see some difference in the TOE of warming pattern when comparing the LMRv2.1 and v2.0 (Figure 5.1a-b). However, they are broadly qualitatively similar. More importantly, the main feature, an earlier emergence of warming in the Indian Ocean and southwest Pacific, remains robust. Hence, we suggest the impacts of a different proxy database on the TOE of warming pattern are minor.

The difference between reanalysis and the model prior also does not depend on

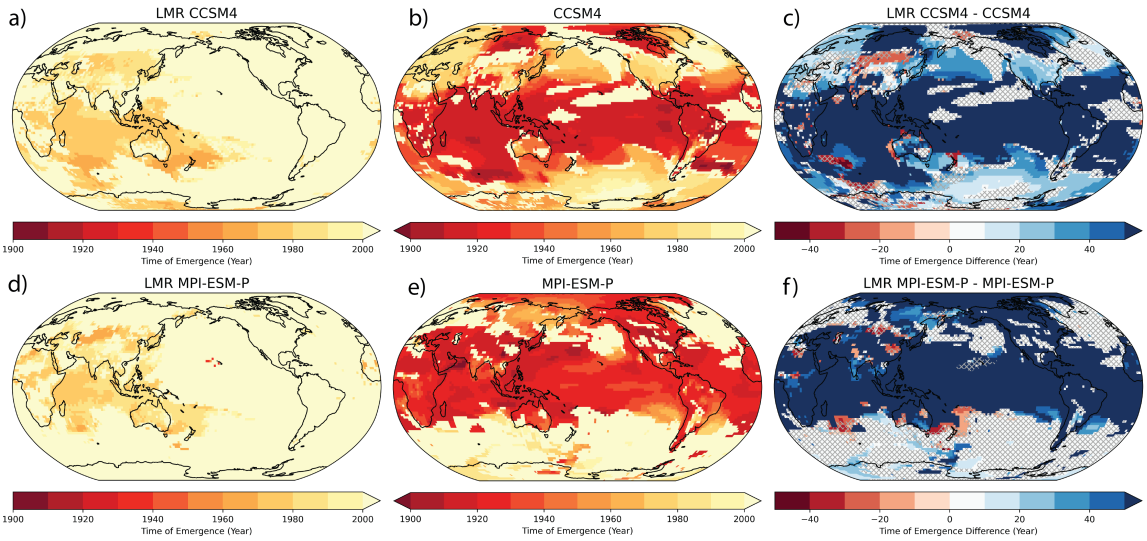

Figure 5.2: Time of emergence of warming in a) LMR CCSM4 (median), b) LMR MPI-ESM-P (median), c) CCSM4, d) MPI-ESM-P. The diference in the time of emergence of warming between e) LMR and CCSM4, and f) LMR and MPI-ESM-P. Hatching indicates less than 9 out of 11 iterations of the LMR has a time of emergence of warming fall in the same direction when compared to the model prior.

the climate model used. The prior model(s) used for data assimilation under the LMR framework has shown to influence the spatiotemporal estimates of past climate (Amrhein et al., 2020). As such, we might expect the TOE of warming estimates would be dependent on the prior model used. However, our comparison between two reanalyses from two different models shows otherwise (Figure 5.2). The TOE of warming spatial pattern are qualitatively similar in the reanalysis products, where the warming emerges earliest in the Indian Ocean. The pattern in the models also show broad consistency, with the warming emerging the earliest in the tropics. Although there are some differences in the exact location of the detectable emergence of warming, the TOE of warming in the Southern Ocean is earlier in CCSM4 than in MPI-ESM-P while the TOE of warming in the Arctic is less spatially coherent in CCSM4 than in MPI-ESM-P (Figures 5.2, S5.3). Nonetheless, the TOE of warming in the climate model is earlier than in LMR in both cases, a result that is consistent with our conclusion made based on LMRv2.1.

Given that the different TOE of warming estimates in LMR and the model is not dependent on the proxy database and the climate model prior used, this suggests proxy records and climate models have a different temperature signal to noise ratio. Our analysis indicates that the signal, as represented by the 20$^{\text{th}}$ century trend, in CCSM4 is larger than LMR in most regions (Figure 5.3). Consequently, the larger signal in CCSM4 than LMR leads to an earlier TOE of warming in the model. This difference in signal amplitude is likely due to the overestimated 20$^{\text{th}}$ century warming in CCSM4 (Meehl et al., 2012). However, because the trend difference and the TOE difference patterns do not match exactly (c.f. Figure 5.1d and 5.3), the large signal amplitude is unlikely to be the only explanation of an earlier TOE of warming in the model compared to LMR. The noise amplitude in proxy records is also likely to be larger than in the climate model. Indeed, previous proxy-model comparison studies have highlighted that climate models may underestimate decadal and longer variability compared to proxy records in the tropics (Laepple & Huybers, 2014; Parsons et al., 2017). Even though we do not have direct evidence to support this argument, our results seem to be consistent with previous conclusions that suggest a larger decadal and longer scale variability in proxy records compared to climate models (Laepple & Huybers, 2014; Parsons et al., 2017).

4 Conclusion

Proxy records and climate models provide contrasting information on the time of emergence of warming over the 20$^{\text{th}}$ century. By analyzing the time of emergence of warming in the LMR and CCSM4, we find that even though proxy records and climate models provide a similar TOE of warming spatial pattern and are consistent with prior studies (e.g., Hawkins & Sutton, 2012; Mahlstein et al., 2011), paleoclimate data assimilation products analyzed here shift the TOE of warming in the tropics later by $\sim$ 50 years. We further suggest that this is due to a combination of too strong estimated

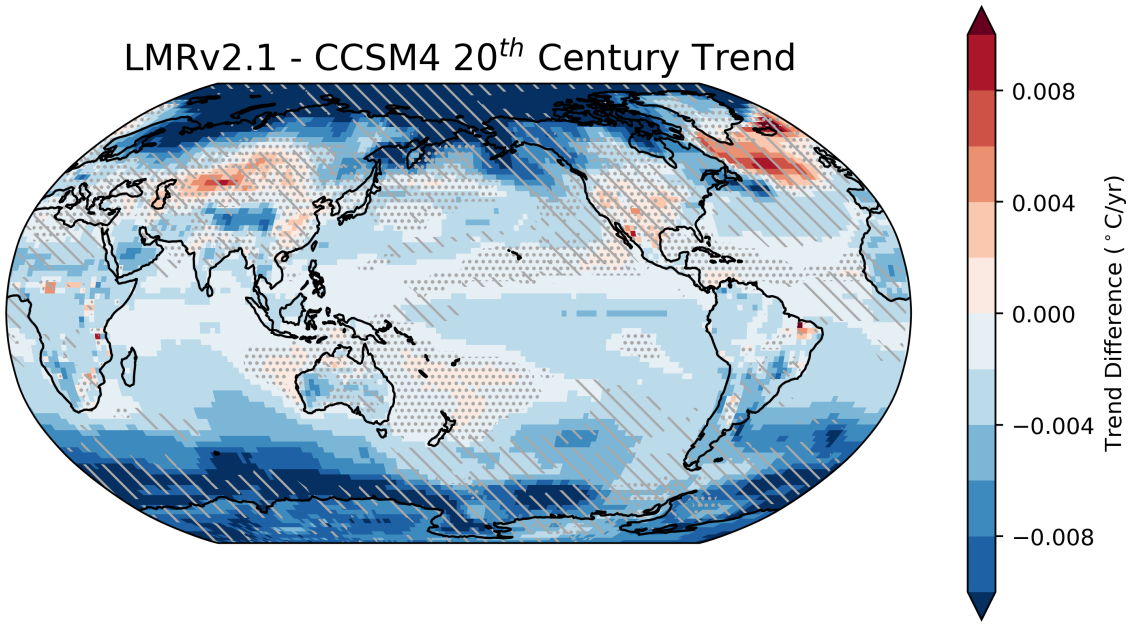

Figure 5.3: Difference in 20$^{\text{th}}$ century temperature trend between LMRv2.1 and CCSM4. Blue regions indicate the trend is smaller in LMRv2.1 than in CCSM4 whereas red regions indicate the trend is larger in LMRv2.1 than in CCSM4. The diagonal hatches represent regions where less than 18 out of 20 iterations of the LMR has a time of emergence of warming fall in the same direction when compared to CCSM4. The stipplings represent regions where the difference in the 20$^{\text{th}}$ century temperature trend between LMRv2.1 and CCSM4 are not statistically significant.

forced signal and a too weak decadal or longer timescale variability. Although this offers hope that the emergence of warming is currently less severe than previously estimated, this also suggests that temperature anomalies observed in recent decades might still be within the range of natural variability, and that the impacts from anthropogenically forced changes will be larger than what we are currently observing. These results together underscore the importance to better quantify the influence of internal climate variability on recent climate, the necessity for more spatial coverage of high quality paleoclimate records to improve our estimates of climate variability, the urgency to reduce anthropogenic greenhouse gases emission to minimize climate change impacts, and the need to revisit climate risk assessments that rely on climate models to estimate emergence of climate signals.

References

Abram, N. J., Mcgregor, H. V., Tierney, J. E., Evans, M. N., Mckay, N. P., & Kaufman, D. S. (2016). Early onset of industrial-era warming across the oceans and continents. *Nature*, *536*(7617), 411–418. https://doi.org/10.1038/nature19082

Abram, N. J., Mulvaney, R., Vimeux, F., Phipps, S. J., Turner, J., & England, M. H. (2014). Evolution of the Southern Annular Mode during the past millennium. *Nature Climate Change*, *4*(7), 564–569.

Amrhein, D. E., Hakim, G. J., & Parsons, L. A. (2020). Quantifying structural uncertainty in paleoclimate data assimilation with an application to the last millennium. *Geophysical Research Letters*, *47*(22), e2020GL090485.

Anderson, D. M., Tardif, R., Horlick, K., Erb, M. P., Hakim, G. J., Noone, D., Perkins, W. A., & Steig, E. (2019). Additions to the Last Millennium Reanalysis Multi-Proxy Database. *Data Science Journal*, *18*(1), 2. https://doi.org/10.5334/dsj-2019-002

Dee, S. G., Parsons, L. A., Loope, G. R., Overpeck, J. T., Ault, T. R., & Emile-Geay, J. (2017). Improved spectral comparisons of paleoclimate models and observations via proxy system modeling: Implications for multi-decadal variability. *Earth and Planetary Science Letters*, *476*, 34–46.

Dee, S. G., Cobb, K. M., Emile-Geay, J., Ault, T. R., Edwards, R. L., Cheng, H., & Charles, C. D. (2020). No consistent ENSO response to volcanic forcing over the last millennium. *Science*, *367*(6485), 1477–1481.

Doblas-Reyes, F., Sorensson, A., Almazroui, M., Dosio, A., Gutowski, W., Haarsma, R., Hamdi, R., Hewitson, B., Kwon, W.-T., Lamptey, B., et al. (2021). Linking Global to Regional Climate change. In Climate Change 2021: The Physical Science Basis. Contribution of Working Group I to the Sixth Assessment Report of the Intergovernmental Panel on Climate Change.

Emile-Geay, J., Cobb, K. M., Mann, M. E., & Wittenberg, A. T. (2013). Estimating central equatorial Pacific SST variability over the past millennium. Part II: Reconstructions and implications. *Journal of Climate*, *26*(7), 2329–2352.

Giorgi, F., & Bi, X. (2009). Time of emergence (TOE) of GHG-forced precipitation change hot-spots. *Geophysical Research Letters*, *36*(6). https://doi.org/https://doi.org/10.1029/2009GL037593

Hakim, G. J., Emile-Geay, J., Steig, E. J., Noone, D., Anderson, D. M., Tardif, R., Steiger, N., & Perkins, W. A. (2016). The last millennium climate reanalysis project: Framework and first results. *Journal of Geophysical Research: Atmospheres*, *121*(12), 6745–6764.

Hawkins, E., & Sutton, R. (2012). Time of emergence of climate signals. *Geophysical Research Letters*, *39*(1).

Laepple, T., & Huybers, P. (2014). Ocean surface temperature variability: Large model–data differences at decadal and longer periods. *Proceedings of the National Academy of Sciences*, *111*(47), 16682–16687.

Landrum, L., Otto-Bliesner, B. L., Wahl, E. R., Conley, A., Lawrence, P. J., Rosenbloom, N., & Teng, H. (2013). Last millennium climate and its variability in ccsm4. *Journal of Climate*, *26*(4), 1085–1111. https://doi.org/10.1175/JCLI-D-11-00326.1

Mahlstein, I., Knutti, R., Solomon, S., & Portmann, R. W. (2011). Early onset of significant local warming in low latitude countries. *Environmental Research Letters*, *6*(3), 034009.

Mann, M. E., Zhang, Z., Hughes, M. K., Bradley, R. S., Miller, S. K., Rutherford, S., & Ni, F. (2008). Proxy-based reconstructions of hemispheric and global surface temperature variations over the past two millennia. *Proceedings of the National Academy of Sciences*, *105*(36), 13252–13257.

Meehl, G. A., Washington, W. M., Arblaster, J. M., Hu, A., Teng, H., Tebaldi, C., Sanderson, B. N., Lamarque, J.-F., Conley, A., Strand, W. G., & White, J. B. (2012). Climate system response to external forcings and climate change projections in ccsm4. *Journal of Climate*, *25*(11), 3661–3683. https://doi.org/10.1175/JCLI-D-11-00240.1

Neukom, R., Gergis, J., Karoly, D. J., Wanner, H., Curran, M., Elbert, J., Gonzalez-Rouco, F., Linsley, B. K., Moy, A. D., Mundo, I., et al. (2014). Inter-hemispheric temperature variability over the past millennium. *Nature climate change*, *4*(5), 362–367.

PAGES 2k-PMIP3 group. (2015). Continental-scale temperature variability in PMIP3 simulations and PAGES 2k regional temperature reconstructions over the past millennium. *Climate of the Past*, *11*(12), 1673–1699. https://doi.org/10.5194/cp-11-1673-2015

PAGES2k Consortium. (2013). Continental-scale temperature variability during the past two millennia. *Nature Geoscience*, *6*(5), 339–346.

PAGES2k Consortium. (2017). A global multiproxy database for temperature reconstructions of the Common Era. *Scientific data*, *4*.

PAGES2k Consortium. (2019). Consistent multidecadal variability in global temperature reconstructions and simulations over the Common Era. *Nature Geoscience*, *12*(8), 643–649.

Parsons, L. A., & Hakim, G. J. (2019). Local regions associated with interdecadal global temperature variability in the Last Millennium Reanalysis and CMIP5 models. *Journal of Geophysical Research: Atmospheres*, *124*(17-18), 9905–9917.

Parsons, L. A., Brennan, M. K., Wills, R. C., & Proistosescu, C. (2020). Magnitudes and spatial patterns of interdecadal temperature variability in cmip6. *Geophysical Research Letters*, *47*(7), e2019GL086588. https://doi.org/https://doi.org/10.1029/2019GL086588

Parsons, L. A., Loope, G. R., Overpeck, J. T., Ault, T. R., Stouffer, R., & Cole, J. E. (2017). Temperature and precipitation variance in CMIP5 simulations and paleoclimate records of the last millennium. *Journal of Climate*, *30*(22), 8885–8912.

Ranasinghe, R., Ruane, A. C., Vautard, R., Arnell, N., Coppola, E., Cruz, F. A., Dessai, S., Saiful Islam, A., Rahimi, M., Carrascal, D. R., et al. (2021). Climate Change Information for Regional Impact and for Risk Assessment. In Climate Change 2021: The Physical Science Basis. Contribution of Working Group I to the Sixth Assessment Report of the Intergovernmental Panel on Climate Change. *IPCC Sixth Assessment Report*.

Schmidt, G. A., Jungclaus, J. H., Ammann, C. M., Bard, E., Braconnot, P., Crowley, T. J., Delaygue, G., Joos, F., Krivova, N. A., Muscheler, R., Otto-Bliesner, B. L., Pongratz, J., Shindell, D. T., Solanki, S. K., Steinhilber, F., & Vieira, L. E. A. (2011). Climate forcing reconstructions for use in PMIP simulations of the last millennium (v1.0). *Geoscientific Model Development*, *4*(1), 33–45. https://doi.org/10.5194/gmd-4-33-2011

Schurer, A. P., Hegerl, G. C., Mann, M. E., Tett, S. F., & Phipps, S. J. (2013). Separating forced from chaotic climate variability over the past millennium. *Journal of Climate*, *26*(18), 6954–6973.

Tardif, R., Hakim, G. J., Perkins, W. A., Horlick, K. A., Erb, M. P., Emile-Geay, J., Anderson, D. M., Steig, E. J., & Noone, D. (2019). Last Millennium Reanalysis with an expanded proxy database and seasonal proxy modeling. *Climate of the Past*, *15*(4), 1251–1273.

Tierney, J. E., Abram, N. J., Anchukaitis, K. J., Evans, M. N., Giry, C., Kilbourne, K. H., Saenger, C. P., Wu, H. C., & Zinke, J. (2015). Tropical sea surface temperatures for the past four centuries reconstructed from coral archives. *paleoceanography*, *30*(3), 226–252.

Trouet, V., Esper, J., Graham, N. E., Baker, A., Scourse, J. D., & Frank, D. C. (2009). Persistent positive North Atlantic Oscillation mode dominated the medieval climate anomaly. *science*, *324*(5923), 78–80.

Zhu, F., Emile-Geay, J., Anchukaitis, K. J., Hakim, G. J., Wittenberg, A. T., Morales, M. S., Toohey, M., & King, J. (2022). A re-appraisal of the ENSO response to volcanism with paleoclimate data assimilation. *Nature communications*, *13*(1), 747.

Zhu, F., Emile-Geay, J., McKay, N. P., Hakim, G. J., Khider, D., Ault, T. R., Steig, E. J., Dee, S., & Kirchner, J. W. (2019). Climate models can correctly simulate the continuum of global-average temperature variability. *Proceedings of the National Academy of Sciences*, *116*(18), 8728–8733.

Supplementary Information

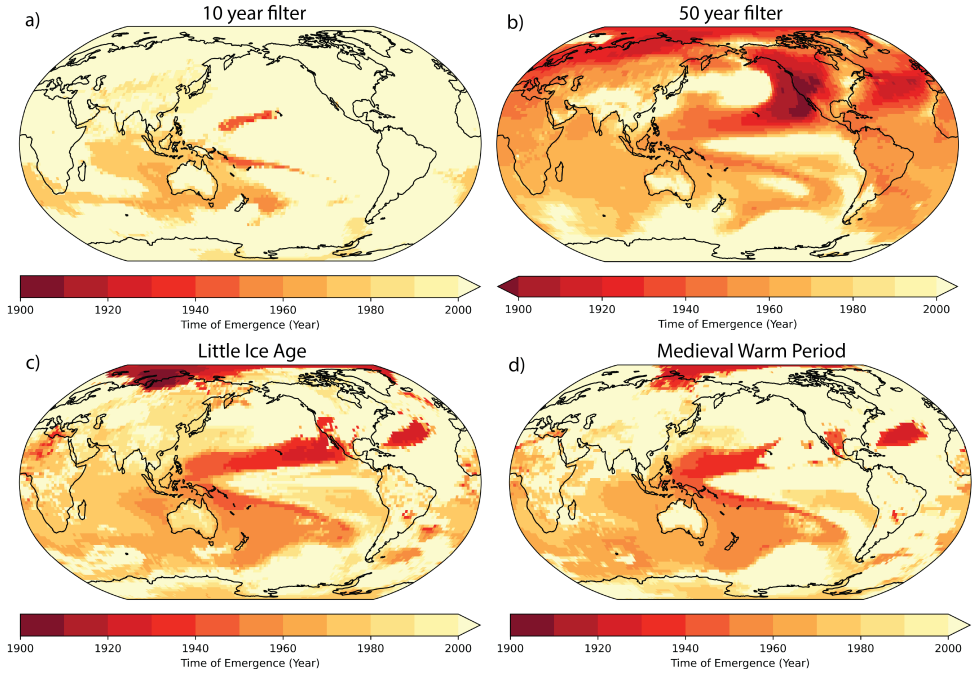

Figure S5.1: The median of time of emergence of warming in LMRv2.1 using a) a 10 year filter, b) a 50 year filter, c) Medieval Warm Period as the reference period, d) Little Ice Age as the reference period.

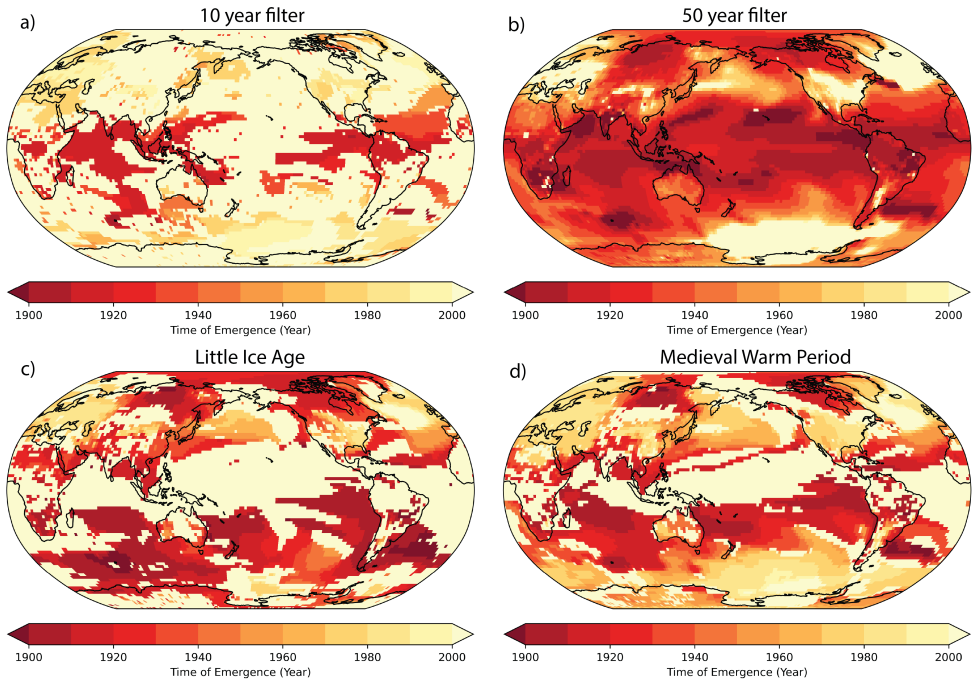

Figure S5.2: The time of emergence of warming in CCSM4 using a) a 10 year filter, b) a 50 year filter, c) Medieval Warm Period as the reference period, d) Little Ice Age as the reference period.

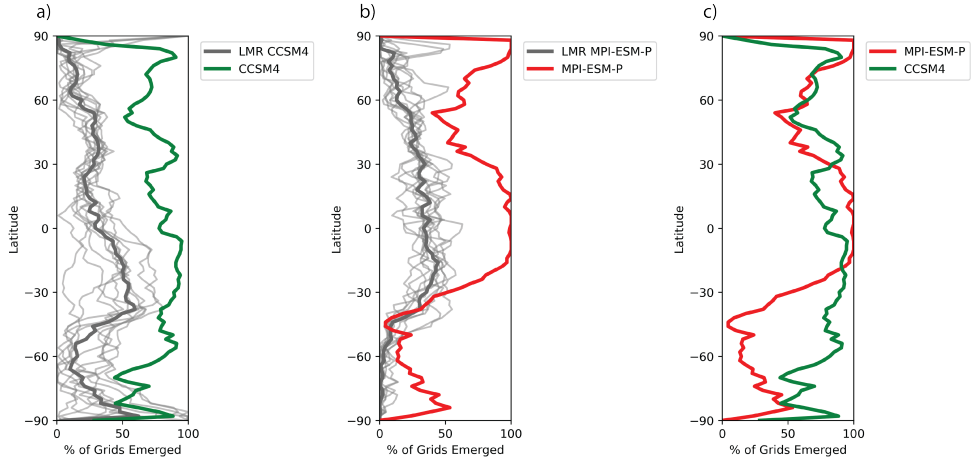

Figure S5.3: A comparison in zonal percentage of grids where the warming has emerged from the background between a) LMR CCSM4 (gray) and CCSM4 (green), b) LMR MPI-ESM-P (gray) and MPI-ESM-P (red), and c) MPI-ESM-P (red) and CCSM4 (green).